Grafting-onto Approaches as Valuable Tool to Access (Bio-Based) Materials for Water Treatment

Zur Erlangung des akademischen Grades eines

DOKTORS DER NATURWISSENSCHAFTEN

(Dr. rer. nat.)

von der KIT-Fakultät für Chemie und Biowissenschaften

des Karlsruher Instituts für Technologie (KIT)

genehmigte

DISSERTATION

von

M. Sc. Timo Sehn

aus Iffezheim

1. Referent: Prof. Dr. Michael A. R. Meier

2. Referent: Prof. Dr. Patrick Théato

Tag der mündlichen Prüfung: 05.05.2025

Für meine Eltern,
Sabine und Roland Sehn

“Most people say that it is the intellect which makes a great scientist.

They are wrong: it is character.”

Albert Einstein

Declaration of Authorship

Die vorliegende Arbeit wurde von Mai 2022 bis März 2025 unter Anleitung von Prof. Dr. Michael A. R. Meier am Institut für Organische Chemie (IOC) und am Institut für Biologische und Chemische Systeme – Funktionelle Molekulare Systeme (IBCS-FMS) des Karlsruher Instituts für Technologie (KIT) angefertigt.

Hiermit versichere ich, dass ich die Arbeit selbständig angefertigt, nur die angegebenen Quellen und Hilfsmittel benutzt und mich keiner unzulässigen Hilfe Dritter bedient habe. Insbesondere habe ich wörtlich oder sinngemäß aus anderen Werken übernommene Inhalte als solche kenntlich gemacht. Die Satzung des Karlsruher Instituts für Technologie (KIT) zur Sicherung wissenschaftlicher Praxis habe ich beachtet. Des Weiteren erkläre ich, dass ich mich derzeit in keinem laufenden Promotionsverfahren befinde und auch keine vorausgegangenen Promotionsversuche unternommen habe. Die elektronische Version der Arbeit stimmt mit der schriftlichen Version überein und die Primärdaten sind gemäß Abs. A (6) der Regeln zur Sicherung guter wissenschaftlicher Praxis des KIT beim Institut abgegeben und archiviert.

Karlsruhe, 26.03.2025

_____

Timo Sehn

Danksagung

Zu Beginn möchte ich mich herzlich bei dir, **Mike**, bedanken. Danke, dass du mich in deinen Arbeitskreis aufgenommen und mich in den letzten drei Jahren fachlich wie persönlich unterstützt hast. Besonders schätze ich deine offene, verständnisvolle und freundliche Art, die die Arbeit in deiner Gruppe und mit dir selbst so angenehm und produktiv gemacht hat. Ein spezieller Dank gilt dir dafür, dass du mir die Teilnahme an verschiedenen Fachkonferenzen ermöglicht hast.

Ein besonderer Dank gilt **Nicolai Kolb** und **Alexander Azzawi** für die inspirierende Zusammenarbeit, die wertvollen und produktiven Projektmeetings sowie eure motivierende und engagierte Art.

I would also like to express my sincere gratitude to you, dear **Audrey**, for hosting me for four amazing months at the LCPO in Bordeaux. I truly appreciated the scientific collaboration, the pleasant working environment, and the wonderful time we spent together. My thanks also go to **all members of LCPO** for integrating me so warmly, for their help, and for the great social events we shared.

Ebenfalls möchte ich mich beim **Karlsruhe House of Young Scientists** (KHYS) für die finanzielle Unterstützung meines Forschungsaufenthalts in Frankreich bedanken.

Ein großer Dank gilt meinen Kolleginnen und Kollegen der Arbeitsgruppe Meier. Danke für drei unglaublich tolle Jahre, für eure stete Hilfsbereitschaft, die angenehme Arbeitsatmosphäre und die unvergesslichen Momente, die wir gemeinsam innerhalb und außerhalb des Labors erlebt haben.

Ein besonderer Dank geht an euch, **Luis** und **Pete**. Ihr wart die besten Laborpartner, die man sich nur wünschen kann! Danke für die zahllosen chemischen Diskussionen – ob über organische Reaktionen oder Polymercharakterisierung. Die Teilnahme an der ACS in San Francisco und der anschließende Urlaub mit dir, Pete, werde ich nie vergessen! Und die berauschende Konferenz in Warwick mit dir, Luis, wird mir ebenfalls immer in Erinnerung bleiben. Diese Erlebnisse haben die letzten drei Jahre zu etwas ganz Besonderem gemacht. Danke, **Luis** und **Pete** (!!!), mit euch habe ich nicht nur großartige Kollegen, sondern auch zwei wahre Freunde gefunden!

Ein spezieller Dank gilt auch dir, **Philipp**. Danke für deine wissenschaftliche Unterstützung, dein offenes Ohr und für die unvergessliche Zeit in den USA. Auch die vielen gemeinsamen Stunden nach der Arbeit haben diese Jahre bereichert!

Danke an **Clara**, **Sandra**, **Leon**, **Hendrik**, **Qianyu**, **Celeste, Luca, Francesca, Nicolas** und **Simon** für die ereignisreichen drei Jahre und all die schönen Momente, die wir zusammen erlebt haben. Ein besonderes Dankeschön gilt **Leon**, **Philipp**, **Clara**, **Luis**, **Pete** und **Hatice** für das Korrekturlesen meiner Arbeit. Außerdem möchte ich mich bei **Brigit Huber**, **Valerian Hirschberg**, **Alexander Schulz**, **Ute Schwotzer**, **Volker Zibat** für das Durchführen verschiedener Messungen bedanken.

Ein großes Dankeschön geht auch an meine Freunde aus der Heimat – **Nico**, **Niclas, Simon** und **Dennis**. Danke für eure kontinuierliche Unterstützung und für die manchmal notwendige Ablenkung vom Laboralltag.

Zum Schluss möchte ich mich von ganzem Herzen bei meiner Familie bedanken – meinen Eltern **Sabine** und **Roland**, meiner Schwester **Sina** und meiner Freundin **Sarah**. Ohne eure bedingungslose Unterstützung wäre dieser Weg nicht möglich gewesen. Ich bin unendlich dankbar, euch alle an meiner Seite zu haben!

Abstract

In recent years, the contamination of drinking water sources by pharmaceuticals, dyes, proteins, hormones, and heavy metals, among others, together with the ongoing climate change and a further increase of human population, led to water shortages on our planet. Nowadays, approximately 2.1 million people have only limited access to fresh drinking water. Thus, the current thesis focuses on the synthesis of functional (bio-based) materials for water decontamination *via grafting-onto approaches*. Herein, to support the transformation of the chemical sector towards a more sustainable future the *Twelve principles of Green Chemistry* acted as a guiding framework.

In a first project, a rapid and homogenous microwave assisted synthesis of high molecular weight (59 kDa ≤ M_n ≤ 116 kDa) short chain (mixed) cellulose esters (CEs) with variable acyl side chain length (2 ≤ C ≤ 8) by using a DMSO/TMG/CO_2 switchable solvent system was introduced. After investigation of structure-property relationships of the resulting materials, selected CEs were tested regarding their applicability in water purification membranes. In a second project, biobased fatty acid cellulose esters (FACEs) with different degrees of substitution (0.38 ≤ DS ≤ 0.62) were inversely vulcanized to obtain high sulfur content composite materials (~95 wt% sulfur). Detailed structural characterization of the crosslinked sections revealed an increased amount of covalently incorporated sulfur (5.67 wt% ≤ sulfur wt% ≤ 56.2 wt%) with higher DS of FACE. Further investigation of the structure-property relationships showed the applicability of the synthesized composites in water treatment, i.e. mercury extraction, and the dependence of the extraction efficiency on the structural constitution, i.e. DS, of the FACE used (70 % ≤ $Hg^{2+}{}_{removal}$ ≤ 95 %). In the third project an efficient one-step synthesis route towards catechol containing polymers from liquid polybutadiene *via* a simple post polymerization modification approach applying acid catalyzed Friedel-Crafts alkylation (FCA) was developed. After model compound synthesis and structural characterization of all synthesized compounds, metal ion removal tests revealed excellent extraction efficiencies (86 % ≤ $M^{n+}{}_{removal}$ < 100%) when using the catechol containing polymer as heavy metal sorbent and thus emphasized the potential application in water treatment. In a final project, a fully renewable catechol containing high oleic sunflower oil-based polyol was synthesized *via* an acid catalyzed FCA. A thermally induced catalyst and solvent-free crosslinking process using the polyol and

a divinyl ether was applied to access fully bio-based covalent adaptable networks which potentially find applications in water treatment in the future.

Zusammenfassung

In den letzten Jahren haben die Verunreinigung von Trinkwasserquellen durch Arzneimittel, Farbstoffe, Proteine, Hormone und Schwermetalle sowie der fortschreitende Klimawandel und eine weitere Zunahme der menschlichen Bevölkerung zu Wasserknappheit auf unserer Erde geführt. Heutzutage haben etwa 2,1 Millionen Menschen nur begrenzten Zugang zu frischem Trinkwasser. Die vorliegende Arbeit befasst sich daher mit der Synthese von funktionellen (biobasierten) Materialien zur Wasserdekontamination durch die Funktionalisierung durch Polymeren. Um den Wandel des Chemiesektors hin zu einer nachhaltigeren Zukunft zu unterstützen, dienten die zwölf Grundsätze der Grünen Chemie als Orientierungsrahmen. In einem ersten Projekt wurde eine schnelle mikrowellenunterstützte Synthese von kurzkettigen (gemischten) Celluloseestern (CE) mit hohem Molekulargewicht (59 kDa ≤ M_n ≤ 116 kDa) und variabler Acylseitenkettenlänge (2 ≤ C ≤ 8) unter Verwendung eines schaltbaren DMSO/TMG/CO2 Lösungsmittelsystems in homogener Lösung entwickelt. Nach eingehender Untersuchung von Struktur-Eigenschafts-Beziehungen der resultierenden Materialien wurden ausgewählte CEs auf ihre Anwendbarkeit in Wasseraufbereitungsmembranen getestet. In einem zweiten Projekt wurden biobasierte Fettsäurecelluloseester (FCE) mit unterschiedlichen Substitutionsgraden (0.38 ≤ DS ≤ 0.62) invers vulkanisiert, um Verbundwerkstoffe mit hohem Schwefelgehalt (~95 Gew.-% Schwefel) zu erhalten. Eine eingehende strukturelle Charakterisierung der vernetzten Abschnitte ergab eine erhöhte Menge an kovalent eingebautem Schwefel (5,67 Gew.-% ≤ Schwefelgew.-% ≤ 56,2 Gew.-%) bei höheren Substitutionsgraden der FCE. Weitere Untersuchungen der Struktur-Eigenschafts-Beziehungen zeigten die Anwendbarkeit der synthetisierten Verbundwerkstoffe bei der Wasseraufbereitung, d.h. der Quecksilberextraktion, und die Abhängigkeit der Extraktionseffizienz von der strukturellen Zusammensetzung, d.h. dem DS, des verwendeten FCE (70 % ≤ Hg^{2+}-Entfernung ≤ 95 %). Im dritten Projekt wurde ein effizienter einstufiger Syntheseweg für Brenzcatechin-haltige Polymere aus flüssigem Polybutadien über einen einfachen Ansatz der nachträglichen Polymermodifizierung unter Verwendung einer säurekatalysierten Friedel-Crafts-Alkylierung (FCA) entwickelt. Nach der Synthese von Modellverbindungen und der eingehenden strukturellen Charakterisierung aller synthetisierten Verbindungen ergaben Tests zur

Entfernung von Metallionen aus wässriger Lösung hervorragende Extraktionseffizienzen (86 % ≤ M^{n+} Entfernung < 100 %), wenn das Brenzcatechin-haltigen Polymer als Schwermetallsorptionsmittel verwendet wurde, und unterstrich damit deren potenzielle Anwendung in der Wasseraufbereitung. In einem abschließenden Projekt wurde ein vollständig erneuerbares, Brenzcatechin-haltiges Polyol auf Basis von Sonnenblumenöl mit einem hohen Ölsäureanteil mittels säurekatalysierter FCA synthetisiert. Ein thermisch induzierter katalysator- und lösungsmittelfreier Vernetzungsprozess zwischen dem Polyol und einem Divinylether wurde angewandt, um vollständig biobasierte kovalent vernetzte, anpassungsfähige Netzwerke zu erhalten, die zukünftig möglicherweise in der Wasseraufbereitung Anwendung finden können.

Table of Contents

1 Introduction

An important turning point for economic sustainability was in 1987, when the World Commission on Environment and Development defined sustainable development as:

"*Development that meets the needs of the present without compromising the ability of future generations to meet their own needs.*"[1]

In accordance with this definition, the 17 Sustainable Development Goals (SDGs) were adopted in 2015 by the General Assembly of the United Nations as part of the 2030 agenda (**Table 1**).[1,2] The SDGs can be considered as economic, environmental, or social system goals representing guidelines for a more sustainable global development.[1,3] The overall aim of the SDGs is to combine the protection of the planet (environmental sustainability) with the end of poverty (economic sustainability) and prosperity for all (social sustainability).[3]

Table 1. 17 Global Goals of Sustainable Development (SDGs).[3]

	Title of SDG		Title of SDG
1	No Poverty	**10**	Reduce inequalities
2	Zero Hunger	**11**	Sustainable cities and communities
3	Good health and well-being	**12**	Responsible consumption and production
4	Quality education	**13**	Climate action
5	Gender equality	**14**	Life below water
6	Clean water and sanitation	**15**	Life on land
7	Affordable and clean energy	**16**	Peace, justice and strong institutions
8	Decent work and economic growth	**17**	Partnerships for the goals
9	Industry, innovation and infrastructure		

The chemical industry, and the polymer sector in particular, does not fulfill several of these SDGs, as they are mainly dependent on depleting fossil resources, affect the climate change, potentially contaminate the environment, and generate high amounts of waste, among others. Thus, to ensure the same quality of life for future generations the chemical sector must undergo a fundamental transformation in terms of economic,

environmental and social sustainability. Key aspects for a sustainable development of the chemical sector, according to Goal 12: "*Ensure sustainable consumption and production patterns.*", are the implementation of renewable resources as raw materials and the optimization of existent processes. The incorporation of renewable feedstocks is essential to replace (bulk) chemicals based on depleting fossil resources, to develop inherently safer reactions, and to reduce the negative impact on humans and the environment. Increasing the effectiveness of established approaches reduces the amount of generated waste and minimizes the need for resources, i.e. energy and chemicals. Nowadays, various concepts such as Green Chemistry,[4] Circular Economy,[5] or Green Engineering[6] have been developed to drive this transition forward.

Another main target of the 17 SDGs is the accessibility of drinking water, which is summarized in Goal 6: "*Ensure availability and sustainable management of water and sanitation for all.*" A person persuing normal activities needs at least 5L of fresh drinking water per day to survive.[7] However, approximately 2.1 billion people on our planet have only limited access to water with a safe drinking quality.[7] Contaminated drinking water causes health risks and can be a platform for waterborne diseases.[8] The reason for the contamination of drinking water in developed countries are mainly problems in chemical disposal processes, whereas in underdeveloped countries agricultural sources are often responsible.[8] Particularly the contamination of freshwater systems with heavy metals, i.e. mercury, lead, cadmium, and chromium, among others, is a major issue due to their adverse effects on human health, aquatic habitats, and agriculture.[9] Heavy metal water pollution is often induced by industrial processes such as coal/mineral mining, textile production, and electronic waste processing, among others.[9]

In line with Goal 6: "*Ensure availability and sustainable management of water and sanitation for all.*" and Goal 12: *"Ensure sustainable consumption and production patterns.*", the current thesis focuses on the synthesis of functional (bio-based) materials for water decontamination to drive the transformation of the chemical sector towards a more sustainable future and overcome global water shortages.

2 Theoretical Backround

2.1 Green Chemistry

The start of a worldwide environmental movement is often ascribed to the books *Silent Spring* by Rachel Carson (1962), in which she also outlined the devasting effects of certain chemicals on the environment and its ecosystem.[10] Within the following years the importance of this issue was recognized, and the National Environmental Policy Act was established to create and maintain conditions for the coexistence of humans in productive harmony.[11] Subsequently, in 1970, the U.S. Environmental Protection Agency (EPA) was founded as a federal regulatory agency, which is responsible for the protection of human health and environment.[12] The first groundbreaking decision based on this agency was the ban of man-made chemicals such as dichlorodiphenyltrichloroethane (DDT) and other pesticides, as these show harmful side-effects and pollute the environment during their manufacturing processes.[13] With the regulation and prohibition of hazardous chemicals the protection of human health and the environment would increase, but simultaneously would raise drastic challenges for the chemical industry. Thus, within the 1980s the concept of reducing environmental pollution was focused more and more on waste prevention at source and not on end-of-pipe solutions.[14] Herein, the US Pollution and Prevention Act, established in 1990, was a key event, which strengthened the focus of government, industry and public society to decrease the amount of pollution by applying cost-effective changes in operating systems and raw materials use.[14,15] Additionally, it was elaborated that the minimization of waste at source would increase the effectiveness of the processes and decrease the costs for subsequent waste treatment, strengthening the economic competitiveness.[14] Accordingly, the EPA underwent a fundamental change in strategy to secure human health and environment.[14]

The term *Green Chemistry*, which is defined as the “design of chemical products and processes to reduce or eliminate the use and generation of hazardous substances”, was subsequently introduced in the early 1990s.[16,17] However, the first formal recognition *Green Chemistry* was received through the pioneering work of Anastas and Warner, who presented the *Twelve Principles of Green Chemistry* in 1998 (**Table 2**).[4] These principles act as guidelines for chemists and chemical products taking all

aspects, i.e. raw materials, reagents, efficiency, safety, toxicity, biodegradability, and waste generation, of the process life-cycle into account.[4,18]

Table 2. The Twelve Principles of Green Chemistry.[4]

	The Twelve Principles of Green Chemistry
1	**Prevention:** It is better to prevent waste than to treat or clean up waste after it is formed.
2	**Atom Economy:** Synthetic methods should be designed to maximize the incorporation of all materials used in the process into the final product.
3	**Less Hazardous Chemical Syntheses:** Wherever practical, synthetic methodologies should be designed to use and generate substances that possess little or no toxicity to human health and environment.
4	**Designing Safer Chemicals:** Chemical products should be designed to preserve efficacy of function while reducing toxicity.
5	**Safer Solvents and Auxiliaries:** The use of auxiliary substances (e.g. solvents, separation agents, etc.) should be made unnecessary whenever possible and, when used, innocuous.
6	**Design for Energy Efficiency:** Energy requirements should be recognized for their environmental and economic impacts and should be minimized. Synthetic methods should be conducted at ambient temperature and pressure.
7	**Use of Renewable Feedstocks:** A raw material or feedstock should be renewable rather than depleting, wherever technically and economically practicable.
8	**Reduce Derivatives:** Unnecessary derivatization should be minimized or avoided, if possible, because such steps require additional reagents and can generate waste.
9	**Catalysis:** Catalytic reagents are superior to stochiometric reagents.
10	**Design for Degradation:** Chemical products should be designed so that at the end of their function they break down into innocuous degradation products and do not persist in the environment.
11	**Real-Time Analysis:** Analytical methodologies need to be further developed to allow for real-time, in-process monitoring and control prior to the formation of hazardous substances.
12	**Inherently Safer Chemistry:** Substances and the form of a substance used in a chemical process should be chosen to minimize the potential for chemical accidents, including releases, explosions, and fires.

Following these guidelines enables chemists to practice chemistry in the most responsible and sustainable fashion possible. In recent years, the twelve principles have been expressed using the mnemonic PRODUCTIVELY, which improves their memorability and comprehensibility.[19] Furthermore, in 2009 , Anastas and Eghbali summarized the three main points of the *Green Chemistry* framework.[18] Herein it was concluded that *Green Chemistry* 1) designs across all stages of the chemical life-cycle, 2) seeks to design the inherent nature of the chemical products and processes to reduce their intrinsic hazards, and 3) works as a cohesive system of principles or design criteria.[18]

2.1.1 Sustainable Chemistry - Metrics

An objective sustainability assessment of chemical processes remains very complex, as many different factors must be considered. Hence, in order to enable a preliminary evaluation and quantification of the sustainability aspects of chemical reactions certain metrics have been introduced. A common example was defined by Trost in 1991, is the so-called atom economy (*AE*).[20] It describes “the ability of a chemical process to incorporate as many as possible atoms” of the starting materials into the final products.[21,22] To clarify, *AE* represents the molecular weight ratio between the starting materials and the desired product and thus indicates the amount of the total molecular weight of the starting materials, which is incorporated into the targeted product.[21,22] The calculation of the *AE* can be performed according to **Eqn. 1.**:

$$AE = \frac{M_{Product}}{\sum_n M_{n,starting\ materials}} \qquad (1)$$

In an ideal reaction, an *AE* of 1 is achieved when every atom of the starting materials is incorporated into the final product, whereas an *AE* of 0 is gained when the starting materials are not implemented at all. The inverse number of the AE can be described as the minimum amount of waste produced in a chemical reaction, making it valuable as preliminary tool for an initial waste assessment of newly planned chemical reactions.[23,24] However, the calculation of the *AE* takes only the reaction equation into account, requires quantitative yields, stochiometric amounts of the reagents and does not include other chemicals, i.e. solvents or auxiliary chemicals, leading to the fact that

AE can be categorized as a purely theoretical value and the actual amount of generated waste will be higher.

The most frequently reported metric to evaluate sustainability in chemical processes was introduced by Sheldon in 1992 and is known as the environmental factor (*E* factor).[23,25] In comparison to the *AE*, this metric takes the waste from auxiliary chemicals, i.e. predominantly solvents used during the reaction or in purification steps, as well as the yield of the reaction into consideration, thus describing more accurate values in waste assessment.[23] The *E* factor is defined as the mass ratio of waste to the desired product generated during a chemical process expressed in kg/kg and represents therefore its environmental footprint.[24] The *E* factor can be calculated according to **Eqn. 2**.:

$$E\ \text{factor} = \frac{m_{waste}}{m_{product}} = \frac{\sum m_{starting\ materials} - m_{product}}{m_{product}} \qquad (2)$$

Accordingly, a higher *E factor* indicates more waste generation and thus an increased negative environmental impact. An ideal chemical reaction achieves an *E* factor of 0, which means that no waste is produced during the process.

Generally, the major source of waste in most of the chemical reactions are solvent losses.[26] Thus, the recyclability of solvents plays a key role in the calculation of reliable *E* factors. However, often such parameters, i.e. solvent recovery, are not investigated or stated in the literature. Hence, to ensure the determination of an *E* factor also in such cases, it is then assumed that 90% of all employed solvents can be recycled.[26] Additionally, it is also worth to mention that water is often excluded from the calculation of *E* factors, as the incorporation would yield exceptionally high values, which are difficult to compare.[27] In order to solve the problems arising from not available experimental research data, the simple *E* factor (*sEF*) and complete *E* factor (*cEF*) were established.[28] Herein, the *sEF* does not include solvents and water and acts therefore as valuable tool in the preliminary waste assessment of early stage processes.[27] The *cEF* takes components such as solvents and water into account, but does not assume their recyclability.[27] Thus, it represents the maximum amount of waste that can be generated in a chemical process. *sEF* and *cEF* can be calculated according to **Eqn. 3.** and **4.**, respectively:

$$sEF = \frac{\sum m_{raw\ materials} + \sum m_{reagents} - m_{product}}{m_{product}} \quad (3)$$

$$cEF = \frac{\sum m_{raw\ materials} + \sum m_{reagents} + \sum m_{solvents} + m_{water} - m_{product}}{m_{product}} \quad (4)$$

The so-called true *E* factor of a specific process can be found between the *sEF* and the *cEF*.[27] Interestingly, nowadays it is well known that the *E* factors of chemical processes correlate with the manufacturing costs of the corresponding products.[26] Herein, it was shown that a decrease of the *E* factor also led to reduced manufacturing costs, which resulted from a lower raw material input and output, reduced costs for waste treatment, less energy consumption, and a more efficient utilization of capacities.[26] Hence, *E* factors not only play an important role in reducing waste to protect human health and prevent environmental pollution, but they also appear to be beneficial to the industry from an economic point of view. The *E* factor in industrial processes differs a lot depending on the desired product. **Table 3** depicts various sectors of the chemical industry and their respective *E* factors.[23] Herein, especially fine chemicals and pharmaceuticals can be categorized as critical revealing *E* factors up to 50 and 100 (or higher), respectively. The high values can be explained by the complex chemical structure of the targeted molecules within these classes, which are often only achievable *via* synthetic multi-step strategies using stoichiometric amounts of reagents.

Table 3. E factors of various sectors of the chemical industry.[23]

Industry segment	Product tonnage	*E*-factor (kg waste/kg product)
Oil refining	10^6 - 10^8	< 0.1
Bulk chemicals	10^4 - 10^6	< 1 - 5
Fine chemicals	10^2 - 10^4	5 - 50
Pharmaceuticals	10 - 10^3	25 - 100

Hence, to reduce the amount of generated waste and increase the process efficiency, especially in these sectors, i.e. fine chemicals and pharmaceuticals, it is necessary to develop more economical multi-step syntheses.[29]

In recent years additional metrics have been proposed to quantify the efficiency of chemical reactions in a more precise manner. However, most of these metrics have not attained the broad acceptance of the *E* factor as they do not provide significant benefits in the early-stage development of chemical processes. A common example is the actual atom economy (*AAE*), which corrects the theoretical *AE* described at the beginning of the current chapter by the reaction yield (*AAE = AE x yield).*[30] Another mass-based metric, which was developed by Glaxo Smith Kline (GSK) and appears nowadays in the literature is the reaction mass efficiency (*RME*).[31] The *RME* can be categorized as a supplemental correction of the *AAE* as it additionally includes the experimental stoichiometry of the reaction. Accordingly, the *RME* can be calculated according to **Equation 5.**:

$$RME = \frac{M_{product}}{\sum_n M_{n,starting\ materials}\ x\ molar\ ratio}\ x\ yield \qquad (5)$$

Indeed, *AAE* and *RME* provide more accurate values than AE, but the determination of both metrics suffers from the need for experimental data. An additional mass-based metric introduced by the GSK group, which should be mentioned in the current chapter, is the mass intensity (*MI*). The *MI* is described as the total mass used in a process divided by the mass of the targeted product and can accordingly also be expressed as: *E* factor + 1.[32] The process mass intensity (*PMI*) represents the *MI* supplemented by the consideration of solvents and water and can thus also be described as: *cEF* + 1.[32]

An additional methodology, which was specifically designed to assess the environmental impact of products is Life Cycle Assessment (LCA).[33,34,35] Herein, the absolute impact of a product on the environment is evaluated starting from raw material separation to production, distribution, application, and disposal as a waste product.[35] The evaluation of the whole life cycle of a specific product is also known as cradle-to-grave analysis and was originally established by the Coca Cola® company in 1969 together with the Midwest Research Institute.[35,36] Unfortunately, LCA often remains very time consuming due to the very difficult to obtain data, which are required.[37] Thus,

LCA is usually only applied to compare the environmental impact of already commercialized products and less frequently employed in fundamental research.[37] Accordingly, mass-based metrics such as *AE* and *E* factor remain herein the most important metrics to evaluate the efficiency and sustainability of processes and products.

2.1.2 Renewable Resources

The world plastic production in 2023 was estimated to be more than 400 million tons. An incredible high amount of more than 90% of the generated polymeric materials were herein synthesized from fossil-based resources. Nowadays, it is well known that the era of chemical sectors focusing exclusively on depleting resources, such as mineral oil, gas, and coal, will end within the current century.[38] Thus, to ensure a sustainable existence of the chemical industry alternative non-depleting resources, which enable the access to bulk chemicals and polymers must be implemented.

Herein, biomass with an annual production of approximately 170 billion tons appear as a prominent candidate.[39] Today, less than 10% of the total biomass is consumed, predominantly as feed, food, or for energy generation.[39] The main constituents of the biomass on earth are carbohydrates (~75 wt%) and lignin (~20 wt%), supplemented by various oils, fats, terpenes and other natural products (~5 wt%, **Scheme 1**).[39]

Carbohydrates, i.e. cellulose, hemicelluloses, starch, pectin, inulin and saccharose, among others, can be classified by mass as the most important renewable carbon source for the chemical industry.[40] Annually, 128 billion tons of carbohydrates are generated, from which roughly 5% are industrially used in fermentative or enzymatic processes to access various platform chemicals that can potentially replace their fossil-based counterparts.[40] Common carbohydrate-based candidates are herein 5-hydroxymethfurfural, furfural, levulinic acid, 3-hydroxypropionic acid, furandicarboxylic acid (FDCA), succinic acid, and fumaric acid.[41,42,43] Among these, particularly FDCA gained a significant importance in recent years, as it can directly be polymerized into poly(ethylene furanoate) (PEF), which is recognized as fully bio-based alternative to poly(ethylene terephthalate) (PET).[44] Interestingly, due to the suppressed ring-flipping in PEF, the respective bio-based alternative possesses even better materials properties, i.e. higher glass transition temperature and less oxygen permeability, than the fossil-derived PET.[45] Thus, PEF is a prominent example that the implementation of renewable resources into the chemical industry can efficiently yield

valuable platform chemicals, which can subsequently be converted into high-performance materials.

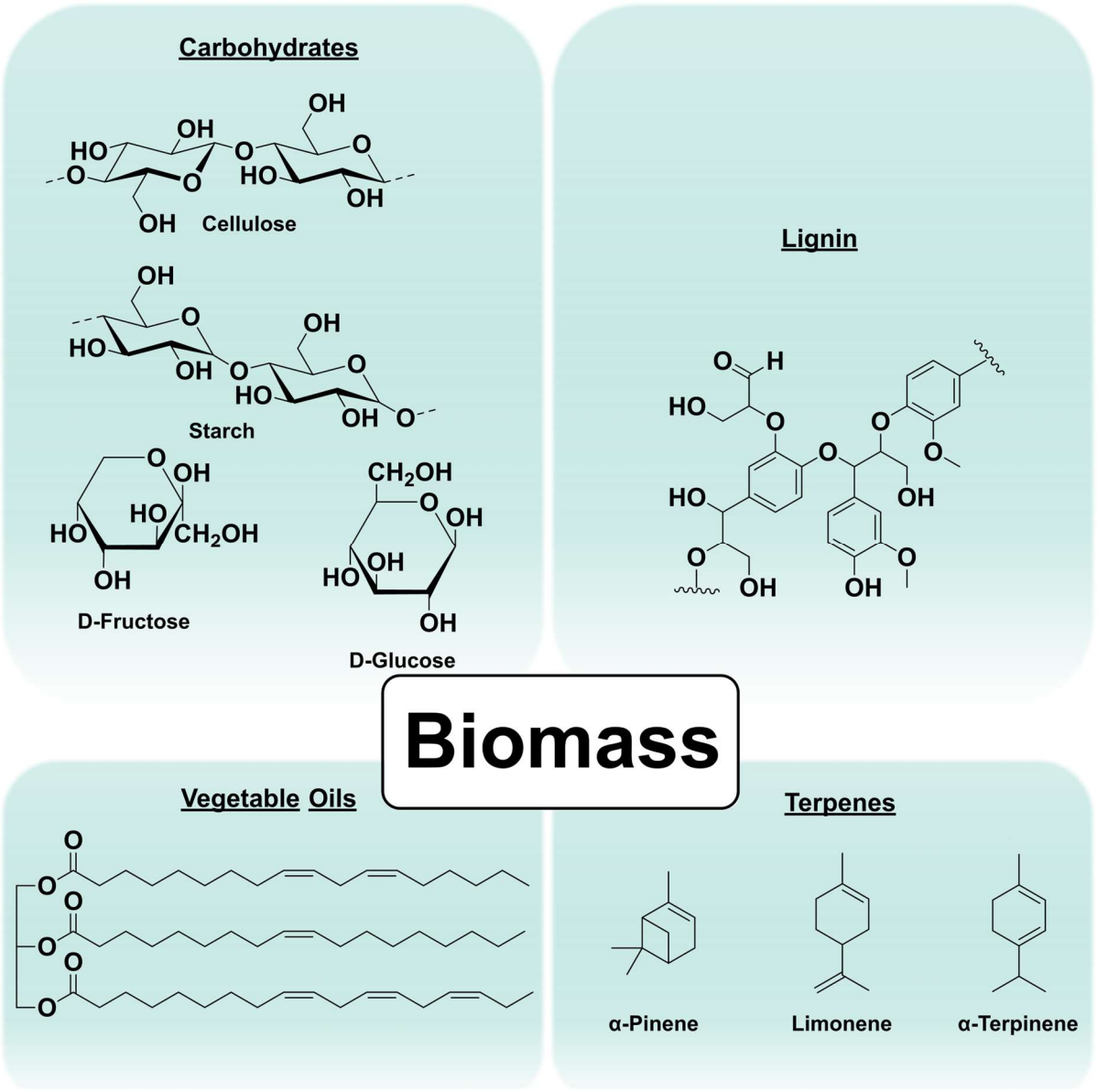

Scheme 1. Schematic overview of renewable resources derived from biomass.

However, even though carbohydrates represent by mass the most important renewable carbon feedstock on earth, plant oils remain the most relevant substance class for the chemical industry.[46] From an estimated global production of 208 million tons per year approximately 25% are used in non-food applications such as surfactants, cosmetics, pesticides, bio-lubricants, and to a small extent as raw material in polymer synthesis.[47] Plant oils are generally composed of a triglyceride structure containing long saturated or unsaturated alkyl side chains (mainly C_{12} to C_{18}).[46] The length, composition, and degree of unsaturation influence the physical and chemical

properties and depend predominantly on the plant source, but also on other parameters such as growing conditions, season, and crop (**Scheme 2**).[46]

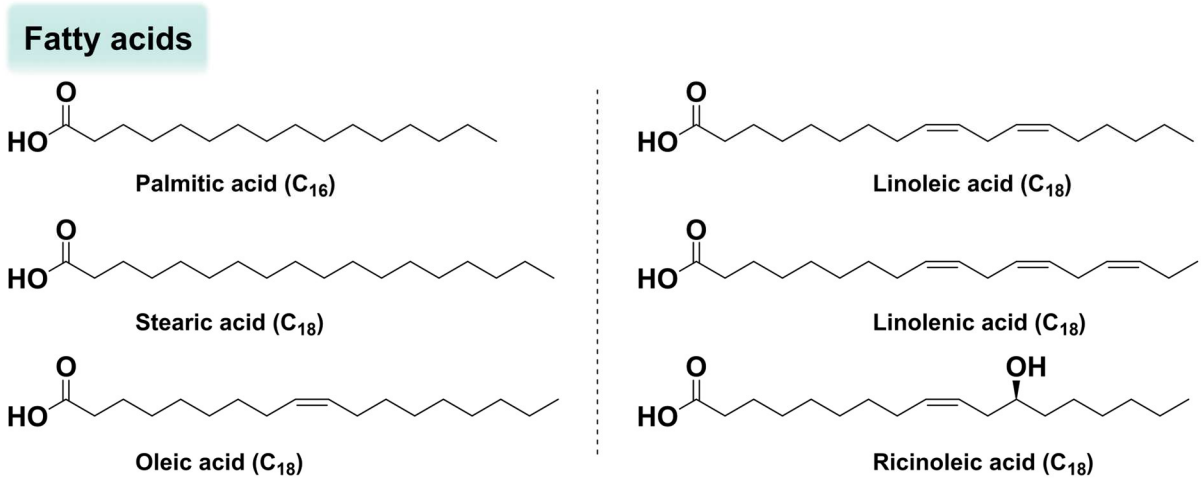

Scheme 2. Chemical structure of selected naturally occurring fatty acids.

Saturated fatty acids find application in surfactants and lubricants, among others, whereas derivatives with a higher degree of unsaturation are frequently used for the synthesis of crosslinked polymeric materials. For example, linseed oil is a key component in the preparation of linoleum, which is a crosslinked material employed for floor covering.[48] In fundamental research, the most frequently applied synthetic strategy to access crosslinked materials from vegetable oils is their use as polyols.[49] However, since most of the naturally occurring plant oils (except for castor oil) do not bear hydroxyl groups in their native chemical structure an initial functionalization is therefore required. The most common synthetic approach towards polyols from plant oils is an epoxidation of the double bonds and a subsequent reaction with e.g. methanol affording the formation of the targeted hydroxyl groups.[50,51,52] In the current literature, such plant-based polyols are often employed for the synthesis of crosslinked polyurethanes.[53,54]

Lignin and terpenes also represent two important renewable feedstocks for the potential synthesis of bio-based materials. Accordingly, up to the present day countless approaches converting these feedstocks into valuable materials exist in the literature.[55,56,57] However, since the current thesis mainly focuses on the synthesis of carbohydrate- and plant oil-based materials, lignin and terpenes are not described further within the current chapter.

2.2 Cellulose

The development of bio-sourced, environmentally friendly, and biocompatible polymeric materials is nowadays a main task of human society to fight against resource depletion, environmental pollution, and climate change. Herein, cellulose, as the most abundant biopolymer on earth with an annual production of 1.5 x 10^{12} tons, displays a key role.[58,59] The term “cellulose” appeared the first time in a work from the French scientist Anselme Payean obtained in 1839.[58,60] Already two years earlier in 1837, Payean reported on a fibrous solid residue after treating plant tissues with acids and ammonia and subsequent extraction steps using water, alcohol, and ether, which can be considered the first successful isolation of cellulose reported in literature.[58,61] Nevertheless, cellulose was already employed thousands of years ago in the form of wood and cotton as a source of energy, for clothing, and as building material.[62] Particularly, the implementation as a building material arose from the high strength of the material, which is based on the unique structural characteristics of cellulose.[63] It was the pioneering work of Hermann Staudinger in 1920, who elucidated the actual structure of the biopolymer.[58,64] More precisely, by acetylation and deacetylation he elaborated that cellulose does not consist of aggregated D-glucose units and thus confirmed the existence of covalently linked macromolecules.[58,64] Nowadays, the structure is frequently described and well known (**Scheme 3**).[58,65,66] Cellulose consists of D-glucopyranose units covalently linked by acetal moieties *via* β-glycosidic bonds between the hydroxyl groups located at the C4 and C1 position. The repeating unit includes two β-1,4 linked glucose units, which are formed *via* a condensation reaction under water elimination, giving the name anhydroglucose unit (AGU). To ensure the favored binding angles of the acetal oxygen participating in the *β*-glycosidic linkage, every second AGU is rotated 180° in plane.

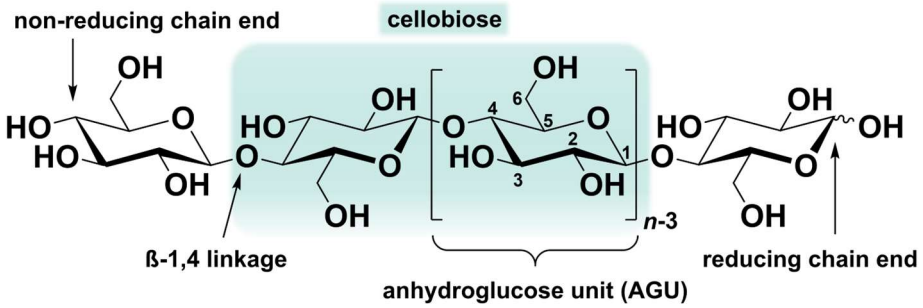

Scheme 3. Chemical structure of cellulose.

If two AGU units are linked accordingly, the disaccharide is defined as cellobiose. The chain ends of cellulose consist on the one hand of an unmodified C4 hydroxyl group (non-reducing end) and on the other hand of a C1 hydroxyl group in an equilibrium with the respective aldehyde structure in a ring opened form (reducing end). The unique chemical structure of the biopolymer equips cellulose with various characteristic material properties such as insolubility, chirality, and degradability.[58,67,68,69] The presence of three hydroxyl groups per AGU additionally ensures a chemical variability and an extensive hydrogen bond network, which is predominantly responsible for the partially crystalline fiber structures and morphologies in cellulose.[70,71] The chain length of the macromolecules in cellulose, which is described by the number of sequentially connected AGUs and known as degree of polymerization (DP), depends on the source and treatment of the raw material (**Table 4**).[58,72,73]

Table 4. Overview of different types of cellulose and the corresponding degrees of polymerization (DP) adapted from Klemm *et al.*[58]

Type of cellulose	Degree of polymerization (DP)
Cotton and other plant fiber cellulose	800 – 10 000
Bacterial cellulose	800 – 10 000
Wood pulp cellulose	300 – 1 700
Regenerated cellulose fibers	250 – 500
Microcrystalline cellulose	150 – 300

A decrease in DP can be achieved by basic and acidic treatment or by cellulase catalyzed hydrolysis of cellulose, which degrade the β-1,4 glycosidic bonds between the AGUs.[74,75,76] Either a complete decomposition towards D-glucose units or a partial degradation, yielding microcrystalline cellulose (MCC), can be targeted. Specifically for cellulose, it was observed that the unique properties of the biopolymer exist for DP values above 20 to 30.[77] The synthesis of cellulose can nowadays be achieved *in vivo* from different biosyntheses and in vitro using synthetic approaches (**Scheme 4**).[58,78,79] The dominant pathway to access cellulose is currently the extraction from plants.[80] A high content of pure cellulose can for example be found in the seed hairs of cotton.[81,82] On the contrary, cellulose from wood must be isolated by chemical pulping and

separated from other renewable biopolymers such as lignin and other polysaccharides like hemicellulose.[83] Other species that can produce cellulose *in vivo* are certain bacteria, algae, and fungi.[84,85,86] The respective cellulose types provided by these organisms were usually employed as model substrates for further investigations and have been investigated in detail during the past decades. Thus, it was discovered that the biosynthesis of cellulose from cyanobacteria has been taking place for more than 3.5 billion years.[87] Common *in vitro* synthesis pathways are cellulase catalyzed reactions based on cellobiosyl fluoride and ring-opening polymerization of substituted D-glucose pivalate derivatives.[88,89,90]

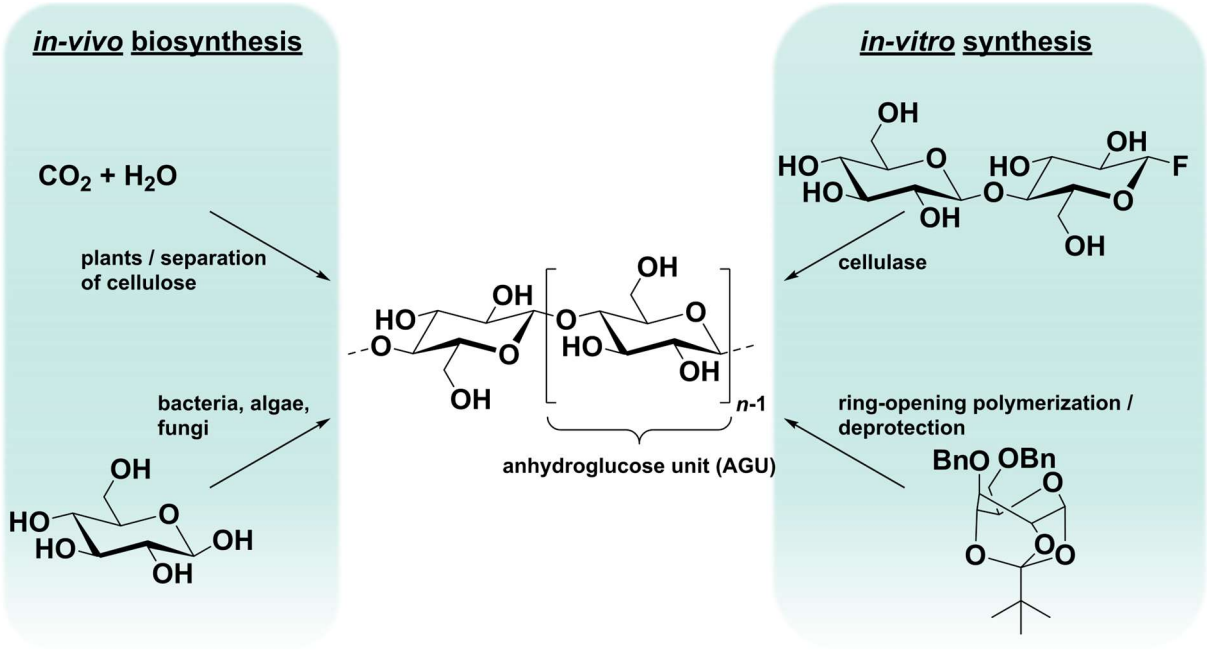

Scheme 4. General pathways to access cellulose adapted from Klemm *et al.*[58]

2.2.1 Raw Material Cellulose - Origin and Isolation

The most abundant and important raw material source to access cellulose nowadays is lignocellulosic biomass (LCB).[91] LCB can be obtained from agricultural residues, cultivated non-food plants, wood or biomass waste, making it cheap and readily available.[40] Globally, approximately 1.3 billion tons of this bio-renewable feedstock are generated every year.[92] The ongoing climate change, petroleum resource depletion, and the general demand for a more sustainable world moved LCB in the spotlight as a valuable candidate to deliver renewable platform chemicals and polymers, such as cellulose, for the synthesis of more sustainable materials.[91] LCB consists of three main components, which are i) cellulose (30 – 60 wt%), ii) hemicelluloses (20 – 40 wt%),

and iii) lignin (10 – 30 wt%).[40] As depicted in **Table 5**, the exact composition of LCB is strongly dependent on the raw material source:[40]

Table 5. Average composition of lignocellulosic biomass from different raw material sources adapted by Peters.[40]

Source	Cellulose (%)	Hemicelluloses (%)	Lignin (%)
Hardwood	43 – 47	25 – 35	16 – 24
Softwood	40 – 44	25 – 29	25 – 31
Monocotyledon stems	25 – 40	25 – 50	10 – 30
Wheat straw	30	50	15
Corn cobs	45	35	15
Corn stalks	35	25	35
Bagasse	40	30	20
Low or nonlignified fiber plants	70 – 95	5 – 25	0 – 6

Next to cellulose (see chapter 2), the second class of carbohydrates appearing in LCB are hemicelluloses, which are heteropolysaccharides with an amorphous, highly branched structure.[91,40] Depending on the constitution of the polymer backbone, i.e. the presence pentoses and hexoses, hemicelluloses can be divided into pentosans and hexosans, respectively.[40] Xylans, arabinogalactans, and glucomannans are the most important examples.[40] The composition of hemicelluloses relies on the LCB origin.[40] For example, hemicelluloses obtained from hardwood exhibit more pentoses, whereas higher amounts hexoses can be observed in hemicelluloses extracted from softwood.[91,40] Due to their branched polymeric structure, these heteropolysaccharides are the least resistant component of LCB and thus undergo hydrolysis and enzymatic degradation already at low temperatures.[40,93] The third component of LCB is a three-dimensional phenolic polymer named lignin.[91,40] It does not possess a typical defined structure or repeating unit.[93] The chemical structure is formed by the oxidative coupling of monolignols, in particular *p*-cumaryl alcohol, coniferyl alcohol, and sinapyl alcohol.[91] Lignin acts in LCB as a “cellular glue”, which means that this component is mainly responsible for the strength and the remarkable resistance against hydrolysis and

other degradation pathways.[91,40] All components together form a complex three-dimensional fiber network increasing the difficulty to separate them.[93]

Nevertheless, the separation of cellulose from hemicellulose and lignin can be achieved by applying different pulping approaches. Pulping can be conducted in a mechanical, chemical or enzymatic manner and targets predominantly the removal of lignin, while keeping the fiber structure of cellulose intact.[83,94] Mechanical pulping is the oldest method using mechanical energy to break the bonds of LCB to convert them into pulp (yield: 90 – 98%).[95] This process retains cellulose and lignin and produces therefore soft and bright pulp with smaller mechanical strength.[95] Mechanical forces in these approaches can exemplarily be induced by rotating metal discs or pressing wood against a grindstone.[95,96]

Nowadays, chemical pulping provides more than 77% of the globally produced pulp and plays the most important role in separating carbohydrates, such as cellulose, from LCB.[97] The efficient removal of lignin and hemicellulose *via* chemical pulping enables the production of fibers with high flexibility and strength, due to extensive intermolecular interactions appearing between the isolated cellulose chains.[98] The general concept behind chemical pulping includes the treatment of wood chips with chemicals in (aqueous) solutions while applying high temperatures and pressures.[96] The most established processes are Kraft (sulfate) and sulfite pulping, which provide 90% and 3.7% of the globally produced chemical pulp, respectively.[99,100] Especially the Kraft pulping possesses several advantages, such as the production of high strength paper, possible energy recovery, and the utilization of different raw materials such as hard- and softwood.[101]

In the Kraft pulping process, LCB containing raw materials like wood are treated with sodium hydroxide (NaOH) and sodium sulfide (Na_2S) under alkaline conditions (pH >12) at elevated temperatures, i.e. 155 to 180 °C, and a pressure of 800 kPa.[102] The previously described conditions swell the wood fibers and lignin is subsequently fragmentated mainly by the cleavage of the β-O-4´ alkyl-aryl ether bonds *via* sequentially occurring ionic reactions.[103,104] Two different pathways for lignin degradation in Kraft pulping are investigated. On the one hand, a sulfide independent endo-depolymerization, which mainly proceeds slowly on non-phenolic moieties (**Scheme 5A**), and on the other hand, a fast sulfide dependent eso-depolymerization, which occurs at the phenolic end-units (**Scheme 5B**).[104,105,106] In the endo-

depolymerization of lignin, a hydroxyl group located in α-position to an aromatic unit is deprotonated and subsequent intramolecular nucleophilic substitutions lead to an epoxide, which enables the cleavage of the alkyl-aryl ether connection.[105,106,107] The mechanism for the eso-depolymerization, which is the main route to degrade lignin in the Kraft process, starts with a phenolate followed by the formation of a quinone methide under elimination of the hydroxyl group in α-position.[107] Particularly this step is important, since this intermediate can afterwards be attacked by a highly nucleophilic hydrosulfide.[107]

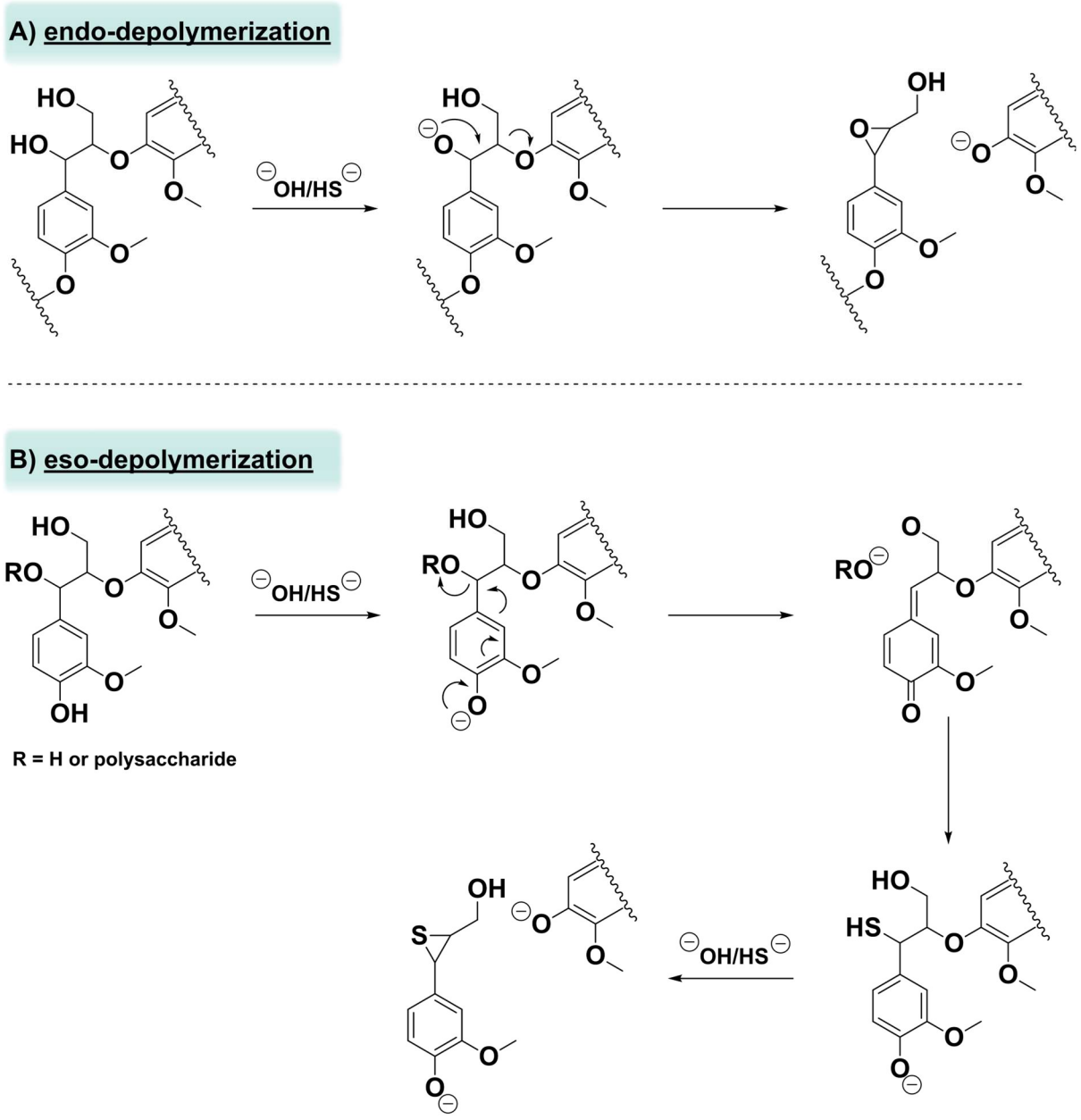

Scheme 5. General mechanistic pathways for the degradation of lignin in the Kraft pulping process adapted by Argyropoulos *et al.*[107]

Subsequent intramolecular substitutions form an episulfide and break the ß-O-4´alkyl-aryl ether bond.[107] Accordingly, after cooking the wood chips for an appropriate time, i.e. 3 - 4 h, under the previously described alkaline conditions, lignin is solubilized in the kraft liquor as polyphenolates.[108] After removing the black liquor (including lignin, hemicelluloses, and extractives) under reduced pressure, the resulting pulp is washed and bleached to obtain the desired cellulose fibers.[108]

2.2.2 Solubilization and Regeneration of Cellulose

The investigation of dissolution processes for cellulose has a remarkable history. However, due to its unique structural characteristics (described in chapter 2) the solubilization of this biopolymer still remains challenging. In other words, the extensive hydrogen bond network and the presence of crystalline regions in the macrostructure of cellulose are responsible for its insolubility in conventional organic solvents, making it difficult to process.[109,110] Nevertheless, various approaches for cellulose dissolution have nowadays been established.[111,112] In general, they can be classified in i) derivatizing and ii) non-derivatizing solvent systems.[113] The concept of derivative solvents is based on the formation of cellulose derivatives, where functional moieties are introduced to interrupt the intra- and intermolecular interactions between the polymer chains.[114] In non-derivatizing solvents, cellulose does not undergo chemical modification, which means that the dissolution results from the disruption of the intra- and intermolecular interactions by the solvent itself.[115]

Derivatizing Solvents

The first milestone regarding derivatizing solvents was reached in 1857, when the Swiss chemist Matthias Eduard Schweizer discovered the solubility of cellulose in a mixture of copper salt and ammonia, the so-called Schweizer´s reagent (**Scheme 6**).[116] On a molecular level, the Schweizer´s reagent, i.e. $[Cu(NH_3)_4](OH)_2$, firstly swells cellulose before the copper ions (Cu^{2+}) start to form strong chelates with the OH groups of the AGU.[117] The latter phenomenon destructs the intermolecular interactions of the biopolymer and thus ensure its solubility.[117] According to the dissolution mechanism, the Schweizer´s reagent can be classified as derivatizing dissolution approach. In the current process, regeneration of cellulose, e.g. in the form of fibers, can be achieved by wet spinning into a diluted H_2SO_4 bath followed by washing steps to remove residual copper traces.[118] The obtained regenerated cellulose fibers are also known as cupro rayon.[119] However, today only a few companies are still using this approach to produce

cellulose fibers, as the process requires the usage of high-price cotton cellulose and copper salts, which makes it uncompetitive against other industrially applied processes.[119]

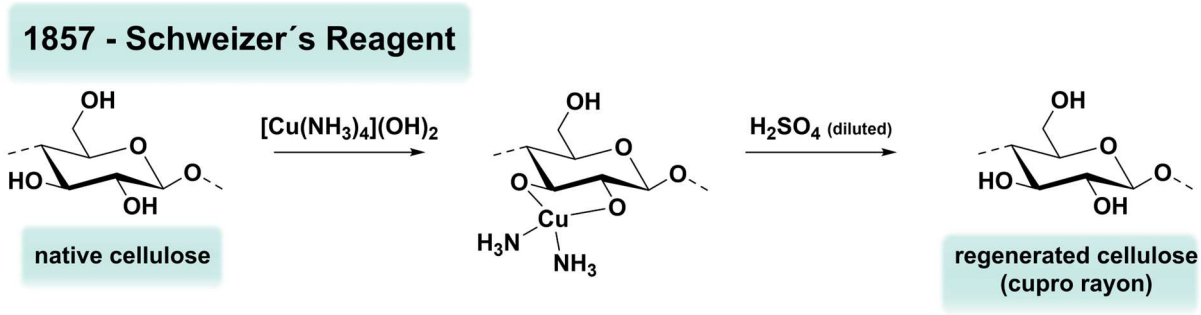

Scheme 6. Schematic overview of cellulose dissolution and regeneration using the Schweizer´s Reagent.

From an industrial point of view, the most important process for cellulose dissolution and regeneration was invented in 1891 and is known as the viscose process (**Scheme 7**).[119,120] Nowadays, it accounts for more than 93% of the regenerated cellulose fibers produced worldwide every year.[119] In the first step of the viscose process cellulose is suspended in a sodium NaOH solution.[113] Herein, NaOH forms hydrates with water molecules, which can interrupt the hydrogen bonds between the cellulose macromolecules.[113] The formed hydrates penetrate first the amorphous regions, which leads to swelling of the cellulose.[113] The actual dissolution of cellulose in form of alkali cellulose starts afterwards when the crystalline segments of the macrostructure break up.[113] In the second part of the viscose process, alkali cellulose reacts with carbon disulfide (CS_2) vapor yielding cellulose xanthate, which solubilizes homogenously in the NaOH solution at the end of the process.[113] However, it has to be mentioned that due to the harsh alkaline conditions depolymerization occurs during the dissolution process lowering the DP of the final materials. Due to the introduction of xanthate units and the corresponding dissolution mechanism, the viscose process is again categorized as a derivatizing dissolution approach for cellulose. In a similar fashion as described for the Schwarzer´s reagent, cellulose can be regenerated by an acidic treatment of the biopolymer solution either as sheets (cellophane) or as fibers (viscose rayon).[119] Even though the viscose process is the most important deliverer for regenerated cellulose fibers, it also possesses drawbacks in terms of sustainability and environmental pollution. Unfortunately, only up to 45% of sulfur can be recovered during the viscose process, which means that the remaining amount can cause

environmental problems through pollution.[121] Moreover, the formation of harmful byproducts, e.g. SO_2, H_2S, and zinc sulfate, during the dissolution process of cellulose as well as the volatility and toxicity of the employed CS_2 remain major issues in terms of sustainability.[122,123]

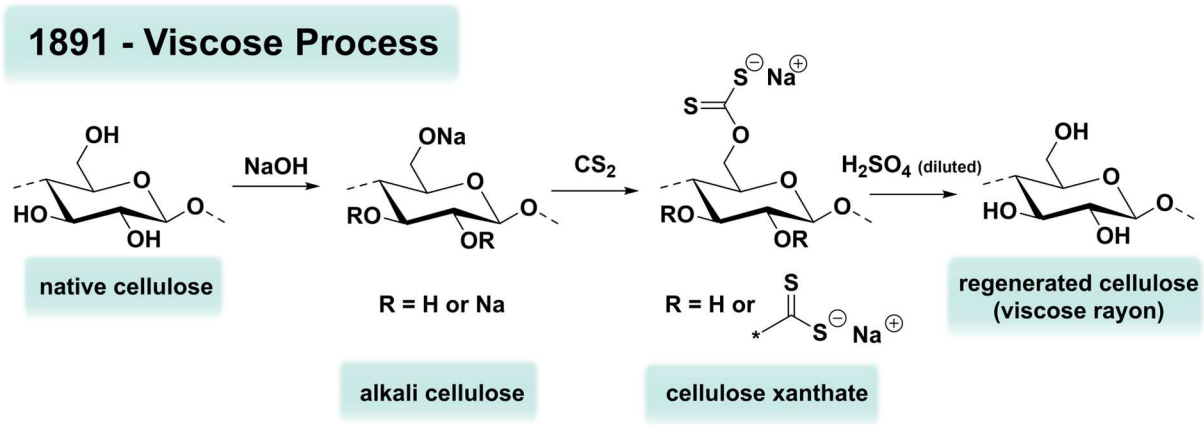

Scheme 7. Schematic overview of cellulose dissolution and regeneration using the viscose process.

An alternative derivatizing dissolution approach avoiding the usage of volatile and toxic CS_2 was investigated by Kemira Oy Saeteri (**Scheme 8**).[124] Herein, CS_2 was substituted by the less toxic chemical urea yielding a cellulose carbamate, which was easily soluble in a diluted NaOH solution.[125,126] Cellulose regeneration in the so-called CarbaCell process is conducted under acidic conditions in the same manner as described for the previous processes.[111] Due to remarkable similarity between the CarbaCell and the viscose process, the regenerated materials possess similar materials properties.[111]

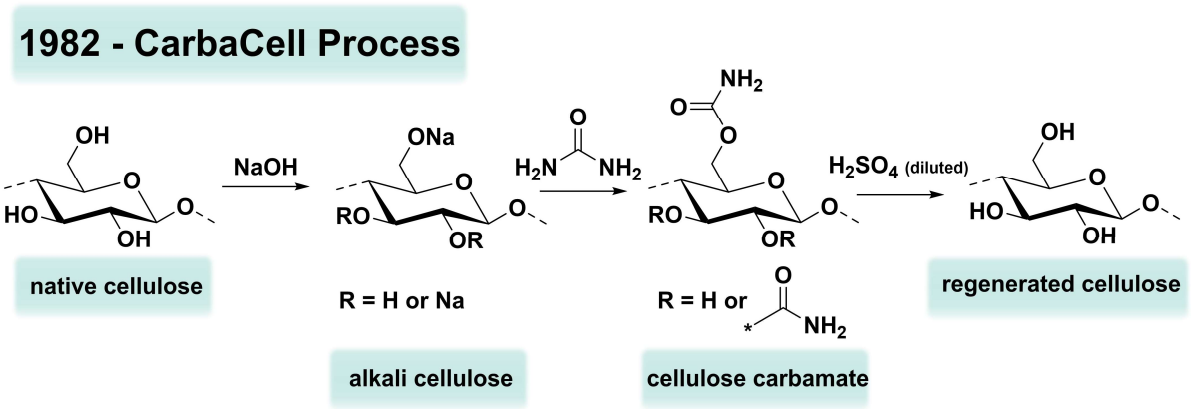

Scheme 8. Schematic overview of cellulose dissolution and regeneration using the CarbaCell process.

Non-derivatizing Solvents

The second solvent class for cellulose dissolution are non-derivatizing solvents. Here, organic solvent systems containing inorganic salt additives play an important role. The most established combination is *N,N*-dimethylacetamide (DMAc) with lithium chloride (LiCl) and was discovered in 1979.[127] As a dissolution mechanism, it is assumed that LiCl forms complexes with DMAc, such as $[Li(DMAc)]^+$, which can enter between the cellulose chains and therefore decrease the intermolecular interactions between the macromolecules of cellulose.[113,114,128] DMAc/LiCl solvent systems are a powerful tool for efficient and tailored functionalization of cellulose. However, high costs and a limited recyclability of the employed components avoid the upscaling of this approach to an industrial level.[111] More recently, a novel non-derivatizing solvent system, which does not contain expensive lithium, was developed. It consists of dimethyl sulfoxide (DMSO) and tetra-butyl-ammonium fluoride (TBAF) and dissolves cellulose samples efficient up to a DP of 650 within 15 minutes.[129]

The most important, non-derivatizing solvent system has industrially been used since the 1990s and is named Lyocell process.[113,119] It includes *N*-methylmorpholine-*N*-oxide (NMMO) and water as components.[119] The mechanism for the efficient cellulose dissolution in NMMO/water mixtures is not fully elucidated today, but can probably be explained by the active N-O moiety, which contains a strong dipole moment.[113,130] Thus, every oxygen of this structural unit can undergo strong hydrogen bonding with the OH groups of cellulose and therefore effectively weaken the intermolecular interactions between the macromolecules enabling the efficient solubilization of cellulose.[130,131] In the Lyocell process, regeneration of cellulose can be achieved by wet spinning into a water bath.[119] The resulting fibers are called Lyocell rayon and account for 5% of the global production of regenerated cellulose fibers.[119] Impressive 99% of the employed solvents in the Lyocell process can be recycled, making it a more environmentally friendly alternative compared to the previously introduced methods.[132]

In 1934, the first non-aqueous *N*-alkylpyridinium salt revealing the potential to dissolve cellulose was described by Charles Greanacher.[133] In 2002, additional studies about similar organic salt systems containing melting points below 100 °C were published.[134,135] Nowadays, such compounds are well known as ionic liquids (ILs) and play a key role in non-derivatizing cellulose dissolution and regeneration.[136,137,138] Thus, within the last years, the number of structurally different ILs has increased dramatically.[139] However, at this point it must be clarified that not every IL is capable of

dissolving polysaccharides such as cellulose. According to the current literature, especially ILs containing ammonium, pyridinium, and imidazolium cations are suitable candidates for cellulose dissolution (**Scheme 9A**).[140,141,142,143,144,145] However, only if the cations possess an unsymmetric structure enabling an efficient interaction with the cellulose backbone dissolution is possible.[137] Regarding anions particularly ILs including carboxylates and alkyl phosphates, showing a strong hydrogen bond basicity and low viscosity, appear as suitable solvents for cellulose dissolution (**Scheme 9B**).[137]

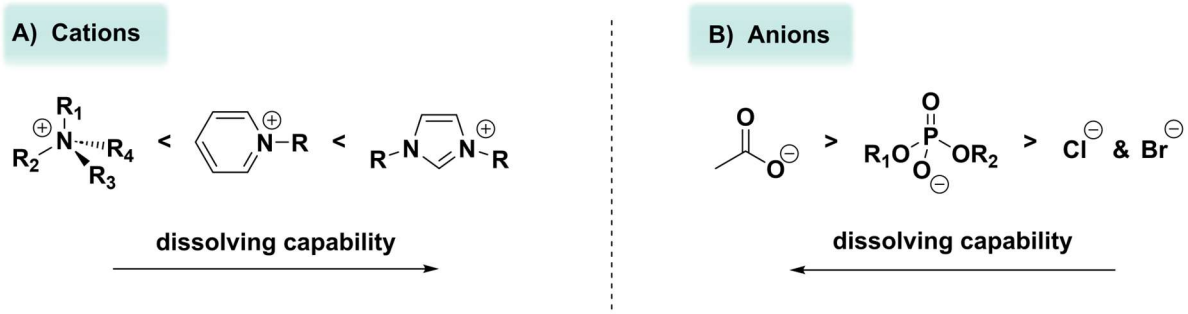

Scheme 9. Overview of the most important cations and anions forming together ionic liquids (ILs) and their respective capability to dissolve cellulose.[137]

A common class of ILs for the solubilization of cellulose are 1-alkyl-3-methylimidazolium salts. Three important examples are 1-butyl-3-methylimidazolium chloride (BMIMCl), 1-allyl-3-methylimidazolium chloride (AMIMCl), and 1-ethyl-3-methylimidazolium acetate (EMIMOAc).[137] The performance of ILs in dissolving cellulose is unique and remarkable at the same time. For example, the usage of ILs such as BMIMCl or AMIMCl as non-derivative solvents for cellulose enable the access to solutions containing a biopolymer content up to 25 and 30 wt%, respectively.[134,137] However, ILs also possess several drawbacks. Main limitations of ILs in terms of sustainability and industrial applicability are their high costs, toxicity, biodegradability, multi-step synthesis, and easy contamination supplemented by a difficult recyclability.[137,146,147,148]

Switchable Solvent System

In 2005, Jessop *et al.* introduced a reversible system in which two non-ILs, i.e. a guanidine superbase and an alcohol, could be converted into an IL by applying a carbon dioxide (CO_2) atmosphere to the reaction mixture.[149] More specifically, they employed an equimolar mixture of 1,8-diazabicyclo-[5.4.0]-undec-7-ene (DBU) and hexanol as non-IL and applied CO_2 at room temperature and ambient pressure.[149]

These reaction conditions converted the alcohol into a carbonate species and DBU into an amidinium ion, i.e. $DBUH^+$, resulting in the respective IL (**Scheme 10**).[149]

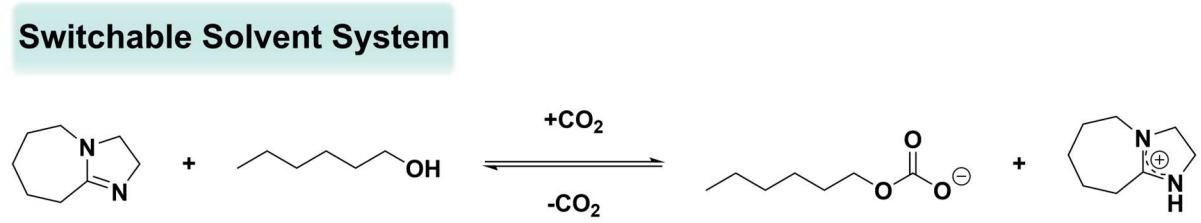

Scheme 10. Switchable solvent system investigated by Jessop *et al.*[149]

After removing CO_2, the system returned to its initial state, which means the formation of a non-IL.[149] Hence, it was possible to establish a reversible solvent system, which can change its polarity drastically using an external stimulus. Initially, this system was developed to avoid tedious solvent removal steps in organic multi-step syntheses by a simple adjustment of the solvent properties, i.e. polarity.[149] In 2013, the switchable solvent approach was simultaneously introduced by Xie *et al.* and Jerôme *et al.* as valuable tool for cellulose dissolution.[150,151] Indeed, Xie *et al.* employed the same concept as already presented by Jessop *et al.* in 2005 (**Scheme 11A**). In this work, a superbase, e.g. DBU or 1,1,3,3-tetramethylguanidine (TMG), together with an additional alcohol, e.g. ethylene alcohol, formed an IL, which was capable of dissolving cellulose in the presence of the co-solvent DMSO.[150] Since no modification was conducted at the chemical structure of cellulose this approach can be classified as a non-derivatizing dissolution method.

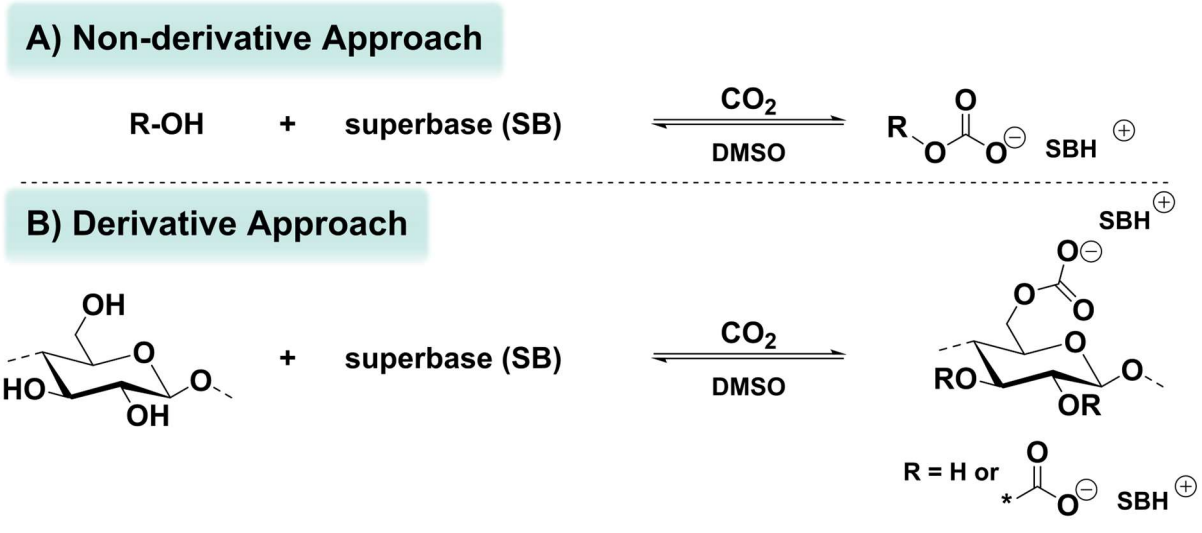

Scheme 11. General concepts for the non-derivative (A) and derivative approach (B) of the switchable solvent system for cellulose dissolution.

On the contrary, Jerôme *et al.* elaborated that the addition of an extra alcohol into the switchable solvent system is not necessarily required to ensure the dissolution of cellulose (**Scheme 11B**).[151] In other words, it was shown that cellulose can directly be solubilized by applying CO_2 to a mixture consisting of biopolymer, superbase, i.e. DBU, and co-solvent, i.e. DMSO.[151] As a mechanism for the derivatizing approach, it was postulated that the carbonate anions are now directly formed at the hydroxyl groups of the cellulose backbone and thus interrupt the intra- and intermolecular interactions enabling the dissolution of cellulose in the co-solvent DMSO.[151] The mechanistic pathway was confirmed by Meier *et al.* by trapping the *in-situ* formed carbonate anions with alkyl halides, i.e. benzyl bromide and methyl iodide, and by subsequent characterization of the correspondingly formed cellulose carbonates *via* infrared (IR) and nuclear magnetic resonance (NMR) spectroscopy.[152] A direct proof of the carbonate formation at the cellulose backbone was provided by Bialik *et al. via in-situ* NMR measurements supplemented by electronic structure calculations and Meier *et al. via* online IR spectroscopy.[152,153]

In line with the earlier presented results investigated by Jessop *et al.* both approaches for cellulose dissolution, i.e. non-derivatizing and derivatizing, show a reversible behavior. Hence, cellulose precipitates from the solution as soon as CO_2 is removed from the system, e.g. by degassing the mixture with an inert gas such as argon or nitrogen.[149,151] The addition of a superbase to the switchable solvent system, such as DBU, is crucial for the efficient solubilization of cellulose. Within recent years, a broad variety of different guanidine based superbase have therefore been investigated. Nowadays the literature reveal several alternatives to DBU, e.g. TBD, 7-methyl-1,5,7-triazobicyclo[4.4.0]dec-5-ene (MTBD), 1,5-Diazabicyclo[4.3.0]non-5-ene (DBN), TMG, or 1,4-diazabicyclo[2.2.2]octane (DABCO), which can be implemented into the approaches.[151,152,154,] However, it is worth to add that the solubilization conditions, i.e. temperature or CO_2 pressure, must be adapted when using different superbases.

The derivatizing approach of the switchable solvent system shows a remarkable similarity to the industrially employed viscose process. The most significant difference is the replacement of volatile and toxic CS_2 by the abundant non-toxic CO_2.[155] Taking additionally into account that DMSO is also categorized as non-toxic and possesses only minor issues in terms of stability and reactivity, the switchable solvent system utilizes fewer amounts of toxic components compared to the viscose process.[156] Even

more, Meier *et al.* showed that the main components of the derivatizing system, i.e. the co-solvent DMSO and the superbase DBU, can be recovered after solubilization (or modification) of cellulose in high yields, i.e. 96% and 87% respectively, which is better than in the viscose process.[157] Hence, it can be concluded that the switchable solvent system is a promising candidate for a more sustainable alternative to the viscose process in the future.

2.2.3 Cellulose Derivatives

Although native cellulose already possesses unique properties resulting from its structural characteristics (see chapter 2) there is a high interest in upgrading them for specific applications in our daily life. A valuable tool to access tailored mechanical properties in cellulose-based materials is chemical modification.[158] Thus, up to the present day, various approaches have been investigated to introduce different functional groups into the cellulose structure to deliver various cellulose derivatives (**Scheme 12**).[159]

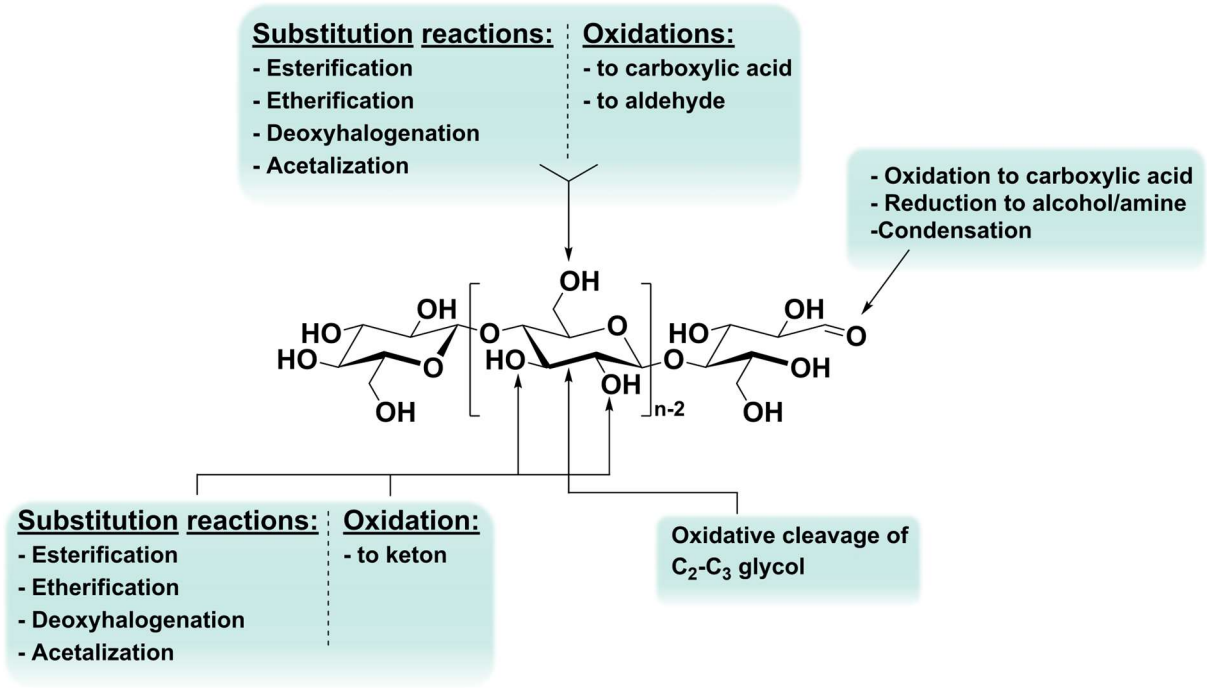

Scheme 12. General overview about potential reactions yielding different cellulose derivatives adapted from Kamel *et al.*[159]

Generally, cellulose modification can be done in a heterogenous or homogenous fashion. From a historical perspective the first approach for cellulose modification was investigated in 1846 by Christian Friedrich Schoenbein. Herein, cellulose was treated

with a mixture of nitric and sulfuric acid (H_2SO_4) yielding cellulose nitrate (**Scheme 13**).[160]

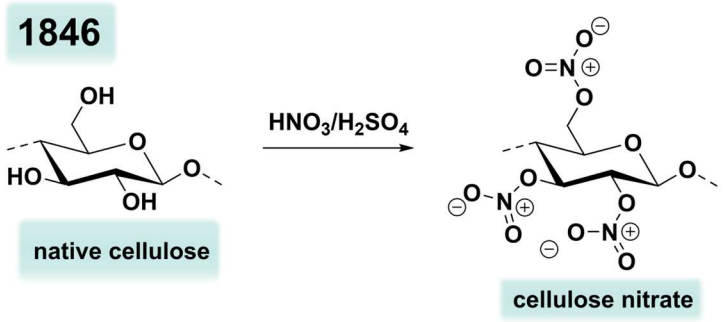

Scheme 13. Schematic overview of the synthesis of cellulose nitrate.

The synthesis of cellulose nitrate in 1846 does not only present the first successful modification process for cellulose, it was also the starting point for the first man made plastic developed in 1865.[161] At this time, John Wesley Hyatt treated cellulose nitrate with camphor as a plasticizer, which led to a plastic material introduced as celluloid.[161] At the early stages, this thermoplastic polymer was applied in billiard balls, gun cotton and film materials.[161,162] The two industrially most important classes of cellulose derivatives are cellulose ethers and esters.[163] The etherification of cellulose can be achieved by the usage of several reagents, e.g. epoxides, alpha halogenated carboxylic acids, and alkyl halides, among others.[164] Carboxymethyl cellulose (CMC), methyl cellulose, ethyl cellulose, and hydroxyethyl cellulose are herein the most prominent examples.[164] Among these cellulose ethers, CMC is the most relevant derivative in industry.[165] It is estimated that the CMC market will grow up to $2.23 billion in 2028 ($1.67 billion in 2021), with a production of then 658kt worldwide per year.[165] CMC finds application in different fields such as in papers, textiles, surfactants, pharmaceuticals, beauty products, packaging and others.[165,] The current chapter, however, focuses more on the class of cellulose esters, as these derivatives, plays a crucial role in the chapters 4.1 and 4.2 as targeted products and starting materials, respectively.

Cellulose Esters

Cellulose esters (CEs) are thermoplastic biopolymers derived from cellulose, which have been known for two centuries.[166] Converting cellulose into the corresponding esters yield a dramatic change in properties enabling for example the solubility in common organic solvents and the meltability before decomposition.[166] Thus, CEs can

be categorized, in comparison to native cellulose, as processable and reshapable polymeric materials.

Nowadays, organic CEs can be synthesized in a heterogenous or homogenous manner *via* a broad variety of different synthetic approaches. From an industrial point of view, the most relevant CEs are cellulose acetate (CA), cellulose acetate propionate (CAP), and cellulose acetate butyrate (CAB).[166,167,168] These materials find applications in textiles, membranes, coatings, drug delivery, and cigarette filters, among others.[166,167] Especially, CA, which is today produced in a multiton scale (980k tons by 2015), can be classified as the major player among these three derivatives.[168,169] The most established approach for CA synthesis in industry is the acetic acid process.[168] Herein, cellulose is heterogenously modified by a simple transesterification reaction using acetic acid as solvent, acetic anhydride as transesterification agent, and sulfuric acid as catalyst (**Scheme 14**).[168]

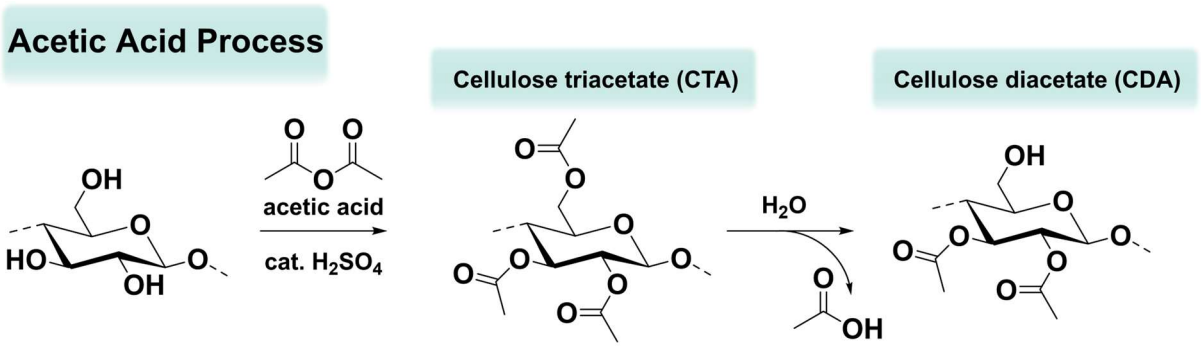

Scheme 14. General concept of the acetic acid process for the synthesis of cellulose acetate.

In the currently describe process, i.e. acetic acid process, high-quality cellulose pulp from cotton or wood with a cellulose content higher than 95% is employed as starting material.[168] During the modification, cellulose is firstly mechanically disintegrated and swelled in acetic acid as a pretreatment to ensure an efficient accessibility of the hydroxyl groups.[168] At the same time, the catalyst, i.e. sulfuric acid, can be added to the reaction mixture.[168] After the addition of acetic anhydride, the exothermic reactions occurs and cellulose triacetate (CTA) is formed, which appears as homogenously solubilized at the end of the process.[168] The modification is subsequently quenched by the addition of water or diluted acetic acid.[168] However, for many applications CTA is often not suitable. For example, CTA cannot be employed for dry spinning and thus not be manufactured into some of targeted materials such as cigarette filters.[168] To

overcome these problems, an additional de-acetylation step is often necessary to achieve CAs with lower DS.[168] The de-functionalization of CTA is herein controlled by the amount of added water (5 - 15 wt%), reaction temperature (60 °C < T < 80 °C), and reaction time (3h < t < 10h).[168] Accordingly, so-called cellulose diacetate can be synthesized with DS values between 2.4 and 2.7, making it processable and therefore usable in many applications.[168] CAP and CAB are industrially produced in a similar manner, just by the variation of the starting materials, i.e. acid and anhydride.[168] However, the acetic acid process also contains some limitations and critical parameters. Firstly, an equal distribution of acetyl moieties along the cellulose backbone as well as a direct adjustment of the DS remain challenging due to the heterogeneity at the beginning of the modification process. Thus, a supplemental de-acetylation step is implemented (as described before), which can be considered as critical in terms of sustainability as it requires additional resources, i.e. chemicals and energy, and produces supplemental waste. Moreover, the reaction temperature plays a crucial role in this system.[168] Since the acetic acid process is an exothermic reaction, it is important to control the temperature in the reaction by cooling or by the addition of frozen acetic acid.[168] On the one hand, because of a competing side reaction, which degrades the cellulose backbone and therefore deteriorate the materials properties of the resulting CAs (**Scheme 15**).[168]

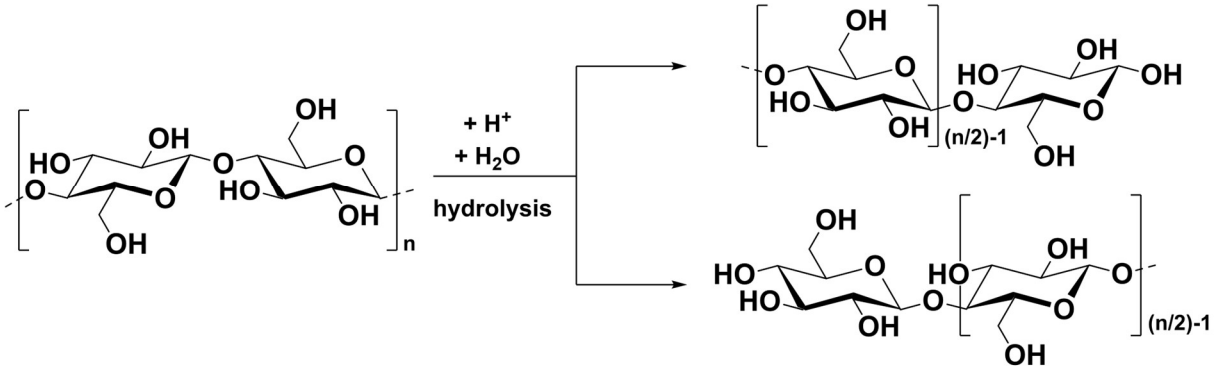

Scheme 15. Schematic overview of cellulose backbone degradation occurring in the acetic acid process.

On the other hand, from a security perspective, as the reaction set-up can fastly overheat, the risk of a potential explosion must be considered. As already previously elucidated, one of the major drawbacks appearing in the acetic acid process remain the harsh acidic reaction conditions inducing an unavoidable backbone degradation of the cellulose structure *via* hydrolysis. In other words, an acid catalyzed cleavage of the 1,4-ß-glycosidic connections between the AGUs decrease the DP, i.e. the molecular

weight, of the initially employed biopolymer and therefore yield CAs with poorer mechanical properties.[168] Even though the main application of CA is nowadays in cigarette filters, it can also replace cellulose nitrate in optical films from the 1920s to the 1970s.[162] In this regard, CA is also known as “safety film”, as it is much more stable and not as highly flammable as the nitrate-based cellulose derivative, which was used before.[162] Nevertheless, CAs films also suffer from an inherent degradation behavior, which is known as “vinegar syndrome” and caused by the humidity of the ambient air and remaining NaOH.[170] Here, a deacetylation occurs based on the reaction between water and the acetyl groups attached to the cellulose backbone forming a hydroxyl unit and acetic acid.[170] The vinegar syndrome is an autocatalytic process, as the present acetic acid can afterwards further catalyze the de-acetylation of the CA films.[170]

To overcome these challenges, i.e. backbone degradation, vinegar syndrome and multi-step adjustment of DS, and to improve the sustainability of the established industrial processes, many different approaches yielding structurally different CEs have nowadays been established.[171,172] Especially, the homogenous synthesis of CEs using ionic liquids or the switchable solvent system reached a significant attention in recent years (**Scheme 16**).[171,172]

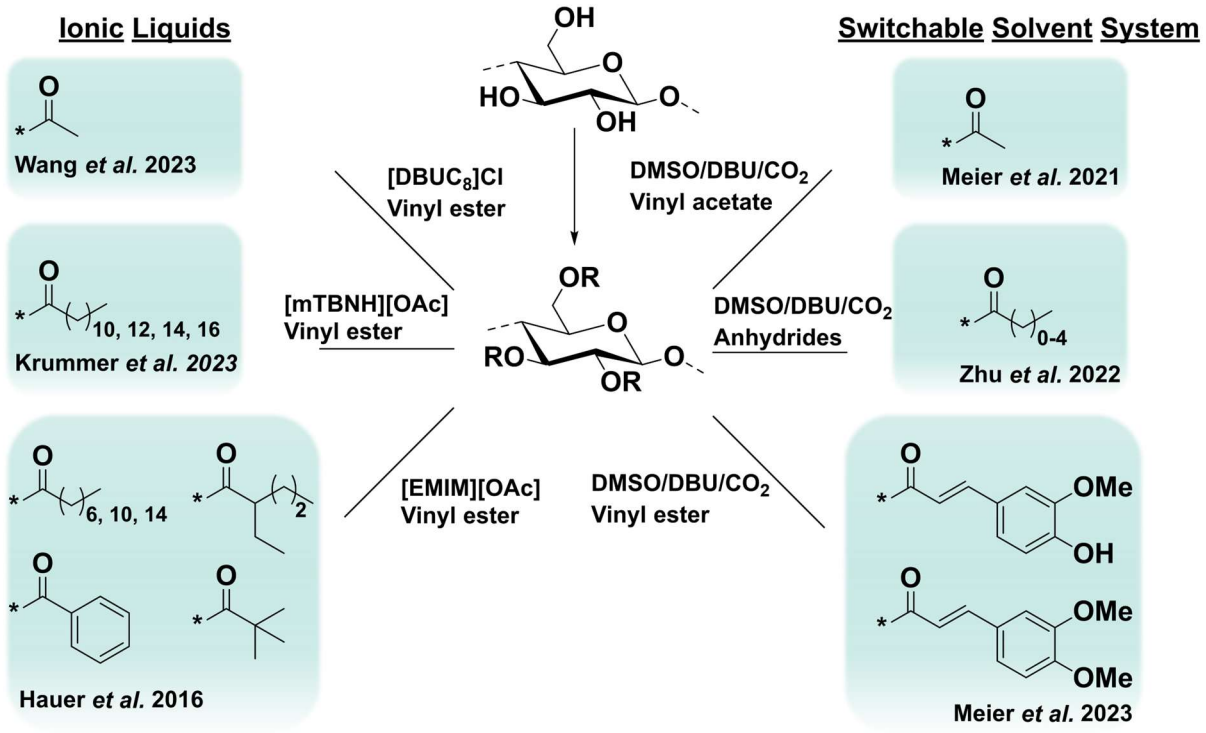

Scheme 16. Overview about recently published homogenous esterification approaches of MCC using ionic liquids or the switchable solvent system.

Both strategies reveal several advantages compared to the industrially applied processes. Firstly, most homogenous approaches delivering CEs proceed under neutral or basic conditions (pH ≥ 7), resulting in less backbone degradation and thus improved mechanical properties of the final materials.[157] Secondly, due to the solubilization of cellulose before the derivatization approach, a statistically even distribution of the introduced functionalities as well as a direct adjustment of the DS by varying the amount of reactants can be achieved.[157,172]

However, since ionic liquids remain critical in terms of sustainability (see chapter 2.2.2), the derivative approach of the switchable solvent system has become a major player in the development of more sustainable homogenous syntheses of CE and other cellulose derivatives.[171,172] The previous statement is underlined by the work of Meier *et al.*, who introduced a more sustainable synthetic pathway to access CA.[157] Herein, MCC was solubilized and subsequently modified in a DMSO/DBU/CO_2 switchable solvent system by a DBU catalyzed transesterification reaction between the hydroxyl groups located at the polymer backbone and vinyl acetate.[157] In this work, it was shown that a direct DS adjustment was feasible, less backbone degradation occurred compared to the industrially employed acetic acid process, and most importantly, that all components used during the modification approach could be recovered in very high yields (87% - 99%).[157] The calculated *E*-factor in this approach was presented as 1.92, which is 3 to almost 10 times lower compared to other methods reported for CA synthesis.[157] Similar approaches were also used to access fully bio-based cellulosic materials combining two different renewable feedstocks. It was again Meier *et al.* directly reacting MCC with high oleic sunflower oil in a DMSO/DBU/CO_2 switchable solvent system, targeting so-called fatty acid cellulose esters.[173] FACEs appear as an important class of 100% bio-based cellulose derivatives showing a better thermal processability, film formation ability, and solubility in common organic solvents compared to their counterparts bearing shorter side chains.[167,174,175] Nevertheless, the most important structural characteristic of FACEs is the potential existence of an alkene functionality in the side chain (depending on the introduced fatty acid derivative) enabling an additional modification step.[154]

The bottle neck in the derivative approach of the switchable solvent regarding sustainability is DBU, which is recognized as toxic. Nowadays, several (non-toxic) alternatives for DBU in the switchable solvent system for cellulose dissolution are

known (see chapter 2.2.2). However, most of them have not been investigated in their dual role affording the solubilization of cellulose and acting as an organocatalyst in a subsequent modification reaction. Hence, the current research is still focusing on the investigation of other non-toxic superbases, which can efficiently replace DBU in the switchable solvent system for the dissolution and modification of cellulose.

Cellulose Esters in Membranes

Membrane technologies are nowadays widely employed in gas separation, food industry, energy generation, and water treatment.[176] The operating principle of membranes is the separation of different mixtures by allowing certain species to pass while others are hindered.[176] Particularly synthetic polymers, such as polysulfones, polyvinylidene fluoride, polypropylene, polyethersulfones, and polyvinyl alcohol find application in this separation technique, due to their easy handling, low costs, and high performance.[176] Nevertheless, the previously mentioned polymers are classified as critical in terms of sustainability. More precisely, these polymers require fossil based starting materials, are not biodegradable, and can cause environmental pollution when distributed in the ecosystem. Thus, within recent years the development of bio-renewable and degradable alternatives to fabricate filtration membranes achieved a significant importance. Indeed, CA showing good film forming properties supplemented by a high chemical and mechanical stability, is a prominent candidate to replace synthetic polymers in membrane applications.[176] Already in 1959, Breton *et al.* showed that CA membranes reveal a high impermeability to salts, but not to water.[177] Hence, the synthesized membranes could be successfully used for seawater desalination.[177] Particularly since 2009, the focus on cellulose-based membranes increased significantly due to the higher attention of human society for environmental aspects.[176]

The main application of CA membranes is currently wastewater treatment. In the last decades, the global demand accessing fresh drinking water increased dramatically.[178] This can be explained by a higher population, more food production, ongoing urbanization, and the climate change, among others.[176] Thus, it is essential to investigate more sustainable membranes for effective water decontamination. Recently, CA membranes are implemented in reverse osmosis, ultrafiltration, and nanofiltration.[179] Accordingly, pollutants such as heavy metal ions, textile dyes, pharmaceuticals, polycyclic aromatic hydrocarbons, and pesticides can be removed from aqueous solutions.[179] For example, in 2020 Ahmed *et al.* showed that CA membranes can remove chromium and selenium ions efficiently from an aqueous

solution at different pH values revealing extraction efficiencies up to 89% and 85%, respectively.[180] Often, in order to tune the properties of the materials and prevent fouling phenomena, other synthetic polymers or nanoparticles are blended with CA to form membranes.[179] This remains critical in terms of sustainability as these additives reduce the biodegradability of the composite materials. An example presents the work of Abdelhameed *et al.*, where the performance of a native CA membrane was compared to a blend material consisting of CA and a metal organic framework regarding the removal of paracetamol from wastewater.[181] Herein, it was found that the introduction of additional functional groups, i.e. amines, dramatically increased the extraction efficiency for paracetamol.[181] A more sustainable approach to achieve higher performances during the separation processes would be the direct functionalization of CA with supplemental functional moieties. As a conclusion of the current chapter, it can be elucidated that CA is already implemented as valuable material in membrane science, particularly for water treatment applications. However, synthetic strategies combining sustainability aspects and material performance must be further investigated in future.

2.3 Inverse Vulcanization

Elemental sulfur (S_8) is an abundant waste material with an annual production of more than 80 million tons.[182] A major source of elemental sulfur in recent years were desulfurization processes of natural gas and oil *via* the Claus process.[183] Although elemental sulfur finds application in the production of vulcanized rubber,[184] sulfuric acid,[185] and fertilizers,[186] not all produced sulfur can be consumed by the industry and therefore accumulates in large deposits.[187] The high flammability of sulfur, which can lead to a potential release of toxic sulfur dioxide (SO_2), and the microbial oxidation into sulfuric acid, which can pollute groundwater, render these storage places a serious environmental risk.[187] However, as the oil industry will continue to be dependent on sulfur containing resources in the coming decades, this problem can only be solved by developing processes that convert large quantities of elemental sulfur into valuable materials. Thus, in recent years, various research fields have evolved that aim at implementing elemental sulfur as a valuable starting material for different applications. Up to the present day, the most important synthetic strategy remains the vulcanization of rubber, which was developed by Goodyear in 1841.[188] Herein, natural rubber is heated with elemental sulfur yielding flexible materials containing network structures with sulfur crosslinks. However, vulcanized materials possess a relatively low sulfur content, i.e. ~2%, and can therefore not resolve the “excess sulfur problem” that has evolved. A supplemental approach, which requires much higher amounts of elemental sulfur and achieved a considerably high attention in recent years, is inverse vulcanization.

Conventional Inverse Vulcanization

In general, inverse vulcanization is the reaction of elemental sulfur with unsaturated organic compounds, which act as crosslinkers in the final materials. In comparison to conventional vulcanization, inverse vulcanization uses much higher amounts of elemental sulfur and can therefore deliver high sulfur content materials (≥ 50 wt% of sulfur). It was the pioneering work of Pyun *et al.* in 2011, that introduced elemental sulfur as abundant waste material for the synthesis of high sulfur content materials.[189] Herein, elemental sulfur was reacted with unsaturated organic comonomers such as divinylbenzene at elevated temperatures (>180°C).[189] On a molecular level a homolytic ring-opening of elemental sulfur occurs by applying specific conditions, i.e. high temperature, light irradiation or catalyst addition, leading to the formation of polysulfur chain containing thiyl radical end groups, which can subsequently react with the double

bonds of the organic co-monomer (also described as crosslinker) delivering the final material (**Scheme 17A**).[190,191,192] Initially, inverse vulcanization was investigated to take place in a temperature range between 160 and 200 °C.[189,190] The high reaction temperature was necessary to induce the ring-opening of elemental sulfur, which is crucial for a successful reaction and does not proceed below 160 °C without additives.[190,193] Generally, the procedures to conduct inverse vulcanization are very simple. Both components, i.e. elemental sulfur and a preferably liquid co-monomer, are homogeneously mixed and heated above 160 °C. However, due to the high reaction temperature, only co-monomers with boiling points far above 160 °C can be employed in the system to avoid evaporation effects. Some common examples for crosslinkers, which have been used for conventional inverse vulcanization at elevated temperatures, are depicted in **Scheme 17B**. By far the most investigated derivatives for inverse vulcanization are di-isopropenylbenzene and 1,2-divinylbenzene, which are liquids with boiling points of 231 °C and 195 °C, respectively.[194]

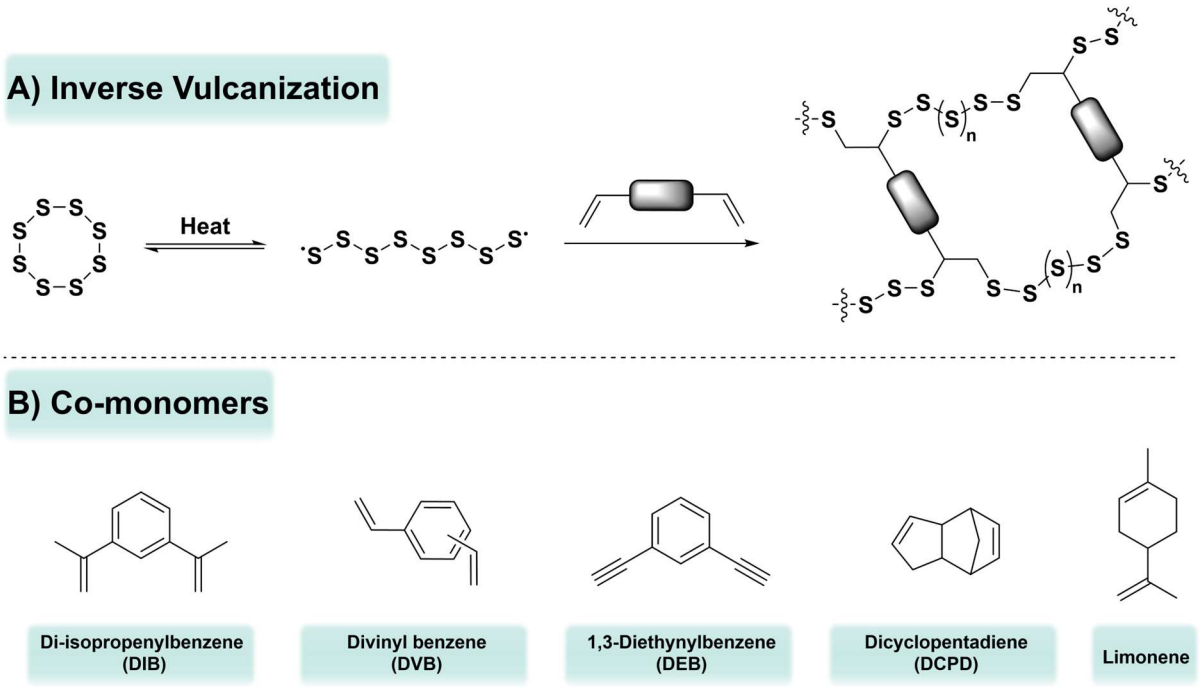

Scheme 17. A) General concept of inverse vulcanization. B) Common co-monomers in conventional inverse vulcanization.[192]

Catalytic Inverse Vulcanization

In 2019, Hasell *et al.* optimized the conventional inverse vulcanization by including a catalyst into the established polymerization approach.[191] Herein, a metal complex, i.e. zinc diethyldithiocarbamate ($Zn(DTC)_2$, **Scheme 18A**), was introduced into the system

to accelerate the reaction.[191] Indeed, for already established unsaturated organic co-monomers, which have previously been used in conventional inverse vulcanization, the addition of $Zn(DTC)_2$ increased the reaction rate and lowered the required reaction temperature significantly (100 °C < T < 135 °C).[191] Moreover, the catalytic approach enabled the polymerization of previously inactive co-monomers such as ethylene glycol dimethacrylate (EGDMA) or glyoxal bis(diallylacetal) (GBDA) with elemental sulfur, expanding the toolbox of potential crosslinkers (**Scheme 18B**).[191] Mechanistic insights showed that in a first step $Zn(DTC)_2$ forms a metal-sulfur bond with elemental sulfur, which enables the ring opening of S_8 at lower temperatures.[191] Subsequently, sulfur inserts between metal and DTC ligand, delivering the active species of the catalyst.[191] Upon bringing sulfur into spatial proximity to the unsaturated co-monomers and lowering the energy barrier for bond formation, the polymerization proceeds and the catalyst is recovered in its initial form.[191] Up to the present day, it is not fully elucidated whether the bond formation step appears in a radical or ionic fashion.[191] In 2021, Hasell *et al.* investigated the role and scope of different catalysts in inverse vulcanization in a more detailed manner.[195] Herein, the performance of several types of catalysts regarding the inverse vulcanization of 1,2-divinyl benzene (DVB) were tested.[195] The conventional heat induced catalyst-free process was used as control experiment, whereas the systems including the most established catalysts $Zn(DTC)_2$ and $Na(DTC)_2$ acted as benchmarks.[195] Initially, it was investigated whether the nature of metal and the ligand structure in metal complexes have an influence on the catalyst performance.[195] Subsequently, alternative types of catalysts, such as inorganic and metal-free derivatives, were introduced as potential candidates.[195] After comparison of reaction rate, yield, and glass transition temperature (T_g) of the final material the authors concluded that the most efficient catalyst for the inverse vulcanization of DVB is $Cu(DTC)_2$.[195] Nevertheless, also other organic and organometallic species revealed a catalytic effect and deserve recognition in future research (**Scheme 18A**).[195] For example, recently Kim *et al.* presented a strategy for the inverse vulcanization of previously unreactive co-monomers such as 1,6-hexanediol dimethacrylate (HDDA) and bisphenol A glycerolate dimethacrylate (BPAGMA), among others (**Scheme 18B**), using low-cost trialkyl amines (TAAs) as nucleophilic sulfur activators and phase transfer catalysts at low temperatures, i.e. 110 °C.[196] Herein, TAAs performed similarly well or better than conventional catalysts, i.e. $Zn(DTC)_2$, in terms of vitrification time, T_g, and yield.[196]

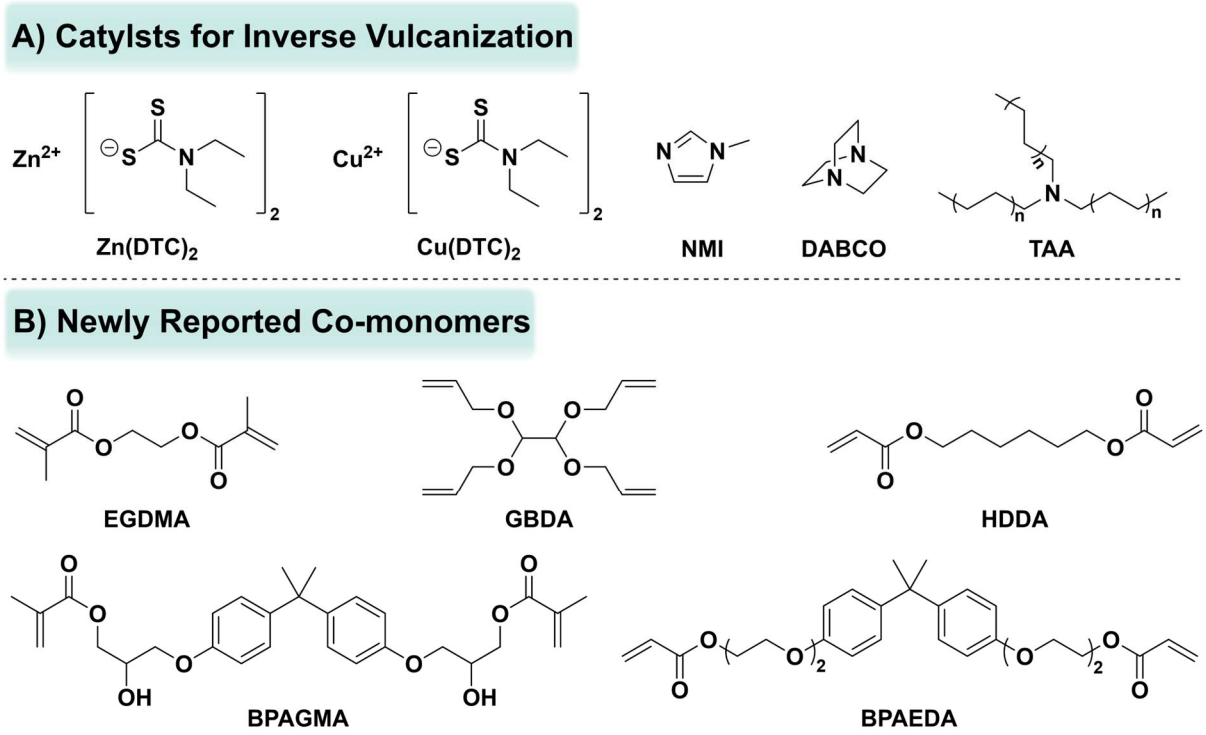

Scheme 18. A) Selected metal based and organic catalysts for inverse vulcanization. B) Newly reported co-monomers polymerizable via catalytic inverse vulcanization.[195,196]

Photoinduced Inverse Vulcanization

The most recently developed method for inverse vulcanization is induced photochemically and can thus be conducted at room temperature.[192] Hence, this reaction system, which was established by Quan *et al.* in 2022, appears as a suitable approach for the inverse vulcanization of thermally sensitive or volatile organic co-monomers.[192] Especially the integration of inexpensive industrial gases such as exemplarily ethylene, propylene, acetylene, and vinyl chloride, among others, into the reaction approach enabled the access to various novel materials and enhanced the prospects of inverse vulcanization for a commercial application.[192]

2.3.1 Inverse Vulcanization of Renewable Resources and Their Application

Inverse vulcanization is nowadays a well-established tool for accessing high sulfur content polymeric materials. In terms of sustainability, this approach fulfils several requirements of Green Chemistry.[197,18] For instance, inverse vulcanization does not require any solvent and no tedious purification steps must be performed, both aspects preventing the formation of waste. Furthermore, the process exhibits a high atom economy, and, also highly importantly, co-monomers from renewable feedstocks can be used.[197] Thus, inverse vulcanization can potentially act as valuable approach to

deliver more sustainable materials, which find possible application as heavy metal sorbents, cathode materials in Li-S batteries, adhesives, fertilizers, and in oil spill remediation.[197,198] Indeed, in line with the further increasing attention on sustainability aspects, the inverse vulcanization of bio-based co-monomers instead of their fossil-based counterparts has gained significant importance in recent years.[199] Today, several approaches integrating crosslinkers derived from renewable resources such as vegetable oils, terpenes, lignin, and cellulose, among others, are described in the literature.[197,199,200,201,202]

Triglycerides

The most extensively investigated renewable resource, which can be employed as co-monomer in inverse vulcanization, are vegetable oils. Especially canola oil was used frequently.[203] High sulfur content materials made from vegetable oils, such as canola oil, find application as more sustainable materials particularly in water treatment, energy storage devices, urban mining, and as fertilizers (**Scheme 19**).

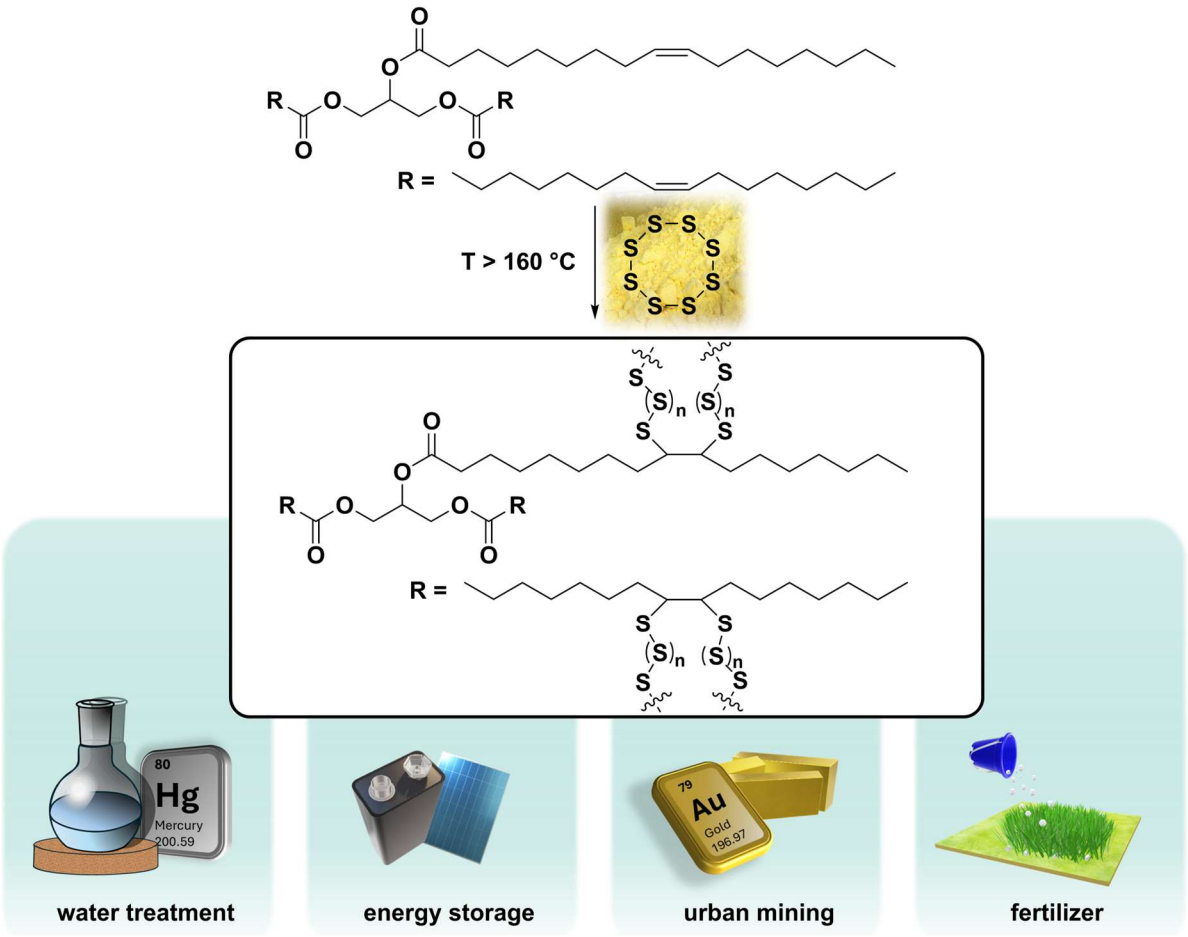

Scheme 19. General concept for the conventional inverse vulcanization of vegetable oils and possible areas of application.

For example, in 2017 Chalker *et al.* directly reacted canola oil with elemental sulfur at 180 °C yielding materials with sulfur contents up to 90 wt%.[204] In this work, it was elaborated that the respective sulfur materials could effectively remove Hg^{2+} and Hg^{0} from aqueous solutions with an extraction efficiency up to 90%. Thus, these materials were introduced to have a potential application in water decontamination.[204] In 2018, the same group synthesized similar materials with slightly lower sulfur contents, i.e. up to 70%, and expanded the toolbox of removable metal ions by showing the effective extraction of Fe^{3+} from water (95%).[205] Within the following years, the scope of implemented vegetable oils into inverse vulcanization gradually increased. Again Chalker *et al.* reported the synthesis of high sulfur content materials (50 wt%) by using structurally different vegetable oils, i.e. canola oil, rice bran oil, and castor oil, as co-monomers (**Scheme 20**).[206] Since it was already known that inverse vulcanized materials can be employed for efficient mercury removal, it was investigated if the structural nature of the introduced co-monomers reveal any influence on the final extraction efficiency.[206] Indeed, a better performance could be observed for the material containing castor oil (**Scheme 20**).[206]

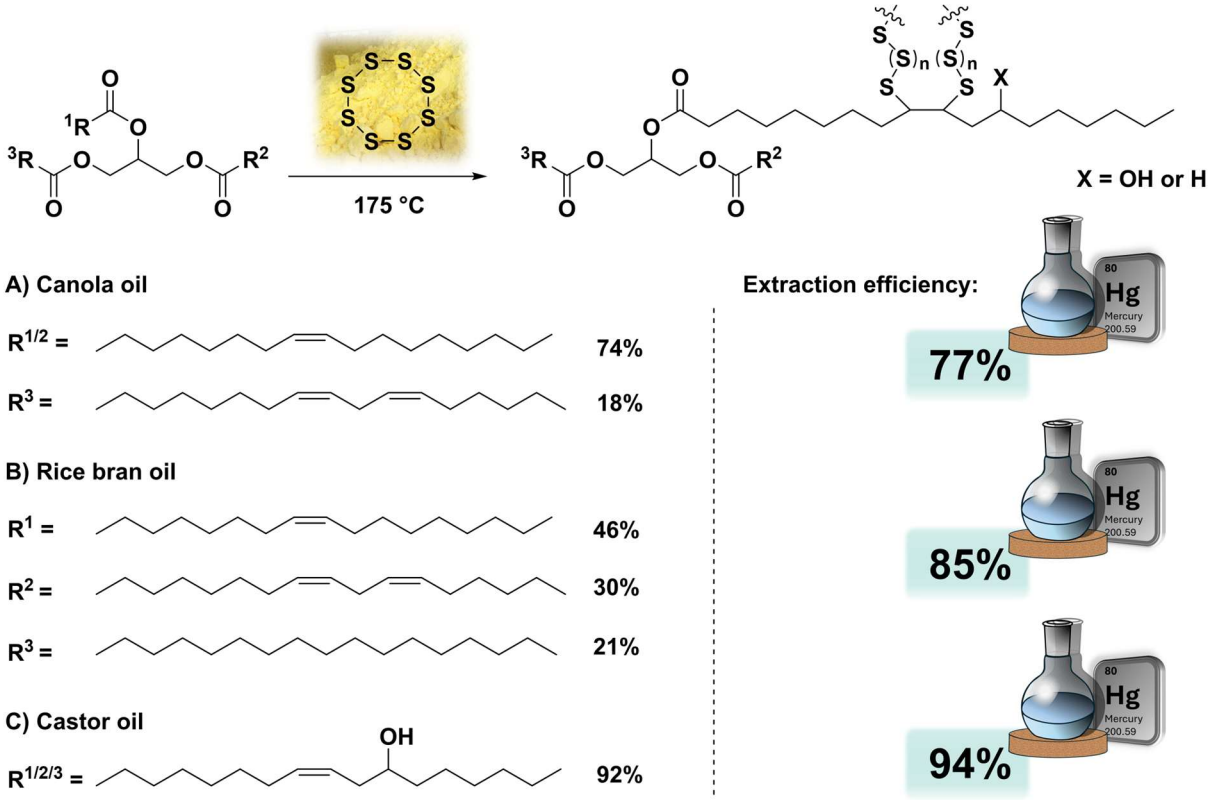

Scheme 20. Inverse vulcanization of three structurally different vegetable oils, i.e. canola oil, rice bran oil, and castor oil, and their respective performance in mercury ion removal from aqueous solutions after 1h treatment.[206]

The higher extraction efficiency can herein probably be explained by the presence of additional hydroxyl groups, as they can also participate in mercury chelation.[206] Due to a continuously increasing population, urban mining of valuable and rare metals has reached nowadays a particular attention. Especially the recovery of gold as a resource, which finds application in military, medical fields, and of course as jewelry, remains important. Accordingly, Yang *et al.* inversely vulcanized an edible oil blend consisting of soybean oil (59%), canola oil (21%), sunflower oil (10%), corn oil (3%), peanut oil (3%), rice oil (3%), sesame oil (0.6%), and linseed oil (0.4%) and investigated the potential of recovering Au^{3+} from aqueous solutions.[207] First, the performance of the materials depending on their sulfur content was investigated.[207] Herein, it could be observed that a higher extraction capacity (up to 20.7 mg g^{-1}) were achieved by increasing the amount of incorporated sulfur from 10 to 50 wt%.[207] However, a further rise in sulfur content led to a brittle material, which revealed a lower capability to extract Au^{3+}.[207] Furthermore, the influence of the surface area was examined. Introducing a porogen, such as sodium chloride (NaCl), into the synthesis approach, which delivered porous structures, increased the surface area and thus improved the Au^{3+} adsorption.[207] The inverse vulcanization of vegetable oils not only provide access to materials, which can be applied in water treatment. Another important field where high sulfur content materials are frequently employed is energy storage.[208,209,210,211] Accordingly, Théato *et al.* introduced sulfur composite materials based on linseed oil, sunflower oil, and olive oil as more sustainable, low-cost, and considerably harmless alternative cathode materials in Li-S batteries.[212] Herein, high specific capacities, good capacity retention abilities, and high coulombic efficiencies were observed.[212] Sulfur appears also as a vital nutrient in the biosynthesis of amino acids.[213] Thus, it is immensely important for plant growth.[213] However, it can be considered the most neglected macronutrient and the deficiency in soils has become a major issue in recent years.[213] The most common sulfur sources are sulfate salts and elemental sulfur.[213] Nevertheless, they suffer from a low sulfur content and inefficient oxidation, respectively.[213] Plants can only uptake sulfur, when it is biologically oxidized by microorganisms.[213] Herein, Ribeiro *et al.* presented that the inverse vulcanization of soybean oil delivered high sulfur content materials (30 – 90 wt%), which can be more easily oxidized and thus act as fertilizer by increasing the sulfur uptake in plants significantly.[213] The more efficient sulfur oxidation in inversely vulcanized materials can

be explained by the improved accessibility of the linear and amorphous sulfur chains.[213]

Carbohydrates

The most abundant class of biopolymers are carbohydrates.[214] Herein, starch and cellulose play the most important role. Both components consist of AGUs, which are connected *via* glycosidic linkages. In cellulose, exclusively β-1,4 connections exist, whereas in starch α-1,4 and α-1,6 glycosidic bonds occur.[215] It is not surprising that this renewable feedstock has already been introduced into inverse vulcanization approaches to access more sustainable high sulfur content materials.[201,202,216,217] However, in comparison to the previously described implementation of triglycerides, the pristine chemical structure of starch and cellulose does not contain alkene functionalities. Hence, a modification to introduce these required moieties must be conducted for both polymers. In 2021, Smith *et al.* modified starch with octenyl succinic anhydride (DS = 0.08) and subsequently inverse vulcanized the obtained derivative at 180 °C.[216] The resulting materials contained sulfur contents of 90 and 95 wt% and were investigated in terms of their materials properties.[216] The authors claimed in this work that the pretreatment was conducted along the principles of green chemistry to follow a pathway, which is as sustainable as possible.[216] However, the use of water as a solvent, leading to contaminated and difficult to purify water, combined with the fact that octenyl succinic anhydride must be synthesized from toxic maleic anhydride make this statement questionable. An extension of the previously presented approaches was established by the same research group. Herein, after reacting starch with octenyl succinic anhydride to the respective ester, the formed carboxylic acid functionalities were consumed in the presence of 1-leucine, yielding starch derivatives with an increased density of alkene moieties in the side chains.[217] In a similar fashion as described before, materials with sulfur contents of 90 and 95 wt%, which included the newly synthesized starch derivative as co-monomer, were prepared.[217] It could be shown that the introduction of additional cross-linking points, i.e. more alkene moieties, into the starch derivative enhanced the thermal and mechanical properties of the final composite materials due to a higher crosslinking density.[217]

Compared to starch, cellulose reveals much better mechanical properties due to its fiber structure, higher crystallinity, and the extensive hydrogen bond network.[218,219] Nevertheless, these characteristics also increase the difficulty to modify cellulose in an

effective fashion (see chapter 2.2.2 and 2.2.3). Thus, nowadays only two approaches for the inverse vulcanization of cellulose derivatives appear in the literature.[201,202] In order to convert cellulose in a valuable co-monomer for inverse vulcanization, Smith *et al.* reacted cellulose with 3-bromo-2-methylpropene, enabling the introduction of polymerizable alkene functionalities (**Scheme 21**).[201] The subsequently synthesized composite materials (80 wt% < sulfur content < 99 wt%) were shown to possess similar mechanical strength as commercial Portland cement.[201]

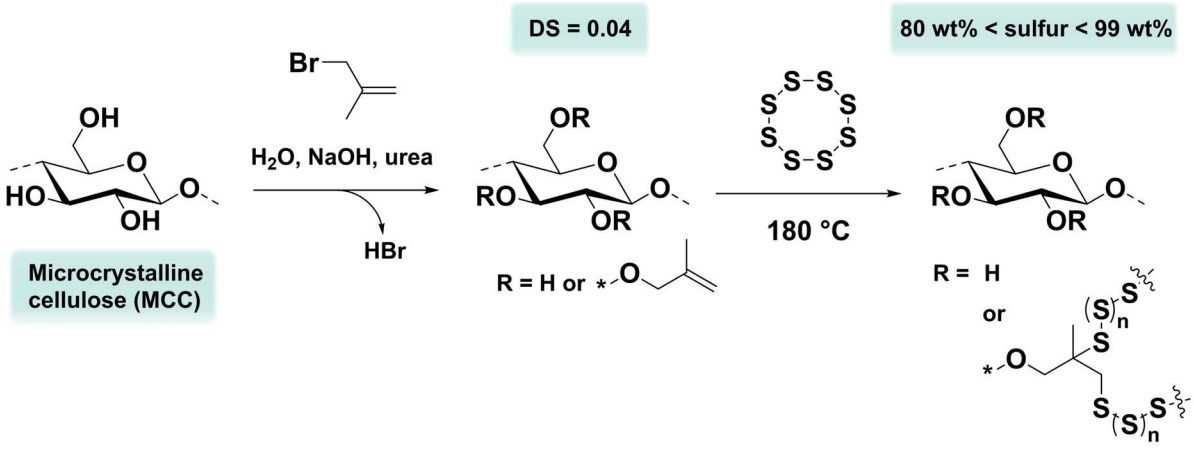

Scheme 21. Pre-functionalization of MCC with 3-bromo-2-methylpropene and subsequent inverse vulcanization.[201]

Furthermore, it was depicted that porous Portland cement filled with cellulose-based high sulfur content composite materials does not degrade in acidic media.[201] However, not only the toxicity of 3-bromo-2-methylpropene, but also the large amounts of waste produced in form of corrosive hydrogen bromide (HBr) make this synthesis approach critical from a sustainability point of view. A more sustainable method was introduced by Smith *et al.* in 2020 (**Scheme 22**).[202] Herein a three step synthesis approach with an atom economy of 90% was employed delivering composite materials with sulfur contents between 80 and 90 wt%.[202] More precisely, native cellulose was selectively oxidized at the C_6-position using sodium hypochlorite, generating carboxylic acid moieties, which were then esterified with a terpenoid, i.e. geraniol, and subsequently inverse vulcanized.[202] The final materials were compared regarding their mechanical properties, but no specific application for the carbohydrate-based sulfur materials was shown in this work.[202] Even though this approach can be classified as more sustainable as the previously described approach for inverse vulcanization of cellulose derivatives, the latter approach also reveals some drawbacks. Especially the reaction time, i.e. 14

days, and the tedious work up of the C_6 oxidation remain critical points regarding energy efficiency and waste production in the current approach.

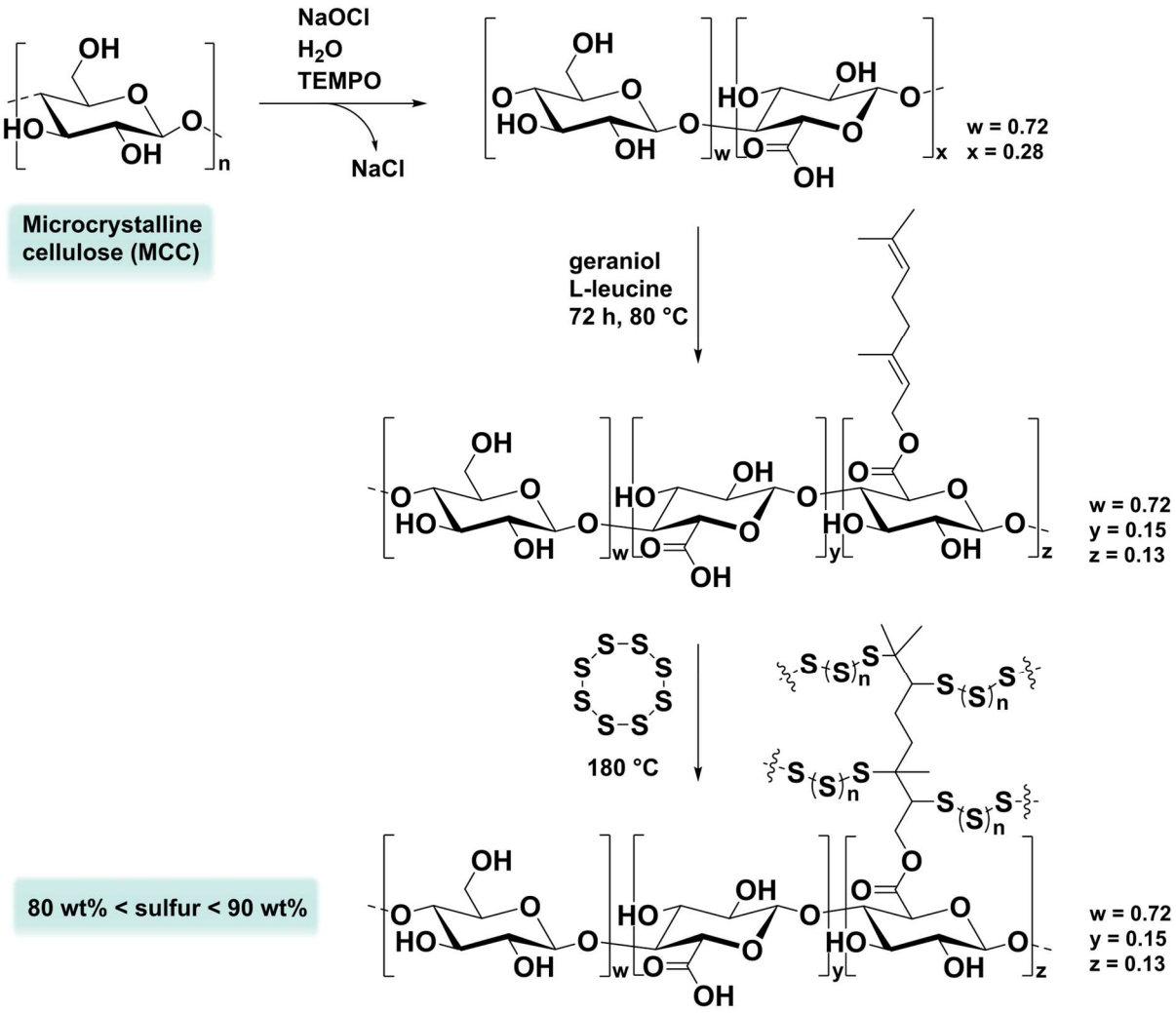

Scheme 22. General concept for the modification of MCC with a terpenoid, i.e. geraniol, and subsequent inverse vulcanization of the corresponding terpenoid cellulose ester.[202]

Other renewable resources

Next to vegetable oils and carbohydrates, terpenes are an additional class of renewable compounds, which have frequently been used in inverse vulcanization.[220,221,222,223] Terpenes are biosynthetically produced by different classes of trees and plants.[224] Hence, this product class represents an abundant and inexpensive feedstock, which does not compete with food sources.[224] Limonene is the most important terpene with an approximated world production between 49 and 74 million kilograms per year.[225] *R*-(+)-Limonene constitutes more than 98% of orange oil.[226] Thus, the peal of citrus fruits, such as oranges, are the main source for this

specific terpene. In 2015, Chalker *et al.* inversely vulcanized limonene at 170 °C without any additives, i.e. catalysts or solvents.[227] The procedure was scalable up to 100 g and the respective materials were able to remove some transition metals, i.e. Pd^{2+} and Hg^{2+}, form water and soil.[227] Particularly the color change from dark red to yellow, which occurred when the limonene based polysulfide encountered a $HgCl_2$ solution, makes this material an effective sensor for mercury detection.[227] Another application for similar materials was introduced by Yu *et al.* using them in combination with various carbon hosts as self-protectable cathode materials in Li-S batteries.[228] Additional work on the inverse vulcanization of other terpenes, such as myrcene, farnesene, and squalene, have also been published.[209,220,221,222] Lignin as the second major component in LCB is also recognized as one of the worldwide most abundant renewable feedstocks next to carbohydrates, vegetable oils, and terpenes.[229,230] Hence, it is not surprising that this aromatic biopolymer has also been introduced as a renewable co-monomer into inverse vulcanization.[200] However, lignin does not contain alkene functionalities in its native chemical structure.[231] Thus, in order to inversely vulcanize this aromatic biopolymer a pre-functionalization with polymerizable double bonds must also be conducted. Tennyson *et al.* reacted lignin with allyl bromide under basic conditions.[200] The alkene decorated lignin was subsequently inversely vulcanized at 180 °C, delivering materials with sulfur contents from 80 up to 99 wt%.[200] In terms of sustainability, particularly the pre-functionalization step can be categorized as very critical. Firstly, the herein employed allyl bromide is a highly toxic chemical, which can cause significant environmental problems. Secondly, during the substitution reaction corrosive hydrogen bromide is eliminated generating a high amount of waste.

2.4 Catechol Containing Polymers

Catechol moieties, i.e. 1,2-dihydroxybenzene, appears as a common structural element in nature and living organisms such as mussels, insects, and gecko´s, among others.[232,233,234,235] Due to its unique chemical structure, i.e. an aromatic scaffold bearing two neighboring (*ortho-)*hydroxyl groups, catechol shows various physico-chemical interactions.[236,237] Herein, especially the occurrence of hydrogen bonding, π-π stacking, and cation-π interactions enable an enhanced adhesion to (un-)polar as well as charged surfaces.[236,238] Furthermore, catechol can undergo reversible bond formation with boronic acids,[239,240] oxide surfaces,[241,242] and metal ions such as Fe^{3+}, Cu^{2+}, and Zn^{2+}.[243,244] Hence, the incorporation of catechol units into polymers (as backbone, pendant or end group, **Scheme 23**) appears nowadays as a valuable tool for the access to biomimetic functional materials. Potential areas of application for such biomimetic catechol containing polymers include coatings,[245] adhesives,[246,247] water treatment,[248] and energy storage.[236] Even though the synthesis of catechol bearing macromolecules remains up to the present day challenging and expensive, several synthetic pathways have been established to incorporate catechol moieties into polymeric structures.

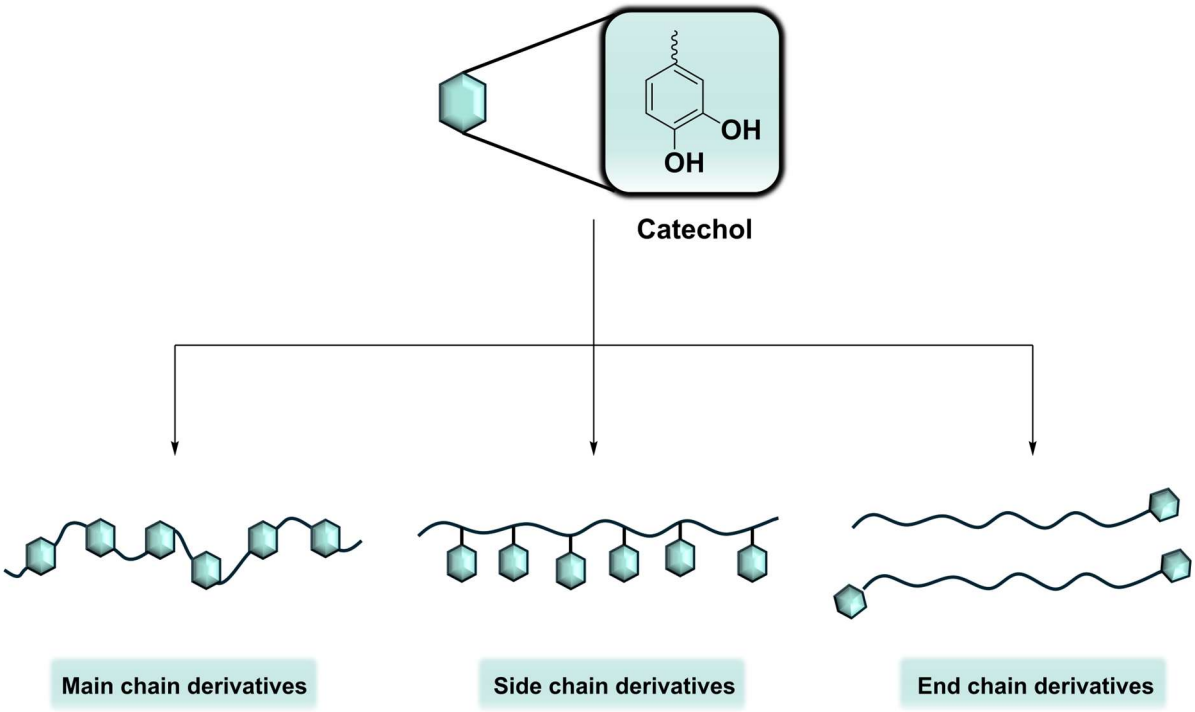

Scheme 23. Schematic representation of the main techniques for the synthesis of catechol containing polymers.[236]

2.4.1 Fundamental Synthetic Approaches

Main Chain Derivatives

Macromolecules containing catechol moieties in the polymer backbone are referred to as main chain derivatives. This specific class of polymers is mainly synthesized by an oxidative polymerization of catechol derivatives, i.e. catecholamines.[236] Interestingly, the resulting polymers reveal a substrate independent tendency to form robust coatings, making them valuable in applications such as surface coating, biotechnology, biomedicine, and water purification.[249,250] In particular, the pioneering work of Messersmith *et al.* in 2007 strongly increased the attention towards catechol containing main chain derivatives, as they discovered a universal approach for the preparation of catecholamine based surface coatings.[249] Herein, a simple dip coating process was used to oxidatively polymerize dopamine under basic conditions (pH = 8.5) on the surface of different substrates, i.e. noble metals, metal oxides, semiconductors, and synthetic polymers.[249] The obtained poly(dopamine) surface coatings revealed a similar chemical structure as mussel foot proteins and appeared therefore as biocompatible and highly adhesive.[249] The proposed mechanism was adapted from biological melanins, which are predominantly constituted of tyrosine derived catecholamines.[251] In the early 20th century, Raper and Mason observed that tyrosinase can efficiently catalyze the oxidation and polymerization of tyrosine yielding melanins.[251] Accordingly, Raper and Mason postulated a possible polymerization mechanism depicted in **Scheme 24**.[250,251]

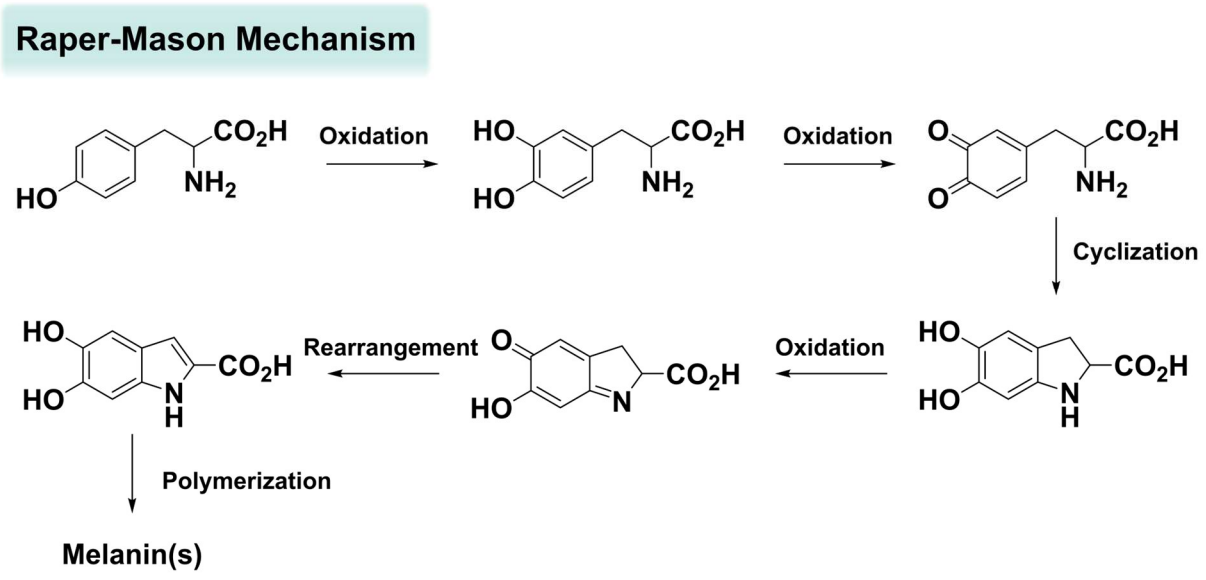

Scheme 24. General concept of the Raper-Mason mechanism.[250,251]

Herein, tyrosine is first oxidized to 3,4-dihydroxyphenyl-l-alanine (DOPA), followed by a second oxidation step leading to dopaquinone, followed by a cyclization *via* a 1,4-aza-Michael type addition delivering the cyclic indoline derivative leucodopachrome.[251] The final oxidation of leucodopachrome connected with a rearrangement step then yields 5,6-dihydroxyindol, which can self-polymerize to the corresponding melanins.[251] For the oxidative polymerization of dopamine Messersmith *et al.* proposed a similar but slightly simplified version of the Raper-Mason mechanism.[251] Herein, dopamine is directly oxidized to the respective quinone derivative, which also undergoes an intramolecular 1,4-aza-Micheal type addition yielding cyclic 5,6-dihydroxyindoline.[251] In the same manner as explained before, a final oxidation step and a subsequent rearrangement result in the self-polymerizable 5,6-dihydroxyindol.[251] Even though dopamine remains the most frequently employed monomer in oxidative polymerization delivering catechol containing main chain derivatives, also other catecholamines, e.g. norepinephrine, and dopamine derivatives e.g. with increased alkyl chain length between the catechol and amine functionalities, have recently been successfully introduced as additional polymerizable derivatives.[252,253] Furthermore, the current literature also reveals reports about the oxidative co-polymerization of catechol and catecholamines, i.e. DOPA, with nucleophilic additives, i.e. amines and thiols. For example, in 2017 Chai *et al.* reported the co-polymerization of *N*-Ac-3,4-dihydroxyphenylalanine methyl ester (NADOPAMe) with several diamines, dithiols, and cysteamine yielding potentially degradable DOPA based coatings.[254] Going one step further, Xu *et al.* polymerized catechol under basic conditions (pH = 8.5) with various polyamines targeting a mussel inspired thermoset coating to change the surface polarity of polypropylene separators in Li-ion batteries without breaking their pore structure.[255]

Side Chain Derivatives

Polymers bearing catechol moieties as pendant side groups can be categorized as side chain derivatives. Compared to the previously introduced main chain derivatives, this polymer class can nowadays be accessed *via* various synthetic strategies.[236,237] Among these, the earliest approach for the synthesis of mussel-mimetic macromolecules bearing catechol units as their side chains are solid- or solution-phase polypeptide synthesis.[256,257] Ring opening polymerization (ROP) of catechol decorated cyclic *N*-carboxyanhydride (NCA) monomers arose within the following years as an alternative method for the synthesis of similar polymers.[258,259,260] In 1998, Deming *et*

al. presented for example the preparation of homo- and copolymers *via* ROP using protected DOPA and lysine based NCA monomers.[261] However, ROP approaches can depict some cases disadvantages such as a limited monomer scope, the requirement of inert conditions, the usage of toxic catalysts, and a low polymerization rate.[262] Thus, ROP is nowadays less frequently employed for the synthesis of side chain catechol derivatives.

Another synthesis approach that corresponds more to conventional polymerization techniques is the direct polymerization of catechol-containing vinyl monomers. Herein, especially anionic or radical polymerization processes have been implemented.[236] However, this synthetic strategy suffers from the fact that catechol is known to act as a radical inhibitor and can undergo side or chain transfer reactions.[263,264] Thus, to avoid unfavorable branching and crosslinking phenomena during the polymerization, the respective monomers are usually protected by introducing methoxy,[246] diphenyl-dioxole,[265] borax,[266] triethylsilyl (TES),[267,268] or *tert*-butyldimethylsilyl (TBDMS)[269,270] protecting groups, among others. An example for the anionic polymerization of protected catechol containing monomers was presented by Wilker *et al.* in 2023 (**Scheme 25**).[246] In this work, 3,4-dimethoxystyrene was synthesized *via* a two-step procedure and subsequently copolymerized with styrene using *n*-butyl lithium (*n*-BuLi) as initiator.[246] Upon deprotection with boron tribromide (BBr_3), the targeted catechol polymers were obtained with M_n values of up to 56 kDa.[246]

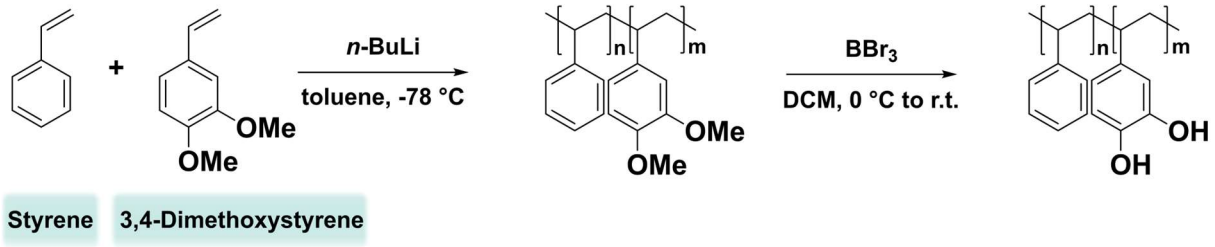

Scheme 25. General concept for the anionic copolymerization of styrene with 3,4-dimethoxy styrene and subsequent deprotection.[246]

Since anionic polymerization remain synthetically demanding, i.e. requiring strictly inert conditions as it is highly sensitive to impurities, also a high interest to introduce radical based approaches for the polymerization of protected catechol monomers evolved. Accordingly, Li *et al.* reported the synthesis of side chain derivatives obtained *via* a diphenyl-dioxole protected catechol monomer by free radical polymerization using azobisisobutyronitrile (AIBN) as an initiator.[265] The deprotection step was performed

by an acidic treatment, i.e. using a mixture of trifluoroacetic acid, hydrobromic acid, and acetic acid, at room temperature.[265] In order to access structurally well-defined side chain derivatives using radical pathways Wilker *et al.* and Topham *et al.* implemented nitroxide mediated polymerization (NMP) and reversible addition fragmentation transfer (RAFT) polymerization, respectively, as valuable synthetic tools for the synthesis of catechol containing polymers.[271,272] Indeed, Wilke *et al.* copolymerized TBDMS protected 3,4-dihydroxystyrene with styrene and 4-vinylbenzyl chloride *via* NMP targeting biomimetic adhesives with different compositions.[271] The deprotection in this work was conducted in a similar manner as described above by treating the protected parent polymer with hydrochloric acid.[271] The final polymers featuring catechol pendant groups were subsequently obtained with narrow dispersities ($1.1 \leq Đ \leq 1.3$) and molecular weights of up to 15 kDa.[271] RAFT polymerization, as a well-established controlled radical polymerization technique in synthetic polymer chemistry, was employed in a similar manner by Topham *et al.* to polymerize methoxy protected 3,4-dihydroxystyrene.[272] Upon deprotection with BBr_3, the targeted catechol containing polymers were obtained with narrow dispersities ($Đ < 1.3$) as it was expected for a controlled radical polymerization.[272]

As highlighted above, a direct polymerization of protected catechol-containing vinyl monomers appears frequently in the literature and can be considered as a well-established approach to access side chain derivatives of catechol polymers. However, this synthetic strategy does not appear as very practicable as it requires a high number of resources, i.e. chemicals, time, and money, particularly due to tedious protection and deprotection steps. Thus, it is not surprising that additional examinations regarding the polymerization of unprotected catechol-containing vinyl monomers have been conducted. Indeed, the current literature includes reports about the polymerization of unprotected catechol derivatives.[273,274,275] However, it must be stated that only the synthesis of copolymers was reported up to the present day. Herein, particularly dopamine methacrylamide (DMA) plays a major role, as it can directly be copolymerized with numerous different synthetic monomers such as acrylamides,[276] methacrylamides,[274] or methacrylates,[277] among others. An example for the copolymerization of DMA with methacrylates was published by Li *et al.* in 2014.[278] In order to synthesize materials, with potential application in multifunctional filtration membranes, DMA was directly copolymerized with 2-hydroxy-3-cardanylpropyl methacrylate (HCPM) *via* free radical polymerization (**Scheme 26**).[278]

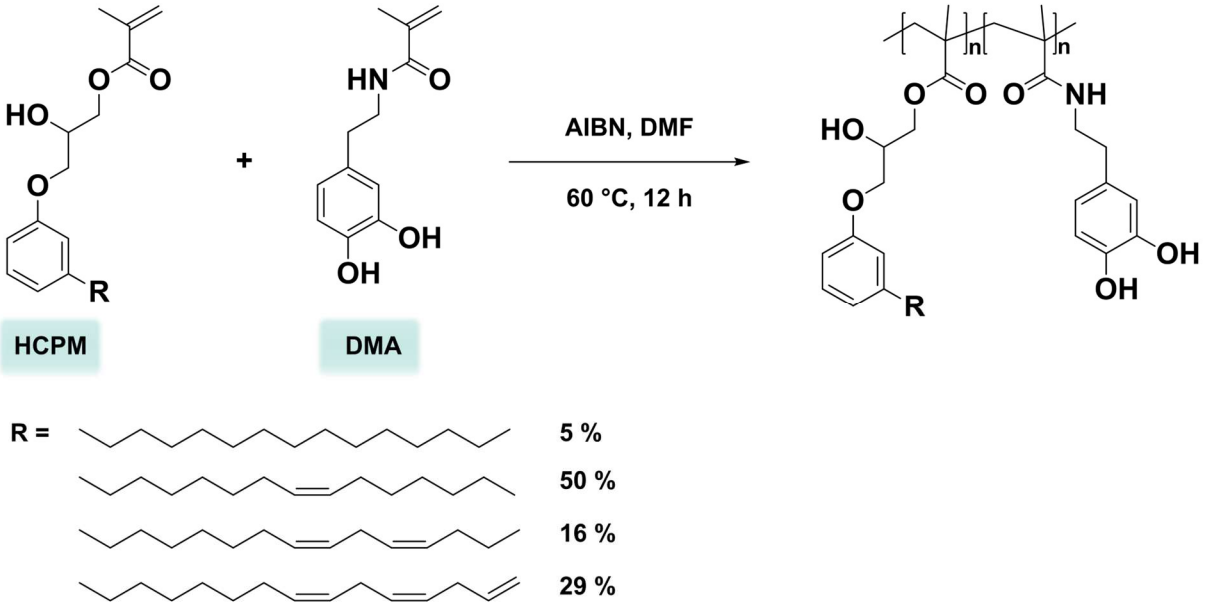

Scheme 26. General synthetic strategy for the direct copolymerization of 2-hydroxy-3-cardanylpropyl methacrylate (HCPM) with dopamine methacrylamide (DMA) *via* free radical polymerization.[278]

In a similar fashion Wilker *et al.* reported the copolymerization DMA with methyl methacrylate and poly(ethylene glycol) methyl ether methacrylate targeting biomimetic adhesives with tailored material properties.[279] Noteworthy, controlled radical polymerization approaches such RAFT can be applied for the direct copolymerization of DMA with other vinyl monomers.[280] However, the incorporation of other unprotected catechol-based vinylic monomers in addition to DMA remain difficult and rarely reported.

In general, the straightforward polymer synthesis from unprotected vinyl monomers benefits from the absence of protection and deprotection steps and requires therefore less resources. Nevertheless, the scope of integrable monomers remains limited and the occurrence of side reactions, which influence the final polymer architecture, is inevitable until now.[236,281] More precisely, the unavoidable side reactions, i.e. branching and crosslinking, can indeed be explained by the presence of unprotected catechol moieties in the polymerization approach.[281,282] It is expected that catechol units can react with carbon-centered propagation radicals forming aryloxy radicals, which can subsequently be scavenged by other carbon-entered radicals yielding intermolecular C-C or C-O bonds or simply oxidize to the respective *ortho*-quinone derivative by a loss of a hydrogen atom (**Scheme 27**).[264] The latter can then undergo again bond formation with other carbon centered radicals in the system (**Scheme 27**).[264]

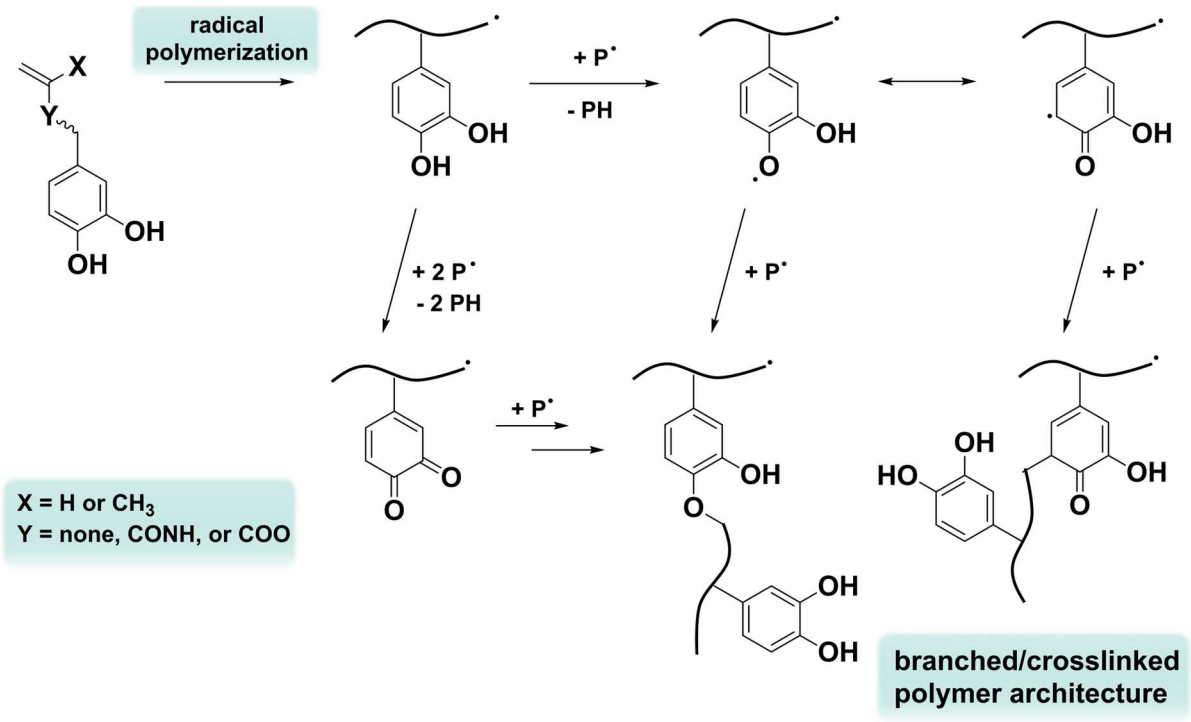

Scheme 27. Potential side and chain transfer reactions occurring during the radical (co)polymerization of unprotected catechol containing vinyl monomers.[236]

To confirm this hypotheses Kamperman *et al.* copolymerized DMA with 2-methoxyethyl acrylate (MEA) *via* free radical polymerization.[282] In this work it was investigated whether the final polymer structure is influenced by the amount of DMA, i.e. unprotected catechol units, incorporated in the polymer structure.[282] Indeed, it was observed that the dispersity, which is related to the amount of branching, of the synthesized copolymers increased with increasing DMA content.[282] Accordingly, a dependence between free catechol moieties and the occurring branching could be confirmed. Even more, when only DMA was homopolymerized, an insoluble product was obtained indicating that the formed polymers crosslinked within the polymerization process.[282] The latter result thus also explain why the synthesis of homopolymers from unprotected catechol-containing vinyl monomers remains challenging.

Nowadays, the most recognized method for the synthesis of polymers containing catechol moieties in their side chains remains post polymerization modification (PPM).[236] Herein, particularly (bio)polymers decorated with functional groups such as -NH_2, -COOH, -OH, and -CHO, among others, can be employed.[236] PPM can again be divided into *grafting-from* and *grafting-onto* approaches. *Grafting-from* approaches describe modification processes, where side chains are formed by the polymerization of monomers directly from the polymer backbone.[283] *Grafting-onto* approaches on the

other hand describe the attachment of side chains to a polymer backbone using specific organic reactions.[283] Biopolymers such as alginate,[284] gelatin,[285] hyaluronic acid,[286] and chitosan,[287] among others, but also synthetic polymers containing pendant functional units are frequently implemented in *grafting-onto* approaches to deliver side chain derivatives of catechol polymers.[288,289] Herein, amidation plays a key role and is readily applied.[236] In 2016, Kang *et al.* for example reported the direct attachment of dopamine onto alginate using carbodiimide coupling chemistry.[284] A follow up physical crosslinking using Fe^{3+} ions enabled the preparation of multilayered antibacterial alginate films.[284] However, due to the use of toxic and phosgene derived chemicals as activators the direct attachment of catecholamines *via* amidation onto (bio)polymers can be categorized as critical regarding sustainability aspects. Thus, to overcome the need for activators in amidation, another strategy involving the incorporation of activated linkages such as pentafluorophenyl,[290] nitrophenyl,[291] or *N*-hydroxy succinimide ester groups[292] into the polymer structure have been established. A recent example was presented by Seferos *et al.* polymerizing various vinyl monomers containing a pentafluorophenyl ester group, i.e. pentafluorophenyl acrylate, pentafluorophenyl methacrylate, and pentafluorophenyl 4-vinylbenzoate, *via* RAFT polymerization and subsequently attached a catecholamine, i.e. dopamine, by conducting an amidation (**Scheme 28A** and **B**).[293]

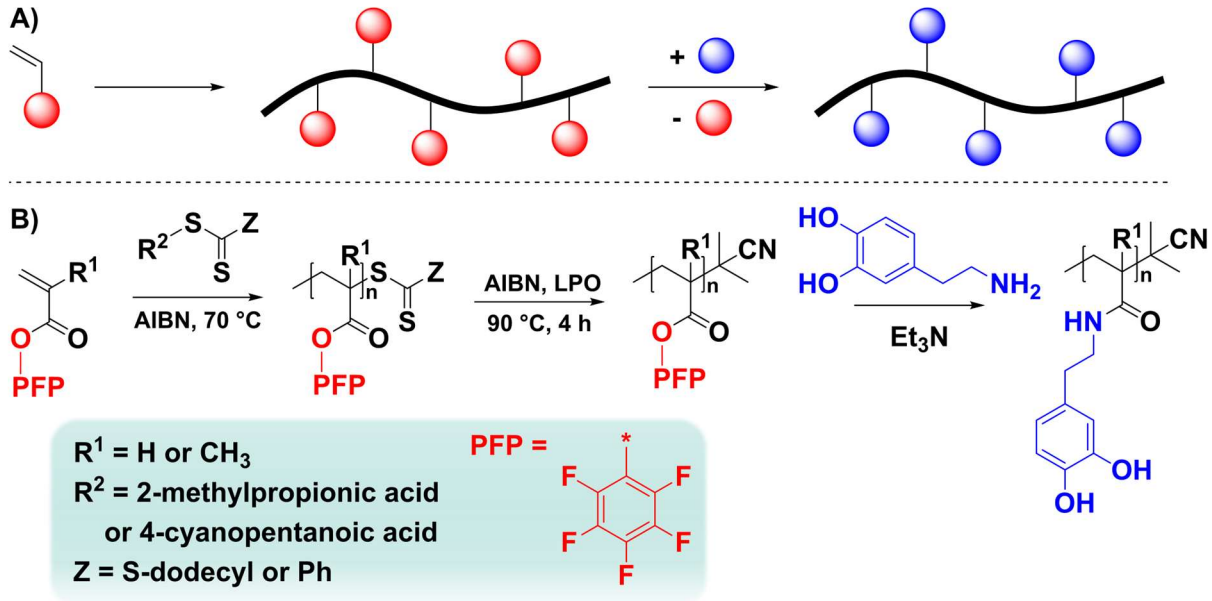

Scheme 28. A) Schematic overview for the polymerization of vinyl monomers and subsequent post polymerization modification (PPM). B) General concept for the RAFT polymerization of pentafluorophenyl ester monomers and subsequent post polymerization modification (PPM) *via* amidation with dopamine.[293]

However, the required synthesis of the respective monomers including activated functional units, their subsequent polymerization, and the actual PPM render this approach a multi-step strategy, consuming a high number of resources, i.e. chemicals, time, and money, and produce therefore also a correspondingly high amount of waste.

In addition to the most frequently employed amidation, supplemental well-established organic reactions such as thiol-ene,[294] diacetal formation,[295] epoxide opening,[296] and cross-metathesis,[297] among others, have been implemented into *grafting-onto* approaches to access side chain derivatives of catechol polymers. On the contrary, up to the present day only two approaches for the attachment of catechol derivatives onto polybutadiene exist in the current literature (**Scheme 29**).[297] In 2016, Bermesheva *et al.* synthesized catechol containing side chain derivatives by connecting TES protected eugenol onto the polymer backbone of polybutadiene *via* cross metathesis.[297]

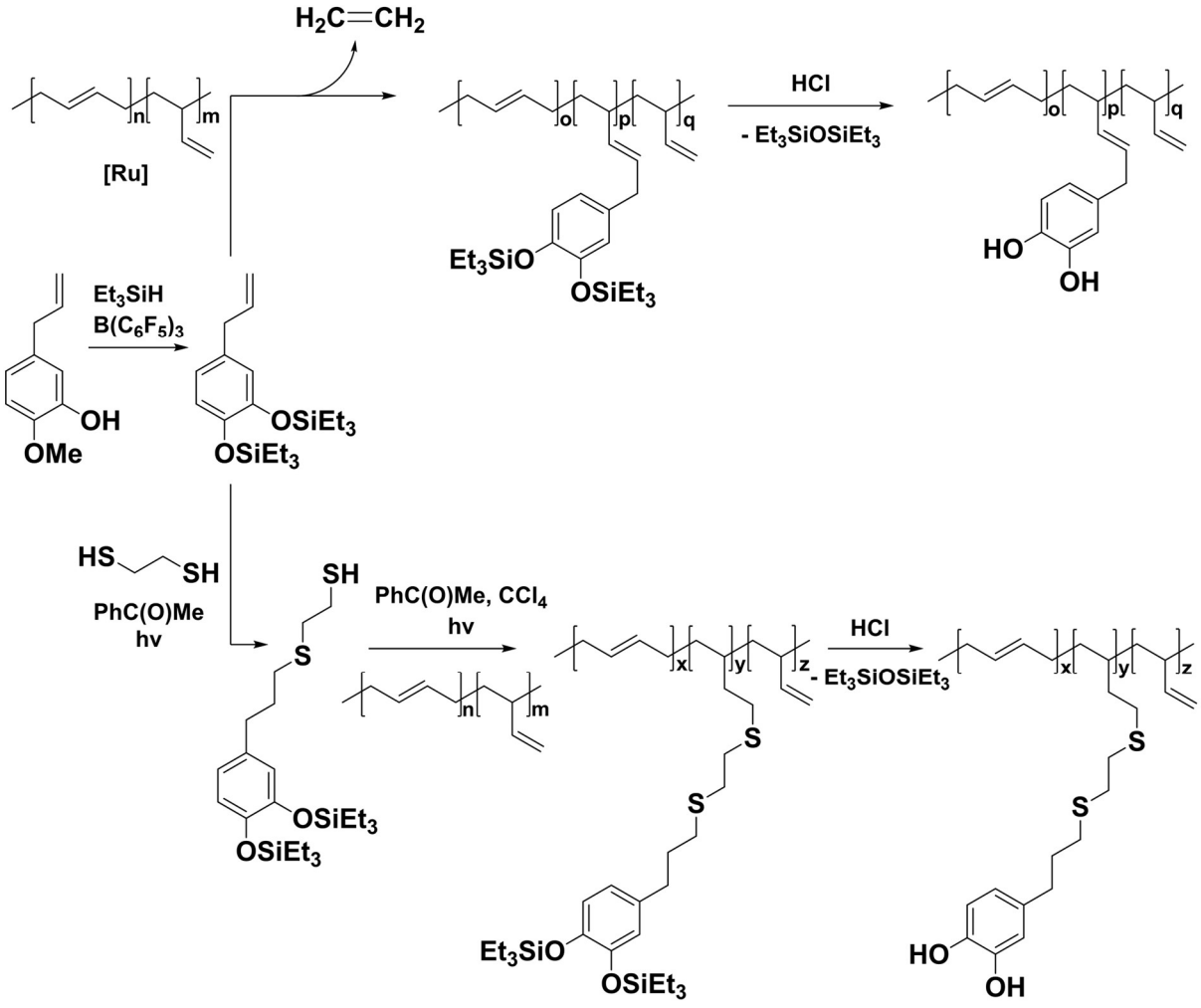

Scheme 29. General synthetic pathways for the attachment of catechol containing side chains onto polybutadiene.[297]

In this approach tedious protection and deprotection steps were necessary as the ruthenium based Grubbs catalyst form stable complexes with the free hydroxyl groups of catechol moieties and would therefore be inactivated.[298] In a second synthetic strategy, which was also described in the same manuscript, 1,2-ethane dithiol was modified monofunctionally with TES protected eugenol and subsequently attached to polybutadiene.[297] Both reaction steps were herein performed *via* thiol-ene chemistry. The targeted catechol polymer was later obtained after a final deprotection step.[297]

End Chain Derivatives

Another class of catechol polymers bearing its catechol unit(s) at the chain-end(s) are named end chain derivatives. With the development of controlled radical polymerization techniques, i.e. atom transfer radical polymerization, ring-opening metathesis polymerization, or RAFT, among others, these macromolecules achieved a high interest in the synthesis of polymer brush-modified substrates using *grafting-from* and *grafting-onto* approaches.[299,300,301] In *grafting-from* approaches the surface of the substrates is functionalized with a catechol or ply(dopamine)-based initiator or controlling agent, which enables the subsequent controlled polymerization yielding the targeted polymer brushes. Generally, a broad variety of different surfaces and substrates including carbon materials, living surfaces, low surface energy polymers and others can be used.[299,302,303] Common initiators, which are employed for different polymerization techniques in *grafting-from approaches,* are depicted in **Scheme 30**.

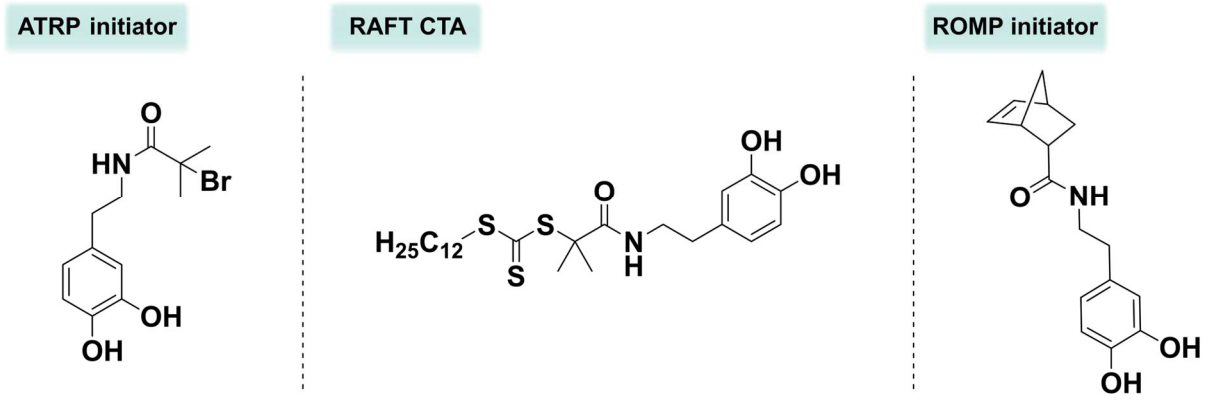

Scheme 30. Exemplary catechol containing initiators and chain transfer agents applicable in controlled radical polymerization.

The inverse way, i.e. the functionalization of substrates with polymer brushes *via grafting-onto* approaches, also appear as frequently employed tool.[304,305,306] Herein, catechol-based initiators or chain transfer agents are first employed to synthesize the

end-chain functionalized polymers, which are then attached to the surface of the desired substrate. For example, Haddleton *et al.* decorated magnetic nanoparticles with several catechol-end functionalized polymers and copolymers *via* this strategy.[307] Herein, especially the attachment of copolymers containing pendant mannose and rhodamine B units was highlighted as these side groups improve the cellular uptake and act as fluorophore, respectively, making the modified nanoparticles suitable in biomedical imaging.[307]

3 Aim

In 2015, the 17 Sustainable Development Goals (SDGs) were adopted by the General Assembly of the United Nations (UN). These goals were established to combine economic, social, and environmental interests and act as guidelines for a more sustainable global development. In this context, the SDGs target no poverty, zero hunger, affordable and clean energy, action against climate change, and the protection of biodiversity, among others, but also a decent economic growth and industrial innovation. An additional aim of the SDGs is to "*ensure the availability and sustainable management of water and sanitation for all"* (Goal 6). Nowadays, approximately 2.1 billion people have limited access to fresh drinking water, often caused by contaminated water sources. In particular, the presence of heavy metal ions, such as mercury or lead, in freshwater systems is still an occurring issue, which is generated by mineral mining or electronic waste processing, among others. Water pollution by heavy metals can especially be considered as critical due to their well-known adverse effects against aquatic habitats, agriculture, and human health.

Thus, in line with Goal 6 of the 17 SDGs, the current thesis targets the synthesis of functional (bio-based) materials for water decontamination *via grafting-onto* approaches. The polymeric materials herein designed were developed using the *Twelve Principles of Green Chemistry* as guiding framework.

Accordingly, the first chapter introduces a fast, microwave mediated modification approach for the synthesis of structurally different short-chain (mixed) cellulose esters, which found application as water purification membranes. The second chapter reveals the inverse vulcanization of fully renewable fatty acid cellulose esters, yielding high sulfur content composite materials, which were applicable for mercury removal from aqueous solutions. The third chapter presents an efficient and straightforward synthetic strategy to decorate unsaturated polymers, i.e. polybutadiene, with catechol units, delivering promising materials for water decontamination showing a high affinity for various heavy metals. The last chapter displays the synthesis of covalent adaptable networks bearing promising structural units for potential water treatment, i.e. catechol groups.

4 Results and Discussion

In this chapter, the results obtained within the current thesis are presented and discussed in detail. It is divided into four subchapters, targeting the synthesis of functional (bio-based) materials for water treatment *via grafting-onto* approaches. Chapter 4.1 introduces a rapid, microwave assisted approach for the modification of cellulose using a DMSO/TMG/CO_2 switchable solvent system that delivers short-chain (mixed) cellulose esters with variable side chain length for water purification membranes. In chapter 4.2, the inverse vulcanization of fully renewable fatty acid cellulose esters is presented, yielding high sulfur content composite materials showing an effective mercury extraction from aqueous solutions. Chapter 4.3 describes an efficient and straightforward synthetic strategy for the decoration of polybutadiene with catechol moieties and the use of the corresponding polymer in water decontamination. The final chapter 4.4 presents a synthetic approach providing a fully renewable polyol by attaching catechol moieties onto high oleic sunflower oil. A subsequent catalyst-free and solvent-free crosslinking process with a bifunctional divinyl ether yielded 100% bio-based covalent adaptable networks with potential applicability in water purification.

4.1 Structure-Property Relationships of Short Chain (Mixed) Cellulose Esters Synthesized in a DMSO/TMG/CO_2 Switchable Solvent System

The results of the current chapter and the corresponding data in the experimental section have been published before:

T. Sehn, M. A. R. Meier, *Biomacromolecules* **2023**, *24*, 5255−5264.[308]

All results related to the membrane part were performed by Jonas Dörr and Sebastian Pusse in the frame of a collaboration between the research groups of Prof. Michael A. R. Meier at Karlsruhe Institute of Technology (KIT) and Prof. Dr.-Ing. Markus Gallei at the University of Saarland.

Abstract

Increasing environmental pollution and petroleum resource depletion are important indicators for the inevitable replacement of fossil-based polymeric materials with more sustainable counterparts. Hence, the development of bio-based materials from renewable resources, such as cellulose, is of great importance. Herein, we introduce a rapid and homogenous microwave assisted synthesis of high molecular weight (59 kDa ≤ M_n ≤ 116 kDa) short chain (mixed) cellulose esters with variable acyl side chain length (2 ≤ C ≤ 8) by using a DMSO/TMG/CO_2 switchable solvent system. Accordingly, (mixed) CEs were synthesized by implementing 1,1,3,3-tetramethylguanidine into a switchable solvent system (DMSO/TMG/CO_2) and simple variation of reaction parameters, followed by in-depth structural characterization *via* IR, ^{1}H NMR, ^{13}C NMR and SEC. Examination of the structure-property relationships revealed a decrease in the glass transition temperature (177 °C ≤ T_g ≤ 204 °C), an increase in surface hydrophobicity, i.e. water contact angle (65° ≤ WCA ≤ 98°) and a decrease of young´s modulus (0.751 GPa ≤ E ≤ 1.36 GPa), with longer alkyl side chains. Selected examples, i.e. cellulose acetate, cellulose octanoate, cellulose

acetate propionate, and cellulose acetate octanoate, were additionally be used for the preparation of membranes that potentially find application in water treatment.

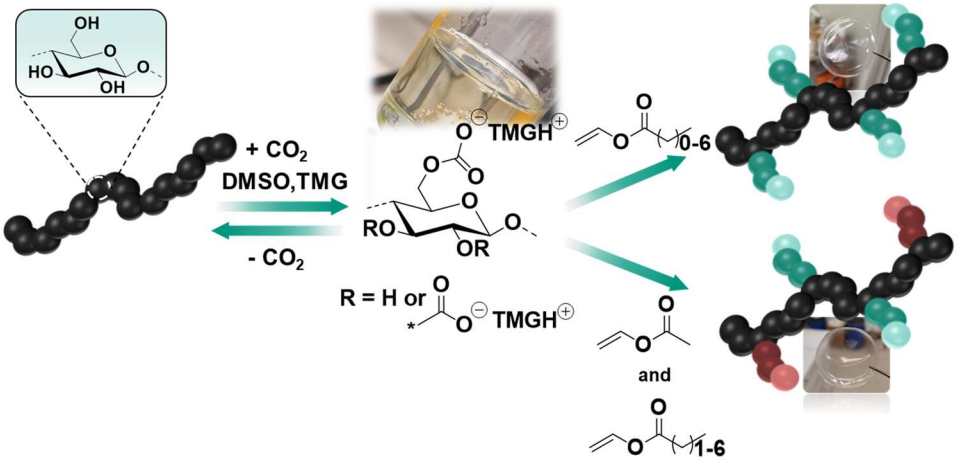

Solubilization and Derivatization of Cellulose in a DMSO/TMG/CO_2 Switchable Solvent System

CO_2 based switchable solvent systems evolved to a versatile tool for homogenous cellulose modifications.[152,309,310,311] These systems are typically based on superbases such as 1,8-diazabicyclo-[5.4.0]-undec-7-ene (DBU) or 1,5,7-triazabicyclo-[4.4.0]-dec-5-en (TBD) and a polar aprotic co-solvent like dimethyl sulfoxide (DMSO).[150,151] Although the derivative approach (see above for details) is currently established as one of the most sustainable possibilities for homogenous cellulose modification, toxicity and expensiveness of the mainly employed superbases, i.e. DBU and TBD, remain as critical points.[157] Thus, the current chapter focuses on the investigation of a cheaper and nontoxic alternative, i.e. 1,1,3,3-tetramethylguanidine (TMG), for cellulose dissolution and subsequent acylation in a CO_2 based switchable solvent system (**Scheme 31**).

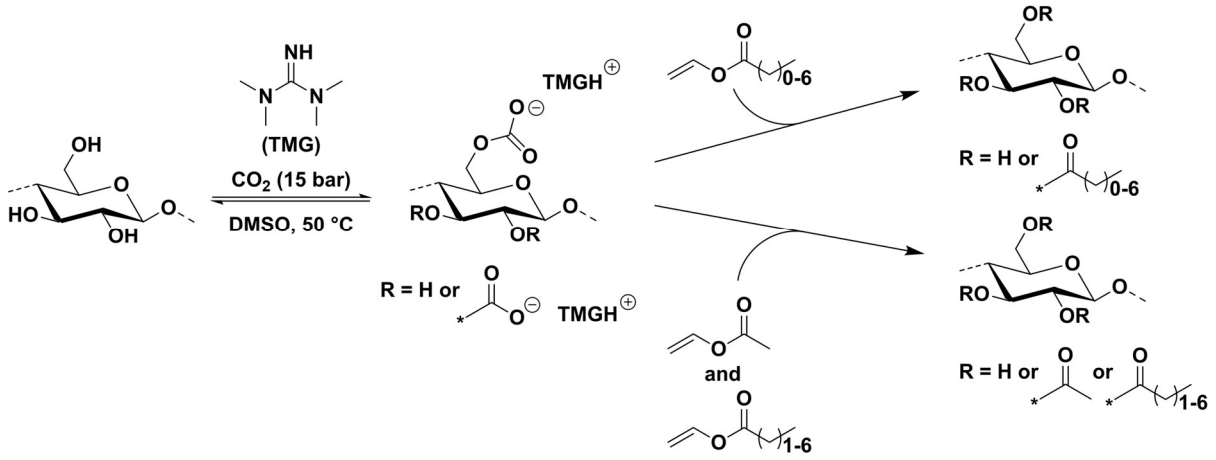

Scheme 31. Cellulose dissolution in DMSO/TMG/CO_2 switchable solvent system and subsequent transesterification reaction towards short chain (mixed) CEs. Top: CEs of different chain lengths are obtained; bottom: mixed CEs containing acetate moieties and one more, different ester, are obtained.

As a first result, we observed that microcrystalline cellulose (MCC, 3 wt%) can be quantitatively dissolved within 30 minutes in the presence of TMG and DMSO when applying a CO_2 atmosphere of 15 bars. Having this information in hand, the subsequent transesterification reaction of cellulose with vinyl acetate (VA) to yield cellulose acetate (CA) was exemplarily studied. Based on previously reported systems for homogenous CA synthesis,[157] the first acylation reactions were conducted in a DMSO/TMG/CO_2 system under traditional heating conditions for 4 hours at 60 °C. In order to optimize the reaction conditions, different parameters, i.e. VA equivalents, TMG equivalents,

heating method and reaction temperature, were investigated. Accordingly, the modification was monitored by following the characteristic carbonyl vibration band at 1740 cm^{-1} in attenuated total reflection infrared (ATR-IR) spectra and additional DS_{1H} determination *via* ^{1}H nuclear magnetic resonance (NMR) spectroscopy. It is important to mention that, in order to afford comparability of all recorded IR spectra, a normalization to the unreacted C-O vibration band of the anhydroglucose unit (~ 1040 cm^{-1}) was essential. Thus, first, the effect of VA and TMG equivalents were investigated, observing that the most promising results were obtained when VA and TMG were used in an equimolar ratio. Hence, the synthesis of **CA-1**, **CA-2**, and **CA-3** were performed with 4.50/4.50, 6.00/6.00 and 9.00/9.00 equivalents of VA and TMG, respectively. **Figure 1** reveals a gradual increase of the characteristic carbonyl vibration band around 1740 cm^{-1} for **CA-1**, **CA-2** and **CA-3**, respectively, indicating a more efficient cellulose modification when using increased VA and TMG equivalents (9.00/9.00 equiv.).

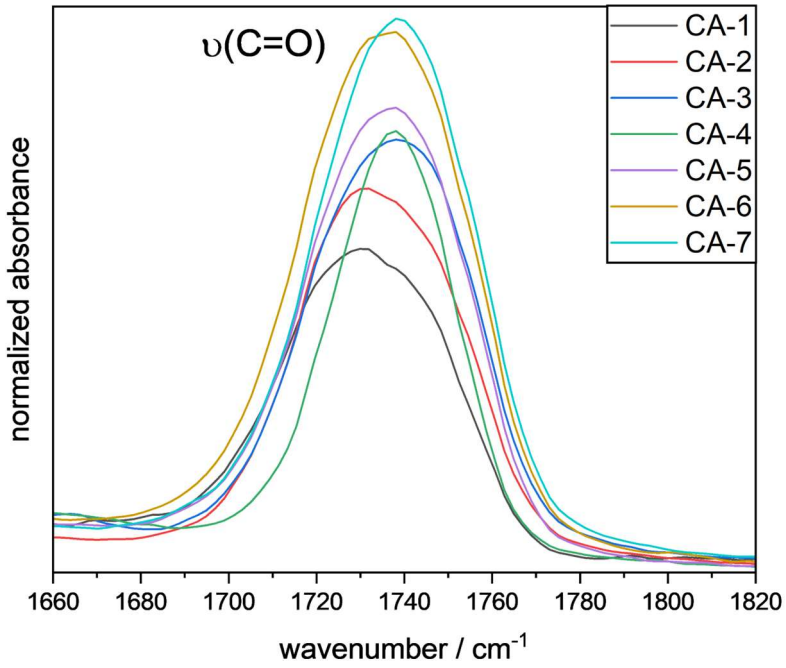

Figure 1. Expanded view of the C=O stretching vibration band for **CA1 – 7** during the optimization process.

The aforementioned trend is additionally underlined by an increase of the degree of substitution (DS_{1H}) from 0.80 (**CA-1**, **Figure S1** and **Table S1**) to 1.51 (**CA-3**, **Figure S3** and **Table S1**). Just recently, Zhu *et. al.* published a rapid microwave assisted acylation approach for cellulose by using anhydrides in a CO_2 switchable solvent

system.[312] Thus, as a second parameter, a different heating method, i.e. microwave heating, was applied. To our delight, **CA-4** could be successfully synthesized within 10 minutes at 60 °C under microwave conditions, i.e. 300 W power input. Despite the short reaction time, **CA-4** showed a more efficient modification (increased carbonyl vibration band at 1740 cm^{-1} and DS_{1H}, **Figure 1** and **Table S1**, respectively) compared to the former synthesized CAs, i.e. **CA-1** to **CA-3**, under otherwise the same conditions. The latter phenomenon, i.e. higher DS at shorter reaction time, results from the improved heat transfer efficiency during microwave irradiation.[312] Subsequently, the effect of different reaction temperatures (60 °C, 100 °C, and 140 °C) was examined. As shown in **Figure 1**, a higher reaction temperature led to a significant increase of the carbonyl vibration band at around 1740 cm^{-1}. Hence, it was not surprising that **CA-6** (140 °C) possessed the highest DS_{1H} (2.06, **Table S1**), compared to **CA-4** (60 °C) and **CA-5** (100°C). In order to finalize the optimization process, VA and TMG equivalents were further increased (to 12.0/12.0 equiv.), as the influence of this parameter was not yet investigated under microwave conditions. At this point, a further increase of functionalization (DS_{1H} = 2.34) could be detected and confirmed by ATR-IR and NMR spectroscopy (**Figure 1** and **Figure S8**). Since the latter optimization step resulted in a minor improvement of DS_{1H} (from 2.06 to 2.34, **Table S1**) and considering sustainability aspects, the investigated reaction conditions (**Scheme 31**) were applied for the subsequent synthesis of polymer libraries (**Scheme 32**).

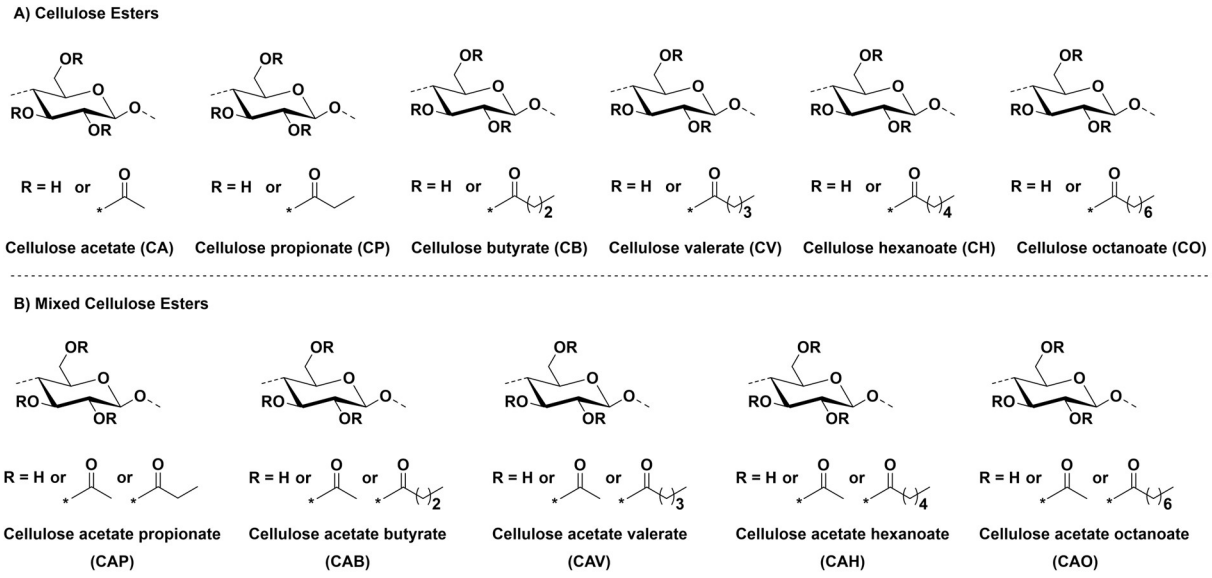

Scheme 32. Libraries of synthesized short chain (mixed) CEs in a DMSO/TMG/CO_2 switchable solvent system.

In the current work, two different polymer libraries of short chain CEs were synthesized by applying the previously described optimized reaction conditions (**Scheme 32**). Particularly, on the one hand, short chain CEs containing side chains with an equal length (using one specific vinyl ester as esterification reagent, **Scheme 32A**) and on the other hand, short chain mixed CEs including side chains with two different lengths (using VA and a second vinyl ester component as esterification reagent simultaneously, **Scheme 32B**). Initially, the structural characterization of all short chain (mixed) CEs shown in **Scheme 32** was performed *via* ATR-IR and ^{1}H NMR spectroscopy (**Figure 2** and **Figure 3**, respectively). For the synthesized short chain CEs, i.e. cellulose acetate (**CA**), cellulose propionate (**CP**), cellulose butyrate (**CB**), cellulose valerate (**CV**), cellulose hexanoate (**CH**) and cellulose octanoate (**CO**), characteristic stretching vibration bands appearing at ~1740 cm^{-1} (C=O, Figure 2A) and 1160 - 1230 cm^{-1} (C-O$_{ester}$, **Figure 2A**) in the corresponding ATR-IR spectra confirmed the successful CE formation. Additionally, a stretching vibration band arising at 2800 – 3020 cm^{-1}, which can be assigned to the CH_3 and CH_2 groups of the aliphatic side chains, underlines the success of the modification process. Furthermore, it was observed, that the intensity of the C-H stretching vibration bands (2800 – 3020 cm^{-1}) increased with the increase of the aliphatic side chain length (**Figure 2A**).

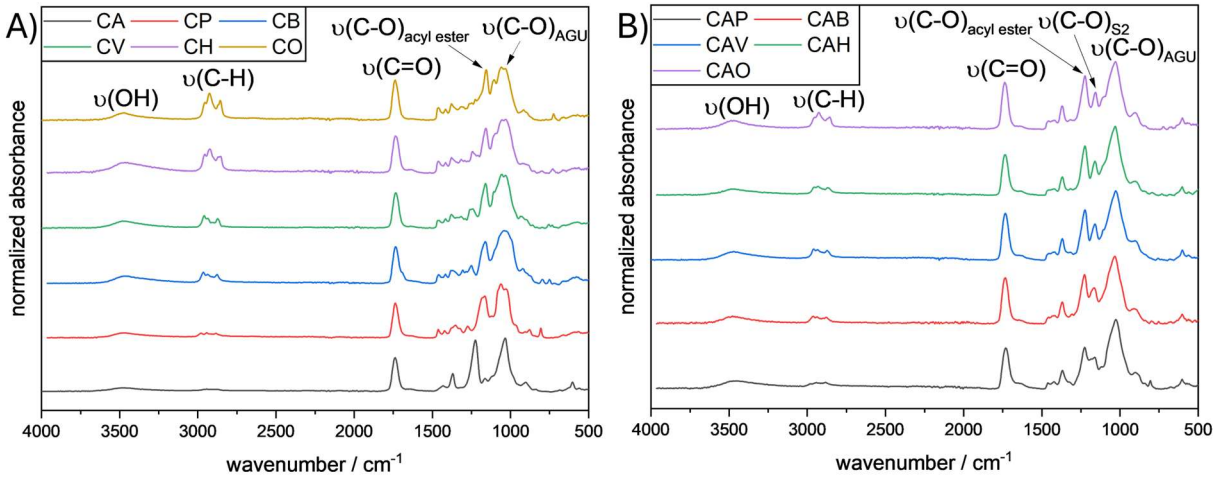

Figure 2. A) ATR-IR spectra of short chain CEs, i.e. **CA** (black line), **CP** (red line), **CB** (blue line), **CV** (green line), **CH** (violet line) and **CO** (yellow line). B) ATR-IR spectra of short chain mixed CEs, i.e. **CAP** (black line), **CAB** (red line), **CAV** (blue line), **CAH** (green line) and **CAO** (violet line).

The aforementioned characterization procedure *via* IR spectroscopy including characteristic vibration bands at 1740 cm^{-1} (C=O), 1160 – 1230 cm^{-1} (C-O$_{ester}$) and 2800 – 3020 cm^{-1} (C-H) is also applicable for short chain mixed CEs (**Figure 2B**), i.e.

cellulose acetate propionate (**CAP**), cellulose acetate butyrate (**CAB**), cellulose acetate valerate (**CAV**), cellulose acetate hexanoate (**CAH**) and cellulose acetate octanoate (**CAO**). However, as shown in **Figure 2B**, an additional vibration band arose at 1155 - 1160 cm^{-1}, which can be associated with the C-O vibration of a supplemental structurally different ester moiety. Hence, the formation of short chain mixed cellulose esters containing ester side chains with two different chain lengths is confirmed by IR spectroscopy. In a complementary way, ^{1}H NMR analysis was conducted for all synthesized short chain and mixed CEs. **Figure 3** shows that all recorded NMR spectra display a similarity by revealing the unaffected anhydroglucose unit (AGU) protons from 2.91 to 5.20 ppm. Additional magnetic resonances at 1.80 – 2.13 ppm for **CA** and 2.04 – 2.42 ppm for **CP**, **CB**, **CV**, **CH** and **CO** can be associated to the protons in α-position next to the ester moiety and thus show further evidence of successful CE formation. In the NMR spectra of mixed CEs containing two structurally different side chains (acetyl and a longer one), magnetic resonances at 1.80-2.13 ppm (-O-C(CO)-CH_3) and 2.04 – 2.42 ppm (-O-C(CO)-CH_2-) could be observed simultaneously. Hence, the formation of short chain mixed CEs including acetyl and longer side chains (3 ≤ C ≤ 8) is evidenced as well. As shown in **Figure 3A** and **B**, ^{1}H NMR spectra of CEs and mixed CEs reveal additional magnetic resonances in the high field region (0.62 – 1.65 ppm) depending on the chain length of the employed vinyl esters.

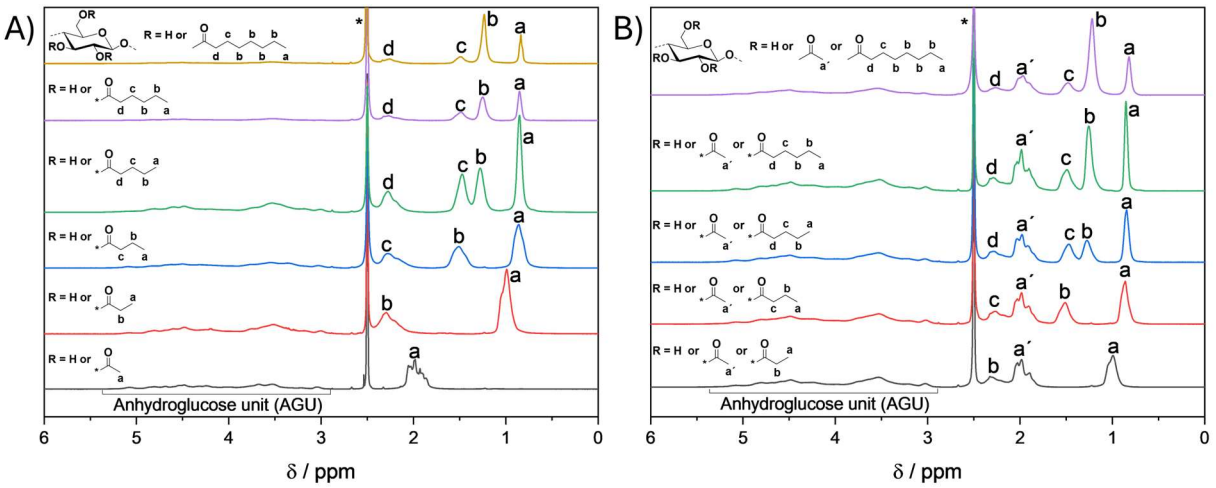

Figure 3. A) ^{1}H NMR (400 MHz) of short chain CEs, i.e. **CA** (black line), **CP** (red line), **CB** (blue line), **CV** (green line), **CH** (violet line) and **CO** (yellow line), in DMSO-d_6 (*) + TFA at ambient temperature. B) ^{1}H NMR (400 MHz) of short chain mixed CEs, i.e. **CAP** (black line), **CAB** (red line), **CAV** (blue line), **CAH** (green line) and **CAO** (violet line), in DMSO-d_6 (*) + TFA at ambient temperature.

In a complementary way, ^{13}C NMR of **CA** and **CAP** were recorded as representative examples of all synthesized CEs and mixed CEs, respectively. In particular, characteristic magnetic resonances in the low-field region at 170, 169, and 168 ppm, which can be assigned to the quaternary carbon atom of the acyl groups at C6, C3, and C2 position, respectively, confirm the successful formation of **CA** (**Figure 4A**). As shown in **Figure 4B**, additional magnetic resonances at 173, 172 and 171 ppm attributable to the -O-C(O)- moiety of propyl ester side chains provide supplemental proof for the formation of mixed CEs, i.e. **CAP**.

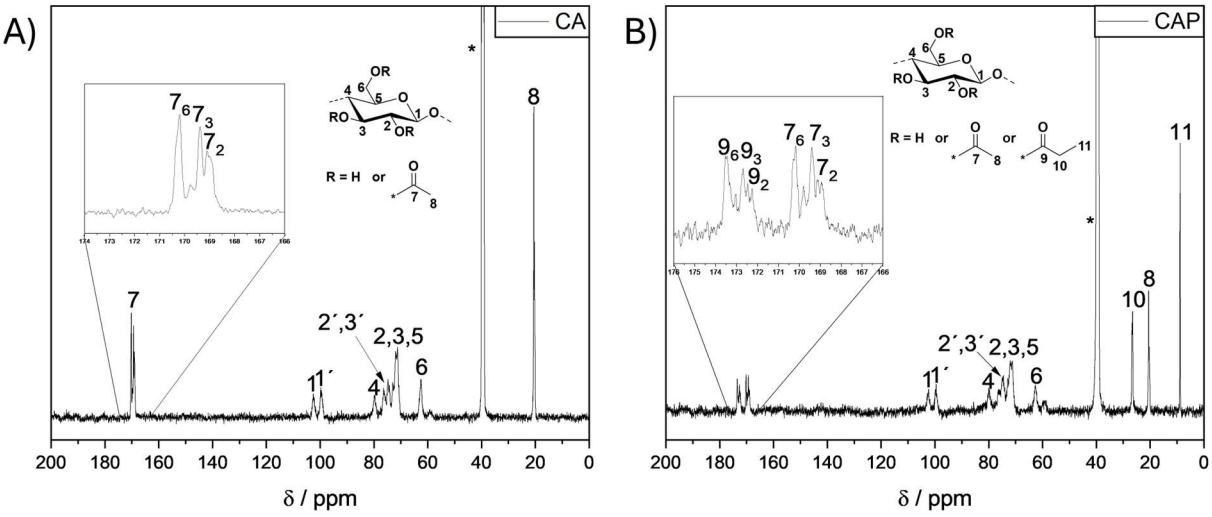

Figure 4. ^{13}C NMR (126 MHz) of **CA** (A) and **CAP** (B) in DMO-d_6 (*) at ambient temperature.

After this structural characterization, the DS of (mixed) CEs was determined according to literature known methodology *via* ^{1}H NMR in order to quantify the efficiency of the cellulose acylation approach in a DMSO/TMG/CO_2 switchable solvent system.[157] Although the current literature postulates that the maximal DS of cellulose derivatives decrease with increasing bulkiness of the attached side chains[154] this phenomenon could not be observed in the existing system. Interestingly, CEs and mixed CEs were all obtained with DS in a similar range, i.e. from 2.05 to 2.16 and 1.99 to 2.16, respectively, as shown in **Table 6**, **Figure S31** and **Figure S32**. It is also worth to mention that the incorporation ratio of VA and vinyl esters with increased chain length, i.e. vinyl propionate, vinyl butyrate, vinyl valerate, vinyl hexanoate and vinyl octanoate, in mixed CEs were determined *via* ^{1}H NMR according to **Equation S3** in chapter 6.3.2. Accordingly, it was observed that the incorporation of VA increased when an additional sterically hindered vinyl ester derivative was used. In other words, the relative content of VA in the corresponding mixed CEs increased from 53% for **CAP** to 61% for **CAO**

(**Figure S32**). Compared to CO_2-based switchable solvent systems containing superbases like DBU and TBD, the DS of acylation seems to be limited when using TMG, likely a result of two main reasons. On the one hand, TMG can undergo an amidation reaction with vinyl esters, due to its increased nucleophilicity at the N atom of the imine functionality (confirmed by ^{1}H NMR and GC-MS, **Figure S33** and **Figure S34**, respectively).[313] On the other hand, the active H atom (-C=NH) of TMG enables hydrogen bond formation among the TMG molecules, which lowers the deprotonation efficiency towards MCC drastically compared to DBU and TBD.[313] Nevertheless, comparable and high DS could efficiently obtained, enabling the investigation of structure property relationships.

Table 6. Molecular and thermal characterization data of short chain (mixed) CEs.

Sample	DS_{1H}[a]	Yield (%)[b]	M_n (kDa)[c]	$Đ$[c]	$T_{d,5\%}$ (°C)
CA	2.34	73	59	2.3	264
CP	2.15	47	65	2.2	299
CB	2.17	58	116	2.2	292
CV	2.05	46	53	2.1	325
CH	2.17	46	102	2.2	333
CO	2.16	52	77	2.4	291
CAP	2.11	61	97	2.1	309
CAB	2.13	47	104	2.1	284
CAV	1.99	39	82	2.0	300
CAH	2.16	58	80	2.2	308
CAO	2.09	41	100	2.1	305

[a]Determined for CEs and mixed CEs *via* ^{1}H NMR according to **Eqn. S1** and **S2** in SI, respectively; [b] determined gravimetrically; [c] obtained by HFIP SEC

Homogenous cellulose modification in CO2-based switchable solvent systems is known for the mild reaction conditions compared to the industrially employed heterogenous counterparts.[154] Hence, less of cellulose backbone degradation was indeed observed for homogenous modification approaches.[157] Size exclusion chromatography (SEC) confirmed high molecular weights for all synthesized CEs, i.e.

53 kDa < M_n < 102 kDa (**Table 6** and **Figure 5A**), and mixed CEs, i.e., 82 kDa < M_n < 104 kDa (**Table 6** and **Figure 5B**). For the mixed short chain CEs, multimodal SEC traces were observed, most likely due to inhomogeneous distribution of the two different acyl side chains.

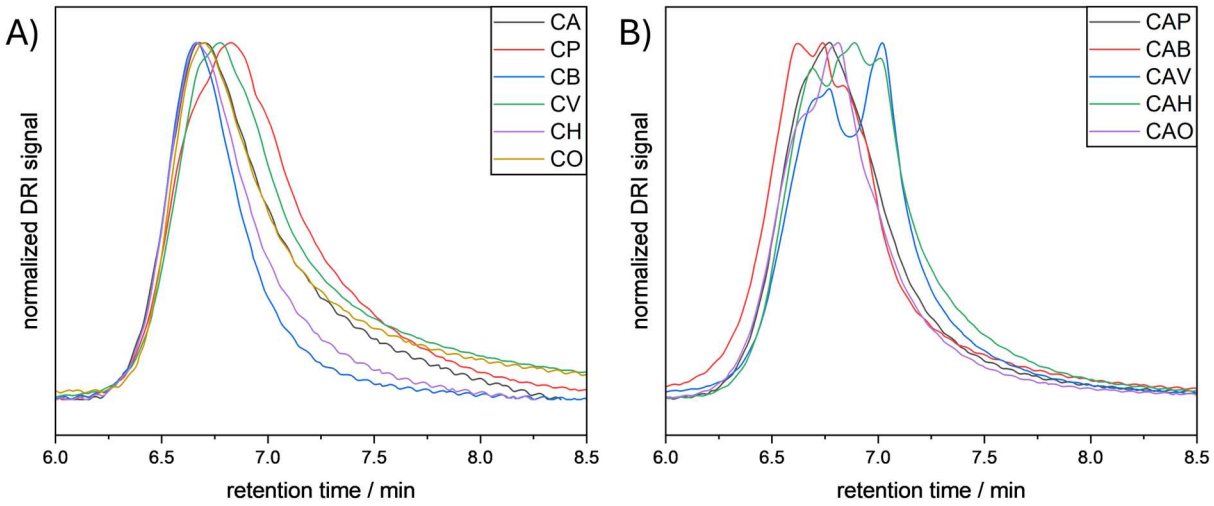

Figure 5. A) SEC traces of short chain CEs, i.e., **CA** (black line), **CP** (red line), **CB** (blue line), **CV** (green line), **CH** (violet line) and **CO** (yellow line) in HFIP + 0.1% w/v KTFA. B) SEC traces of short chain mixed CEs, i.e., **CAP** (black line), **CAB** (red line), **CAV** (blue line), **CAH** (green line) and **CAO** (violet line) in HFIP + 0.1% w/v KTFA.

Investigations of Structure-Property Relationships

In addition to the so far presented structural characterization, materials properties play an important role in polymer materials in terms of potential industrial applicability. First, the decomposition temperatures, defined as the temperatures at which 5% weight loss occurs were determined by thermogravimetric analysis (TGA) measurements. All synthesized (mixed) CEs revealed a single major degradation step in the range of 200 to 400 °C, which can be assigned to the pyrolytic decomposition of the polymer chain skeleton. As shown in **Figure S35**, **CA** reveals a lower degradation temperature ($T_{d,5\%}$ = 264 °C) compared to native cellulose ($T_{d,5\%}$ = 316 °C), due to decreased intra- and intermolecular interactions. An increase of the side chain length from C=2 (CA) to C=6 (CH) resulted in a rise of $T_{d,5\%}$ up to 333 °C (**Figure S35**). However, the aforementioned trend was not continued by **CO**, which showed a lower degradation temperature ($T_{d,5\%}$ = 291 °C). Mixed CEs showed degradation temperatures in a similar range from 300 °C (**CAV**) to 308 °C (**CAP**) except for **CAB**, which possesses a lower one ($T_{d,5\%}$ = 284 °C, **Figure S36**). Complementary to TGA, differential scanning calorimetry (DSC) measurements were conducted for all CEs and mixed CEs. An amorphous state for all

synthesized CEs in a temperature range of -20 to 250 °C by only revealing glass transitions (**Figure 6A** and **B**) was observed. Thus, thermal characteristics are stated by the corresponding glass transition temperatures (T_g). According to the internal plasticizer effect already known from literature,[314] it was found that T_g decreased with increasing side chain length from 203 °C (**CA**) to 172 °C (**CB**) for CEs and from 204 °C (**CAP**) to 177 °C (**CAO**) for mixed CEs. An increased molecular size of n-alkyl side groups increasingly limits the formation of inter- and intramolecular interactions (here hydrogen bonding of the cellulose backbone) and hence promotes backbone motion.[312,315,316]

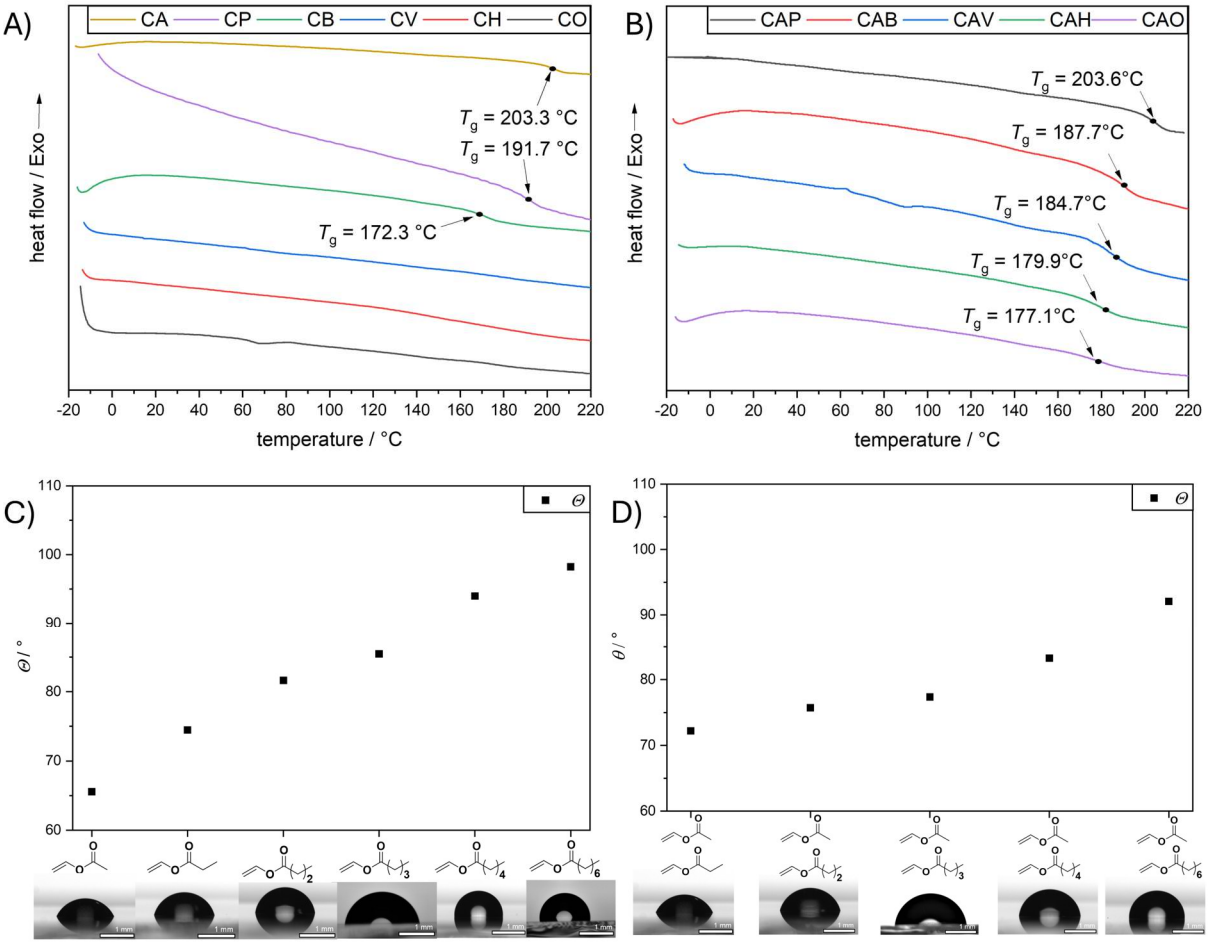

Figure 6. A) DSC studies (second heating run) of short chain CEs, i.e., **CA** (yellow line), **CP** (violet line), **CB** (green line), **CV** blue line), **CH** (red line) and **CO** (black line) from -20°C to 220 °C with a heating rate of 20 °C min^{-1} under a nitrogen flow. B) DSC studies (second heating run) of short chain mixed CEs, i.e., **CAP** (black line), **CAB** (red line), **CAV** (blue line), **CAH** (green line) and **CAO** (violet line) from -20°C to 220 °C with a heating rate of 20 °C min^{-1} under a nitrogen flow. C) Static WCA measurements of short chain CEs at ambient conditions. D) Static WCA measurements of short chain mixed CEs at ambient conditions.

For **CV**, **CH**, and **CO**, no thermal transitions were observed, which can be attributed to the poor cellulose backbone interactions. More precisely, due to the limited inter- and intramolecular interactions, i.e. hydrogen bonding, in **CV**, **CH**, and **CO**, a T_g was not detectable for these polymers. In addition to thermal characterization, the wettability properties of the synthesized materials were investigated by static water contact angle (WCA) measurements. Current literature postulates that particularly the introduction of long alkyl side chains, such as fatty acids, as well as the DS results in a significant influence regarding the hydrophobicity of CEs. Nevertheless, as to our knowledge, the dependence of WCA on the side chain length is only reported for long chain cellulose esters (C ≥ 6) containing low DS.[317] Therefore, the structure-property relationship of side chain length and hydrophobicity was studied separately for short chain CEs (2 ≥ C ≥ 8) and short chain mixed CEs (2 ≥ C ≥ 8). The incorporation of longer alky side chains resulted in a linear increase of WCA, i.e. in hydrophobicity, for short chain CEs and short chain mixed CEs (**Figure 6C** and **D**, respectively). More specifically, the WCA of short chain CEs increased from 65° for **CA** to 98° for **CO** (ΔWCA = 33°, **Figure 6C**) and of short chain mixed CEs from 72° for **CAP** to 92° for **CAO** (ΔWCA = 20°, **Figure 6D**). Subsequently, tensile strength measurements of mixed short chain cellulose esters, i.e. **CAP** to **CAO**, have been performed (**Figure 7**).

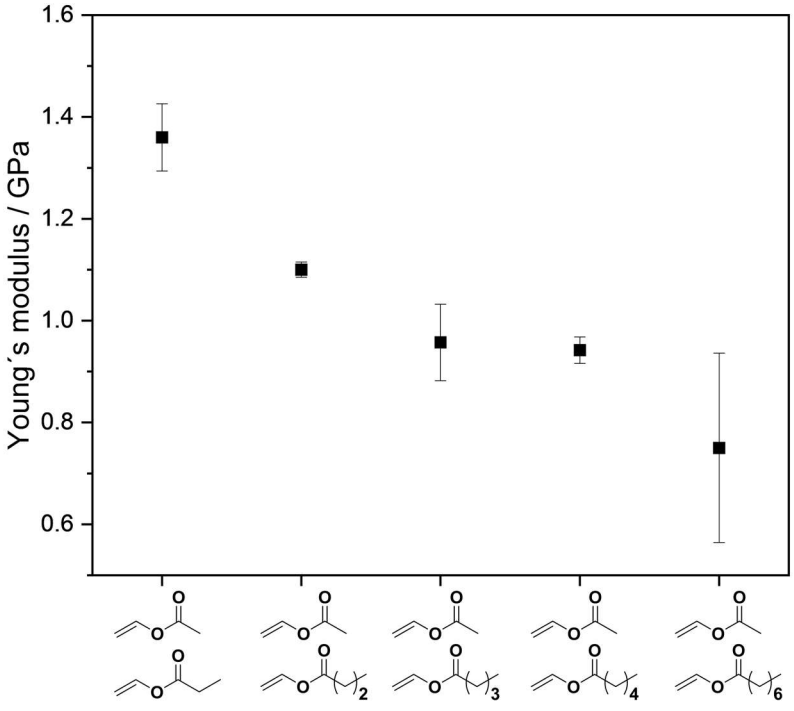

Figure 7. Young´s moduli of mixed short chain cellulose esters at ambient conditions.

According to the previously described internal plasticizer effect, it was observed that the Young´s moduli of the respective materials decreased with increasing length of the second incorporated ester side chain from 1.36 GPa for **CAP** to 0.751 GPa for **CAO** (**Figure 7**). On a molecular level, the incorporation of longer side chains decreases intra- and intermolecular interactions between the cellulose backbones, i.e. mainly hydrogen bonding, and thus leads to a loss in the Young´s modulus.

Membrane Preparation

The 32 billion USD membrane market is nowadays dominated by synthetic fossil-based polymers such as PVDF, due to their outstanding performance.[318] However, in recent years particularly CA as a more sustainable alternative has gained an increased attention as valuable material for membranes (see chapter 2.2.3). Thus, as a continuation of the previously conducted work, in collaboration with partners from the University of Saarbrücken, we investigated if selected CEs would be suitable materials for membrane preparation. Accordingly, structurally different (mixed) CEs containing short and long alkyl side chains, i.e. **CA**, **CO**, **CAP**, and **CAO**, were implemented as starting materials into the so-called nonsolvent induced phase separation (NIPS) method, targeting cellulose-based membranes. Herein, the polymers were solubilized in an appropriate solvent, i.e. DMSO or DMAc, the solution was added onto a solid support and subsequently the entire system was put into a coagulation bath containing an antisolvent, i.e. water. Preliminary results revealed that the NIPS method delivered membranes for all employed CEs. Herein, scanning electron microscopy (SEM) revealed the most promising results for **CA** and **CAO,** as these CE yielded porous structures revealing the fewest number of defects and a narrow pore size distribution. Frist successful permeance measurements of the **CA**- and **CAO**-derived membranes also underlined their potential applicability in water purification processes. Accordingly, the ongoing research focuses now on the search for potential adsorbents, i.e. hormones, proteins, pharmaceuticals, and dyes, among others, which could be removed from water streams by using these membranes.

Conclusion

In the first chapter, a rapid homogeneous microwave assisted synthesis of short chain (mixed) cellulose esters (CEs) with high molecular weight (59 kDa ≤ M_n ≤ 116 kDa) and variable acyl side chain length (2 ≤ C ≤ 8) was developed in a DMSO/TMG/CO_2

switchable solvent system. Thus, 1,1,3,3-tetramethylguanidine was first implemented into the switchable solvent concept for cellulose esterification as a cheap and nontoxic alternative superbase. Upon the quantitative dissolution of cellulose and the optimization of the subsequent transesterification reaction with vinyl acetate, two polymer libraries including short chain CEs and short chain mixed CEs were synthesized. In-depth structural characterization of (mixed) CEs *via* IR, ^{1}H NMR, ^{13}C NMR and SEC confirmed the successful formation within 10 minutes. The homogenous modification approach yielded (mixed) CEs with similar DS, i.e. $2.05 \leq DS \leq 2.34$ (CEs) and $1.99 \leq DS \leq 2.16$ (mixed CEs), which affords a comparability of materials properties. Thus, in order to understand structure property relationships, all synthesized CEs were investigated regarding their thermal characteristics (*via* DSC and TGA) and wettability (*via* WCA). For mixed short chain cellulose esters, mechanical properties (tensile strength) have also been investigated. After detailed characterization of the structure-property relationships, membranes of **CA**, **CO**, **CAP** and **CAO** were synthesized using the NIPS method and subsequently characterized by SEM and permeation measurements.

4.2 High Sulfur Content Composite Materials from Renewable Fatty Acid Cellulose Esters (FACE) *via* Inverse Vulcanization

The results of the current chapter and the corresponding data in the experimental section have been published before:

T. Sehn, J. Fanelli, L. Wahl, M. A. R. Meier, *RSC Sustainability* **2025**, *3*, 291–299.[319]

The author was responsible for the conceptualization of the project, investigation, formal analysis, and writing of the original draft.

J. Fanelli (“wissenschaftliche Hilfskraft”) and L. Wahl (Bachelor thesis supervised by the author) contributed to the synthetic part of the work, i.e. synthesis of the starting materials and high sulfur content composite materials.

Abstract

Herein, we introduce an efficient inverse vulcanization of fully renewable cellulose-based monomers. Therefore, biobased fatty acid cellulose esters with different degrees of substitution (0.38 ≤ DS ≤ 0.62) were inversely vulcanized to obtain high sulfur content composite materials (~95 wt% sulfur). In-depth structural characterization of the crosslinked sections *via* differential scanning calorimetry, thermogravimetric analysis, energy dispersive X-ray spectroscopy, and scanning electron microscopy revealed an increased amount of covalently incorporated sulfur (5.67 wt% ≤ sulfur wt% ≤ 56.2 wt%) with a higher degree of substitution of fatty acid cellulose ester. Investigating structure-property relationships further revealed an increase in thermal stability (227 °C ≤ $T_{d,5\%}$ ≤ 247 °C) accompanied by a decreased wettability (87° ≤ Θ ≤ 99°) with higher degree of substitution. The obtained materials showed application possibilities for water purification, i.e. for mercury extraction (70 % ≤ $Hg^{2+}_{removal}$ ≤ 95 %).

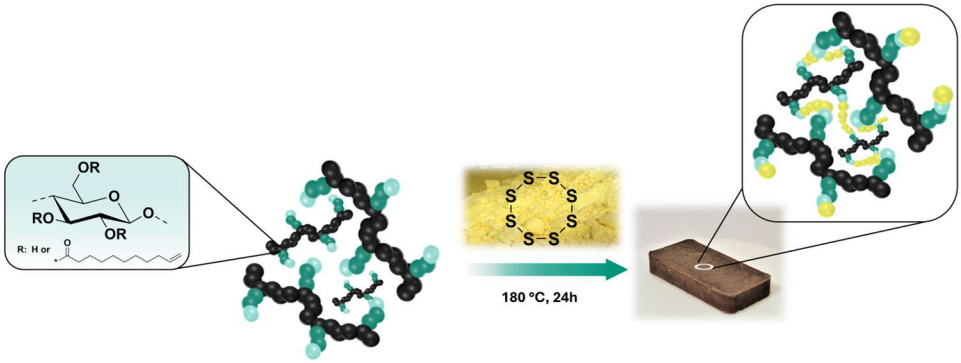
OR
O
RO
O
OR
R: H or
180 °C, 24h

Synthesis and Characterization of Fatty Acid Cellulose Esters (FACEs)

Using the so-called derivative approach for cellulose modification in a DMSO/TBD/CO_2 switchable solvent system, cellulose (microcrystalline, dried at 100 °C at 10 mbar overnight) was esterified with biobased methyl-10-undecenoate (**Scheme 33A**). By applying different amounts of methyl-10-undecenoate (i.e. 0.66, 1.16, and 3.00 equivalents), **FACE-1**, **FACE-2** and **FACE-3**, respectively, were obtained.

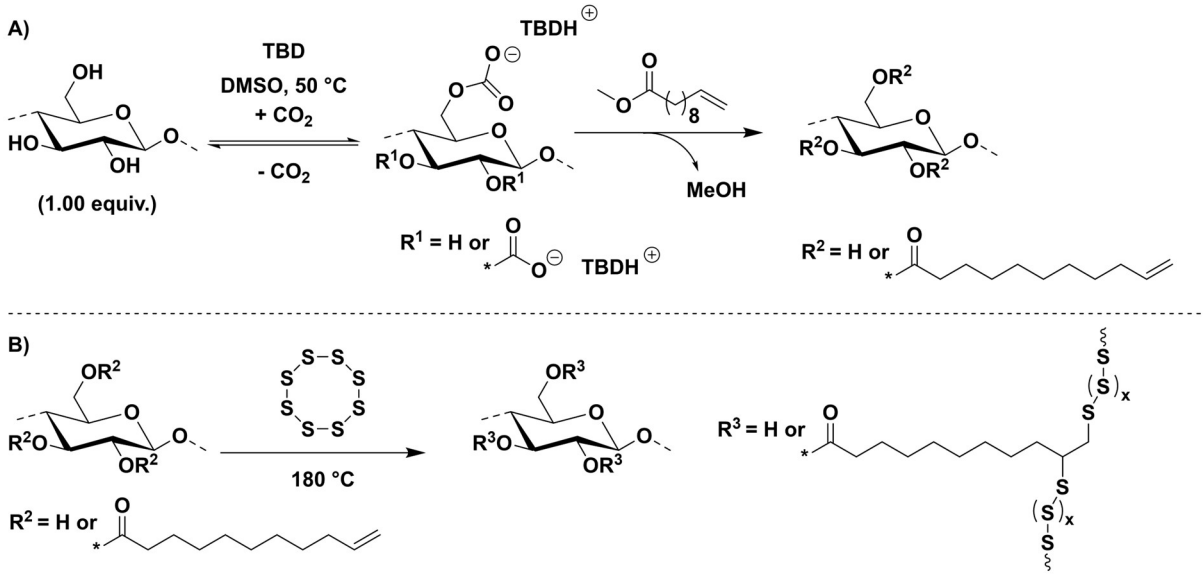

Scheme 33. (A) General concept for cellulose dissolution in a DMSO/TBD/CO_2 switchable solvent system with subsequent transesterification using methyl-10-undecenoate to fatty acid cellulose esters (FACE). (B) Synthetic approach for the inverse vulcanization of FACE towards high sulfur content composite materials.

The structural characterization of these FACEs was performed by attenuated total reflection infrared (ATR-IR) spectroscopy supplemented by ^{1}H and ^{31}P nuclear magnetic resonance (NMR) spectroscopy. ATR-IR spectra of all synthesized FACEs (**Figure 8**) revealed characteristic stretching vibration bands at ~1641 cm^{-1} (C=C) and ~1730 cm^{-1} (C=O), indicating the successful incorporation of ester and alkene functional groups into cellulose. In ^{1}H NMR (**Figure S37**,**Figure S39** and **Figure S41**), magnetic resonances appearing from 2.95 to 5.64 ppm, assigned to the unmodified protons of the anhydroglucose unit (AGU), and magnetic resonances at 4.97 ppm and 5.80 ppm, attributed to the introduced double bond protons, additionally confirmed the success of the synthetic approach. The following degree of substitution (DS) determination of the synthesized FACE materials was conducted according to an established ^{31}P NMR spectroscopy method.[320] Thus, the free hydroxyl groups of the respective FACE were converted into phosphite esters by reaction with the

phosphitylation agent 2-chloro-4,4,5,5-tetramethyl-1,3,2-dioxaphospholane (2-Cl-TMDP).

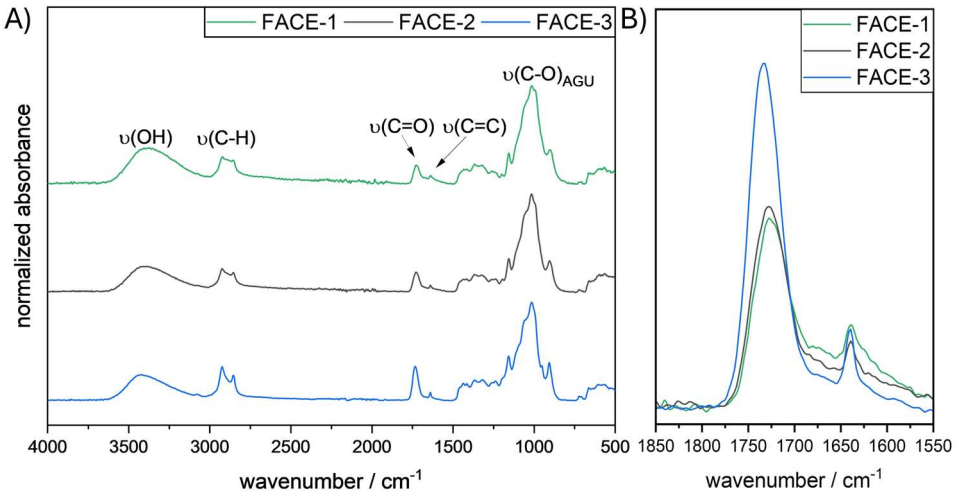

Figure 8. (A) ATR-IR spectra of **FACE-1** (green line), **FACE-2** (black line), and **FACE-3** (blue line). (B) Expanded view of the C=O and C=C stretching vibration bands for **FACE-1** (green line), **FACE-2** (black line), and **FACE-3** (blue line).

A subsequent quantitative determination of the corresponding phosphite esters *via* ^{31}P NMR spectroscopy using an internal standard (*endo*-*N*-hydroxy-5-norbornene-2,3-dicarboximide) allowed the calculation of the average DS as previously reported by Kilpeläinen *et al.* (**Figure S38**, **Figure S40**, **Figure S42**, **Eqn. S7**, and **S8**).[320] Unsurprisingly, the DS of the synthesized FACE correlated with the amount of employed transesterification agent, i.e. methyl-10-undecenoate. Thus, **FACE-1** appeared as the material with the lowest DS, i.e. 0.38, followed by **FACE-2** (DS = 0.42) and **FACE-3** (DS = 0.62), respectively. Conventional inverse vulcanization is usually conducted at elevated temperatures above 160 °C. Therefore, to evaluate if the synthesized FACEs can potentially be employed as comonomers for inverse vulcanization, the thermal properties of the respective materials were investigated *via* thermogravimetric analysis (TGA, **Figure S43**) and differential scanning calorimetry (DSC, **Figure S44**). As shown in **Figure S43** in chapter 6.4.4, TGA curves revealed a higher thermal stability for FACE with lower DS. The higher degradation temperatures, which are defined as the temperature of 5% weight loss ($T_{d,5\%}$), can be explained by the inherently existing strong intra- and intermolecular interactions (predominantly hydrogen bonding) between the hydroxyl groups of the cellulose backbones. An increased amount of incorporated bulky alkyl side chains, i.e. a higher DS, affords a partial interruption of the intra- and intermolecular interactions between the cellulose

backbones and therefore explains the slightly lower thermal stability of **FACE-3** ($T_{d,5\%}$ = 221 °C). DSC measurements of all synthesized FACEs did not show any thermal transition. Size exclusion chromatography (SEC) was performed to determine the molecular weight of the FACEs. Unfortunately, **FACE-1** was not soluble in the available SEC eluent, i.e. hexafluoro isopropanol (HFIP), and therefore no measurement could be conducted. SEC traces of **FACE-2** and **FACE-3** (**Figure S45**) revealed high molecular weights (53 kDa ≤ M_n ≤ 64 kDa; 1.85 ≤ $Đ$ ≤ 1.99), a result of the mild reaction conditions during the modification approach using the switchable solvent system,[157] i.e. less backbone degradation, which is also beneficial for the materials properties. The thermal and structural characterization of the FACEs revealed that they are potential fully renewable comonomers for inverse vulcanization, which was an aim of this study (**Scheme 33B**).

Network Structure Investigations

The corresponding FACEs (5 wt%) were mixed with elemental sulfur (95 wt%) and reacted for 24 h at 180 °C. The optical appearance of the final composite materials, i.e. **FACE-1S**, **FACE-2S** and **FACE-3S** (**Figure 9**) was brown to black. At this point it is worth mentioning that the synthesis of the cellulose-based high sulfur content composite materials was achieved without the employment of any solvent, toxic chemicals, purification steps, and most importantly without the production of any waste, thus an E-Factor of 0 is the result of this synthesis procedure.

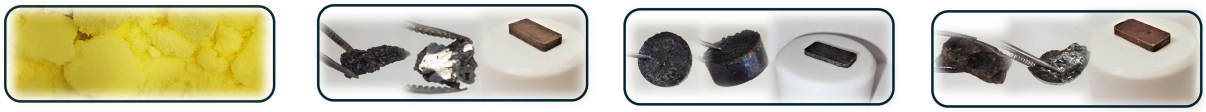

Figure 9. Optical appearance of the synthesized high sulfur content composite materials **FACE-1S**, **FACE-2S**, and **FACE-3S.**

First, the thermal properties of the obtained inverse vulcanizates were investigated by conducting DSC measurements (**Figure 10**). Herein, the synthesized composite materials revealed a thermal transition, i.e. a significant melting peak, at 120 °C, indicating the presence of unreacted crystalline elemental sulfur. Accordingly, DSC measurements did not confirm if the expected reaction between the FACE comonomers and elemental sulfur proceeded successfully.

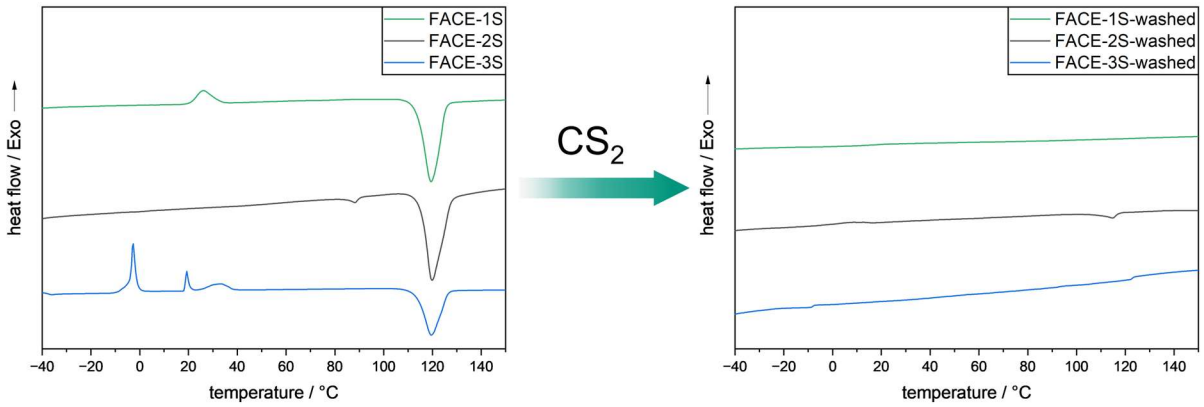

Figure 10. DSC studies of **FACE-1S** (green line), **FACE-2S** (black line), and **FACE-3S** (blue line) before and after the washing step with CS_2.

For a more detailed understanding of the networks structure, unreacted elemental sulfur was thus removed from the synthesized materials to obtain and characterize the formed crosslinked networks. Hence, a washing procedure implementing carbon disulfide (CS_2), which is known to dissolve elemental sulfur at room temperature, was applied to the obtained inverse vulcanizates. Subsequent DSC measurements of the potentially crosslinked residual materials, i.e. **FACE-1S-washed**, **FACE-2S-washed**, and **FACE-3S-washed**, did not show any melting peak at 120 °C (**Figure 10**), indicating that no crystalline elemental sulfur remained after the washing procedure. However, potentially covalent incorporation of sulfur could not be confirmed *via* DSC. Interestingly, a two-step degradation behavior was observed by TGA after sulfur extraction (**Figure 11A**).

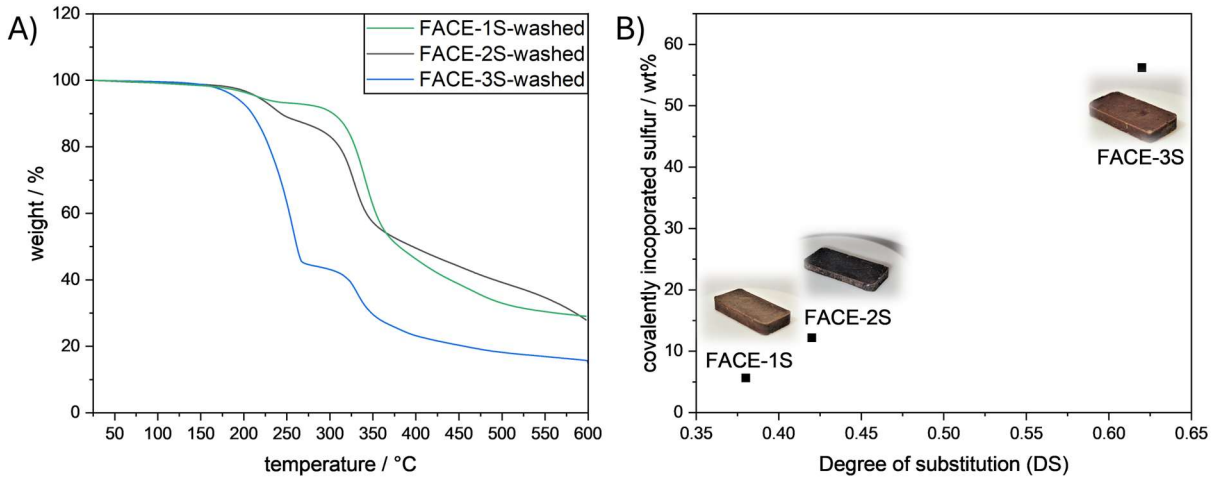

Figure 11. A) TGA curves of **FACE-1S-washed** (green line), **FACE-2S-washed** (black line), and **FACE-3S-washed** (blue line) from 25 to 600 °C with a heating rate of 10 K min^{-1} under a nitrogen flow. B) Correlation between covalently incorporated sulfur and DS of the starting materials, i.e. **FACE-1**, **FACE-2**, and **FACE-3**.

It can be assumed that the first degradation step corresponds to the degradation of covalently incorporated S-S moieties, whereas the second one is attributed to the degradation of the FACE backbone. Correspondingly, with increasing DS of the FACEs, the intensity of the first degradation step (corresponding to the decomposition of S-S bonds) also increased from 5.64 wt% in **FACE-1S-washed** to 56.2 wt% for **FACE-3S-washed**. In other words, the amount of covalently incorporated sulfur related to the DS of the employed FACE comonomer and increased with increasing DS (**Figure 11B**). The previously investigated phenomenon might be explained by the more hydrophobic character of the FACE containing higher DS, which enabled an improved solubility in molten sulfur and thus a more efficient reaction, i.e. covalent implementation of sulfur. In order to verify the presence of covalently incorporated sulfur in the residue materials, **FACE-XS-washed** (X = 1, 2 or 3) were investigated by energy-dispersive X-ray (EDX) spectroscopy. EDX spectra of the FACE comonomers before inverse vulcanization revealed characteristic bands for the elements carbon and oxygen (**Figure 12A**), which was expected according to their chemical structure (depicted in **Scheme 33A**). Additional bands for **FACE-XS-washed** particularly appeared between 2.0 and 2.5 keV (**Figure 12A**), confirming the existence of sulfur in the washed materials. The absence of sulfur crystals in supplemental SEM images of the previously mentioned residue materials combined with smooth surface areas confirmed that the sulfur species, which were detected by EDX, were covalently incorporated (**Figure 12B**).

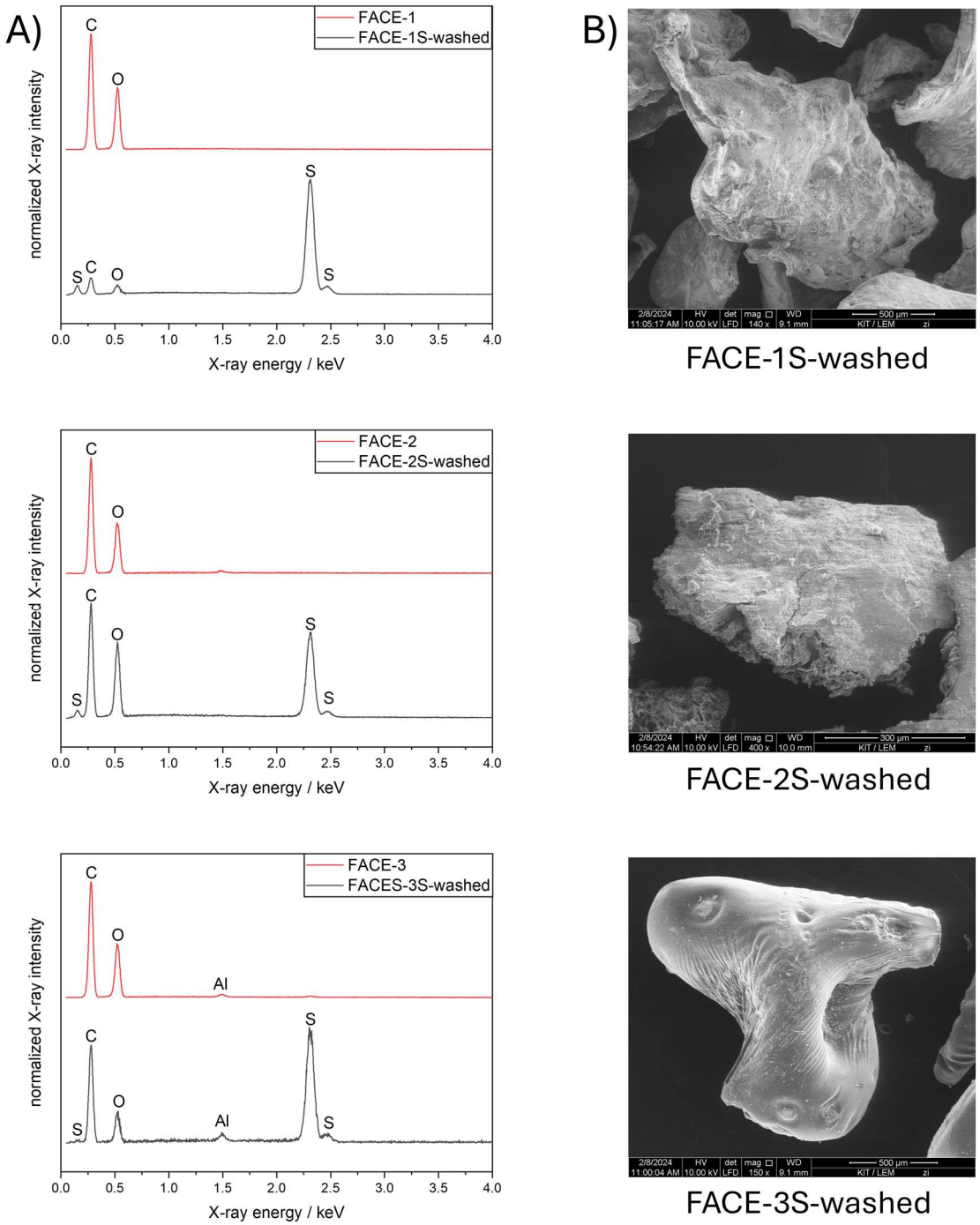

Figure 12. A) EDX spectra of the starting materials, i.e. **FACE-1**, **FACE-2**, and **FACE-3**, and washed high sulfur content composite materials, i.e. **FACE-1S-washed** (top), **FACE-2S-washed** (middle), and **FACE-3S-washed** (bottom). B) SEM images of high content composite materials after washing with CS_2.

Investigations of Structure-Property Relationships

After understanding the formed network structure and confirming that cross-linked composite materials were formed, structure property-relationships were examined. An increased degradation temperature (temperature at which 5% weight loss occurred) was observed by TGA if FACEs with higher DS were incorporated as comonomers (**Figure 13A**). More precisely, **FACE-1S** (DS_{FACE-1} = 0.38) revealed the lowest degradation temperature ($T_{d,5\%}$ = 227 °C) followed by **FACE-2S** ($T_{d,5\%}$ = 233 °C) and **FACE-3S** ($T_{d,5\%}$ = 247 °C), respectively. The improved thermal stability of the composite materials including FACEs with higher DS resulted from the increased amount of covalently bonded sulfur (5.67, 12.2 and 56.2 wt% for **FACE-1S**, **FACE-2S**, and **FACE-3S**, respectively) and thus more extensive crosslinking. Interestingly, the composite materials show a one- step degradation behaviour, resulting from the high sulfur content that prevents the observation of the FACE degradation step.

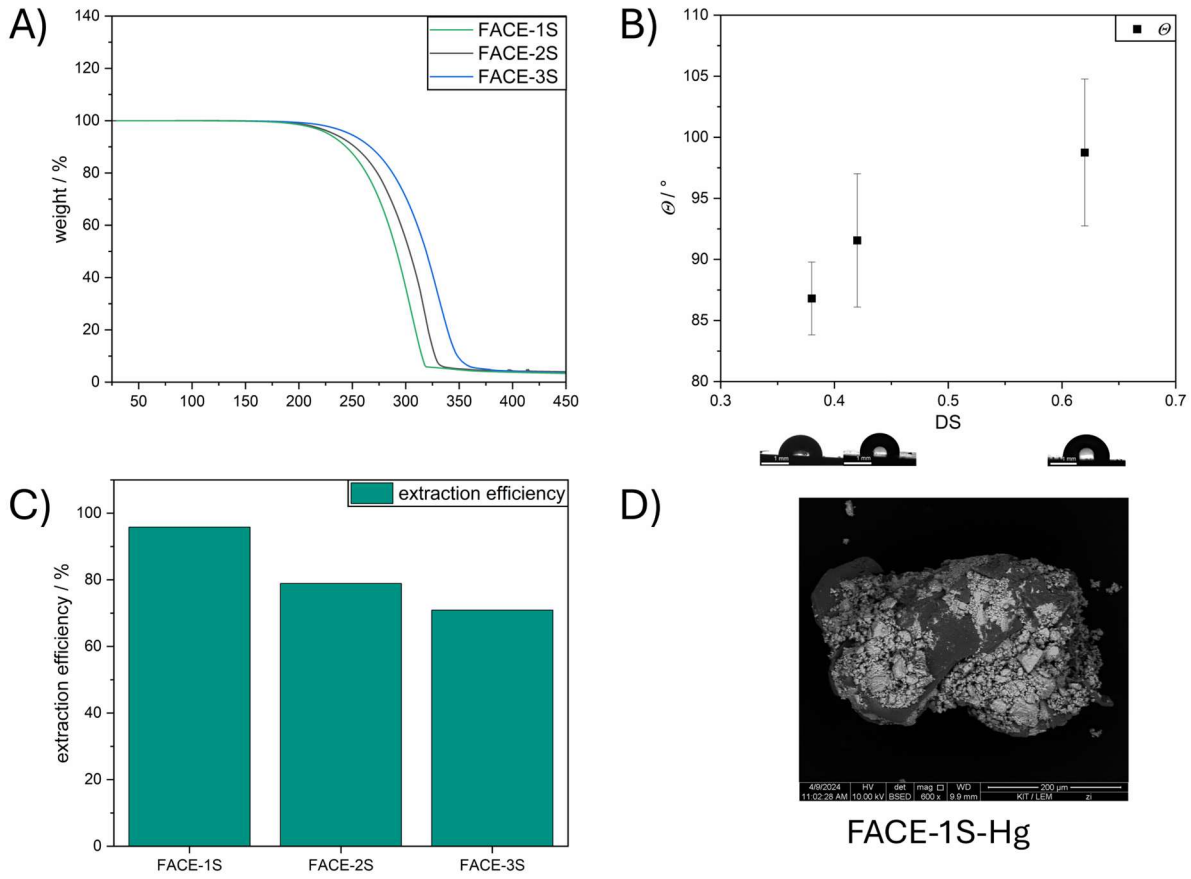

Figure 13. (A) TGA curves of **FACE-1S** (green line), **FACE-2S** (black line), and **FACE-3S** (blue line). (B) Static WCA measurements **of FACE-1S**, **FACE-2S**, and **FACE-3S**. (C) Mercury removal efficiency of **FACE-1S**, **FACE-2S**, and **FACE-3S** from an aqueous $HgCl_2$ solution (1.00 mg L^{-1}) after 24 h at ambient temperature. (C) Backscattered electron image of **FACE-1S** after mercury uptake *via* SEM.

The hydrophobic character of **FACE-1S**, **FACE-2S**, and **FACE-3S** was investigated by conducting static WCA measurements (**Figure 13B**). In the current literature,[321] it has been frequently described that an increased DS leads to a higher hydrophobicity for CEs. Hence, it was not surprising that the static contact angels increased from 87° for **FACE-1S** (DS_{FACE-1} = 0.38) to 99° for **FACE-3S** (DS_{FACE-2} = 0.62).

Application for Water Treatment

Inverse vulcanized materials are known as excellent heavy metal sorbents and can therefore be applied in water purification processes.[227,221,204,191,322,323] Thus, to emphasize a potential application for the synthesized high sulfur content composite materials, their potential for mercury uptake from an aqueous $HgCl_2$ solution (C_i = 1.00 mg L^{-1}) was investigated. The chemical structure, i.e. the DS of the incorporated FACE comonomers, revealed a significant impact on the extraction efficiency and capacity of the materials. As shown in **Figure 13C**, **FACE-1S** synthesized from **FACE-1** occurred as the most efficient mercury sorbent with an extraction efficiency up to 95%, followed by **FACE-2S** (78%) and **FACE-3S** (70%), respectively. The equilibrium mercury concentrations were subsequently employed for the calculation of the distribution coefficient (K_d), which assess the affinity of the synthesized sorbents for Hg^{2+} ions. K_d values can generally be calculated according to **Eqn. 6**:

$$K_d = \frac{(C_i - C_f)}{C_f} \; x \; \frac{V}{m} \qquad (6)$$

Here, C_i is the initial mercury concentration (mg L^{-1}), C_f is the final mercury concentration (mg L^{-1}), V is the volume of mercury solution (mL), and m is the mass of polymer (g). In line with the investigated extraction efficiencies, **FACE-1S** possessed the highest calculated K_d of 1.13 x 10^4 mL g^{-1}, followed by **FACES-2S** (1.87 × 10^3 mL g^{-1}) and **FACE-3S** (1.22 x 10^3 mL g^{-1}), respectively. Excellent and commercially available mercury sorbents usually exhibit K_d values > 10^5 mL g^{-1}. Thus, particularly **FACE-1S** (K_d = 1.13 x 10^4 mL g^{-1}) can be categorized as a promising mercury sorbent.

The equilibrium extraction capacities (q_e) of all synthesized composite materials can be calculated according to **Eqn. 7:**

$$q_e = (C_i - C_f) \; x \; \frac{V}{m} \qquad (7)$$

Unsurprisingly, **FACE-1S** showed the highest q_e (0.48 mg g^{-1}) compared to **FACE-2S** (0.39 mg g^{-1}) and **FACE-3S** (0.35 mg g^{-1}). As a final proof for the adsorption of mercury at the surfaces of the sorbent materials, i.e. **FACE-1S**, **FACE-2S**, and **FACE-3S**, backscattered electron (BSE) images after mercury uptake were recorded *via* SEM (**Figure 13D**, **Figure S47A** and **Figure S47B**, respectively). **Figure 13D** exemplarily reveals bright and dark surface areas, where the dark spots correspond to the initial composite material and the bright spots represent areas with adsorbed mercury.

Table 7. Summary of mercury sorption studies of cellulose-based high sulfur content composite materials.

Material	Extraction efficiency / %[a]	Distribution coefficient / mL g^{-1}	Extraction capacity / mg g^{-1}
FACE-1S	95	1.13 x 10^4	0.48
FACE-2S	78	1.87 x 10^3	0.39
FACE-3S	70	1.22 x 10^3	0.35

[a] from an aqueous $HgCl_2$ solution (C_i = 1.00 mg L^{-1}) after 24 h at ambient temperature.

Conclusion

In the current chapter of the thesis, microcrystalline cellulose was solubilized in a DMSO/TBD/CO_2 switchable solvent system and subsequently transesterified by using the biobased transesterification agent methyl-10-undecenoate by adopting a literature known procedure.[154] Upon the synthesis of renewable fatty acid cellulose esters (FACEs) containing three different DS (0.38 ≤ DS ≤ 0.62), an in-depth structural characterization, i.e. ^{1}H NMR, ^{31}P NMR, ATR-IR, DSC and TGA, was conducted. The subsequent inverse vulcanization of the synthesized FACEs resulted in high sulfur content composite materials (~95 wt% sulfur). A detailed investigation of the structural composition of the crosslinked sections *via* DSC, TGA, EDX, and SEM showed an increased amount of covalently implemented sulfur (5.67 wt% ≤ wt% sulfur ≤ 56.2 wt%), depending on the degree of substitution (DS) of the employed FACE. Additionally, it was also shown that the structural composition of the FACEs, i.e. their DS, also influence the material properties of the synthesized high sulfur content composite materials. More precisely, a higher DS of the used FACEs afforded a higher thermal stability (227 °C ≤ $T_{d,5\%}$ ≤ 247 °C), an elevated surface hydrophobicity (87° ≤ Θ ≤ 99°) and a lower mercury extraction efficiency (70 % ≤ $Hg^{2+}_{removal}$ ≤ 95 %).

4.3 Efficient One-Step Synthesis of Catechol Containing Polymers *via* Friedel-Crafts Alkylation and Their Use for Water Decontamination

The results of the current chapter and the corresponding data in the experimental section have been published before:

T. Sehn, N. Kolb, A. Azzawi, M. A. R. Meier, *Macromolecules* **2024**, *57*, 10802−10811.[324]

Parts of the project were conducted in collaboration with Evonik Operation GmbH as an industrial partner.

The author was responsible for the investigation, formal analysis, and writing of the original draft.

N. Kolb (Evonik Operation GmbH) and A. Azzawi (Evonik Operation GmbH) contributed to the conceptualization of the work.

Abstract

We herein present an efficient one-step synthesis route towards catechol containing polymers from liquid polybutadiene *via* a simple post polymerization modification approach applying acid catalyzed Friedel-Crafts alkylation. Accordingly, 100% modification of polybutadiene was achieved within 30 minutes in bulk at 120 °C. The final structure of the polymer was analyzed by ^{1}H NMR, ^{13}C NMR, 2D NMR, ART-IR, DOSY, and SEC. Material properties were investigated *via* TGA and DSC. Subsequent metal ion removal tests revealed excellent extraction efficiencies (86 % ≤ $M^{n+}_{removal}$ < 100%) when using the catechol containing polymer as heavy metal sorbent and thus emphasize a potential application for water purification processes.

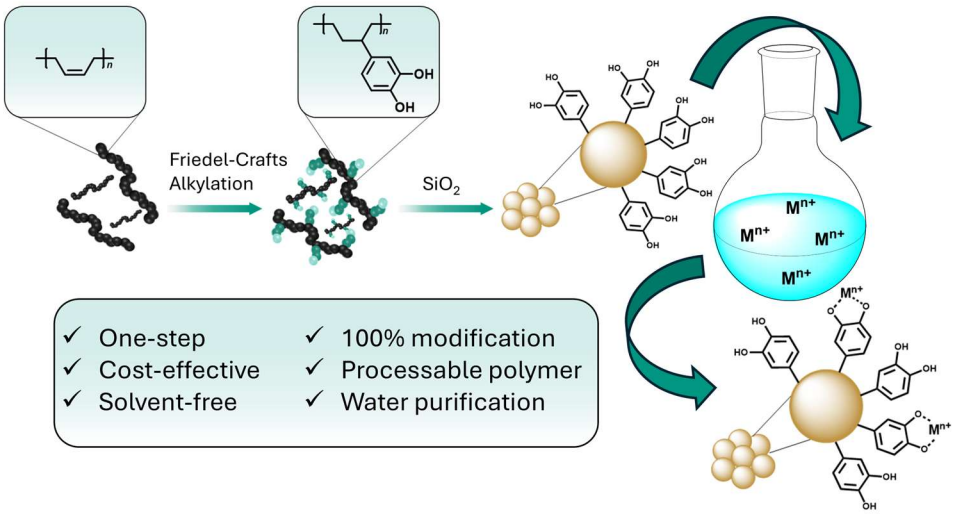
Friedel-Crafts
Alkylation
SiO2
Mn+
✓ One-step
✓ Cost-effective
✓ Solvent-free
✓ 100% modification
✓ Processable polymer
✓ Water purification

Investigation of Reaction conditions and Model Compound Synthesis

First, to find suitable and generally applicable conditions for Friedel-Crafts alkylation (FCA) with catechol, limonene was used as a model compound, offering different types of double bonds with different reactivities.

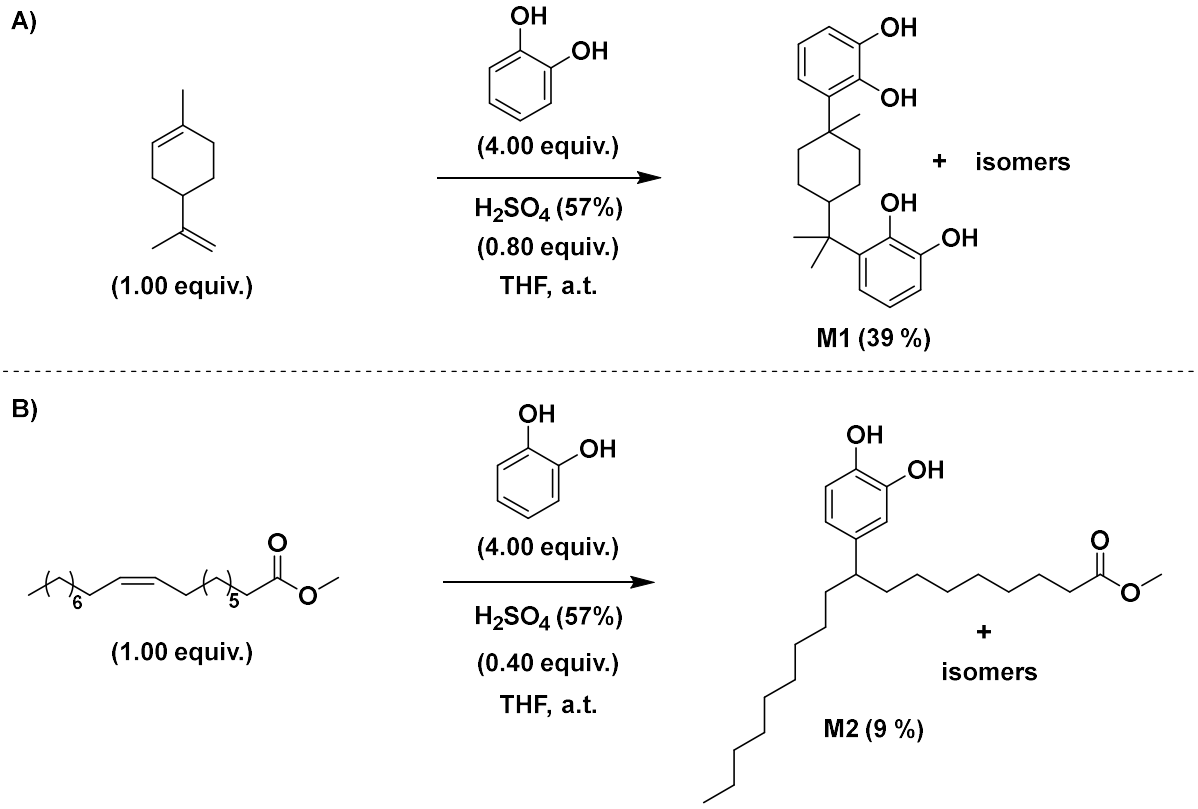

Scheme 34. General reaction conditions for the synthesis of A) **M1** and B) **M2**.

In the current literature, catechol modification approaches of organic compounds *via* FCA are rarely described.[325,326,327] Frequently, the reactions proceed in bulk at a temperature above the melting point of catechol (m_p = 105°C) around 120 °C.[325,326] The most common side reaction in acid catalyzed FCA is cationic polymerization, which can trigger crosslinking for substrates containing more than one double bond.[328] Thus, to investigate if cationic oligomerization occurs, limonene was first stirred in the presence of three different concentrated Brønsted acids, i.e. perchloric acid ($HClO_4$), sulfuric acid (H_2SO_4), and phosphoric acid (H_3PO_4). Size exclusion chromatography (SEC) revealed additional signals at higher retention times for all systems, indicating the previously mentioned oligomerization (**Figure S54**). Nevertheless, using the respective acids more diluted (57%) suppressed the oligomerization (**Figure S55**) and diluted acids were therefore applied for the following FCA modifications.

Subsequently, a gas chromatography (GC) screening of the conversion of limonene at different reaction conditions, i.e. catalyst, temperature, and solvent, was performed (**Table S3**). It was observed that the conversion of limonene in the presence of catechol and acid catalyst, i.e. $HClO_4$ (57%), H_2SO_4 (57%), and H_3PO_4 (57%), were quantitative within 10 minutes at 120 °C in bulk (**Table S3**). Adding a solvent, i.e. tetrahydrofuran (THF), resulted in a less efficient modification when using H_3PO_4 (57%) as catalyst, whereas $HClO_4$ (57%) and H_2SO_4 (57%) still provided almost quantitative conversion (**Table S3**). A decrease of reaction temperature to 60 °C lowered the efficiency of the reaction, i.e. full conversion could only be achieved for $HClO_4$ (57%) and H_2SO_4 (57%) within 120 minutes (**Table S3**). On the contrary, H_3PO_4 (57%) showed no conversion after 120 minutes reaction time (**Table S3**). Since $HClO_4$ (57%) and H_2SO_4 (57%) appeared equally efficient and due to cost effectiveness, H_2SO_4 (57%) was chosen as catalyst for all subsequent reactions reported herein. An additional GC screening showed that a decrease in catalyst (down to 0.10 equiv. H_2SO_4 (57%)) yielded a slower reaction rate and thus high conversions (≥ 99%) could only be achieved after 24 hours. At ambient temperature the modification process proceeded again less efficiently, i.e. conversions from 24.2% up to 80.6% could be reached within one day dependent on the catalyst loading (**Table S4**). After these GC screenings, reaction 13 of **Table S4** (also shown in **Scheme 34A**) was purified to confirm that the targeted catechol modified products were successfully synthesized. Hence, ^{1}H nuclear magnetic resonance (NMR) spectroscopy of model compound **M1** was performed (**Figure 14A**).

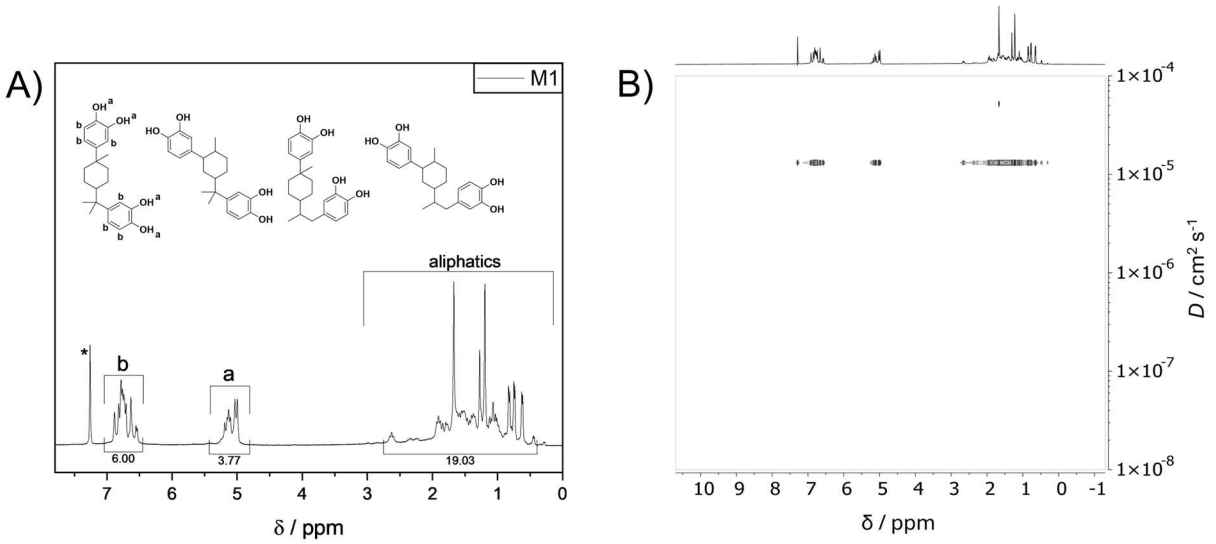

Figure 14. (A) ^{1}H NMR (400 MHz) of **M1** in $CDCl_3$ (*) at ambient temperature. (B) DOSY spectrum of **M1** in $CDCl_3$ at ambient temperature.

The spectrum revealed characteristic magnetic resonances (0.24 – 2.75 ppm) in the upfield region, which can be assigned to the terpene scaffold of the product. Additional signals in the range from 4.86 to 5.35 and 6.47 to 6.96 ppm correspond to the hydroxyl and aromatic protons, respectively, introduced by the catechol moieties (**Figure 14A**). At this point it must be mentioned that a direct assignment of every peak in the spectrum of **M1** was not feasible, due to isomer formation (**Figure 14A**). Thus, diffusion ordered spectroscopy (DOSY) and size exclusion chromatography (SEC) were performed to investigate the structure of the synthesized products. As shown in **Figure 14B**, DOSY revealed the same diffusion coefficient for all magnetic resonances appearing in ^{1}H NMR, indicating that all compounds are of similar molecular weight.

This is further confirmed by SEC of **M1**, showing only one peak with a dispersity of 1.00 (**Figure S56**). Supplemental structural characterization of **M1** was performed *via* ^{13}C NMR, gradient selected correlation (COSY), and heteronuclear single quantum coherence (HSQC) spectroscopy, showing all expected signals and correlations (**Figure S49**, **Figure S57**, and **Figure S58**, respectively). The disappearance of the C=C vibration band around 1645 cm^{-1} and the arising OH vibration band (~3337 cm^{-1}) in the ATR-IR spectrum of **M1** (**Figure S59**) combined with the observed mass of the sodium adduct of **M1** in electrospray ionization mass spectrometry (ESI-MS, **Figure S60**) further confirmed the formation of the targeted products. Subsequently, a structurally more similar substrate to polybutadiene, i.e. methyl oleate, was introduced to further investigate catechol addition onto *cis* double bonds *via* acid catalyzed FCA (**Scheme 34B**). For the synthesis of model compound **M2**, again a GC screening was conducted to investigate if the reaction appears as efficient as for **M1**. Generally, the FCA using methyl oleate as starting material worked less efficiently when using THF as solvent (1M) and H_2SO_4 (57%, 0.40 equiv. per DB) as catalyst (compare R9 in **Table S4** with R10 in **Table S5**). Interestingly, the reaction however still proceeded also with low catalyst loading (0.05 equiv. per DB) and at ambient temperature, but slower. This indicates that the isolated double bond of methyl oleate is somewhat less reactive than the geminal disubstituted or the trisubstituted double bonds of limonene, as can be expected for FCA. The structural characterization of **M2** was performed in a similar manner as described for **M1**. Most importantly, ^{1}H NMR revealed magnetic resonance from 4.79 to 5.63 ppm and from 6.52 to 6.81 ppm, corresponding to the attached hydroxyl and aromatic protons of the catechol unit (**Figure 15A**). An additional signal appearing from 2.77 to 2.98 ppm underlined the attachment of catechol groups onto

methyl oleate, as this signal can be assigned to the tertiary proton formed during the reaction (**Figure 15B**). DOSY, 13C NMR, SEC, 2D NMR, IR, and ESI-MS additionally confirmed the structure of **M2**, as explained before for **M1** (**Figure 15B**, **Figure S51** and **Figure S61** to **Figure S65**, respectively).

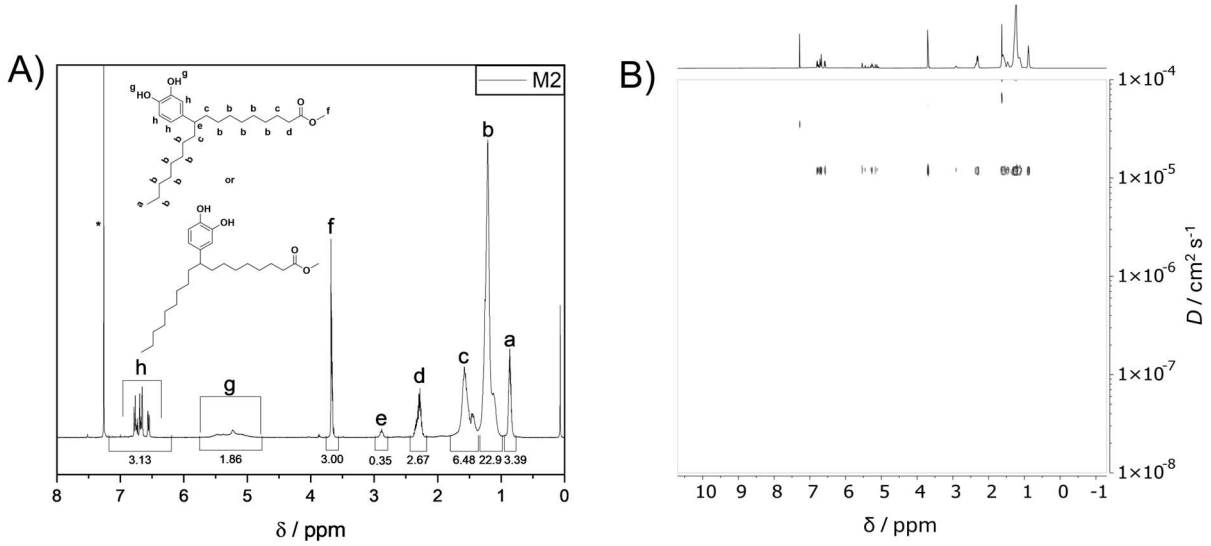

Figure 15. (A) ^{1}H NMR (400 MHz) of **M2** in $CDCl_3$ (*) at ambient temperature. (B) DOSY spectrum of **M2** in $CDCl_3$ at ambient temperature.

Polymer Modification and Characterization

After the previously described initial investigations, the post polymerization modification (PPM) of polybutadiene with catechol was investigated, revealing that the modification had to be conducted at harsher reaction conditions, i.e. in bulk and at 120 °C (**Scheme 35**).

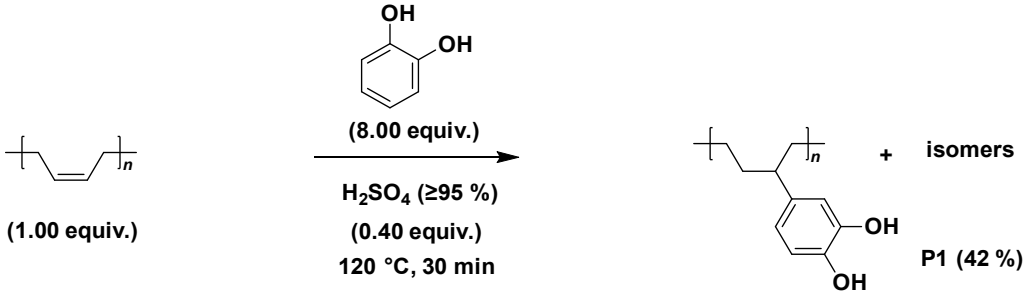

Scheme 35. General conditions for the post polymerization modification of polybutadiene *via* Friedel-Crafts alkylation.

The harsher reaction conditions for PPM were likely required due to the increased steric hindrance of the double bonds within the polymer backbone. Nevertheless, FCA in bulk at 120 °C yielded a degree of modification of 100% within 30 minutes. Reducing the equivalents of catechol to 6.00 and the catalyst loading to 2.5% still resulted in full

functionalization, however then a much longer reaction time, i.e. 6h, was required. Further reduction of either catechol or catalyst led to incomplete conversion and possibly side reactions such as cross-linking. After simple purification, i.e. washing and distillation of excess catechol, structural characterization of the modified polybutadiene (**P1**) was conducted. First, ^{1}H NMR of **P1** was recorded, revealing broad magnetic resonances from 0.27 to 2.23, 6.04 to 6.91, and 8.14 to 8.79 ppm, which can be assigned to the aliphatic polymer backbone, the aromatic hydroxyl groups and the aromatic protons of the introduced catechol moieties, respectively (**Figure 16A**). An additional DOSY experiment, showing a similar diffusion coefficient for all appearing magnetic resonances observed by ^{1}H NMR, confirmed the attachment of catechol groups onto the polymer backbone (**Figure 16B**). Supplemental proof for the success of the PPM was provided by the appearance of characteristic magnetic resonances in ^{13}C NMR from 111 to 121 and 141 to 148 ppm, which can be attributed to the aromatic carbon atoms of the pendant catechol side groups (**Figure S53**).

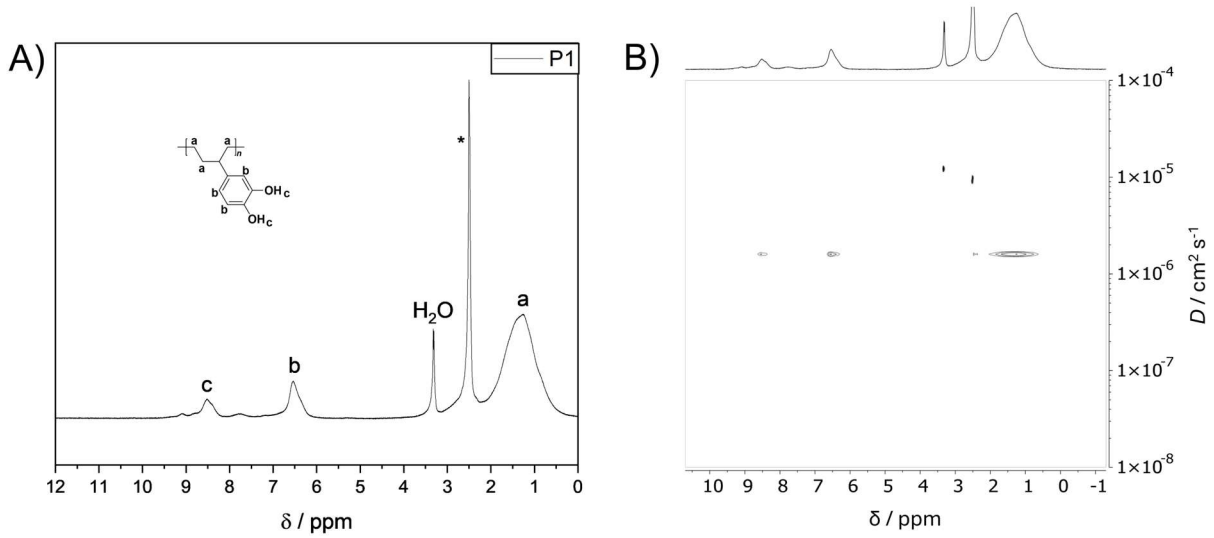

Figure 16. (A) ^{1}H NMR (400 MHz) of **P1** in DMSO-d_6 (*) at ambient temperature. (B) DOSY spectrum of **P1** in DMSO-d_6 at ambient temperature.

Expected correlations in 2D NMR, i.e. COSY and HSQC spectroscopy (**Figure S66** and **Figure S67**, respectively), combined with the presence of a characteristic hydroxyl vibration band (~3381 cm^{-1}, **Figure S68**) in the IR spectrum of **P1** underline again the success of the modification approach. SEC of the starting polybutadiene and **P1** were conducted, showing a decrease in hydrodynamic volume for **P1** after modification, probably due to an increased number of intramolecular interactions, i.e. hydrogen bonding and π-π stacking (**Figure 17A**). Thermal properties of **P1** were investigated

via thermogravimetric analysis (TGA) and differential scanning calorimetry (DSC). Thermal degradation, which is defined as the temperature at which 5% mass loss occurs ($T_{d,5\%}$), of **P1** was observed at 377 °C (**Figure S69**) and thus started in the same temperature range as for polybutadiene ($T_{d,5\%}$ = 373 °C, **Figure S69**). DSC of **P1** revealed one thermal transition, i.e. a glass transition (T_g) at 143 °C, which is 242 °C higher than the T_g of the parent polybutadiene (**Figure 17B**). The significant increase of T_g resulted from the introduction of bulky side groups, i.e. catechol moieties, onto the polymer supplemented by additional inter- and intramolecular interaction, i.e. mainly hydrogen bonding and π-π stacking, which limits the chain flexibility of **P1** dramatically compared to the starting polymer. Noteworthy, similarly efficient modifications were also observed for other polybutadiene samples, i.e. for hydroxyl terminated polybutadiene.

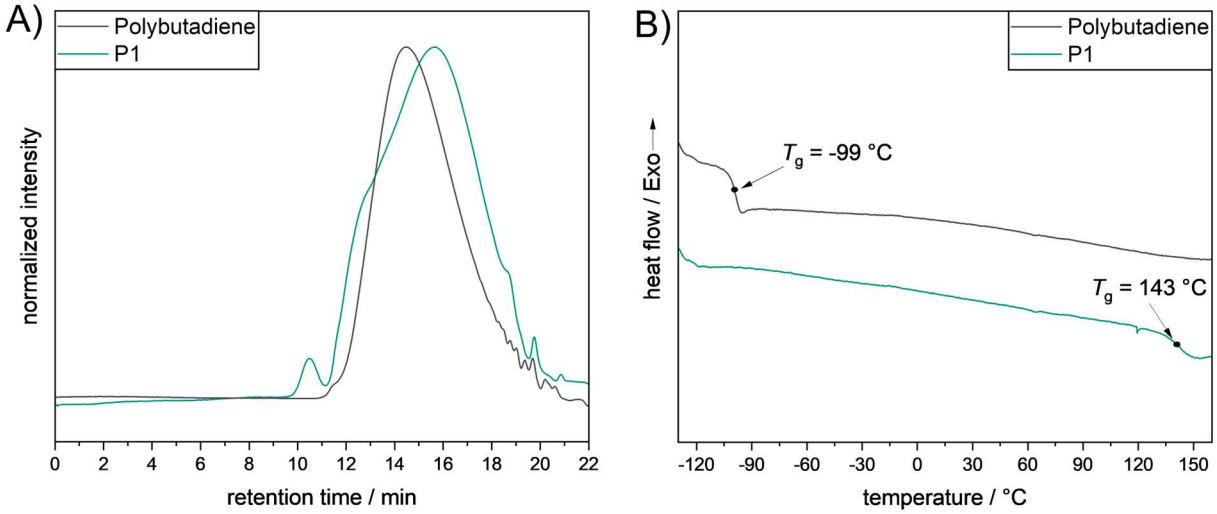

Figure 17. (A) SEC traces of polybutadiene (black, M_n = 1.6 kDa) and **P1** (green, M_n = 1.8 kDa) in THF + 0.025% w/v BHT. (B) DSC thermograms (second heating run) of polybutadiene (black) and **P1** (green) from -130 to 160 °C with a heating rate of 10 °C min^{-1} under a nitrogen flow.

Application of P1 as Heavy Metal Ion Sorbent in Water Decontamination

After the synthetic part of the current chapter, i.e. synthesis of two model compounds to develop suitable reaction conditions and a fully catechol modified polymer *via* PPM, a potential application for **P1** was targeted. It is well known that catechol forms stable complexes with metal ions. Therefore, the applicability of **P1** in water treatment was investigated to further improve the availability and sustainable management of clean water, as envisaged by UN Sustainable Development Goal 6. Particularly the fact that **P1** is a thermoplastic material enables an easy processability and hence affords a

broad versatility in sample preparation. In the current work, the polymer was coated onto the surface of silica particles by a simple technique (5 wt%, **Scheme 36**), i.e. **P1** was dissolved in THF, silica particles were added, and the solvent was afterwards evaporated under reduced pressure. The polymer coated silica particles provided a large surface area, which was beneficial for subsequent metal ion removal tests.

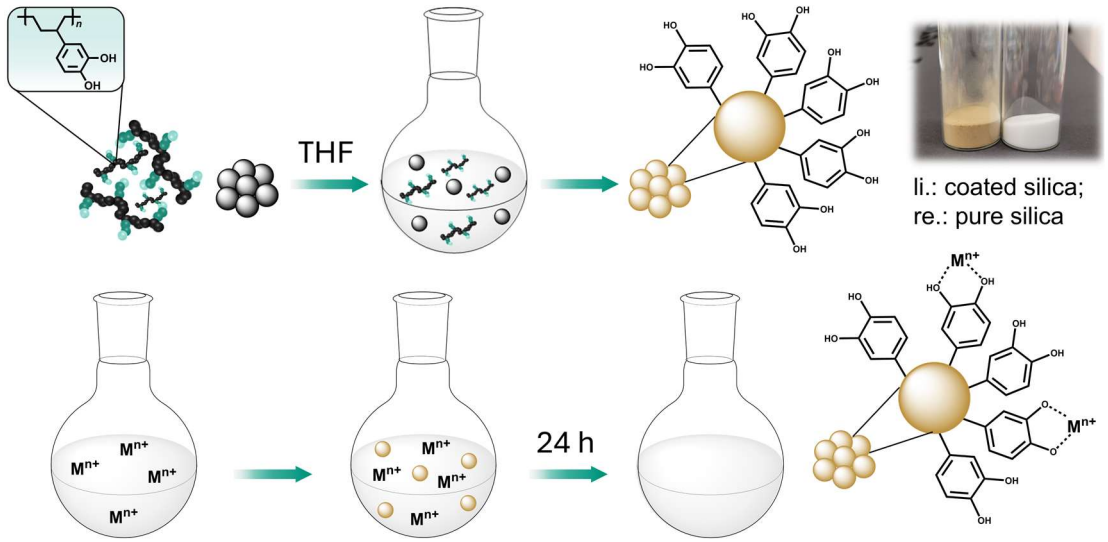

Scheme 36. General concept of the loading technique for polymer coating onto silica particles (top) and schematic overview of the metal ion removal tests (bottom).

The polymer coated silica particles provided a large surface area, which was beneficial for subsequent metal ion removal tests. The coating of **P1** onto the silica particles was observed by a color change from white to beige (**Scheme 36**) and confirmed by an additional carbon signal around 0.28 keV in energy dispersive X-ray (EDX) spectroscopy (**Figure 18A**).

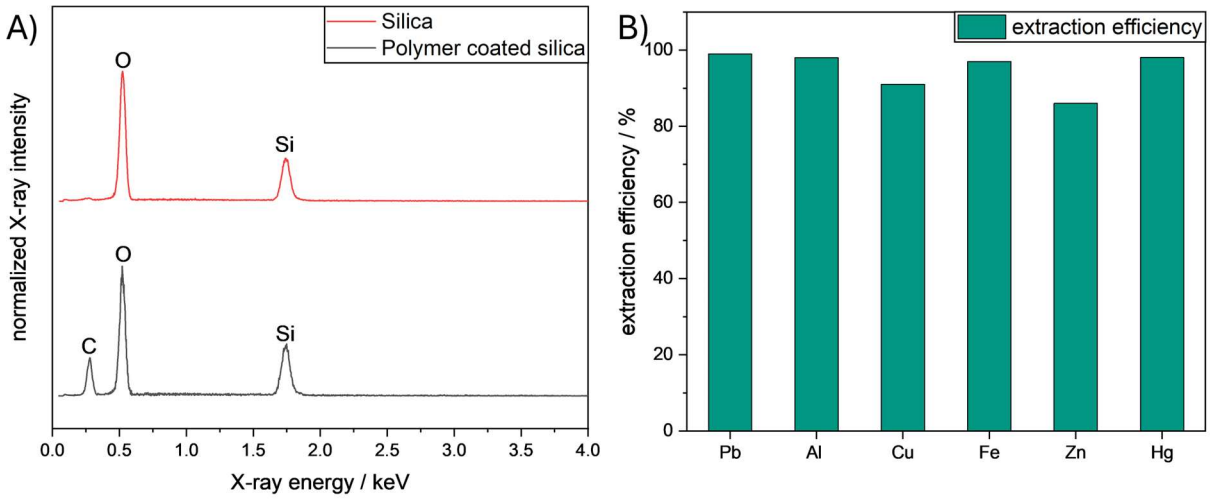

Figure 18. A) EDX spectra of uncoated and polymer coated silica particles. B) Extraction efficiencies of **P1** coated silica particles from aqueous metal ion solution (C_i = 1.00 mg L^{-1}) for different cations.

For metal ion removal tests, 200 mg of the polymer coated silica particles were stirred in aqueous solutions containing different metal ions (c_i = 1.00 mg L^{-1}), i.e. Pb^{2+}, Al^{3+}, Cu^{2+}, Fe^{3+}, Zn^{2+}, or Hg^{2+}, for 24 h at ambient conditions and subsequently filtered off (**Scheme 36**). Interestingly, **P1** coated silica particles revealed a high affinity towards all tested metal ions. In other words, extraction efficiencies from 86% for Zn^{2+} up to >99% for Pb^{2+} were achieved during the experiments (**Figure 18B** and **Table 8**). To quantify the affinity of the synthesized sorbent to the respective metal ion, the equilibrium metal ion concentrations were employed to calculate the corresponding distribution coefficient (K_d). K_d values can be calculated, as already introduced in chapter 4.2, according to **Eqn. (8)**:

$$K_d = \frac{(C_i - C_f)}{C_f} \; x \; \frac{V}{m} \qquad (8)$$

In **Eqn. 8**, C_i is the initial metal ion concentration (mg L^{-1}), C_f is the final metal ion concentration (mg L^{-1}), V the volume aqueous metal ion solution (mL), and m is the mass of coated silica particles (g). Accordingly, two different K_d values were calculated. One referred to the employed mass of coated silica particles, i.e. 200 mg, and the other referred to the actual polymer mass coated onto the silica particles, i.e. 10 mg (**Table 8**). According to the current literature, K_d values of 1 x 10^4 mL g^{-1} are considered as good for extractions, whereas values above 1 x 10^5 mL g^{-1} are recognized as excellent for commercially available metal ion sorbents.[329,330,331] Thus, especially the K_d values referred to the actual polymer mass (6.14×10^4 mL $g^{-1} \leq K_d \leq 9.90 \times 10^5$ mL g^{-1}, Table1) reveal that **P1** can be recognized as a good to excellent metal ion sorbent for each tested metal. Especially the removal of Pb^{2+} from an aqueous solution (C_i = 1.00 mg L^{-1}) appears as very efficient, resulting in a final concentration < 0.01 mg L^{-1}, fulfilling the criteria for drinking water according to the World Health Organization (WHO) and thus underlining the potential of the developed scavenger.[332] Furthermore, the equilibrium extraction capacities (q_e), which describe the amount of adsorbed metal ions referred to the employed polymer mass, were calculated again according to **Eqn. 9.**, which was previously introduced in chapter 4.2:

$$q_e = (C_i - C_f) \; x \; \frac{V}{m} \qquad (9)$$

As shown in **Table 8**, q_e values were also calculated referring to the coated particle and actual polymer mass. Generally, the q_e values correlate with the extraction efficiencies, thus the highest values were obtained for Pb^{2+} and Hg^{2+} removal, i.e. 9.90 mg g^{-1} and 9.98 mg g^{-1}, respectively.

Table 8. Overview of metal ion sorption studies of **P1** coated silica particles.

Metal	Extraction efficiency / %	Distribution coefficient (K_d) / mL g^{-1}	Extraction capacity / mg g^{-1}	Distribution coefficient (K_d) / mL g^{-1} [(a)]	Extraction capacity / mg g^{-1} [(a)]
Pb	>99	4.95×10^4	0.49	9.90×10^5	9.90
Al	98	2.45×10^4	0.49	4.90×10^5	9.80
Cu	91	5.05×10^3	0.46	1.01×10^5	9.20
Fe	97	1.62×10^4	0.49	3.24×10^5	9.80
Zn	86	3.07×10^3	0.43	6.14×10^4	8.60
Hg	98	2.50×10^4	0.49	5.00×10^5	9.80

[a] referred to the actual coated polymer mass of **P1**.

Conclusion

In the current chapter, an efficient and straightforward synthetic pathway to attach catechol moieties directly onto polybutadiene *via* post polymerization modification using Friedel-Crafts alkylation (FCA) was introduced. First, to achieve a detailed understanding of the reaction and screen reaction parameters, two model compounds, i.e. **M1** and **M2**, were synthesized from two organic molecules including at least one double bond, i.e. limonene and methyl oleate, respectively. Upon synthesis, an in-depth structural characterization of **M1** and **M2** *via* ^{1}H NMR, ^{13}C NMR, 2D NMR, DOSY, SEC, IR, and ESI-MS was conducted. The targeted polymer bearing catechol moieties as pendant side groups, derived from polybutadiene, was subsequently synthesized *via* H_2SO_4 (≥95%) catalyzed FCA in bulk within 30 minutes at 120 °C, resulting in a final degree of modification of 100%. The success of the modification approach was confirmed *via* ^{1}H NMR, ^{13}C NMR, 2D NMR, DOSY, SEC, IR, TGA, and DSC. Additional metal ion removal tests revealed the excellent performance of the synthesized polymer (86 % ≤ $M^{n+}_{removal}$ < 100 %) and hence emphasize a potential application in water purification. Further application possibilities of catechol functionalized polymers, as

discussed in the introduction, can potentially also be realized in the future using the introduced direct functionalization approach.

4.4 Fully Renewable High Oleic Sunflower Oil (HOSO)-based Acetal Covalent Adaptable Networks (CANs)

Context

Chapter 4.3 introduced an efficient one-step strategy for the attachment of catechol units onto polybutadiene *via* Friedel-Crafts alkylation (FCA). Within this chapter, the same chemistry was applied to a renewable substrate, i.e. high oleic sunflower oil (HOSO), targeting a fully bio-based polyol for the synthesis of 100% renewable covalent adaptable networks (CANs). CANs are classified as dynamically crosslinked materials, which combine the advantages of thermoplastic and permanently crosslinked materials.[333,334] More specifically, CANs possess material properties similar to thermosets, but can be reprocessed and reshaped like thermoplastics by applying certain external stimuli such as temperature or pressure.[335] This behavior can be explained by the occurrence of exchange reactions that can either proceed in an associative or in a dissociative fashion under specific conditions (**Scheme 37**).[336] Associative CANs, also named vitrimers, undergo this rearrangement process without reduced time-averaged crosslinking density, whereas dissociative CANs show a temperature dependent equilibrium between bond breaking and formation, leading to fluidization of the initial material at a certain temperature, the so-called sol-gel transition.[336]

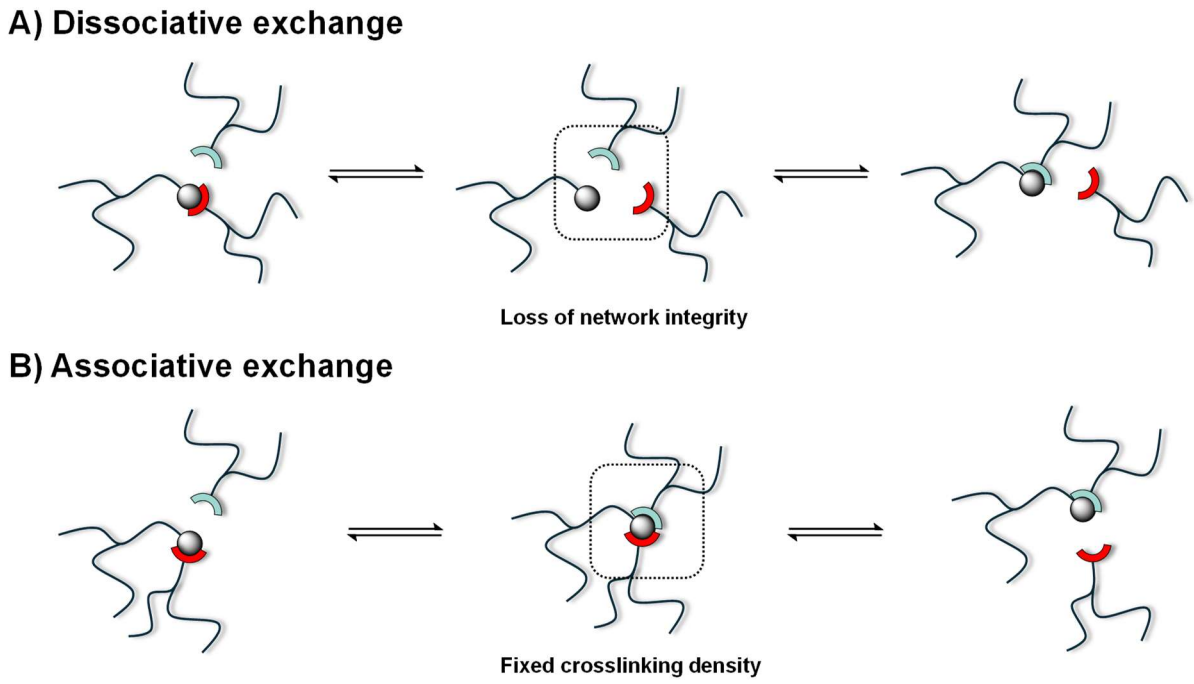

Scheme 37. Illustrative representation of potential bond exchange mechanisms.

Common functional groups that can undergo reversible exchange reactions and therefore often find application in CANs are for instance disulfides,[337] esters,[338] ureas,[339] and imines,[340] among others. Less frequently employed dynamic functional groups are acetal units, which can efficiently be formed *via* a catalyst-free click-reaction between alcohol and vinyl ether groups.[341,342] According to the current literature, dynamic acetal linkages follow a dissociative mechanism that involves their cleavage into hydroxyl and vinyl ether groups that can react back, thus re-forming acetal units and thus the crosslinked network.[341,342] CANs are frequently investigated, as these materials possess improved material properties and overcome limitations regarding reprocessing. Thus, CANs reveal a high potential for the development of reusable and therefore more sustainable crosslinked materials.

Synthesis of a Fully Renewable Polyol

Inspired by the chemistry presented in chapter 4.3, i.e. attachment of catechol functionalities onto double bonds via acid catalyzed FCA, a fully renewable polyol based on HOSO was targeted. Catechol is accessible from the renewable resource lignin *via* demethylation and subsequent hydrogenation.[343] HOSO was reacted with an excess of catechol in the presence of H_2SO_4 (>95%) at 120 °C (**Scheme 38**). Quantitative conversion of the alkene moieties was achieved within 30 minutes, similar to the results using polybutadiene in chapter 4.3.

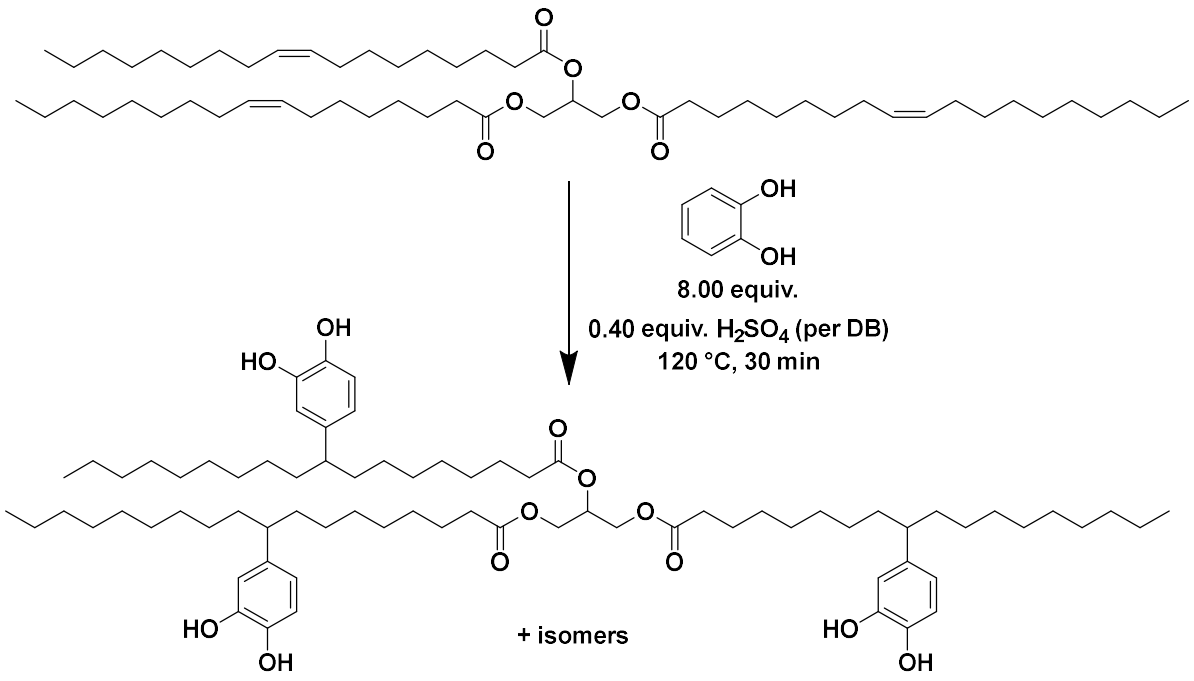

Scheme 38. Synthesis of a fully renewable polyol from high oleic sunflower oil (HOSO) via acid catalyzed Friedel-Crafts alkylation (FCA).

Structural characterization of the synthesized polyol, i.e. *via* nuclear magnetic resonance (NMR) and attenuated total reflection infrared (ATR-IR) spectroscopy, was performed. As shown in **Figure 19A**, ^{1}H NMR confirmed the attachment of catechol moieties onto the triglyceride structure of HOSO by revealing characteristic magnetic resonances from 5.30 ppm to 5.77 ppm and from 6.35 ppm and 7.10 ppm, which can be assigned to the introduced hydroxyl and aromatic protons, respectively. Two additional characteristic magnetic resonances (arising at 2.57 ppm and 2.92 ppm), corresponding to the methine protons formed during the modification process, appeared in the spectrum and provided supplemental proof for the successful implementation of catechol units. The presence of more than one magnetic resonance associated with the tertiary proton can be explained by carbocation shifts and rearrangements occurring after protonation of the double bonds.[344] In other words, depending on the formed carbocation and the actual position of the attached catechol unit, various magnetic resonances can appear at different ppm values.

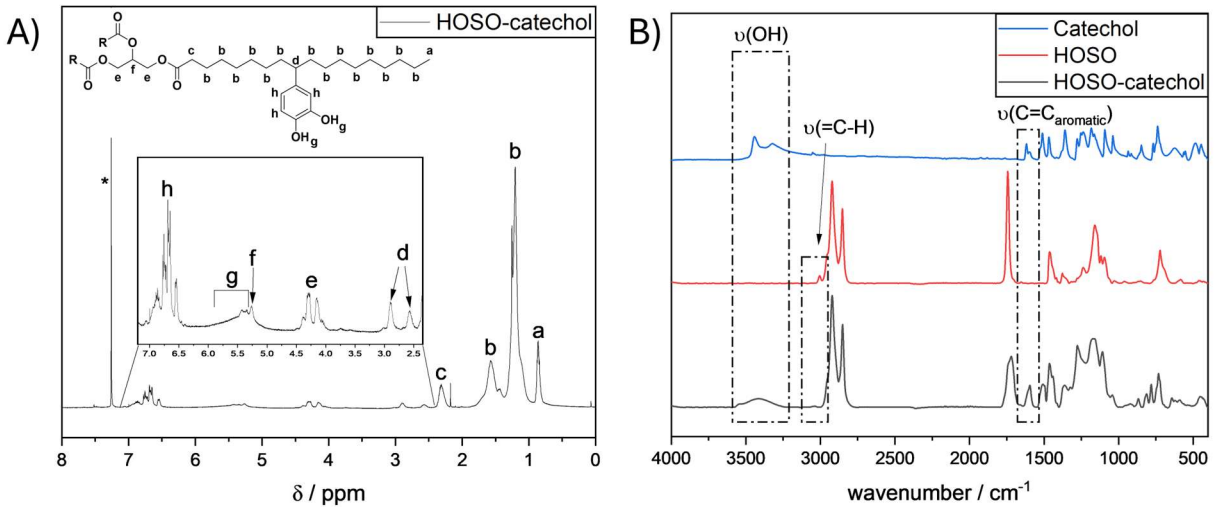

Figure 19. A) ^{1}H NMR (400 MHz) of **HOSO-catechol** in $CDCl_3$ (*) at ambient temperature. B) ATR-IR spectra of catechol (blue), HOSO (red), and **HOSO-catechol** (black).

Furthermore, ^{13}C NMR showed the expected magnetic resonances for catechol moieties in the aromatic region (112 ppm to 122 ppm and 132 ppm to 144 ppm), which was complemented by 2D NMR experiments, i.e. gradient selected correlation (COSY), and heteronuclear single quantum coherence (HSQC) spectroscopy, revealing the predicted correlations (**Figure S72**). For additional indication of the attachment of catechol groups onto HOSO, ATR-IR spectroscopy was conducted. Herein, especially the appearance of two stretching vibration bands at 3418 cm^{-1} (O-

H) and 1597 cm^{-1} ($C=C_{aromatic}$) supplemented by the disappearance of the C=C stretching vibration band at 3007 cm^{-1} confirmed the formation of the polyol (**Figure 19B**). Subsequently, thermal properties of HOSO and the corresponding polyol were investigated *via* differential scanning calorimetry (DSC) and thermogravimetric analysis (TGA). DSC measurement of HOSO revealed a melting point at -7°C, which occurred due to the crystallization of the aliphatic chains of the triglyceride structure (**Figure S75**). After the introduction of bulky catechol moieties into the HOSO structure, crystallization was suppressed and thus no melting point could be observed. Instead, the newly formed polyol still displayed a thermal transition, i.e. glass transition, at -9 °C (**Figure S75**). Investigations regarding the thermal stability of the unmodified and catechol decorated HOSO revealed that the modified derivative degraded at lower temperatures than the pristine vegetable oil. Accordingly, a weight loss of 5% was observed at 356 °C for HOSO and at 296 °C for **HOSO-catechol** (**Figure S76**).

Crosslinking Process

After structural characterization of the synthesized polyol, the preparation of fully renewable HOSO-based acetal CANs was targeted. To access such kind of materials, a thermally initiated, catalyst and solvent-free click reaction between a bifunctional vinyl ether (VE) and hydroxyl groups was chosen for crosslinking. The polyol was therefore reacted with 1,4-cyclohexanedimethanol divinyl ether (CVDE), which can be obtained from terpenes such as limonene and is therefore recognized as bio-based (**Scheme 39**).[345,346]

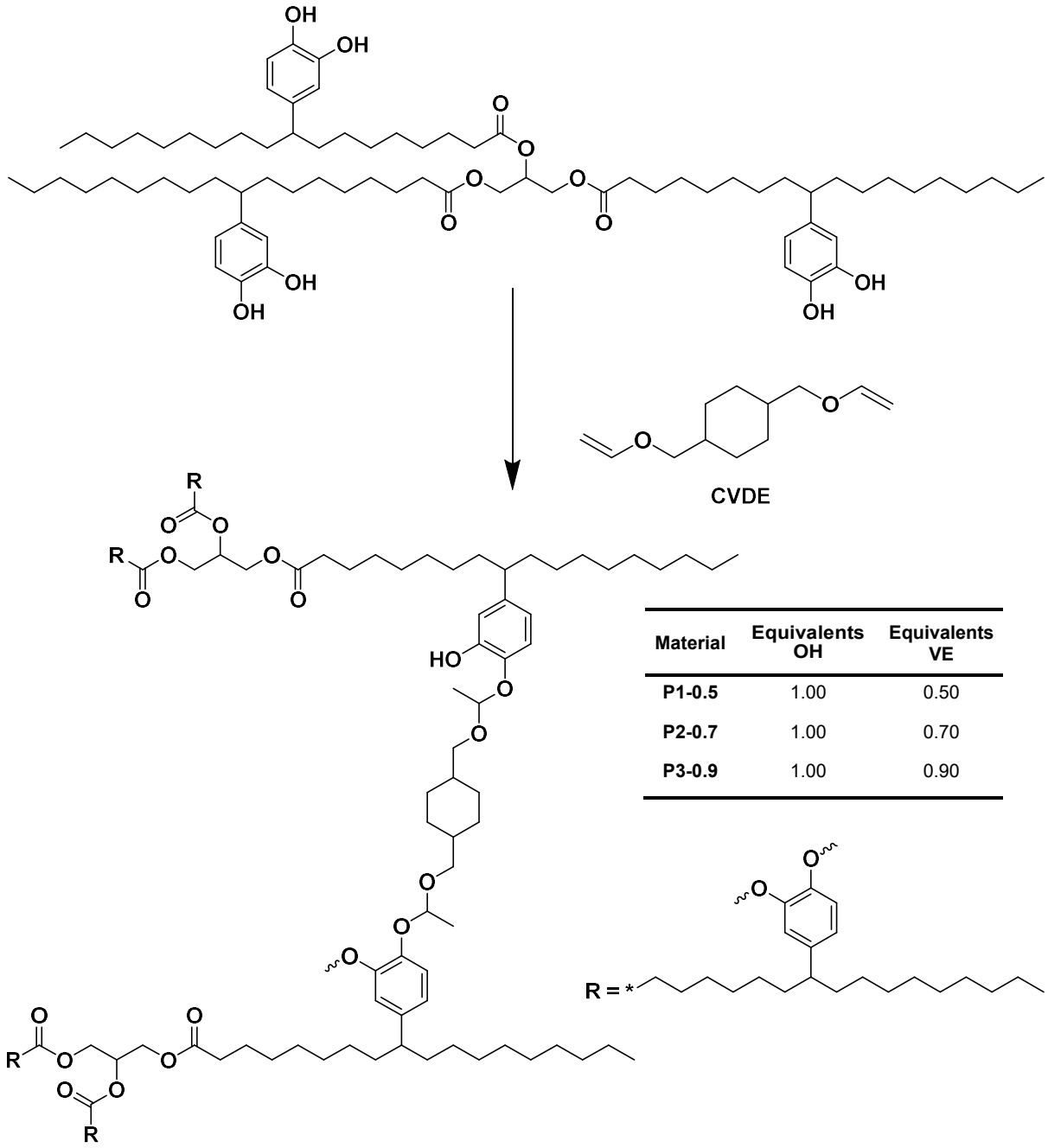

Material	Equivalents OH	Equivalents VE
P1-0.5	1.00	0.50
P2-0.7	1.00	0.70
P3-0.9	1.00	0.90

Scheme 39. Preparation of fully renewable high oleic sunflower oil (HOSO)-based acetal CANs.

Based on already described approaches to prepare acetal based CANs using a click reaction between vinyl ether and hydroxyl groups, the crosslinking in the current system was first investigated.[341,342,347] Thus, the polyol and CVDE were mixed (OH 1:0.5 VE) without any additional solvent and a non-isothermal DSC measurement was conducted. Herein, a broad exothermic peak was observed, indicating that the crosslinking reaction between vinyl ether and hydroxyl groups started slowly at around 100 °C and reached its maximum at 147 °C (**Figure S77**). Thus, the reaction was

expected to proceed efficiently at 147 °C and higher temperatures. However, in order to reach a high amount of crosslinking, i.e. high gel contents, it is recommended to start the curing at a lower temperature to provide enough time and flexibility for the starting materials to react quantitatively. Thus, it was decided to cure the final materials for 1h at 120 °C and subsequently for 3h at 150 °C to ensure an efficient crosslinking. By applying these curing conditions, three materials, i.e. **P1-0.5**, **P2-0.7**, and **P3-0.9**, with different compositions, i.e. OH 1:0.5 VE, OH 1:0.7 VE, and OH 1:0.9, were synthesized, respectively. As depicted in **Figure 20**, the materials were obtained as dark red to black materials.

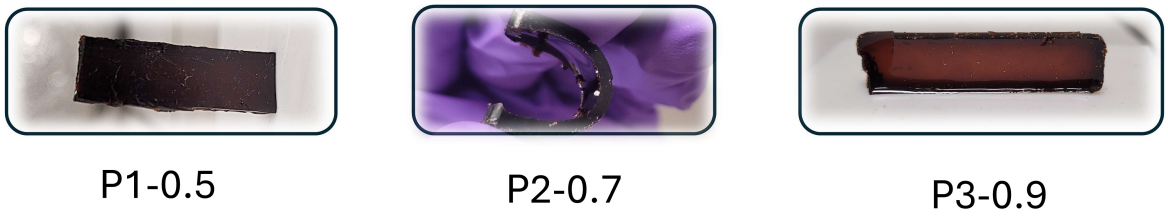

Figure 20. Optical appearance of the fully renewable acetal CANs **P1-0.5** (left), **P2-0.7** (middle), and **P3-0.9** (right).

The structural characterization after the curing process was mainly performed by IR spectroscopy. The absorption ATR-IR spectra of the polyol and the potential CANs, i.e. **P1-0.5**, **P2-0.7**, and **P3-0.9**, were first normalized to the C=O stretching vibration band (1740 cm^{-1}), which was expected not to undergo any changes as the carbonyl moieties are not affected during the crosslinking process. The groups that are expected to undergo changes are the hydroxyl groups provided by the polyol and the formed C-O-C groups of the targeted acetal groups. Accordingly, ATR-IR spectra of **P1-0.5**, **P2-0.7**, and **P3-0.9** revealed a decrease of the O-H stretching vibration band (3418 cm^{-1}) and an increase of the C-O-C stretching vibration band (1101 cm^{-1}), depending on the amount of introduced crosslinker (**Figure 21**). More precisely, **P3-0.9**, with the highest amount of crosslinker, correspondingly revealed the most significant change in signal intensity of the O-H and C-O-C stretching vibration bands. These observations can be explained by a successful acetal formation reaction. The decrease of the O-H vibration band indicated the consumption of hydroxyl groups provided by the polyol, whereas the increase of the C-O-C vibration band illustrated the formation of the targeted acetal groups. Additionally, no characteristic stretching vibration band corresponding to residual vinyl ether groups (1608 cm^{-1}) could be observed in the ATR-IR spectra of the materials, suggesting an efficient and quantitative crosslinking.

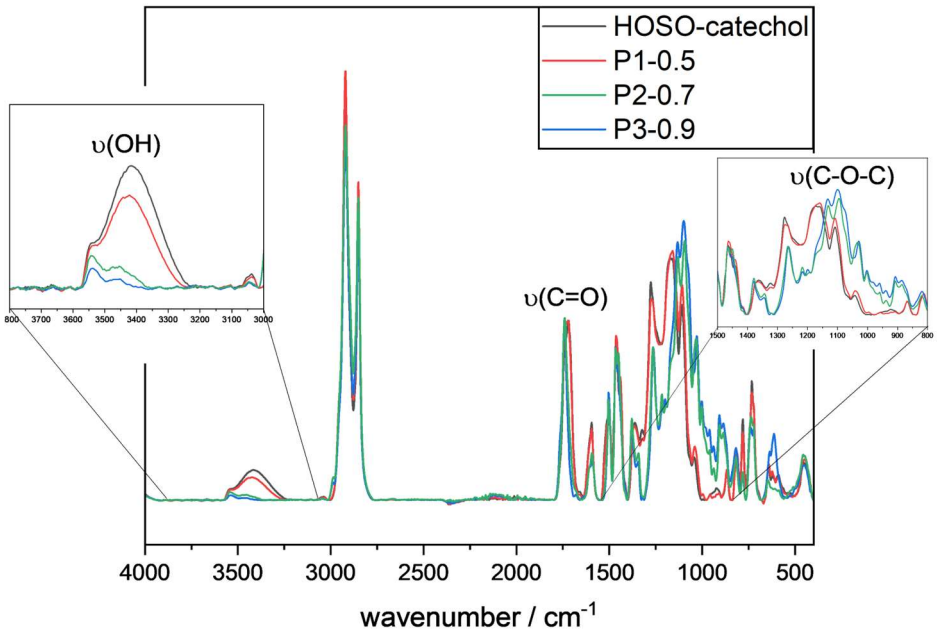

Figure 21. ATR-IR spectra of **HOSO-catechol** (black), **P1-0.5** (red), **P2-0.7** (green), and **P3-0.9** (blue).

Nevertheless, to quantify the degree of crosslinking in the synthesized materials, the gel contents of **P1-0.5**, **P2-0.7**, and **P3-0.9** were evaluated in tetrahydrofuran (THF). THF was chosen as the solvent for gel content tests, as both the polyol and the crosslinker, were completely soluble in the respective organic solvent. Accordingly, all materials (~60 mg) were stored in 1.5 mL of THF for 24h at ambient temperature, dried under reduced pressure, and weighed. The corresponding gel contents were subsequently calculated according to **Eqn. 10**:

$$Gel\ content\ (\%) = \frac{m_1}{m_o}\ x\ 100 \qquad (10)$$

Herein, m_1 is the dried sample mass after storing the respective material in THF whereas m_0 is recognized as the initial sample mass before the gel content tests. As shown in **Figure 22A**, **P2-0.7** and **P3-0.7** revealed a high gel content of 99%, which confirmed the already assumed efficient crosslinking. However, **P1-0.5** possessed a gel content of 72%, indicating that an appropriate amount of crosslinker, i.e. more than 0.50 equivalents of VE groups related to OH groups, is crucial to achieve solvent resistance in the material. Moreover, swelling tests in THF were conducted revealing higher swelling ratios for the materials showing less crosslinking. Thus, **P1-0.5** showed the highest swelling ratio with 604% followed by **P2-0.7** (374%) and **P3-0.9** (338%). Additional to gel content and swelling tests, thermal properties were investigated. DSC

measurements of the crosslinked materials revealed that the glass transition temperatures of the polymer networks (-5 °C ≤ T_g ≤ -3 °C) were higher than the one of the polyol (T_g = -9 °C), which can be explained by the reduced flexibility of the polymer chains after crosslinking (**Figure 22B** and **Figure S75**). The obtained T_g values were in accordance with the current literature for crosslinked triglycerides. For instance, Meier *et al.* reported HOSO-based thermosets using the Passerini three-component reaction revealing T_g´s between -18 and 9 °C.[348]

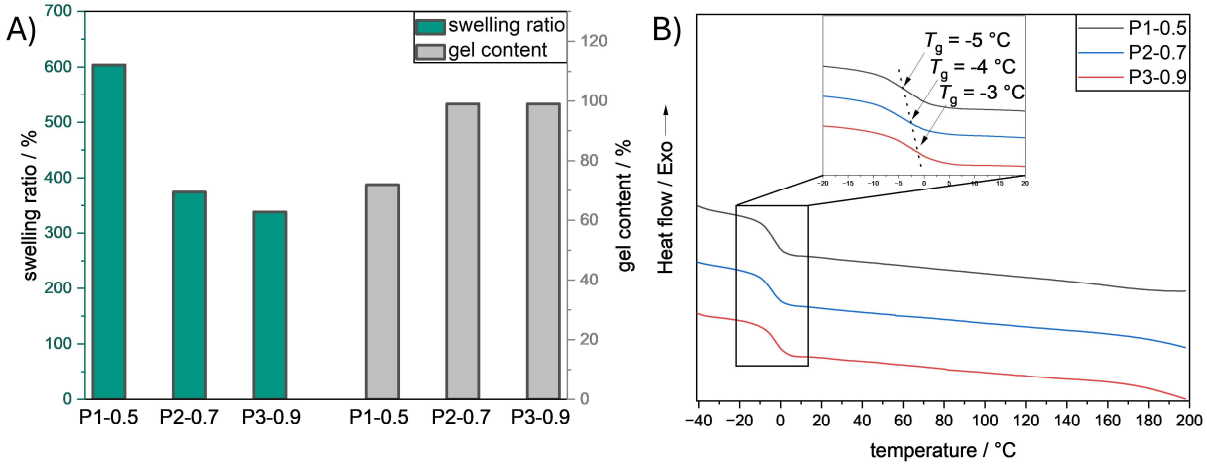

Figure 22. A) Swelling and gel content tests of **P1-0.5**, **P2-0.7**, and **P3-0.9**. B) DSC traces of **P1-0.5** (black), **P2-0.7** (blue), and **P3-0.9** (red) from -40 to 200 °C with a heating rate of 10 °C min^{-1} under a nitrogen flow.

P1-0.5, which included the least amount of crosslinker and possessed therefore also the smallest crosslinking density, revealed the lowest glass transition temperature (T_g = -5 °C, **Figure 22B**). The implementation of more crosslinker into the materials in **P2-0.7** and **P3-0.9** resulted in a more rigid polymer network and led to a slight increase of T_g to -4 °C and -3 °C (**Figure 22B**), respectively. The thermal stability of **P1-0.5**, **P2-0.7**, and **P3-0.9** was subsequently investigated *via* TGA. Thermal degradation of the materials, which is defined as the temperature at which 5% weight loss occurs, was observed at 258 °C, 274 °C, and 248 °C for **P1-0.5**, **P2-0.7**, and **P3-0.9**, respectively, which is in line with the literature on acetal based covalent adaptable networks (**Figure S78**).[342]

Investigation of Dynamic Properties

The introduction of acetal moieties into **P1-0.5**, **P2-0.7**, and **P3-0.9** enabled a potential dynamic behavior, i.e. the crosslinked materials could potentially be reprocessed and reshaped by applying specific external stimuli such as temperature and pressure. On

a molecular level, acetal groups can undergo exchange reactions like acetal metathesis and transacetalization, enabling the previously described dynamic character. A conventional characterization method to estimate the dynamic nature of materials are stress relaxation experiments. In these measurements, a specific strain is applied to the materials and the occurring stress in the samples is measured over time. Stress relaxation was measured for two out of three materials at different temperatures. The stress applied to the materials was found to decrease exponentially for **P1-0.5** and **P3-0.9**, which already indicated the dynamic behavior of the materials. The relaxation time (τ*), which is defined as the time required to reach 1/e of the initially applied stress, enabled a comparison of stress relaxation rates. As shown in **Figure 23A** and **B**, the relaxation of the materials occurred faster at higher temperatures and with higher free hydroxyl group content.

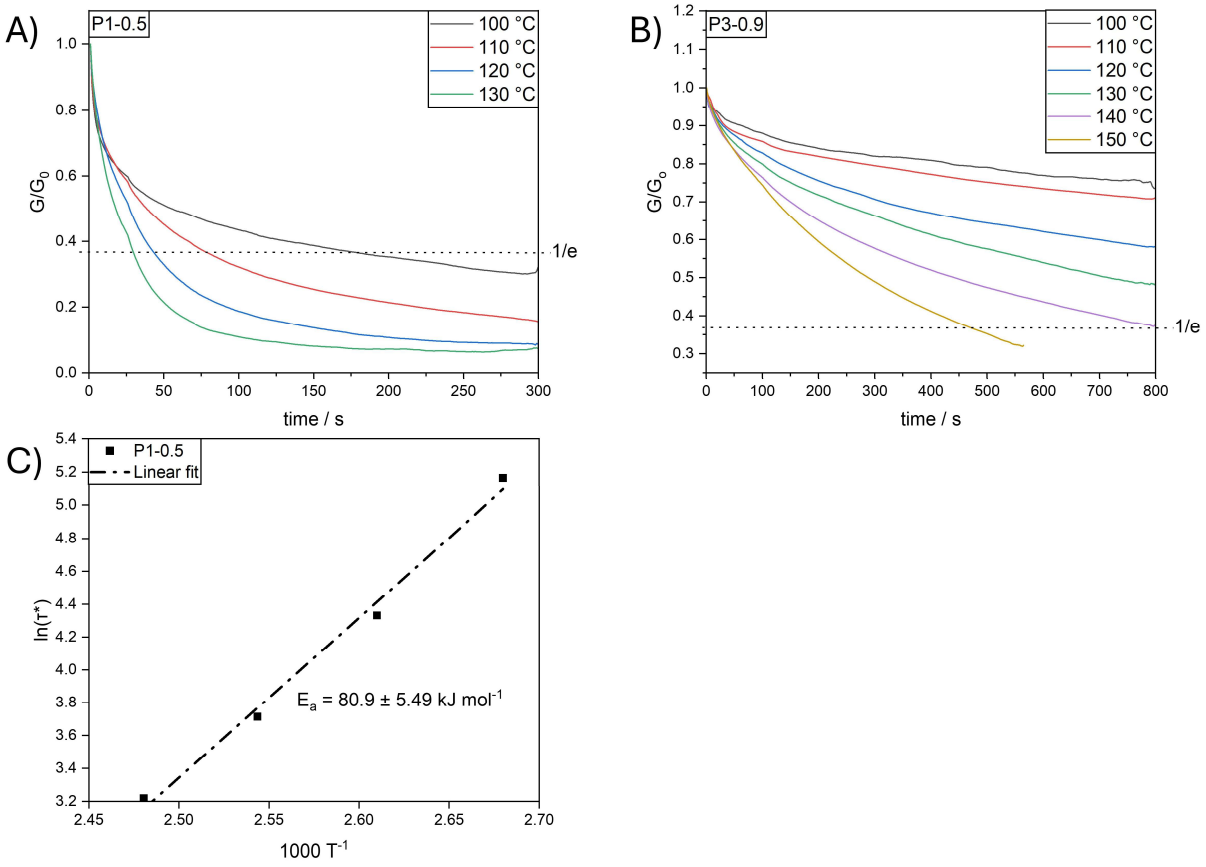

Figure 23. A) Stress relaxation measurements of **P1-0.5** at different temperatures with an applied strain of 1%. B) Stress relaxation measurements of **P3-0.9** at different temperatures with an applied strain of 1%. C) Arrhenius plot of the characteristic relaxation time τ* versus 1000 T^{-1} for **P1-0.5**.

More specifically, the stress relaxation time τ* decreased from 161 to 24 s for **P1-0.5** when increasing the temperature from 100 to 130 °C. Unfortunately, due to the slow

relaxation behavior of P3-0.9, the respective 1/e values of this material could only be reached at 150 °C (τ* = 480 s). As depicted in **Figure 23A and B**, the previous measurements at lower temperatures, i.e. 100 to 140 ° C, already clearly indicated that the stress relaxation in **P3-0.9** proceeded much slower than in **P1-0.5.** The occurrence of a comparatively slow relaxation in **P3-0.9** led to the assumption that free hydroxyl groups, which enable transacetalization reactions, were crucial for a fast relaxation and are therefore mainly responsible for the dynamic behavior of the materials. Having determined τ* values of **P1-0.5** at four different temperatures, i.e. 100 °C, 110 °C, 120 °C, and 130 °C, the characteristic activation energy of the occurring exchange reactions in this specific material was calculated according to the Arrhenius equation (**Eqn. 11**):

$$\tau^* = \tau_0 \, x \, e^{\frac{E_a}{RT}} \quad <=> \quad \ln\left(\frac{\tau^*}{\tau_0}\right) = \frac{E_a}{R} x \, \frac{1}{T} \qquad (11)$$

Here, τ* represents the characteristic stress relaxation time, τ^0 is the Arrhenius factor, R the universal gas constant, and T the temperature. Correspondingly, when plotting ln(τ*) against 1000 T^{-1} an activation energy of 80.8 ± 5.49 kJ mol^{-1} could be calculated for **P1-0.5** (**Figure 23C**). This value is lower than the activation energy in other systems containing acetals as dynamic linkages.[342] Thus, the relaxation in **P1-0.5** can occur significantly faster and further supposably at lower temperatures, due to the low T_g of the material enabling a high flexibility of the polymer chains.

Conclusion

In the current chapter, a fully renewable catechol containing high oleic sunflower oil-based polyol was accessed within 30 minutes at 120 °C *via* a H_2SO_4 (≥95%) catalyzed FCA. The structural characterization of the resulting product was conducted *via* ^{1}H NMR, ^{13}C NMR, 2D NMR, DOSY, ATR-IR, TGA, and DSC. Subsequently, a thermally induced catalyst and solvent-free reaction between hydroxyl groups of the polyol and a bifunctional vinyl ether, i.e. 1,4-cyclohexanedimethanol divinyl ether, was employed to synthesize fully renewable covalent adaptable networks (CANs) with different compositions. The successful crosslinking and the chemical composition of the CANs was herein confirmed by ATR-IR, swelling and gel content tests. Additionally, thermal properties of the obtained CANs were examined *via* DSC and TGA, as well as their potential dynamic behavior *via* stress relaxation measurements.

5 Conclusion and Outlook

The current thesis targeted the synthesis of functional (bio-based) materials for water decontamination *via grafting-onto* approaches. Herein, the *Twelve Principles of Green Chemistry* acted as a guiding framework.

In the first project, a cheap and comparably nontoxic superbase, i.e. 1,1,3,3-tetramethylguanidine, was implemented into the switchable solvent concept for cellulose dissolution. Upon investigation of the optimal solubilization conditions for cellulose in a DMSO/TMG/CO_2 switchable solvent system, a rapid homogenous microwave assisted modification approach, delivering short chain (mixed) cellulose esters with high molecular weights (59 kDa ≤ M_n ≤ 116 kDa) and variable side chain length (2 ≤ C ≤ 8) was developed. Therefore, cellulose was first transesterified with vinyl acetate to investigate the optimal reaction conditions. Subsequently, two polymer libraries including short chain cellulose esters and short chain mixed cellulose esters were synthesized. The structural characterization of all synthesized materials was subsequently performed *via* IR, ^{1}H NMR, ^{13}C NMR and SEC and confirmed the successful modification of cellulose within 10 minutes. The obtained DS values were determined using ^{1}H NMR and appeared for all synthesized (mixed) cellulose esters in the same range, i.e. 1.99 ≤ DS ≤ 2.34. In the second part of the chapter, structure-property relationships were examined *via* TGA, DSC, WCA, and tensile strength measurements. It was observed that the glass transition temperature and the Young´s modulus decreased, whereas the hydrophobicity increased with longer alkyl side chains. In order to show a potential application for the synthesized materials, selected cellulose esters were further used in collaboration with another research group for the preparation of water purification membranes.

In a second project, a literature known procedure using a DMSO/TBD/CO_2 switchable solvent system was employed to synthesize fully renewable fatty acid cellulose esters with different degrees of substitution (0.38 ≤ DS ≤ 0.62). These cellulose derivatives were inversely vulcanized delivering high sulfur content composite materials (~95 wt% sulfur). Upon successful inverse vulcanization, the structural composition of the crosslinked sections in the synthesized materials was investigated in detail *via* DSC, TGA, EDX, and SEM. Herein, it was shown that the content of covalently incorporated sulfur increased with higher degree of substitution, i.e. from 5.67 to 56.2 wt% and was therefore dependent on the structural constitution of the starting materials.

Furthermore, it was elaborated that the degree of substitution also influences the material properties of the pristine high sulfur content composites. More precisely, an increased functionalization in the starting materials, i.e. higher DS, led to a higher thermal stability (227 °C ≤ $T_{d,5\%}$ ≤ 247 °C), an elevated surface hydrophobicity (87° ≤ Θ ≤ 99°), and a lower mercury extraction efficiency (70 % ≤ $Hg^{2+}_{removal}$ ≤ 95 %).

In the third project, an efficient and straightforward synthetic strategy for the decoration of polybutadiene with catechol units *via* post polymerization modification using a Friedel Crafts alkylation was established. Therefore, two model compounds based on organic substrates with at least one alkene functionality, i.e. limonene and methyl oleate, were synthesized to understand and screen reaction parameters. The structural characterization for the successful synthesis of these model compounds was conducted *via* ^{1}H NMR, ^{13}C NMR, 2D NMR, DOSY, SEC, IR, and ESI-MS. The final decoration of polybutadiene with catechol was subsequently performed in bulk within 30 minutes at 120 °C using a sulfuric acid (≥95%) catalyzed Friedel Crafts alkylation. Herein, a degree of modification of 100% could be achieved. Upon synthesis, the final catechol containing polymer was characterized using ^{1}H NMR, ^{13}C NMR, 2D NMR, DOSY, SEC, IR, TGA, and DSC. Furthermore, it was shown that the respective polymer revealed excellent performance in metal ion removal tests (86 % ≤ $M^{n+}_{removal}$ < 100 %) which emphasized a potential application in water treatment.

In the final project, a sulfuric acid catalyzed Friedel Crafts alkylation was presented as a valuable tool to access a fully renewable catechol containing high oleic sunflower oil-based polyol. The modification was conducted in bulk within 30 minutes at 120 °C and the respective polyol was characterized *via* ^{1}H NMR, ^{13}C NMR, 2D NMR, DOSY, SEC, IR, TGA, and DSC. Subsequently, fully renewable covalent adaptable networks with different compositions were synthesized *via* a thermally induced solvent and catalyst-free click reaction between the polyol and a bifunctional vinyl ether. The structural characterization of the crosslinked materials was performed by IR, swelling and gel content tests. Material properties were examined by performing DSC and TGA and were supplemented by stress relaxation measurements that confirmed the dynamic behavior of selected materials.

6 Experimental Section

6.1 Materials

Microcrystalline cellulose (MCC, Sigma Aldrich) was dried under reduced pressure at 100 °C for 24 hours prior to use. Dimethyl sulfoxide (DMSO, dried and stored over molecular sieve, Acros Organics, >99.7%), carbon dioxide (CO_2, 999.995%, Air Liquide), vinyl acetate (Sigma Aldrich, >99%), vinyl propionate (TCI, >98%), vinyl butyrate (TCI, >98%), vinyl valerate (Sigma Aldrich, 97%), vinyl hexanoate (TCI, 99%), vinyl octanoate (TCI, >99%), tetramethylguanidine (TMG, TCI, >99%), pyridine (Sigma Aldrich, 99.8%), 1,5,7-triazabicyclo[4.4.0]dec-5-ene (TCI, ≥98%), methanol (VWR, ≥99.8%), methyl-10-undecenoate (Sigma Aldrich, 96%), *endo*-*N*-hydroxy-5-norbornene-2,3-dicarboximide (Alfa Aesar, 97%), catechol (Thermo Scientific, 99%), (+)-limonene (Acros Organics, 96%), liquid polybutadiene (Polyvest 110®, Evonik Operations GmbH, M_n = 2.6 kDa), sulfuric acid (Fisher Scientific, ≥95%), phosphoric acid (Fisher Scientific, 85%), perchloric acid (TCI, 70%), sodium sulfate (Thermo Scientific, 99%), tetrahydrofuran (Honeywell, ≥99.9%), mercury(II) chloride (Fisher Scientific, 99.5+%), copper(II)sulfate (Sigma Aldrich, ≥99.9%), iron(III) chloride (Fluka, >97%), zinc(II) chloride (Alfa Aesar, 98+%), aluminum(III) chloride (Thermo Scientific, 98.5%), lead(II) nitrate (Sigma Aldrich, 99%), silica gel (Sigma Aldrich, pore size 60 Å, mesh size of 230–240, particle size of 40–63 µm), high oleic sunflower oil (Lesieur), 1,4-cyclohexanedithenal divinyl ether (mixture of isomers, Sigma Aldrich, 98%), DMSO-d_6 (Eurisotop, 99.8%), and $CDCl_3$ (Eurisotop, 99.8%) were used without further purification. Elemental sulfur and all other solvents were employed in technical grade.

6.2 Instrumentation

Infrared Spectroscopy (IR)

Infrared spectra of all samples were recorded using a Bruker Alpha-p instrument with ATR technology in a range of v = 500–4000 cm^{-1} with 24 scans per measurement and a resolution of 4 cm^{-1}.

Nuclear magnetic resonance (NMR) spectroscopy

^1H NMR spectra were recorded using a Bruker Ascend 400 MHz with 16 scans and a delay time d_1 of 5 seconds at 298 K. The chemical shift was reported in ppm and referenced to the solvent signal of partly deuterated DMSO-d_6 at 2.50 ppm or $CDCl_3$

at 7.26 ppm. ^{13}C NMR spectra were recorded using a Bruker Avance DRX at 126 MHz with 8192 scans for cellulose samples and polymers and 1024 scans for organic molecules and a delay time d_1 of 3 seconds at 298 K. The signals were referenced to the solvent peak of partly deuterated DMSO-d_5 at 39.52 ppm or $CDCl_3$ at 77.16 ppm. ^{31}P NMR spectra were recorded using a Bruker Ascend instrument at 162 MHz with 1024 scans and a delay time d_1 of 5 seconds at 298 K.

Size Exclusion Chromatography (SEC)

SEC measurements of all cellulose samples were performed in HFIP containing 0.1 wt% potassium trifluoroacetate (KTFA) using a Tosoh EcoSEC HLC8320 SEC system. The solvent flow was 0.40 mL min^{-1} at 30 °C, and the concentration of the samples was 1 mg mL^{-1}. The analysis was performed using a three-column system: PSS PFG Micro precolumn (3.0 × 0.46 cm, 10,000 Å), PSS PFG Micro (25.0 × 0.46 cm, 1000 Å), and PSS PFG Micro (25.0 × 0.46 cm, 100 Å). The system was calibrated with linear poly(methyl methacrylate) standards (Polymer Standard Service, Mp: 102− 981 kDa).

A PSS SECcurity^2 GPC system based on Agilent Infinity 1260 II hardware was used for the measurements of all other samples. The system is equipped with a refractive index detector SECcurity^2 RI, a column oven "(Bio)SECcurity^2 column compartment TCC6500", a "standard SECcurity^2" autosampler, and an isocratic pump "SECcurity^2 isocratic pump". THF (flow rate, 1 mL/min) at 30 °C was used as the mobile phase. The analysis was performed using the following column system: two PSS SDV analytical columns (3 µm, 300 × 8.0 mm^2, 1000 Å) with a PSS SDV analytical precolumn (3 µm, 50 × 8.0 mm^2). For the calibration, narrow linear poly(methyl methacrylate) standards (Polymer Standards Service, PPS, Germany) ranging from 102 to 62.200 Da were used.

Differential Scanning Calorimetry (DSC)

<u>Cellulose esters – Chapter 4.1</u>

Thermal properties were measured on a TA DSC 2500 with a heating rate of 20 K·min^{-1} between -20 °C and 220 °C in TA Tzero sample holders. The glass transition temperature (T_g) was determined from the second heating run to eliminate possible interference from the polymer's thermal history.

Inverse Vulcanization of Fatty Acid Cellulose esters – Chapter 4.2

DSC measurements were performed on a Mettler Toledo DSC821e instrument using 100 µL aluminium crucibles under nitrogen atmosphere. The samples were measured in two heating cycles: 25–150 °C, 150 to −40 °C, and −40–150 °C at a heating/cooling rate of 10 K min^{-1}. The second heating cycle is shown in the DSC curves.

Catechol Containing Polymers – Chapter 4.3

Differential scanning calorimetry was performed on a 214 Polyma DSC device from NETZSCH (Selb, Germany). Around 5 mg of sample were precisely (Δ = 0.005 mg) weighed in an aluminum pan with a pierced lid for measurement. An aluminum pan filled with air was used as a reference and the heating rate was typically set to 10 K min^{-1} for all measurements. The samples were measured in two heating cycles using a liquid nitrogen cooling system: 25–160 °C, 160 to −130 °C, and −130 to 160 °C. The second heating cycle is shown in the DSC curves.

Acetal-based Covalent Adaptable Networks (CANs) – Chapter 4.4

Thermal properties were measured on a TA DSC 2500 with a heating rate of 10 K·min^{-1} between -40 °C and 200 °C in TA Tzero sample holders. The glass transition temperature (T_g) was determined from the second heating run to eliminate possible interference from the polymer's thermal history.

Thermogravimetric Analysis (TGA)

TGA measurements of all samples were carried out on the TA Instruments TGA 5500 under nitrogen atmosphere using platinum TGA sample pans and with a heating rate of 10 °C min^{-1}. Herein, the following temperature ranges were used for the different samples:

Cellulose esters – Chapter 4.1

25 to 500 °C

Inverse Vulcanization of Fatty Acid Cellulose esters – Chapter 4.2

25 °C to 500 °C for FACEs

25 °C to 600 °C for FACE-XS-washed

25 °C to 450 °C for FACE-XS

Catechol Containing Polymers – Chapter 4.3

25 °C to 800 °C.

Acetal-based Covalent Adaptable Networks (CANs) – Chapter 4.4

25 °C to 800 °C.

Water contact angel (WCA) measurements

Polymer films of cellulose esters were spin cast (4000 rpm, 30 s, in air) from a polymer/pyridine solution (100 µL, c = 1.67 g mL^{-1}) onto a glass surface at ambient temperature. Subsequent contact angle measurements of cellulose ester films and FACE-XS were performed with a DSA 25 contact angle goniometer (Krüss) using the sessile drop technique. A water droplet with a size of 5 µL was slowly added onto the spin cast films by a micrometer syringe and contact angles of the spin cast films against the water droplet were measured. The average value of five measurements was calculated for each sample with a standard deviation less than 1 for the cellulose ester films and between 3 and 6° for the high sulfur content composite materials FACE-XS.

Tensile strength measurement

Polymer films of cellulose esters were prepared by dissolving 100 mg of the respective material in 1.5 mL of pyridine and casting the solution into poly(tetrafluoro ethylene) plates (40 mm diameter). The solvent was evaporated overnight at room temperature. Subsequently, the polymer films were cut into dog bones (16 mm x 2 mm) and the thickness was determined with a digital vernier caliper. Tensile strength was measured using a Inspect table 10kN from Hegewald & Peschke with a 1.5 kN sensor. The initial speed was set to 5 mm min^{-1} and three samples were analyzed for each ester.

Gas Chromatography-Mass Spectrometry (GC-MS)

Gas chromatography-mass spectrometry (GC-MS) measurements were performed on a Varian 431 GC instrument with a HP-5 column (30 m × 0.32 mm × 0.25 µm) and a Varian 210 ion trap mass detector. Scans were performed from 40 to 650 m/z at a rate of 1.0 scan s^{-1}. Initial temperature at 95 °C for 1 min, heating to 220 °C with a rate of 15 °C min^{-1}, heating to 300 °C with a rate of 15 °C min^{-1}, heating to 325 °C with a rate of 15 °C min^{-1}, retaining 325 °C for 3 min. The injector transfer line temperature was set to 250 °C. Measurements were performed with a split ratio of 50:1 using helium as carrier gas with a flow rate of 1.0 mL min^{-1}.

Gas Chromatography (GC)

Gas chromatography (GC) measurements were performed on an Agilent 8860 gas chromatography instrument with a HP-5 column (30 m × 0.32 mm × 0.25 µm) and a flame ionization detector (FID). Samples were prepared by dissolving 1.5−5.0 mg of the respective compound in 1.5 mL of ethyl acetate. All samples were filtered via syringe filter (polytetrafluoroethylene, 13 mm diameter, 0.2 µm pore size, Agilent) prior to measurement. The heating program was as follows: Initial temperature at 95 °C, heating to 200 °C with a rate of 15 K min^{-1}, retaining 200 °C for 4 min, heating to 300 °C with a rate of 15 K min^{-1}, retaining 300 °C for 2 min. The injector transfer line temperature was set to 220 °C. Measurements were performed with a split ratio of 20:1 using nitrogen as make-up gas and helium as carrier gas with a flow rate of 1.87 mL min^{-1}.

Electrospray Ionization Mass Spectroscopy (ESI-MS)

Electrospray ionization (ESI) experiments were recorded on a Q-Exactive (Orbitrap) mass spectrometer (Thermo Fisher Scientific) equipped with a HESI II probe to record high resolution. The spectra were evaluated by molecular signals $[M+Na]^+$ and indicated with their mass-to-charge ratio (*m/z*).

Scanning electron microscopy (SEM)

For SEM analysis, the samples were sputtered with a thin layer of carbon. All analysed materials were investigated with a QUANTA FEG 650 scanning electron microscope from FEI with an accelerating voltage of 5–10 kV.

Energy dispersive X-ray (EDX) spectroscopy

For EDX spectroscopy, a QUANTAX (Esprit 1.9) from Bruker was used.

Atomic Absorption Spectrometry (AAS)

Cold-vapor AAS measurements were performed using a QuickTrace M-7600 from Teledyne Leeman Labs. Bromination reagent was added prior to measurements.

Inductively Coupled Plasma Atomic Emission Spectroscopy (ICP-AES)

ICP-AES measurements were performed on an ICP-AES 5100 SVDV, type G8010A from Agilent equipped with an SPS3 648480A autosampler. Samples were filtered through 0.45 µm pores and acidified with 100 µL 65% HNO_3 per 10 mL sample volume.

Rheometer

Rheology measurements were performed on an Anton Paar MCR302 equipped with disposable parallel aluminum plates (d = 5 mm). The sample was loaded and subsequently heated to the desired temperature (between 100 and 150 °C depending on the sample) before 1% of strain was applied under nitrogen.

6.3 Short Chain (Mixed) Cellulose Esters – Chapter 4.1

The experimental data of the current chapter have been published before:

T. Sehn, M. A. R. Meier, *Biomacromolecules* **2023**, *24*, 5255−5264.[308]

Text, figures, and data are reproduced from this article and were partially edited and extended.

6.3.1 Synthesis of Short Chain Cellulose Esters

Degree of substitution (DS) calculation

The degree of substitution (DS) of short chain cellulose esters was determined according to **Eqn**. **S1**:

$$DS_{1H} = \frac{7\ x\ I_{CH_3}}{3\ x\ I_{AGU}} \quad \text{(S1)}$$

I_{CH3}: Integral of the magnetic resonance signal, which is assigned to methyl groups in the ^{1}H NMR spectrum.

I_{AGU}: Integral of the magnetic resonance signal, which is assigned to the anhydroglucose unit (AGU) in the ^{1}H NMR spectrum.

Yield Calculation

Yields of short chain cellulose esters were determined according to **Eqn. S2**:

$$Yield = \frac{\left(\frac{m_{CE}}{M_{repunit}}\right)}{\left(\frac{m_{cellulose}}{M_{AGU}}\right)} \quad \text{(S2)}$$

$$M_{repunit} = M_{AGU} + (M_S - 1{,}01\ g\ mol^{-1})\ x\ DS_{1H}$$

m_{CE}: mass of cellulose ester

$m_{cellulose}$: mass of cellulose educt

$M_{repunit}$: average molar mass of CE repeating unit

M_{AGU}: molecular weight of anhydroglucose unit (162.14 g mol^{-1})

Optimization of Cellulose Acetate Synthesis in a DMSO/TMG/CO_2 Switchable Solvent System

In a microwave vial, microcrystalline cellulose (MCC, 0.10 g, 0.62mmol) was suspended in 3.33 mL of anhydrous DMSO followed by the dropwise addition of TMG (4.50 to 12.0 equiv. per AGU, depending on the derivative, **Table S1**). Subsequently, a CO_2 atmosphere (15 bar) was applied in a pressure reactor for 30 min at 50 °C until a homogeneous solution was obtained. Vinyl acetate (4.50 to 12.0 equiv. per AGU, depending on the derivative, **Table S1**) was then added, and the transparent reaction mixture was either conventional heated (4h at 60 °C) or subjected to microwave irradiation (300 W,10 min, 100-140 °C, depending on the derivative, **Table S1.** Results of the optimization process for the synthesis of cellulose acetate in a DMSO/TMG/CO2 switchable solvent system.. The desired CAs were precipitated under vigorous stirring in 60 mL of isopropanol and filtrated. In order to remove residual impurities and DMSO, the products were additionally stirred in 80 mL of isopropanol under reflux for 1 h, vacuum filtrated, and dried overnight under reduced pressure at 100 °C. The final products were obtained as white powdery solids.

Table S1. Results of the optimization process for the synthesis of cellulose acetate in a DMSO/TMG/CO_2 switchable solvent system.

	Conditions	Equivalents (VA/TMG)	Temperature / °C	Reaction time / min	Degree of Substitution (DS)
CA-1	heating	4.50/4.50	60	240	0.80
CA-2	heating	6.00/6.00	60	240	1.33
CA-3	heating	9.00/9.00	60	240	1.51
CA-4	microwave	9.00/9.00	60	10	1.49
CA-5	microwave	9.00/9.00	100	10	1.81
CA-6	microwave	9.00/9.00	140	10	2.06
CA-7	microwave	12.0/12.0	140	10	2.34

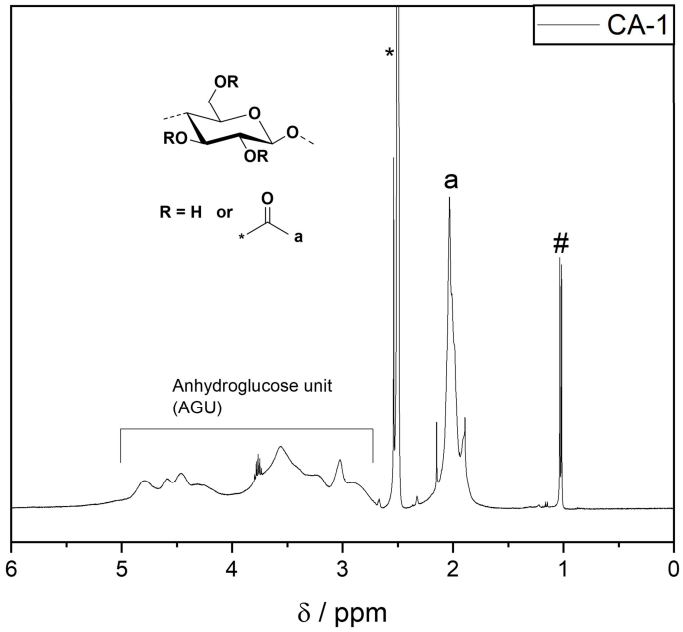

Figure S1. ^{1}H NMR (400 MHz) of **CA-1** in DMSO-d_6 (*) + TFA at ambient temperature. – DS_{1H} = 0.80; # - *iso*-propanol

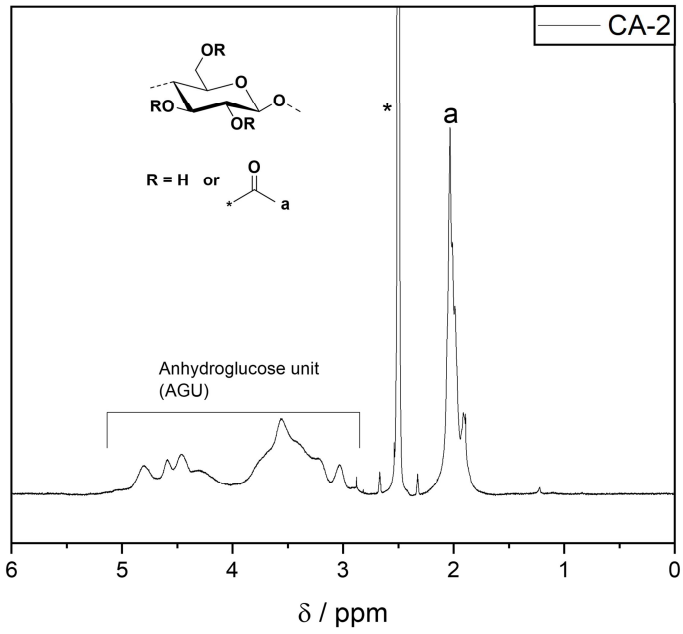

Figure S2. ^{1}H NMR (400 MHz) of **CA-2** in DMSO-d_6 (*) + TFA at ambient temperature. – DS_{1H} = 1.33

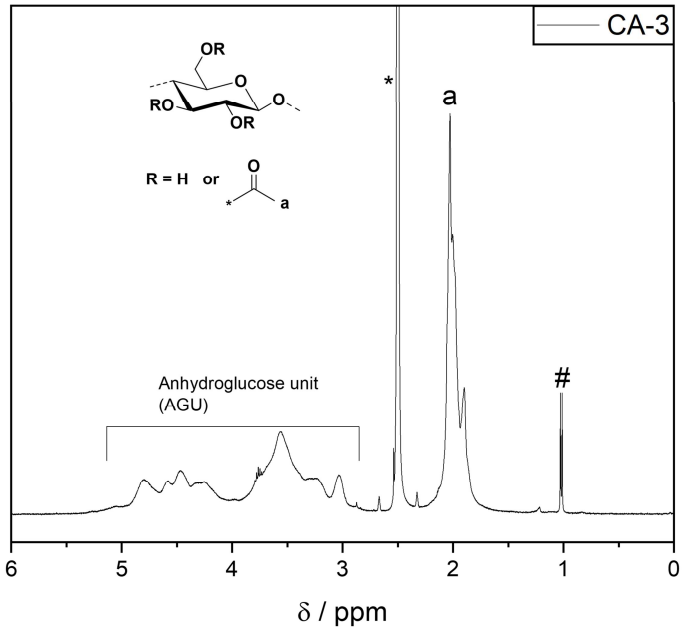

Figure S3. ^{1}H NMR (400 MHz) of **CA-3** in DMSO-d_6 (*) + TFA at ambient temperature. – DS_{1H} = 1.51; # - *iso*-propanol

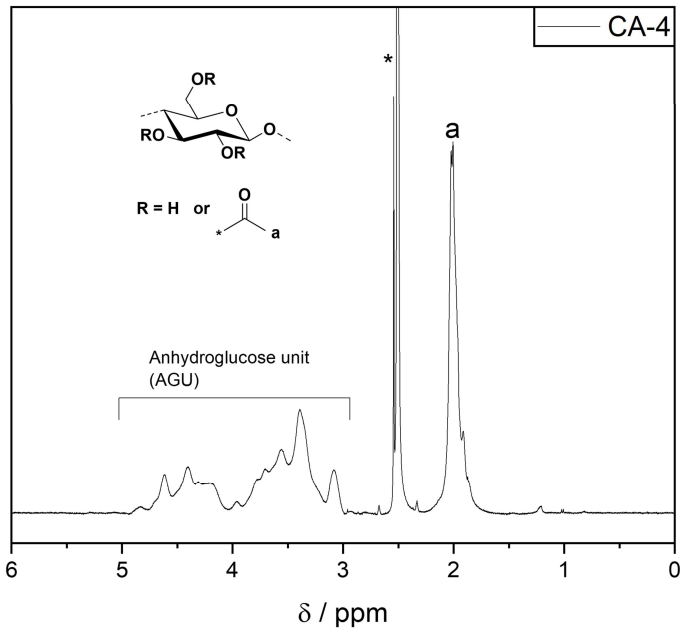

Figure S4. ^{1}H NMR (400 MHz) of **CA-4** in DMSO-d_6 (*) + TFA at ambient temperature. – DS_{1H} = 1.49

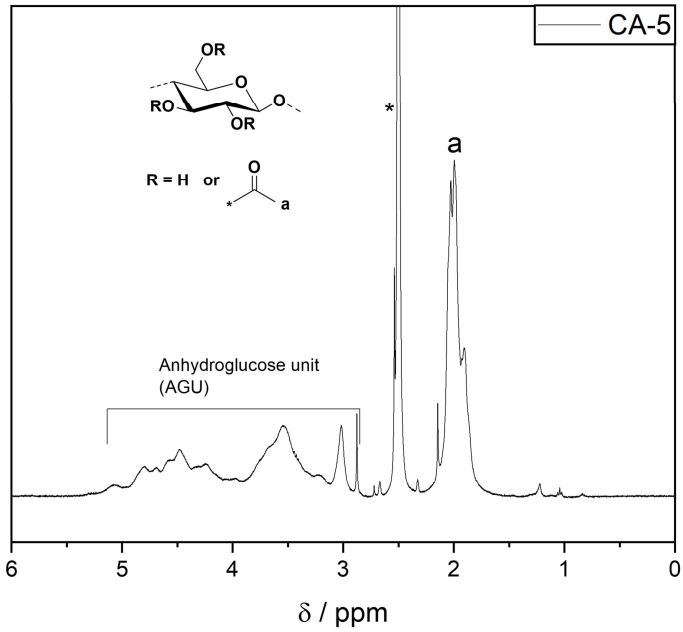

Figure S5. ^{1}H NMR (400 MHz) of **CA-5** in DMSO-d_6 (*) + TFA at ambient temperature. – DS_{1H} = 1.81

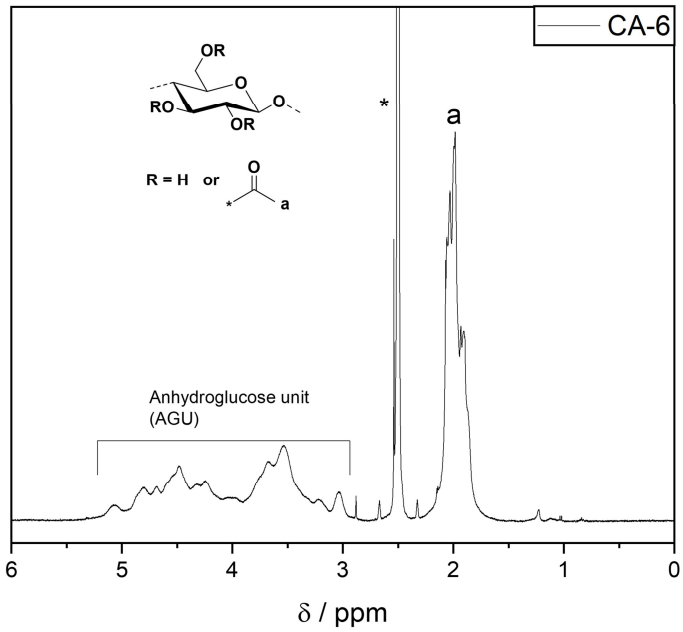

Figure S6. ^{1}H NMR (400 MHz) of **CA-6** in DMSO-d_6 (*) + TFA at ambient temperature. – DS_{1H} = 2.06

General Procedure for the Synthesis of Short Chain CEs

In a microwave vial, microcrystalline cellulose (MCC, 0.10 g, 0.62 mmol) was suspended in 3.33 mL anhydrous DMSO followed by the dropwise addition of TMG (0.93 mL, 0.86 g, 7.44 mmol, 12.0 equiv. per AGU). Subsequently, a CO_2 atmosphere (15 bar) was applied in a pressure reactor for 30 minutes at 50 °C until a homogeneous solution was obtained. The corresponding vinyl ester (7.44 mmol, 12.0 equiv. per AGU) was then added and the transparent reaction mixture was subjected to microwave irradiation (300 W) for 10 minutes at 140 °C. The desired CEs were precipitated under vigorous stirring in 60 mL isopropanol (or isopropanol/water mixture 3:1 wt% for CH and CO) and filtrated. In order to remove residual impurities and DMSO, the products were additionally stirred in 80 mL isopropanol under reflux for 1 h, vacuum filtrated and dried overnight under reduced pressure at 100 °C. The final products were obtained as white powdery solids. The corresponding yields were determined according to **Eqn. S2** (based on DS_{1H}) and ranged from 46 to 73%.

Cellulose Acetate (CA) – Yield: 73%

ATR-IR: v(cm^{-1}) = 3126 - 3711 v(O-H), 2812 - 3033 v(C-H), 1738 v(C=O), 1225 v(C-O_{ester}), 1034 v(C-O_{AGU}).

^{1}H NMR: (400 MHz, DMSO-d_6 + TFA) δ (ppm) = 5.37 – 2.88 (m, AGU, 7H), 2.20 – 1.63 (m, H_a, 3H).

DS_{1H} = 2.34

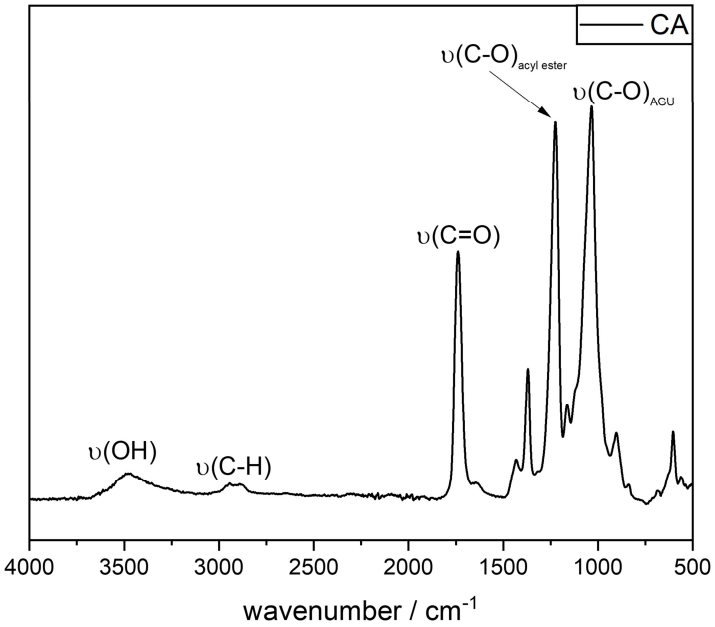

Figure S7. ATR-IR spectrum of **CA**.

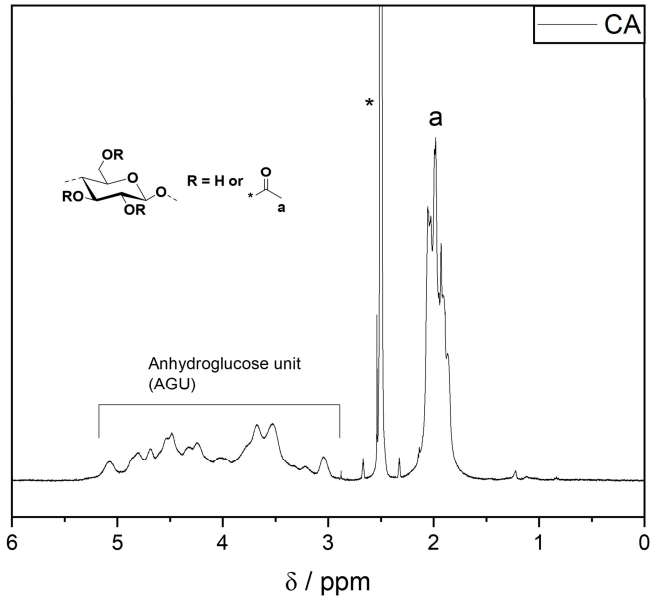

Figure S8. ^{1}H NMR (400 MHz) of **CA** in DMSO-d_6 (*) + TFA at ambient temperature.

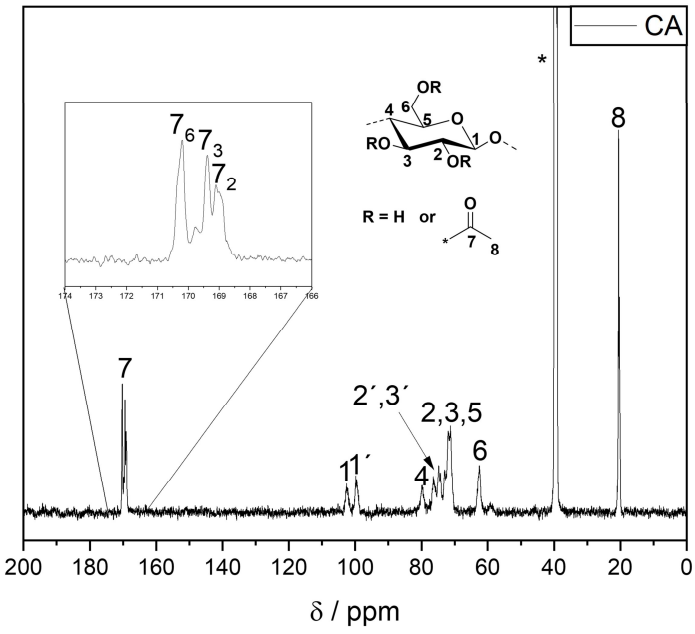

Figure S9. ^{13}C NMR (126 MHz) of **CA** in DMSO-d_6 (*) at ambient temperature.

Cellulose Propionate (CP) – Yield: 47%

ATR-IR: v(cm^{-1}) = 3094 - 3664 v(O-H), 2840 - 3041 v(C-H), 1738 v(C=O),1164 v(C-O_{ester}), 1061 v(C-O_{AGU}).

^{1}H NMR: (400 MHz, DMSO-d_6 + TFA) δ (ppm) = 5.30 – 2.76 (m, AGU, 7H), 2.43 – 1.83 (m, H_b, 2H), 1.29 – 0.43(m, H_a, 3H).

$DS_{^1H}$ = 2.15

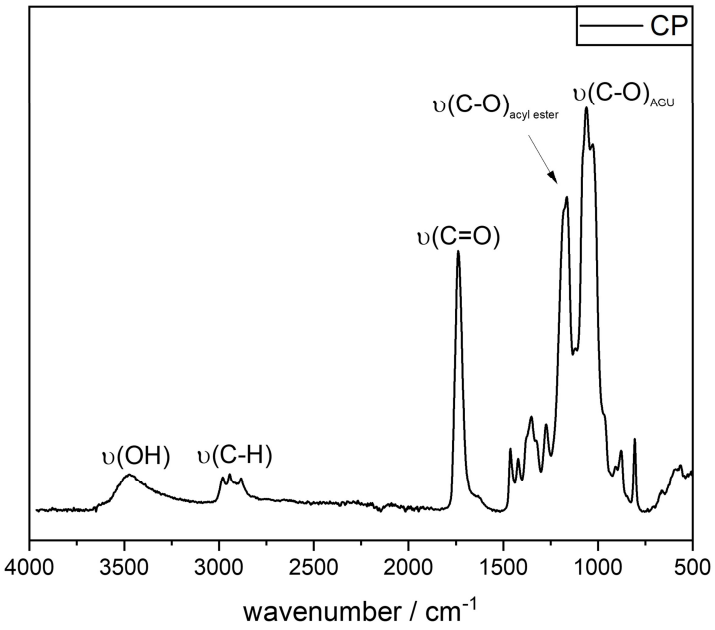

Figure S10. ATR-IR spectrum of **CP**.

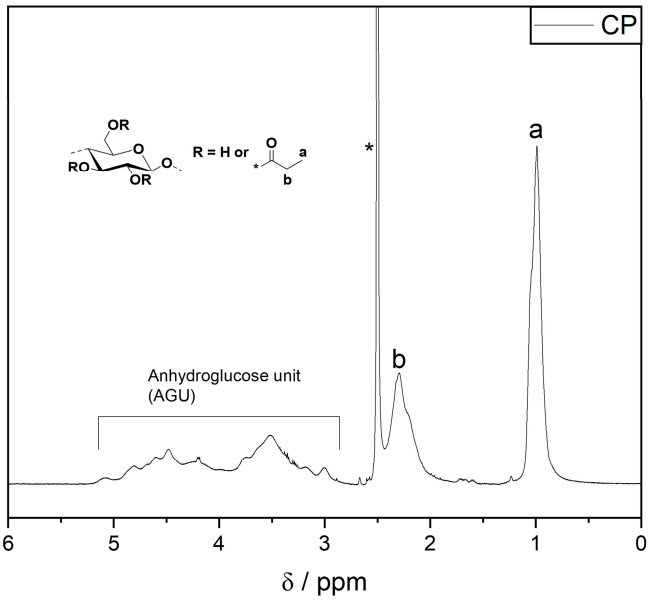

Figure S11. ^{1}H NMR (400 MHz) of **CP** in DMSO-d_6 (*) + TFA at ambient temperature.

Cellulose Butyrate (CB) – Yield: 58%

ATR-IR: v(cm^{-1}) = 3062 - 3674 v(O-H), 2772 - 3039 v(C-H), 1733 v(C=O), 1162 v(C-O_{ester}), 1038 v(C-O_{AGU}).

^{1}H NMR: (400 MHz, DMSO-d_6 + TFA) δ (ppm) = 5.32 – 2.75 (m, AGU, 7H), 2.39 – 1.84 (m, H_c, 2H), 1.54 (br, H_b, 2H), 0.88 (br, H_a, 3H).

DS_{1H} = 2.17

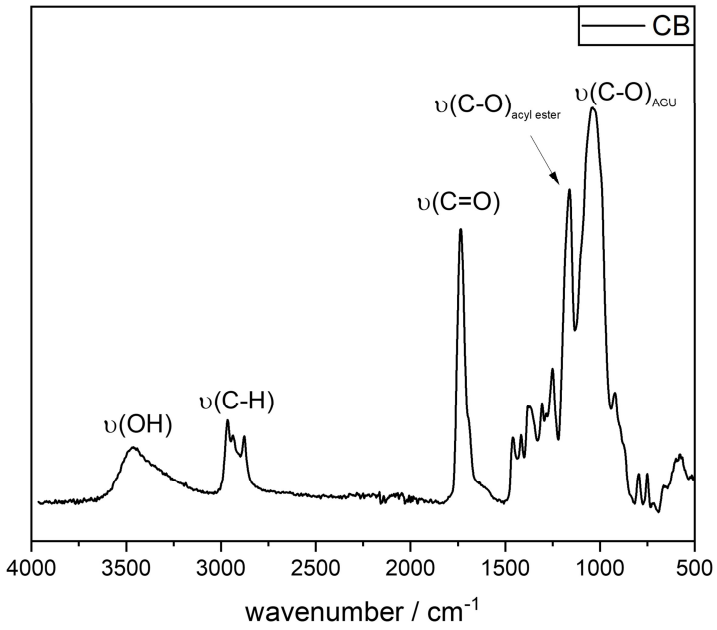

Figure S12. ATR-IR spectrum of **CB**.

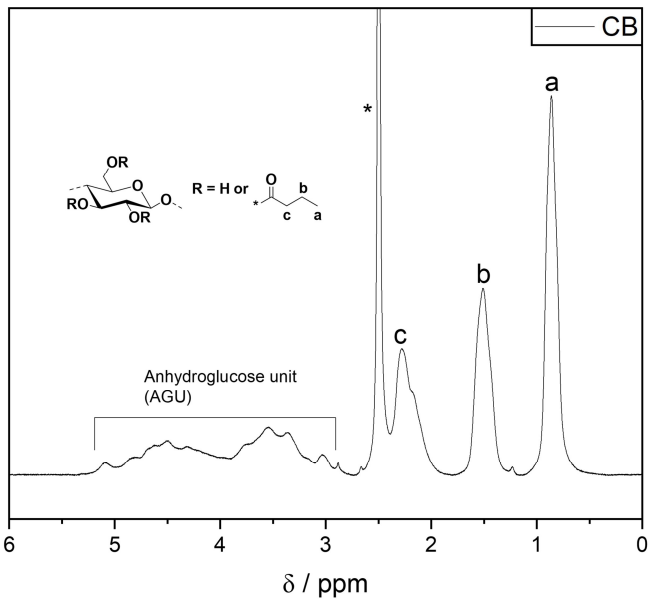

Figure S13. ^{1}H NMR (400 MHz) of **CB** in DMSO-d_6 (*) + TFA at ambient temperature.

Cellulose Valerate (CV) – Yield: 46%

ATR-IR: v(cm^{-1}) = 3083 - 3667 v(O-H), 2787 - 3027 v(C-H), 1733 v(C=O), 1160 v(C-O_{ester}), 1032 v(C-O_{AGU}).

^{1}H NMR: (400 MHz, DMSO-d_6 + TFA) δ (ppm) = 5.42 – 2.78 (m, AGU, 7H), 2.40 – 1.86 (m, H_d, 2H), 1.47 (br, H_c, 2H), 1.28 (br, H_b, 2H), 0.85 (br, H_a, 3H).

DS_{1H} = 2.05

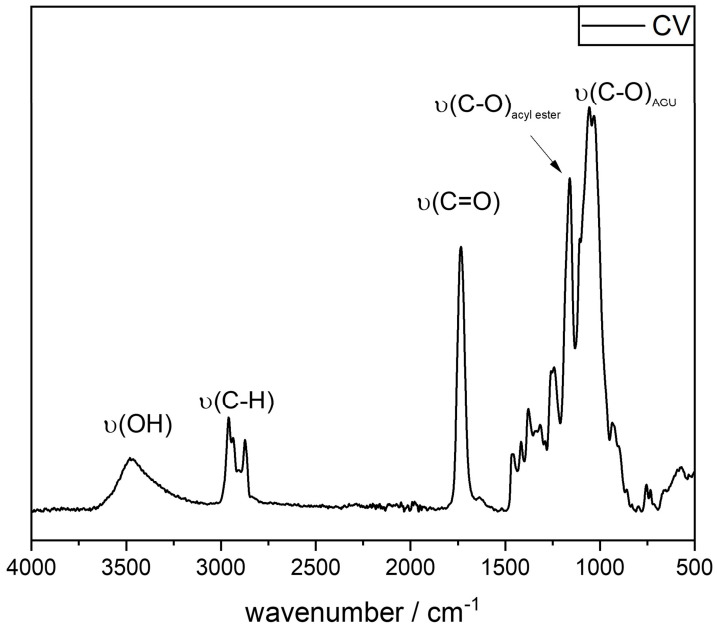

Figure S14. ATR-IR spectrum of **CV**.

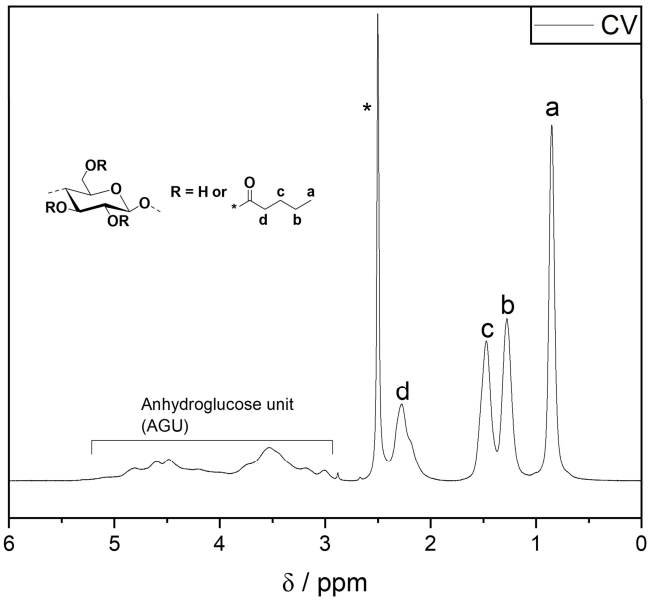

Figure S15. ^{1}H NMR (400 MHz) of **CV** in DMSO-d_6 (*) + TFA at ambient temperature.

Cellulose Hexanoate (CH) – Yield: 46%

ATR-IR: v(cm^{-1}) = 3068 - 3680 v(O-H), 2783 - 3033 v(C-H), 1738 v(C=O), 1158 v(C-O_{ester}), 1032 v(C-O_{AGU}).

^{1}H NMR: (400 MHz, DMSO-d_6 + TFA) δ (ppm) = 5.38 – 2.83 (m, AGU, 7H), 2.39 – 1.84 (m, H_d, 2H), 1.49 (br, H_c, 2H), 1.25 (br, H_b, 4H), 0.85 (br, H_a, 3H).

DS_{1H} = 2.17

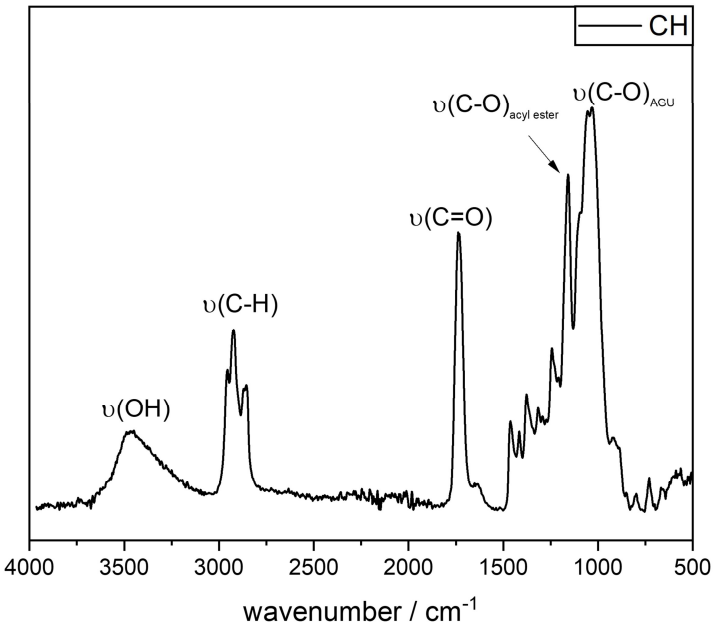

Figure S16. ATR-IR spectrum of **CH**.

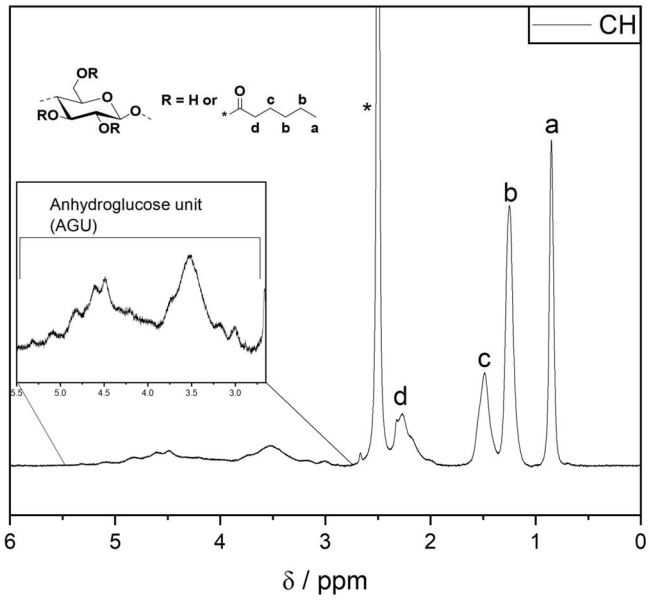

Figure S17. ^{1}H NMR (400 MHz) of **CH** in DMSO-d_6 (*) + TFA at ambient temperature.

Cellulose Octanoate (CO) – Yield: 52%

ATR-IR: v(cm^{-1}) = 3113 - 3667 v(O-H), 2769 - 3040 v(C-H), 1738 v(C=O), 1155 v(C-O_{ester}), 1034 v(C-O_{AGU}).

^{1}H NMR: (400 MHz, DMSO-d_6 + TFA) δ (ppm) = 5.42 – 2.93 (m, AGU, 7H), 2.37 – 1.89 (m, H_d, 2H), 1.49 (br, H_c, 2H), 1.25 (br, H_b, 8H), 0.84 (br, H_a, 3H).

DS_{1H} = 2.16

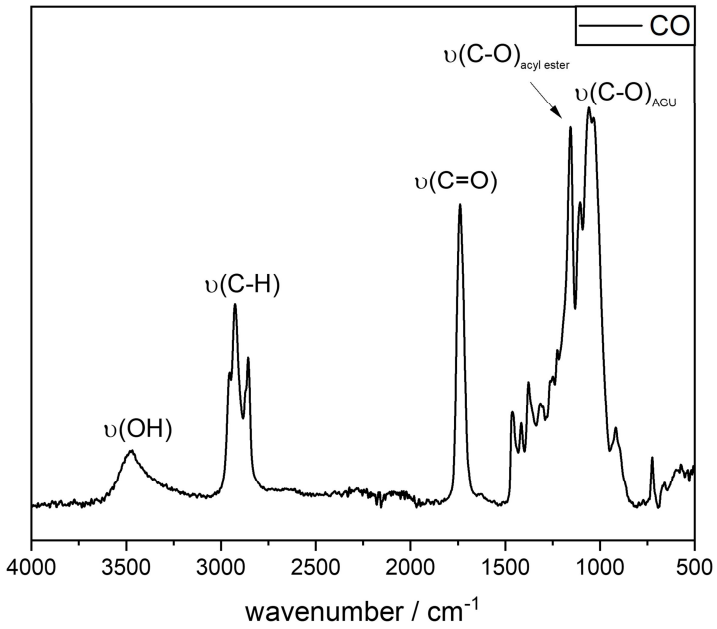

Figure S18. ATR-IR spectrum of **CO**.

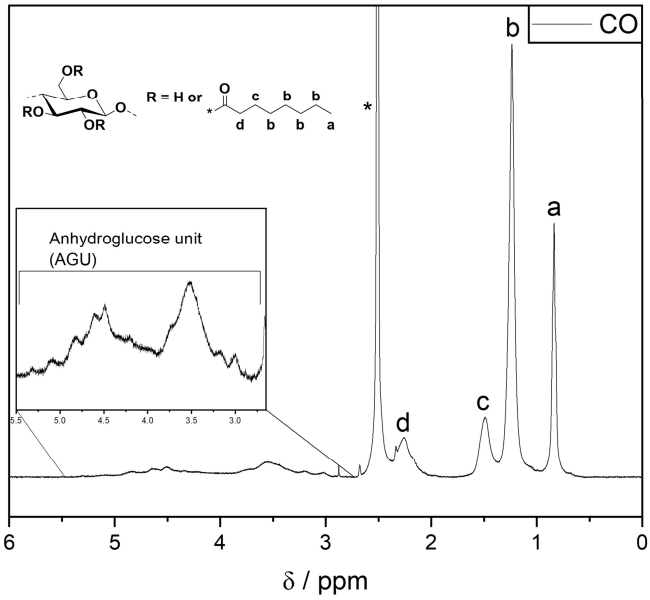

Figure S19. ^{1}H NMR (400 MHz) of **CO** in DMSO-d_6 (*) + TFA at ambient temperature.

6.3.2 Synthesis of Short Chain Mixed Cellulose Esters

Degree of substitution (DS) calculation

The degree of substitution (DS) of short chain mixed cellulose esters was determined according to **Eqn. S3**:

$$DS_{1H} = \frac{7\ x\ (I_{CH_3,Ac} + I_{CH_3,S2})}{3\ x\ I_{AGU}} \quad \text{(S3)}$$

$I_{CH3,\ Ac}$: Integral of the magnetic resonance signal, which is assigned to the methyl group of the acetyl side chain in the ^{1}H NMR spectrum.

$I_{CH3,\ S2}$: Integral of the magnetic resonance signal, which is assigned to the methyl group of the second ester side chain in the ^{1}H NMR spectrum.

I_{AGU}: Integral of the magnetic resonance signal, which is assigned to the anhydroglucose unit (AGU) in the ^{1}H NMR spectrum.

Yield Calculation

Yields of short chain mixed cellulose esters were determined according to **Eqn. S4**:

$$Yield = \frac{\left(\frac{m_{mixed\ CE}}{M_{repunit}}\right)}{\left(\frac{m_{cellulose}}{M_{AGU}}\right)} \quad \text{(S4)}$$

$$M_{repunit} = M_{AGU} + ((M_{S1} - 1{,}01\ g\ mol^{-1})\ x\ DS_{1H(Ac)}) + ((M_{S2} - 1{,}01\ g\ mol^{-1})\ x\ DS_{1H\ (S2)})$$

$m_{mixed\ CE}$: mass of mixed cellulose ester

$m_{cellulose}$: mass of cellulose educt

$M_{repunit}$: average molar mass of CE repeating unit

M_{AGU}: molecular weight of anhydroglucose unit (162.14 g mol^{-1})

General Procedure for the Synthesis of Short Chain Mixed CEs

In a microwave vial, microcrystalline cellulose (MCC, 0.10 g, 0.62 mmol) was suspended in 3.33 mL DMSO (anhydrous 99.9%) followed by the dropwise addition of TMG (0.93 mL, 0.86 g, 7.44 mmol, 12.0 equiv. per AGU). After transferring the reaction mixture into a pressure reactor, a CO_2 atmosphere (15 bar) was applied for 30 minutes at 50°C until a transparent yellowish solution was obtained. Subsequently, vinyl acetate

(0.34 mL, 0.32 g, 3.72 mmol, 6.00 equiv. per AGU) as well as the corresponding second vinyl ester (3.72 mmol, 6.00 equiv. per AGU) were added and the transparent reaction mixture was subjected to microwave irradiation (300 W) for 10 minutes at 140 °C. The desired CEs were precipitated under vigorous stirring in 60 mL isopropanol and filtrated. In order to remove residual impurities and DMSO, the products were additionally stirred in 80 mL isopropanol under reflux for 1 h, vacuum filtrated and dried overnight under reduced pressure at 100 °C. The final products were obtained as white powdery solids. The corresponding yields were determined according to **Eqn. S4** (based on DS_{1H}) and ranged from 39 to 60%.

Cellulose Acetate Propionate (CAP) – Yield: 61%

ATR-IR: v(cm^{-1}) = 3144 – 3691 v(O-H), 2778 - 3033 v(C-H), 1731 v(C=O), 1225 v(C-O_{ester}), 1162 v(C-O_{S2}), 1026 v(C-O_{AGU}).

^{1}H NMR: (400 MHz, DMSO-d_6) δ (ppm) = 5.49 – 2.82 (m, AGU, 7H), 2.42 – 2.11 (m, H_b, 2H), 2.10 – 1.60 (m, $H_{a'}$, 3H), 1.02 (br, H_a, 3H).

DS_{1H} = 2.11

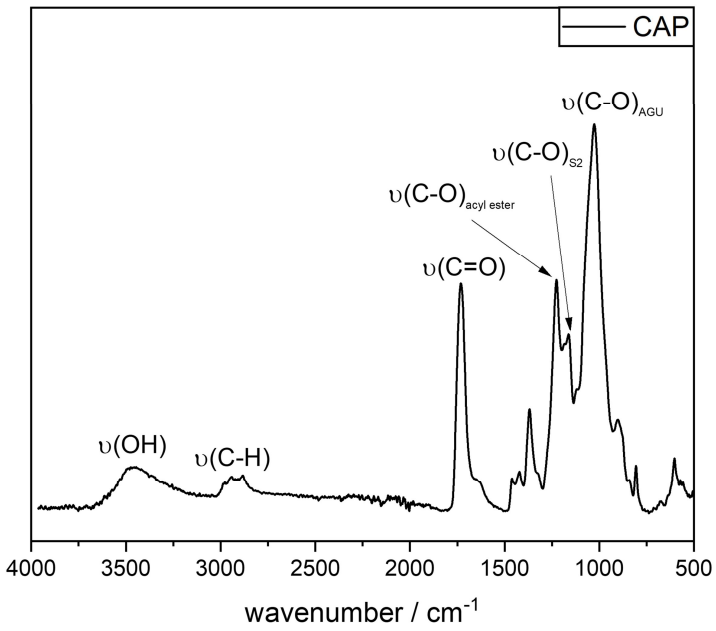

Figure S20. ATR-IR spectrum of **CAP**.

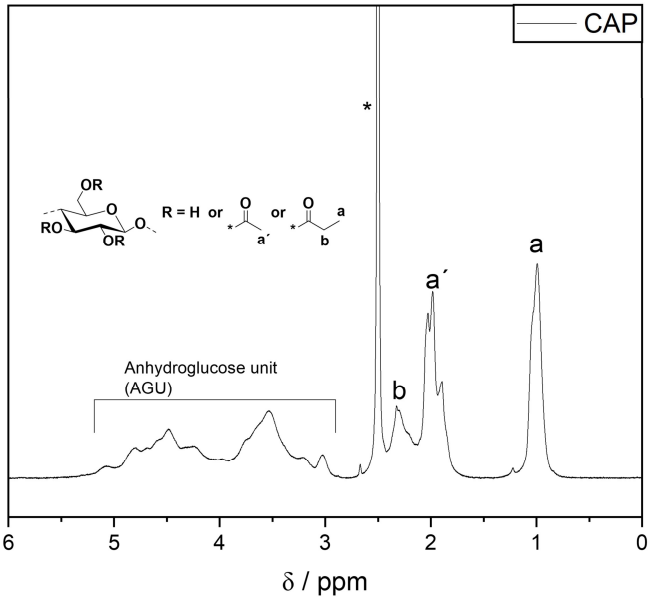

Figure S21. ^{1}H NMR (400 MHz) of **CAP** in DMSO-d_6 (*) + TFA at ambient temperature.

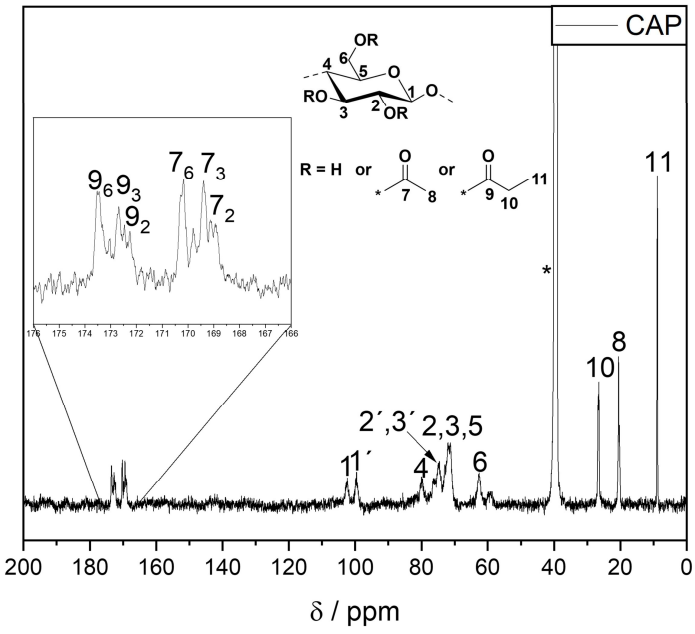

Figure S22. ^{13}C NMR (126 MHz) of **CAP** in DMSO-d_6 (*) at ambient temperature.

Cellulose Acetate Butyrate (CAB) – Yield: 47%

ATR-IR: v(cm^{-1}) = 3115 – 3651 v(O-H), 2807 - 3033 v(C-H), 1731 v(C=O), 1227 v(C-O_{ester}), 1165 v(C-O_{S2}), 1032 v(C-O_{AGU}).

^{1}H NMR: (400 MHz, DMSO-d_6) δ (ppm) = 5.43 – 2.76 (m, AGU, 7H), 2.39 – 2.12 (m, H_c, 2H), 2.10 – 1.68 (m, $H_{a'}$, 3H), 1.52 (br, H_b, 2H), 0.87 (br, H_a, 3H).

DS_{1H} = 2.13

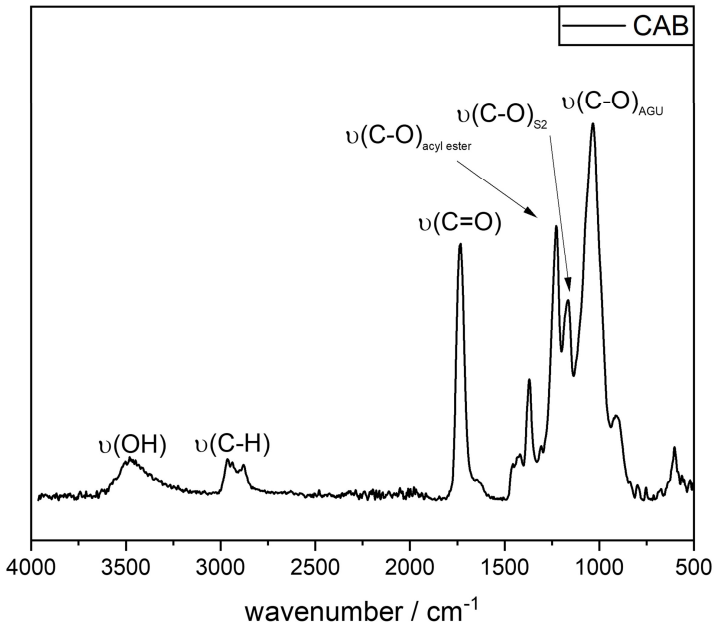

Figure S23. ATR-IR spectrum of **CAB**.

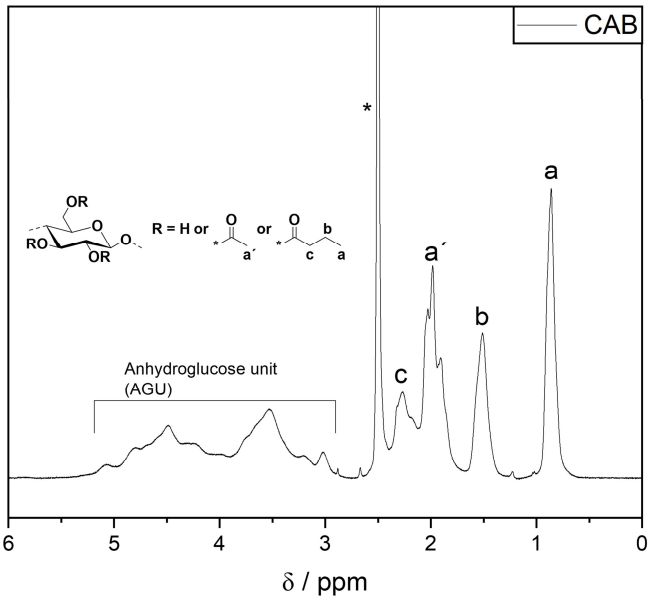

Figure S24. ^{1}H NMR (400 MHz) of **CAB** in DMSO-d_6 (*) + TFA at ambient temperature.

Cellulose Acetate Valerate (CAV) – Yield: 39%

ATR-IR: v(cm^{-1}) = 3095 – 3674 v(O-H), 2762 - 3033 v(C-H), 1733 v(C=O), 1223 v(C-O_{ester}), 1160 v(C-O_{S2}), 1028 v(C-O_{AGU}).

^{1}H NMR: (400 MHz, DMSO-d_6) δ (ppm) = 5.41 – 2.75 (m, AGU, 7H), 2.40 – 2.12 (m, H_d, 2H), 2.11 – 1.67 (m, $H_{a'}$, 3H), 1.47 (br, H_c, 2H), 1.27 (br, H_b, 2H), 0.84 (br, H_a, 3H).

DS_{1H} = 1.99

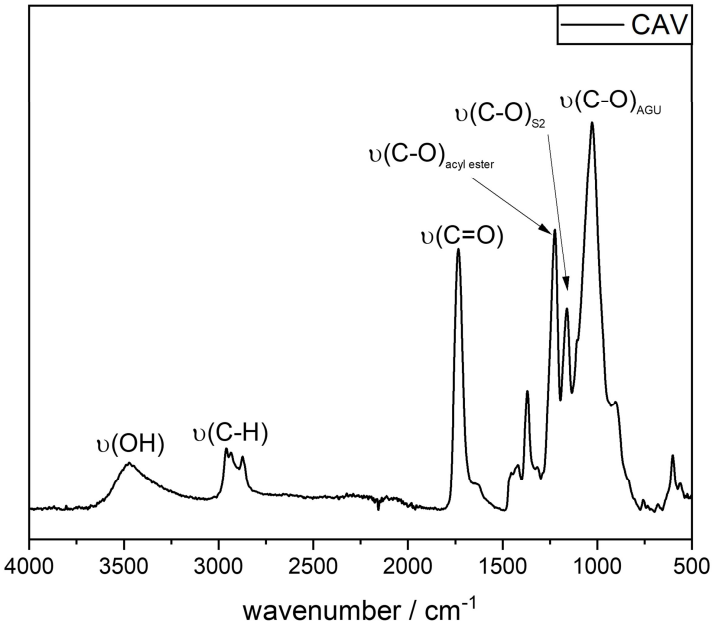

Figure S25. ATR-IR spectrum of **CAV**.

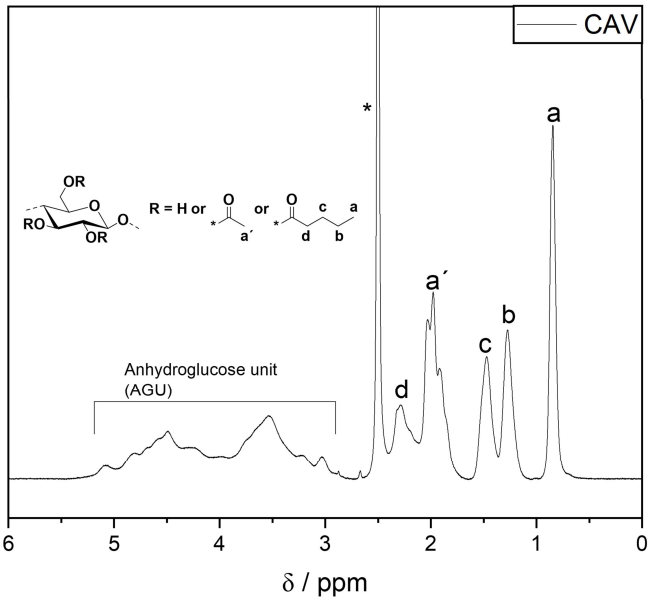

Figure S26. ^{1}H NMR (400 MHz) of **CAV** in DMSO-d_6 (*) + TFA at ambient temperature.

Cellulose Acetate Hexanoate (CAH) – Yield: 58%

ATR-IR: v(cm^{-1}) = 3115 – 3686 v(O-H), 2783 - 3033 v(C-H), 1733 v(C=O), 1223 v(C-O_{ester}), 1160 v(C-O_{S2}), 1030 v(C-O_{AGU}).

^{1}H NMR: (400 MHz, DMSO-d_6) δ (ppm) = 5.34 – 2.77 (m, AGU, 7H), 2.40 – 2.14 (m, H_d, 2H), 2.12 – 1.66 (m, $H_{a'}$, 3H), 1.51 (br, H_c, 2H), 1.26 (br, H_b, 4H), 0.84(br, H_a, 3H).

DS_{1H} = 2.16

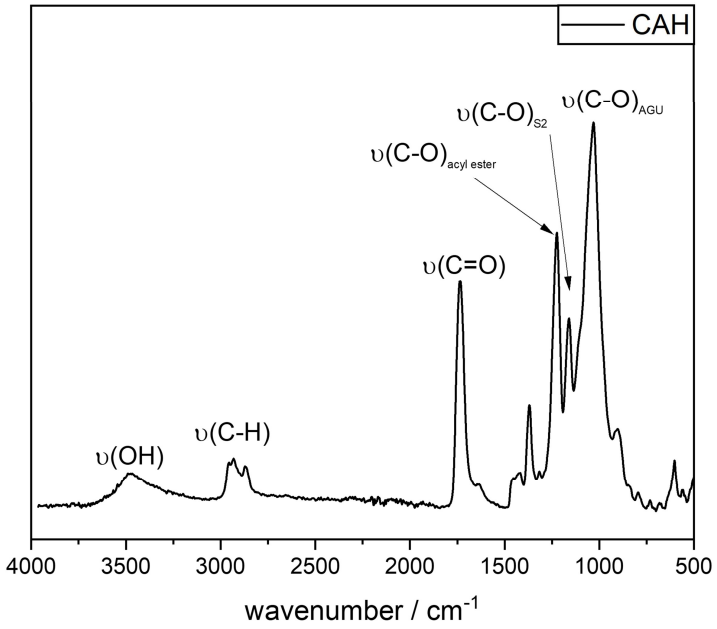

Figure S27. ATR-IR spectrum of **CAH**.

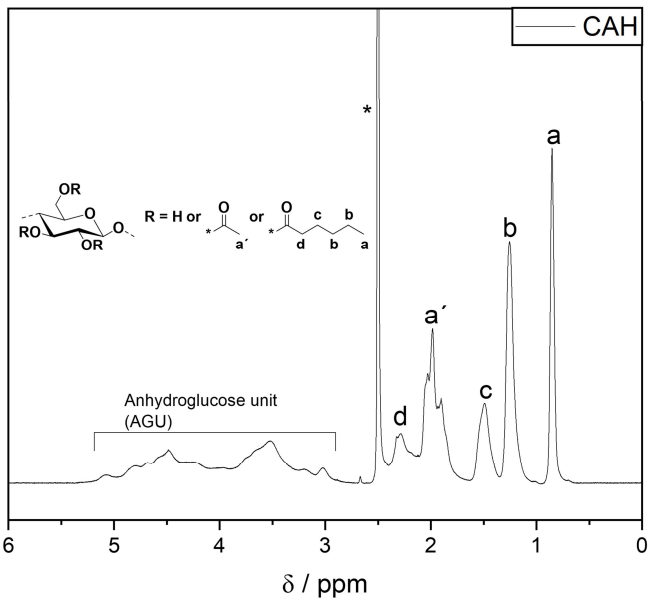

Figure S28. ^{1}H NMR (400 MHz) of **CAH** in DMSO-d_6 (*) + TFA at ambient temperature.

Cellulose Acetate Octanoate (CAO) – Yield: 41%

ATR-IR: v(cm^{-1}) = 3221 - 3686 v(O-H), 2760 - 3033 v(C-H), 1738 v(C=O), 1223 v(C-O_{ester}), 1154 v(C-O_{S2}), 1028 v(C-O_{AGU}).

^{1}H NMR: (400 MHz, DMSO-d_6) δ (ppm) = 5.44 – 2.83 (m, AGU, 7H), 2.39 – 2.12 (m, H_d, 2H), 2.13 – 1.67 (m, $H_{a'}$, 2H), 1.48 (br, H_c, 2H), 1.22 (br, H_b, 6H), 0.82 (br, H_a, 3H).

DS_{1H} = 2.09

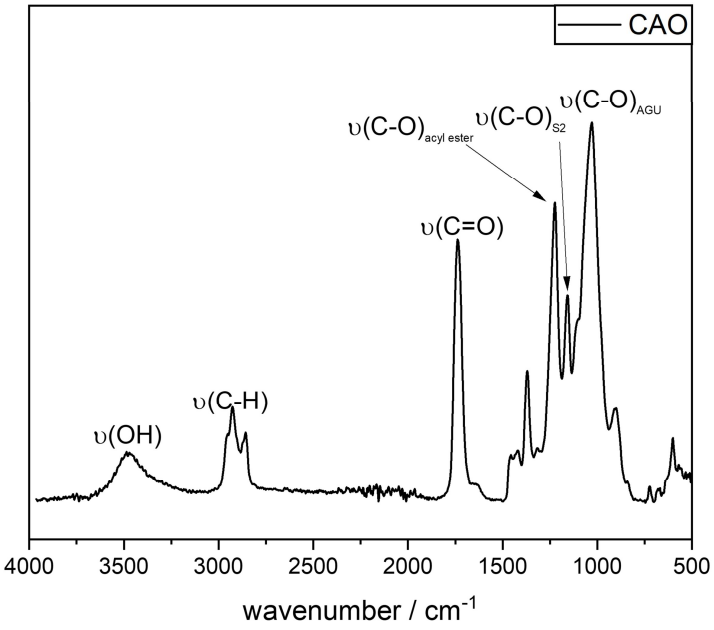

Figure S29. ATR-IR spectrum of **CAO**.

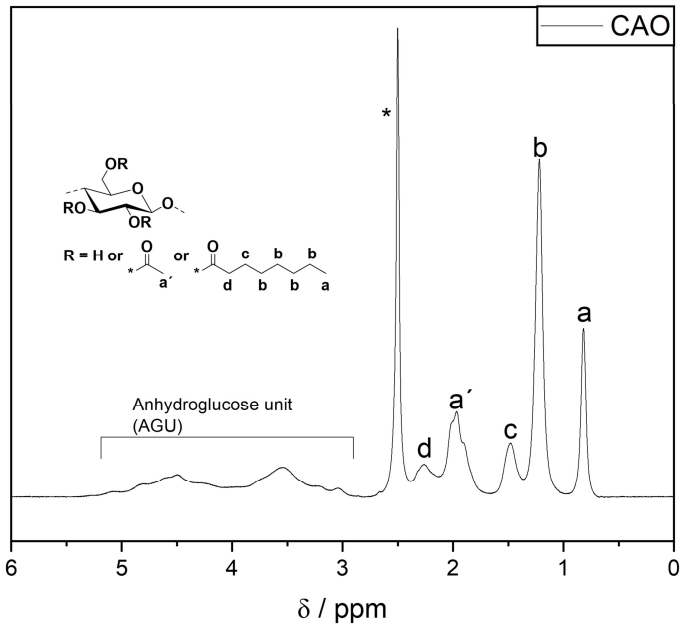

Figure S30. ^{1}H NMR (400 MHz) of **CAO** in DMSO-d_6 (*) + TFA at ambient temperature.

6.3.3 Supporting Figures

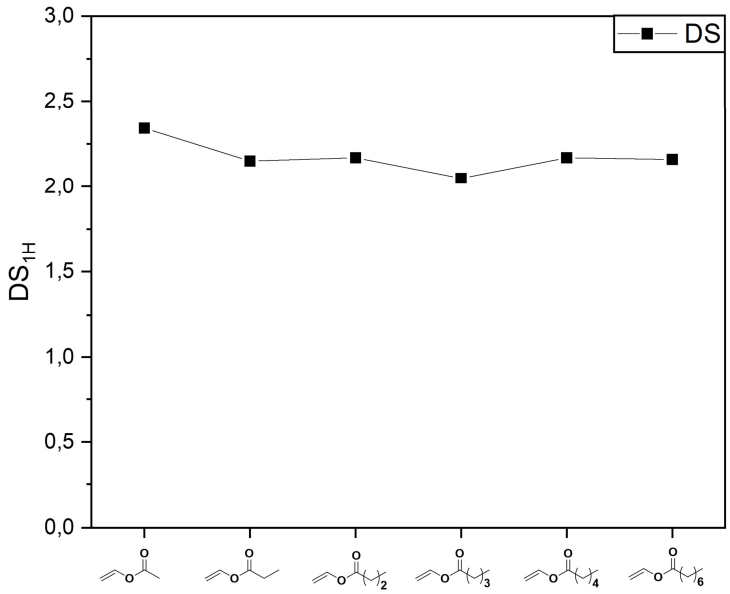

Figure S31. Degree of substitution (DS_{1H}) of short chain cellulose esters synthesized in a DMSO/TMG/CO_2 switchable solvent system.

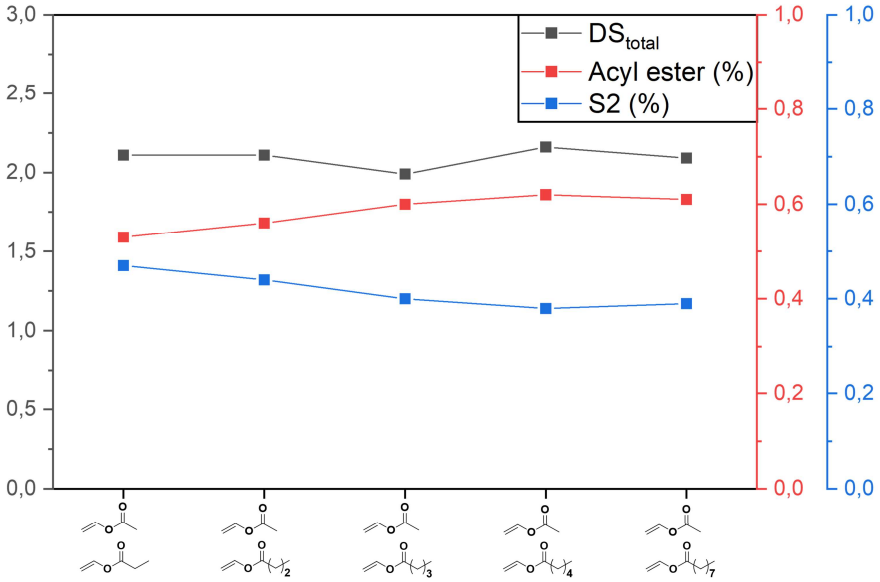

Figure S32. (1) Degree of substitution (DS_{1H}) of short chain mixed cellulose esters synthesized in a DMSO/TMG/CO_2 switchable solvent system (black line). (2) Incorporation ratio of introduced ester side chains.

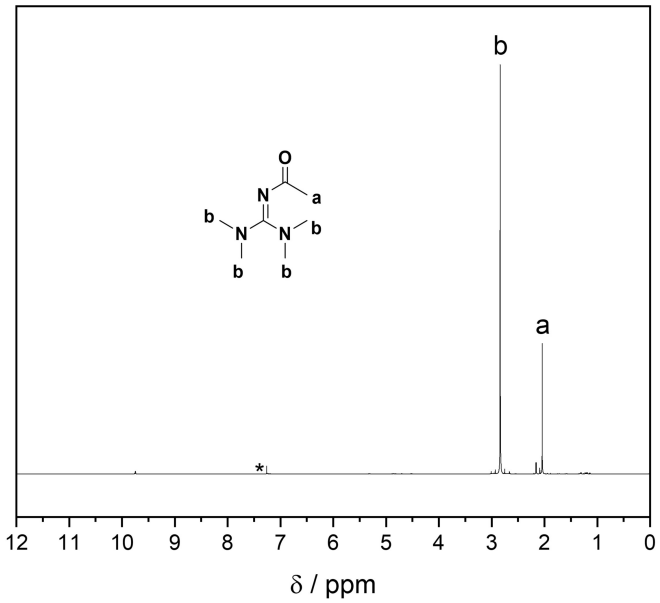

Figure S33. ^{1}H NMR (400 MHz) of acyl-TMG in $CDCl_3$ (*) at ambient temperature.

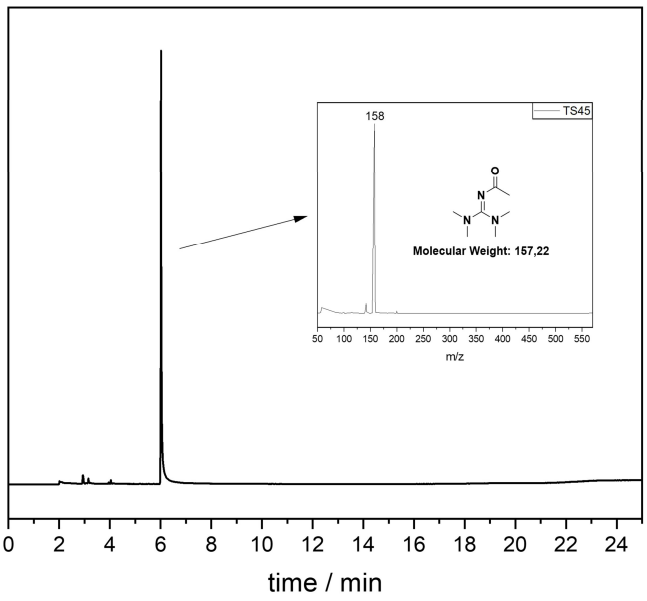

Figure S34. GC-MS spectrum of acyl-TMG.

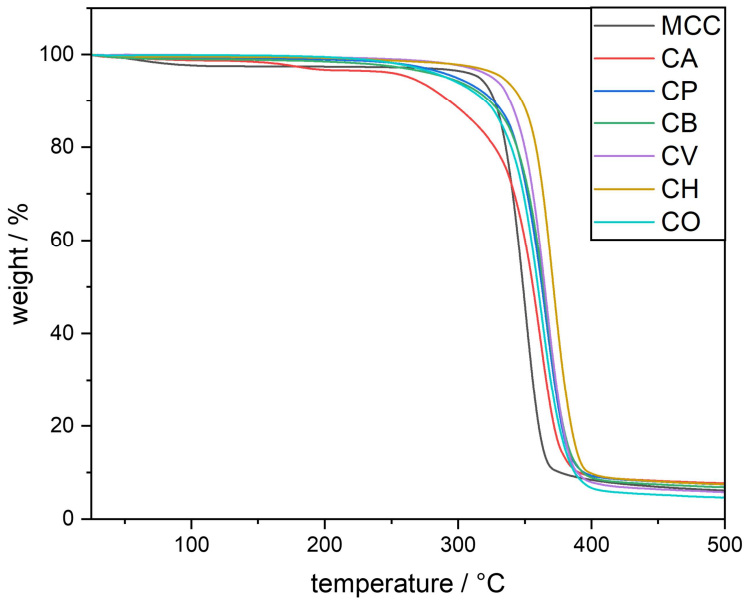

Figure S35. Thermogravimetric analysis (TGA) of MCC (black line), **CA** (red line), **CP** (blue line), **C**B (green line), **CV** (violet line), **CH** (yellow line) and **CO** (light blue line) from 25 to 500 °C with a heating rate of 10 K min^{-1} under a nitrogen flow.

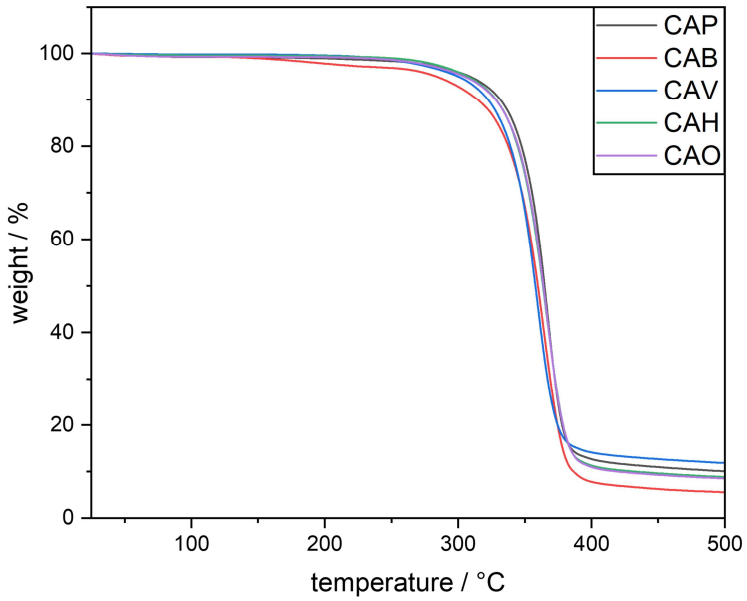

Figure S36. Thermogravimetric analysis (TGA) of **CAP** (black line), **CAB** (red line), **CAV** (blue line), **CAH** (green line) and **CAO** (violet line) from 25 to 500 °C with a heating rate of 10 K min^{-1} under a nitrogen flow.

6.4 High Sulfur Content Composite Materials from Renewable Fatty Acid Cellulose Esters – Chapter 4.2

The experimental data of the current chapter have been published before:

T. Sehn, J. Fanelli, L. Wahl, M. A. R. Meier, *RSC Sustainability* **2025**, *3*, 291–299.[319]

Text, figures, and data are reproduced from this article and were partially edited and extended.

6.4.1 Synthesis of Fatty Acid Cellulose Esters (FACEs)

Yield Calculation for FACEs

The corresponding yields of the synthesized FACE were determined according to **Eqn. S5** and **S6**:

$$\text{Yield} = \frac{\left(\frac{m_{CE}}{M_{repunit}}\right)}{\left(\frac{m_{cellulose}}{M_{AGU}}\right)} \quad \text{(S5)}$$

$$M_{repunit} = M_{AGU} + (M_S - 1{,}01\ \text{g mol}^{-1})\ \text{x}\ DS_{1H} \quad \text{(S6)}$$

m_{CE}: mass of cellulose ester

$m_{cellulose}$: mass of cellulose educt

$M_{repunit}$: average molar mass of CE repeating unit

M_{AGU}: molecular weight of anhydroglucose unit (162.14 g mol^{-1})

M_S: molecular weight of the substituent (without the linking oxygen atom between the substituent and the cellulose backbone; 167.27 g mol^{-1})

^{31}P NMR for DS determination

The DS of the synthesized FACEs were calculated as previously published by Kilpeläinen et al.[320] according to **Eqn. S7** and **S8**:

$$DS = DS_{max} \times \frac{\frac{1}{OH_S} - \frac{1}{OH_C}}{M_S + \frac{1}{OH_S} - 1} \quad (S7)$$

$$OH_S = \frac{C_{IS} \text{ x } V_{IS} \text{ x } I_R}{1000000 \text{ x } m_S} \quad (S8)$$

DS_{max}: highest achievable DS value (3 for unsubstituted cellulose)

M_S: molecular weight of the substituent (without the linking oxygen atom between the substituent and the cellulose backbone; 167.27 g mol^{-1})

c_{IS}: concentration of the internal standard (mmol L^{-1})

V_{IS}: volume of the employed internal standard (μL)

I_R: integration ratio of remaining functionalized cellulose hydroxyl groups against internal standard

m_S: sample mass (mg)

OH_S: free hydroxyl groups per weight unit of substrate (mol g^{-1})

OH_C: free hydroxyl groups per weight unit of cellulose ($OH_C = DS_{max}/M_{AGU}$ = 3 /162.14 g mol^{-1})

General Procedure for the Synthesis of FACEs

Fatty acid cellulose esters (FACE) were synthesized according to a literature known procedure.[154]

Accordingly, microcrystalline cellulose (MCC, 0.50 g, 3.08 mmol) was suspended in 10 mL DMSO (anhydrous, 99.9%) in a two neck round bottom flask. Subsequently, TBD (1.28 g, 9.25 mmol) was added, and the reaction mixture was stirred after applying a continuous CO_2 flow for 20 minutes at 50 °C. The homogenous solution was then heated to 95 °C and methyl-10-undecenoate (0.66 equiv., 1.16 equiv. and 3.00 equiv. per AGU for FACE-1, FACE-2, and FACE-3, respectively.) was added in a dropwise manner. The dark brown mixture was stirred for 6 h under air flow, diluted with 10 mL

of anhydrous DMSO and precipitated under vigorous stirring in 200 mL of water. The residue was filtered, stirred in methanol again filtrated and subsequently dried under reduced pressure at 80 °C. The corresponding yields were determined dependent on the DS_{31P} according to **Eqn. S5** and **S6.**

General procedure for DS determination via ^{31}P NMR spectroscopy

An exact amount of the corresponding FACE (20 mg) was dissolved in 1.00 mL of pyridine. Subsequently, 1.00 mL of $CDCl_3$ and 2-chloro-4,4,5,5-tetramethyl-1,3,2-dioxaphospholane (2-Cl-TMDP, 200 µL, 1.26 mmol) were added and the reaction mixture was stirred until a visibly homogenous solution was obtained. After adding the internal standard *endo*-*N*-hydroxy-5-norbornene-2,3-dicarboximide (125 µL, 105.59 mM in pyridine/$CDCl_3$ = 3:2, 0.0132 mmol) the solution was again stirred for at least 10 minutes before 0.60 mL were transferred into an NMR tube and a ^{31}P NMR was conducted. The DS values were calculated according Kilpeläinen *et al.* by applying **Eqn. S7** and **S8.**

Fatty Acid Cellulose Ester (FACE-1) – Yield: 43%

ATR-IR: ν(cm^{-1}) = 3644 – 3035 ν(O-H), 3009 – 2789 ν(C-H), 1728 ν(C=O), 1639 ν(C=C), 1016 ν(C-O)$_{AGU}$.

^{1}H NMR: (400 MHz, DMSO-d_6) δ (ppm) = 5.79 (br, H$_f$, 1H), 5.52 – 2.96 (m, AGU, 7H), 4.96 (br, H$_e$, 2H), 2.32 (br, H$_d$, 2H), 2.01 (br, H$_c$, 2H), 1.51 (br, H$_b$, 2H), 1.38 – 1.17 (br, H$_a$, 10H).

DS$_{31P}$ = 0.38

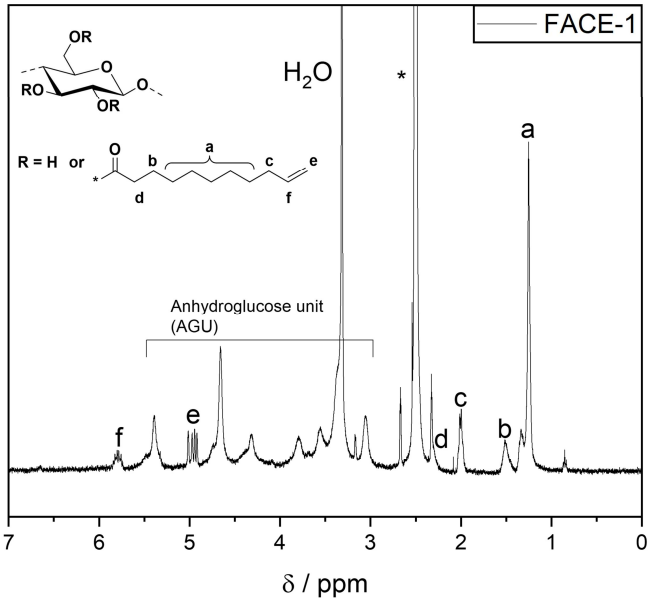

Figure S37. ^{1}H NMR (400 MHz) of **FACE-1** in DMSO-d_6 (*) at ambient temperature.

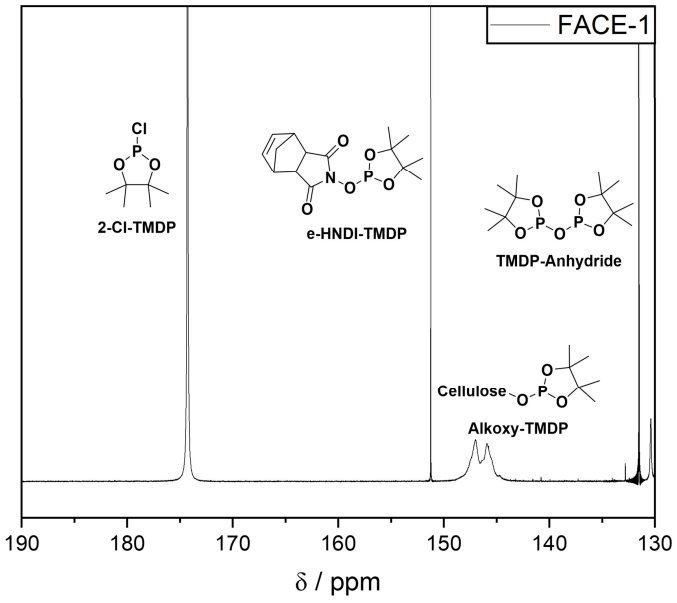

Figure S38. ^{31}P NMR of phosphorylated **FACE-1** in $CDCl_3$ at ambient temperature.

Fatty Acid Cellulose Ester (FACE-2) – Yield: 52%

ATR-IR: ν(cm^{-1}) = 3653 – 3029 ν(O-H), 3003 – 2799 ν(C-H), 1728 ν(C=O), 1639 ν(C=C), 1016 ν(C-O)$_{AGU}$.

^{1}H NMR: (400 MHz, DMSO-d_6) δ (ppm) = 5.79 (br, H$_f$, 1H), 5.56 – 2.96 (m, AGU, 7H), 4.96 (br, H$_e$, 2H), 2.32 (br, H$_d$, 2H), 2.01 (br, H$_c$, 2H), 1.51 (br, H$_b$, 2H), 1.40 – 1.15 (br, H$_a$, 10H).

DS$_{31P}$ = 0.42

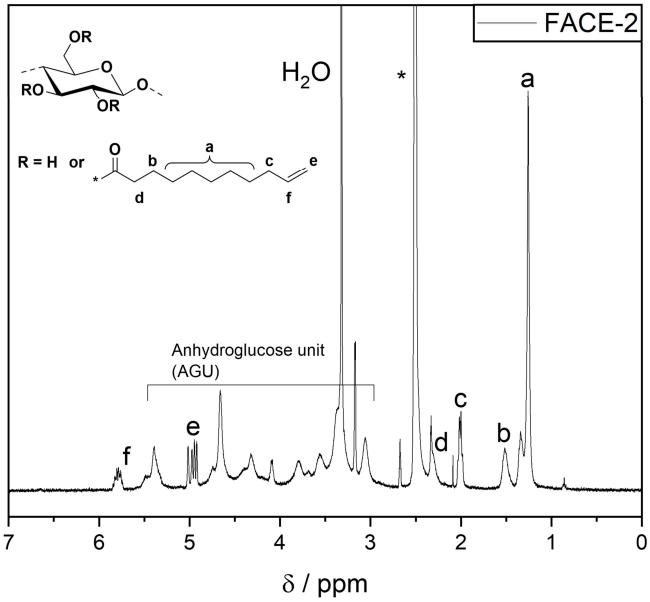

Figure S39. ^{1}H NMR (400 MHz) of **FACE-2** in DMSO-d_6 (*) at ambient temperature.

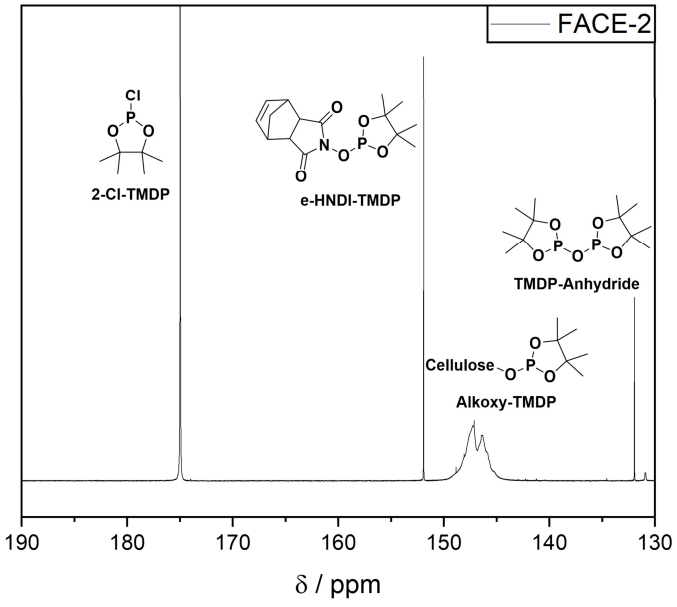

Figure S40. ^{31}P NMR of phosphorylated **FACE-2** in $CDCl_3$ at ambient temperature.

Fatty Acid Cellulose Ester (FACE-3) – Yield: 57%

ATR-IR: ν(cm^{-1}) = 3651 – 3105 ν(O-H), 3013 – 2793 ν(C-H), 1734 ν(C=O), 1639 ν(C=C), 1016 ν(C-O)$_{AGU}$.

^{1}H NMR: (400 MHz, DMSO-d_6) δ (ppm) = 5.78 (br, H$_f$, 1H), 5.61 – 2.82 (m, AGU, 7H), 4.94 (br, H$_e$, 2H), 2.32 (br, H$_d$, 2H), 2.00 (br, H$_c$, 2H), 1.51 (br, H$_b$, 2H), 1.40 – 1.15 (br, H$_a$, 10H).

DS$_{31P}$ = 0.62

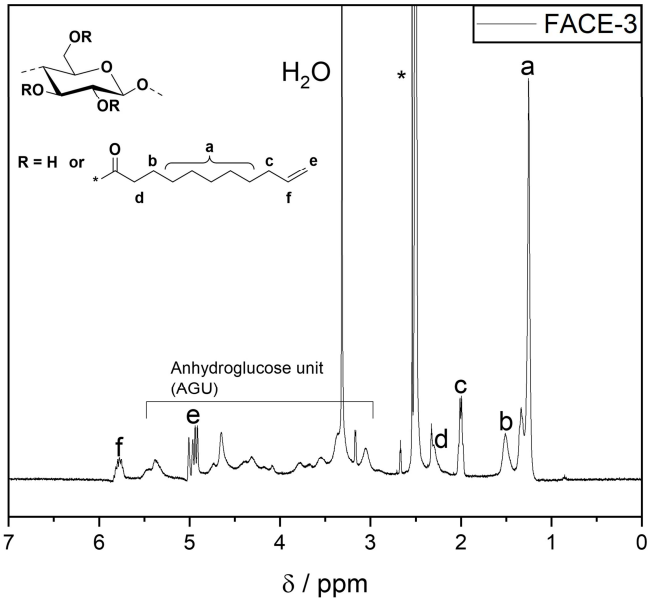

Figure S41. ^{1}H NMR (400 MHz) of **FACE-3** in DMSO-d_6 (*) at ambient temperature.

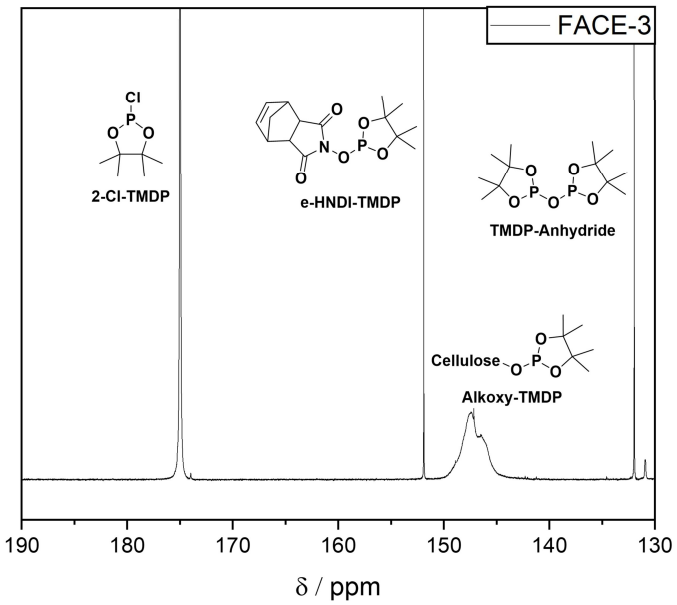

Figure S42. ^{31}P NMR of phosphorylated **FACE-3** in $CDCl_3$ at ambient temperature.

6.4.2 Synthesis of High Sulfur Content Composite Materials (FACE-XS, X = 1, 2 or 3)

General Procedure for the Synthesis of FACE-XS (X = 1, 2 or 3)

A crimp vial was charged with elemental sulfur (2.85 g, 95 wt%) and the corresponding FACE (150 mg, 5.00 wt%). Subsequently, the reaction mixture was heated to 180 °C and stirred for 24 h until the black reaction medium appeared homogenous. After cooling to room temperature, the targeted composite materials were obtained.

FACE-1S: Yield: 100 %

FACE-2S: Yield: 100 %

FACE-3S: Yield: 100 %

6.4.3 Mercury Sorption Studies

General procedure for mercury sorption studies

200 mg of the respective high sulfur content composite material were crushed into a powder and subsequently added to 100 mL of an aqueous $HgCl_2$ solution (C_i = 1.00 mg L^{-1}). After stirring the solution for 24 h at ambient temperature, the inverse vulcanized material was filtered off and the mercury concentration in the solution was determined via Cold Vapor Atomic Absorption spectroscopy (AAS).

6.4.4 Supporting Figures

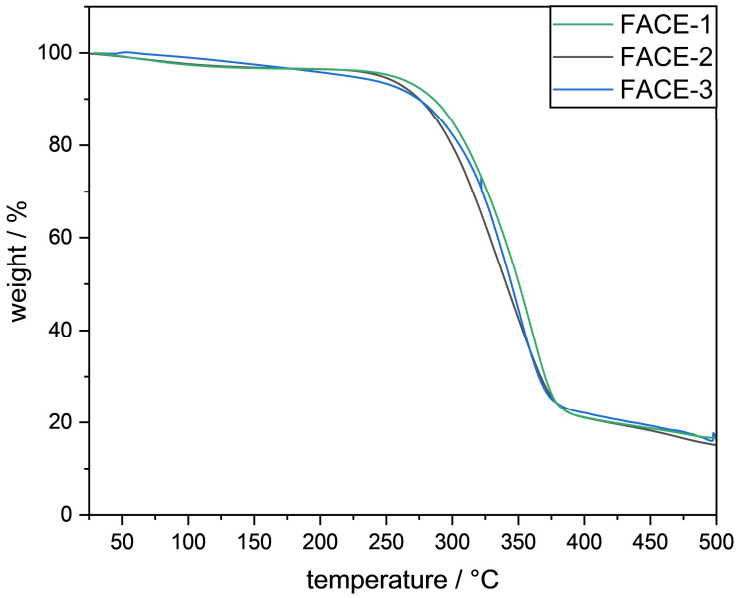

Figure S43. Thermogravimetric analysis (TGA) of **FACE-1** (green line), **FACE-2** (black line), and **FACE-3** (blue line) from 25 to 500 °C with a heating rate of 10 K min^{-1} under a nitrogen flow.

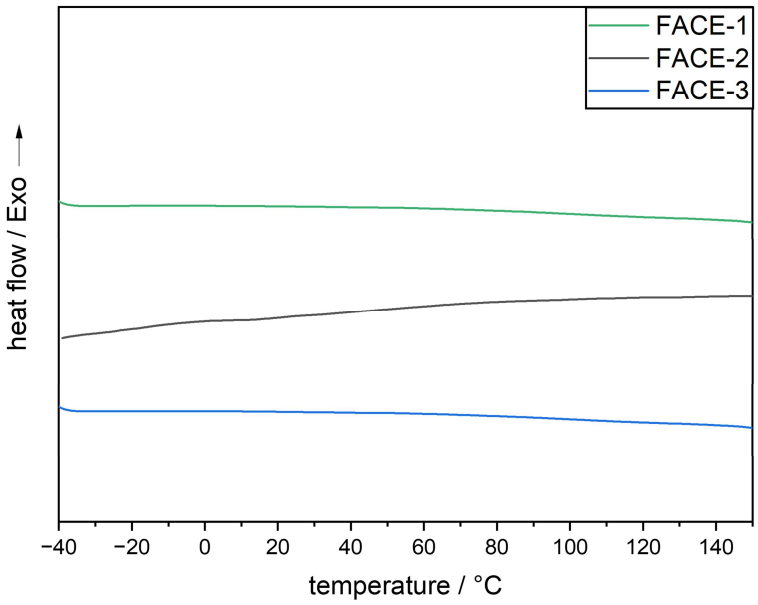

Figure S44. DSC studies (second heating run) of **FACE-1** (green line), **FACE-2** (black line), and **FACE-3** (blue line) from −40 to 220 °C with a heating rate of 20 °C min^{-1}under a nitrogen flow.

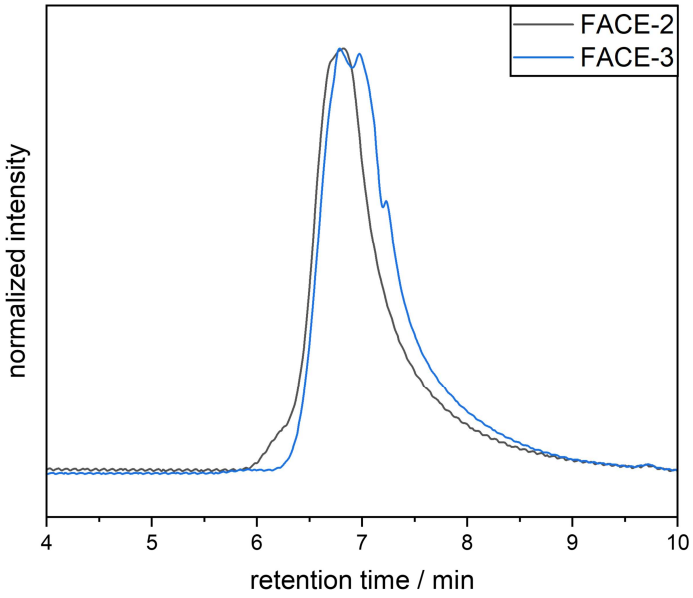

Figure S45. SEC traces of **FACE-2** (black line) and **FACE-3** (blue line) in in HFIP+ 0.1%w/v KTFA.

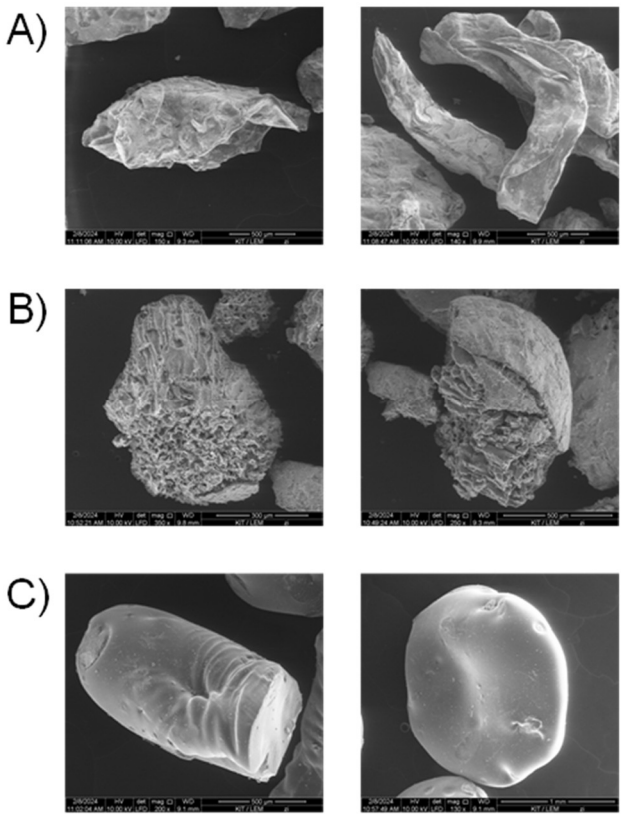

Figure S46. Additional SEM images of **FACE-1S-washed** (A), **FACE-2S-washed** (B), and **FACE-3S-washed** (C).

Table S2. Mercury concentrations before and after treatment with high sulfur content composite materials.

Material	C_i (µg L^{-1})	C_t (µg L^{-1})[a]
FACE-1S	1 000	41.8
FACE-2S	1 000	211
FACE-3S	1 000	291

[a]after stirring for 24 h at ambient temperature.

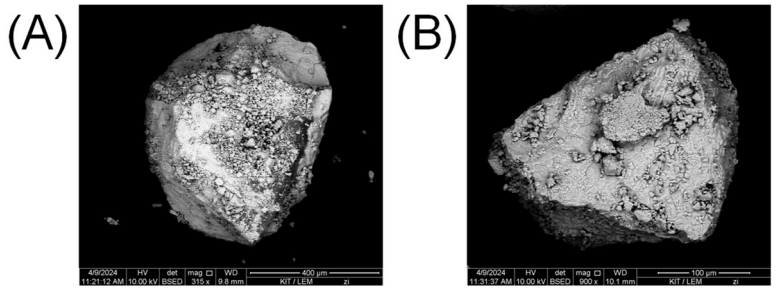

Figure S47. BSE-SEM images of FACE-2S (A) and FACE-3S (B).

6.5 Efficient One-Step Synthesis of Catechol Containing Polymers via Friedel-Crafts Alkylation – Chapter 4.3

The experimental data of the current chapter have been published before:

T. Sehn, N. Kolb, A. Azzawi, M. A. R. Meier, *Macromolecules* **2024**, *57*, 10802−10811.[324]

Text, figures, and data are reproduced from this article and were partially edited and extended.

6.5.1 Synthesis of Catechol Bearing Model Compounds

Procedure for the Synthesis of Model Compound 1 (M1)

A crimp vial was charged with catechol (1.62 g, 14.7 mmol, 4.00 equiv.), limonene (0.59 mL, 500 mg, 3.67 mmol, 1.00 equiv.), tetrahydrofuran (THF, 1M) and a stirring bar. After quantitative solubilization of catechol and limonene in THF, sulfuric acid (57%, 0.28 mL, 2.94 mmol, 0.40 equiv. per double bond) was added as a catalyst and the reaction mixture was subsequently stirred overnight at ambient temperature. For purification, THF was removed under reduced pressure, the solid residue resolubilized in diethyl ether, washed with water (3×) and the organic phase was dried over anhydrous sodium sulfate. After removal of the solvent under reduced pressure, the crude solid was purified by vacuum distillation in a Kugelrohr oven (1 mbar, 300°C). The products (structural isomers) were obtained as orange to red solid (505 mg, 38.8 %).

^{1}H NMR: (400 MHz, $CDCl_3$) δ (ppm) = 6.96 – 6.47 (m, H_b, 6H), 5.35 – 4.86 (m, H_a, 4H), 2.75 – 0.24 (m, $H_{aliphatic}$, 18H).

^{13}C NMR: (126 MHz, $CDCl_3$) δ (ppm) = 147 - 139 (C_b, 4C), 121 – 112 (C_a, 6C), 53.2 – 14.3 ($C_{aliphatic}$, 12C).

ATR-IR: ν (cm^{-1}) = 3337 (m), 2952 (m), 2927 (m), 2866 (m), 1604 (m), 1511 (s), 1438 (m), 1366 (m), 1275 (vs), 1259 (vs), 1190 (vs), 1106 (s), 1041 (w), 928 (w), 866 (m), 809 (s), 783 (s), 728 (w), 642 (m), 606 (w), 595 (w).

m/z: $[M + Na]^+$ calculated for $C_{22}H_{28}O_4$ = 379.1885; found: 379.1879

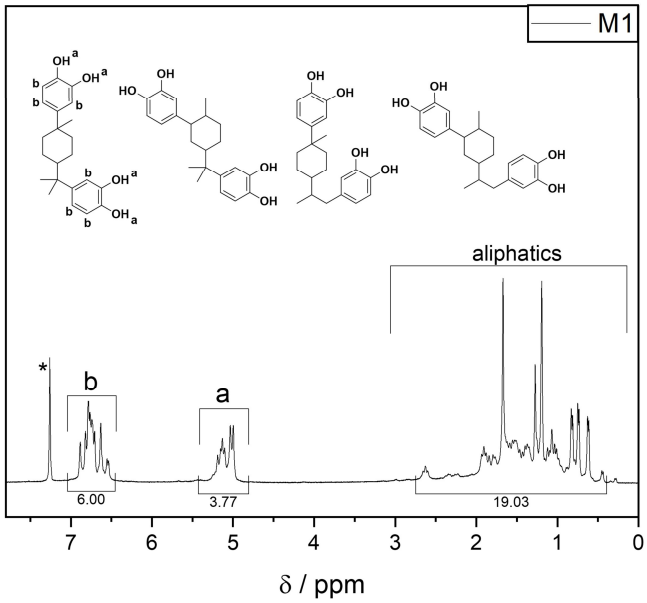

Figure S48. ^{1}H NMR (400 MHz) of **M1** in $CDCl_3$ (*) at ambient temperature.

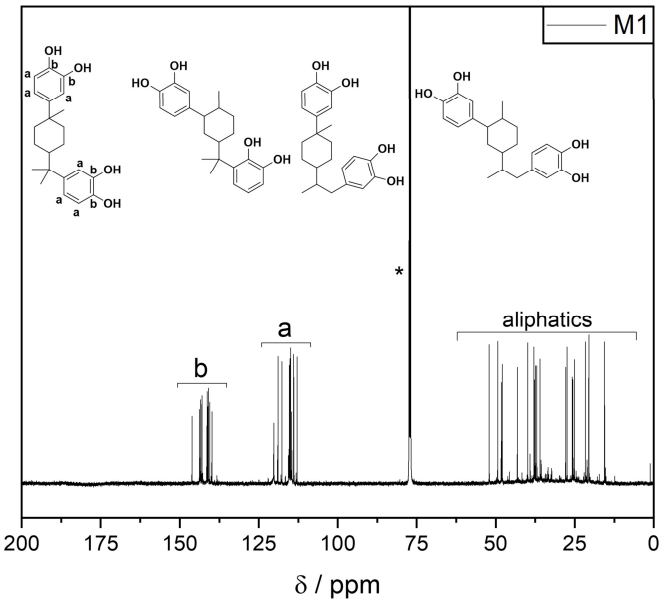

Figure S49. ^{13}C NMR (126 MHz) of **M1** in $CDCl_3$ (*) at ambient temperature.

Procedure for the Synthesis of Model Compound 2 (M2)

A crimp vial was charged with catechol (1.62 g, 14.7 mmol, 4.00 equiv.), methyl oleate (1.25 mL, 1.09 mg, 3.67 mmol, 1.00 equiv.), tetrahydrofuran (THF, 1M) and a stirring bar. After quantitative solubilization of catechol and methyl oleate in THF, sulfuric acid (57%, 0.14 mL, 1.47 mmol, 0.40 equiv. per double bond) was added as a catalyst and the reaction mixture was subsequently stirred overnight at ambient temperature. For purification, THF was removed under reduced pressure, the solid residue resolubilized in diethyl ether, washed with water (3×) and the organic phase was dried over anhydrous sodium sulfate. After removal of the solvent under reduced pressure, the crude solid was purified by vacuum distillation in a Kugelrohr oven (1 mbar, 200 to 250 °C). The products (structural isomers) were obtained as orange to red solid (138 mg, 9.26 %).

^{1}H NMR: (400 MHz, $CDCl_3$) δ (ppm) = 6.81 – 6.52 (m, H_h, 3H), 5.63 – 4.79 (m, H_g, 2H), 3.88 – 3.34 (m, H_f, 3H), 2.98 – 2.77 (m, H_e, 1H), 2.45 – 2.15 (m, H_d, 2H), 1.73 – 1.32 (m, H_c, 6H), 1.35 – 1.01 (m, H_b, 22H), 0.91 – 0.80 (m, H_a, 3H).

^{13}C NMR: (126 MHz, $CDCl_3$) δ (ppm) = 175 (C_h, 1C), 145 – 130 (C_g, 3C), 122 - 110 (C_f, 3C), 51.7 (C_e, 1C), 45.4 (C_d, 1C), 38.2 (C_c, 1C), 37.6 – 20.8 (C_b, 14C), 14.1 (C_a, 1C).

ATR-IR: v (cm^{-1}) = 3393 (w), 2922 (vs), 2851 (s), 1738 (w), 1713 (m), 1605 (w), 1511 (w), 1458 (m), 1439 (m), 1361 (m), 1324 (m), 1276 (s), 1193 (s), 1180 (s), 1108 (m), 867 (w), 812 (w), 782 (w), 732 (w), 646 (w), 595 (w), 484 (w), 441 (w).

m/z: $[M + Na]^+$ calculated for $C_{25}H_{42}O_4$ = 429.2981; found: 429.2977

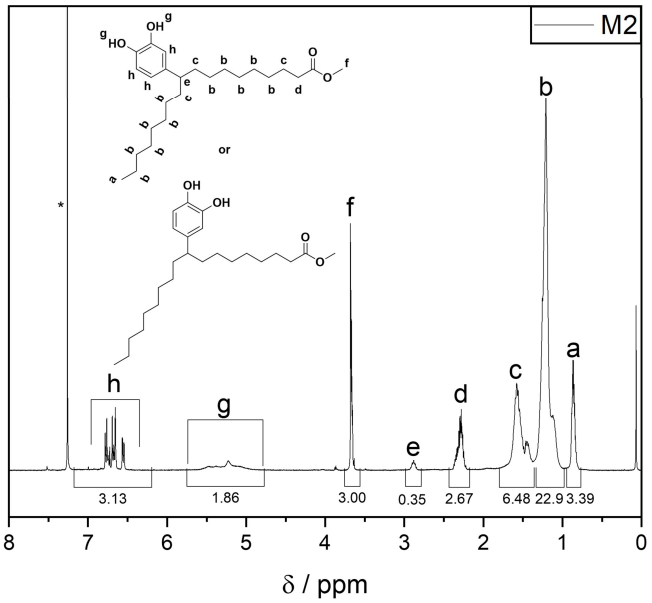

Figure S50. ^{1}H NMR (400 MHz) of **M2** in $CDCl_3$ (*) at ambient temperature.

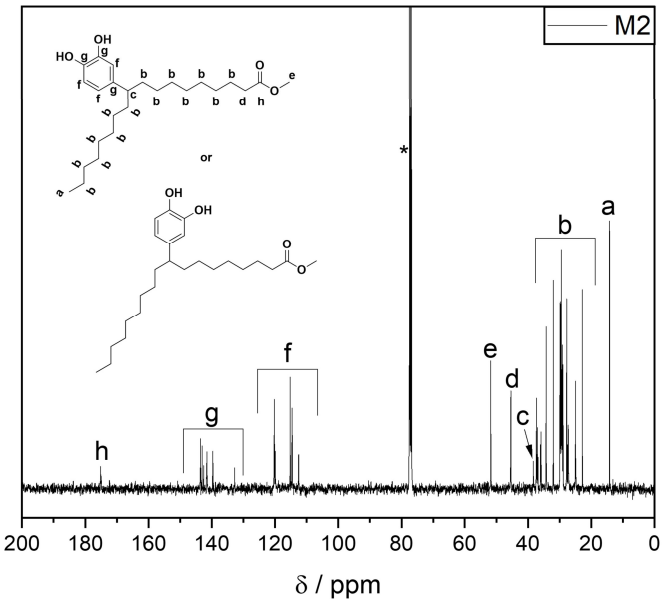

Figure S51. ^{13}C NMR (126 MHz) of **M2** in $CDCl_3$ (*) at ambient temperature.

6.5.2 Synthesis of Catechol Containing Polymer

Procedure for the Synthesis of Polymer 1 (P1)

Initially, a 250 mL three-neck flask was charged with polybutadiene (198 mg, 3.67 mmol, 1.00 equiv.) and catechol (3.24 g, 29.4 mmol, 8.00 equiv.). The three-neck flask was equipped with an air cooler and the reaction apparatus was flooded with argon at room temperature. After an inert atmosphere was established in the apparatus, the reaction mixture was heated to 120 °C and stirred until the catechol was completely melted. Sulfuric acid (≥95%, 78.0 µL, 1.47 mmol, 0.40 equiv. per double bond) was then added carefully to the reaction solution and stirring was continued at 120 °C for additional 30 minutes. After cooling the reaction mixture to ambient temperature, the solid residue was taken up in a minimal amount of diethyl ether, washed with water, sodium carbonate solution and again with water. The organic phase was dried over anhydrous sodium sulfate, the solvent was removed under reduced pressure, and the excess catechol was distilled off by short path distillation (Kugelrohr) in vacuum (120 °C to 230 °C, 4.2 x 10^{-2} mbar). The product was obtained as a dark red to black solid (254 mg, 42.2%) and revealed a degree of modification of 100% (^{1}H NMR).

^{1}H NMR: (400 MHz, DMSO-d_6) δ (ppm) = 8.79 – 8.14 (br, H_c, 2H), 6.91 – 6.04 (br, H_b, 3H), 2.23 – 0.27 (br, H_a, 7H).

^{13}C NMR: (126 MHz, DMSO-d_6) δ (ppm) = 148 – 141 (C_c, 2C), 121 – 111 (m, C_b, 3C), 38.6 – 17.39 (br, C_a, 4C).

ATR-IR: ν (cm^{-1}) = 3381 (m), 2918 (s), 2851 (s), 1604 (w), 1510 (m), 1493 (m), 1443 (m), 1343 (m), 1235 (vs), 1183 (s), 1154 (s), 1106 (s), 983 (w), 809 (m), 781 (m), 731 (w), 436 (w), 398 (w).

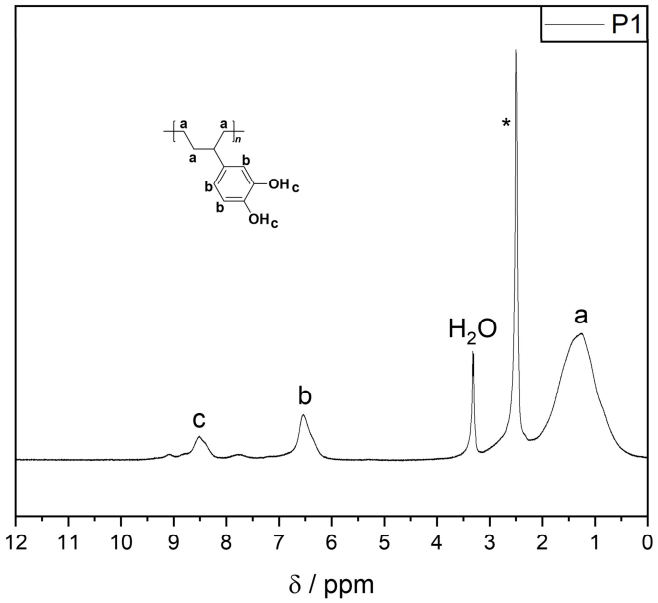

Figure S52. ^{1}H NMR (400 MHz) of **P1** in $CDCl_3$ (*) at ambient temperature.

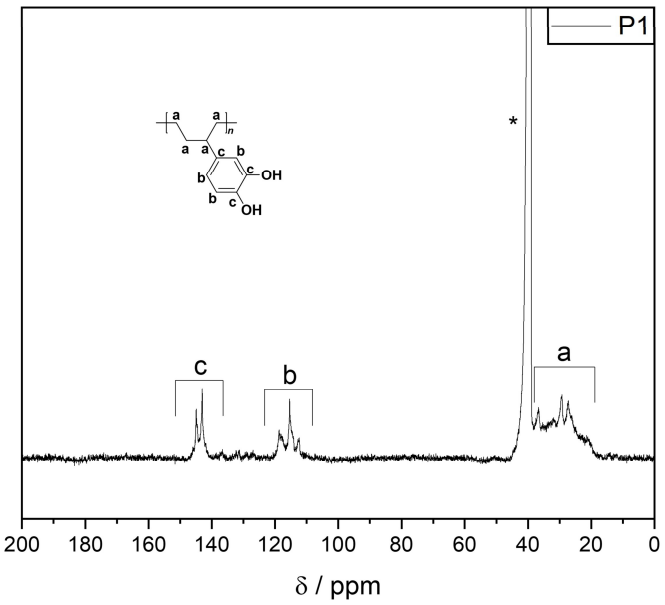

Figure S53. ^{13}C NMR (126 MHz) of **P1** in $CDCl_3$ (*) at ambient temperature.

6.5.3 Metal Sorption Studies

Coating of silica particles (5 wt%)

156 mg of P1 were dissolved in 50 mL THF. After complete dissolution of the polymer, 3.00 g silica particles were added, and the solvent was slowly removed under reduced pressure. The coated silica particles were obtained as beige solid.

Procedure for Metal Sorption Studies

200 mg of the coated silica particles were added into 100 mL of an aqueous metal ion solution (C_i = 1.00 mg L^{-1}, pH ≤ 7). After stirring the heterogenous mixture for 24 h at ambient conditions, the particles were filtered off and the remaining metal ion concentration was determined via Inductively Coupled Plasma Atomic Emission Spectroscopy (ICP-AES) or Atomic Absorption Spectrometry (AAS).

6.5.4 Supporting Tables and Figures

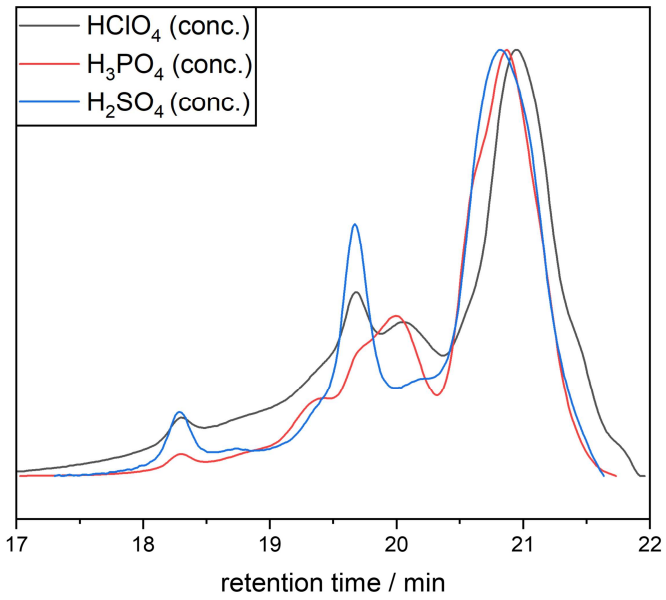

Figure S54. SEC traces after stirring limonene with concentrated $HClO_4$ (black), H_3PO_4 (red) or H_2SO_4 (blue) for 10 minutes at 120 °C.

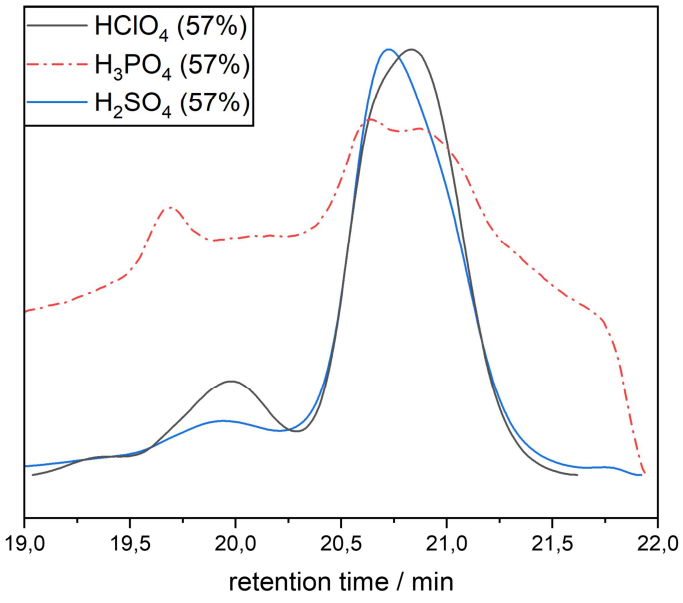

Figure S55. SEC traces after stirring limonene with 57% $HClO_4$ (black), H_3PO_4 (red) or H_2SO_4 (blue) for 10 minutes at 120 °C.

Table S3. GC screening for the conversion of limonene in the presence of various Brønsted acids (0.80 equiv.) at different reaction conditions.

	Catalyst	T / °C	Solvent[a]	Conversion of limonene (10 min)[b]	Conversion of limonene (60 min)[b]	Conversion of limonene (120 min)[b]
R1	$HClO_4$ (57%)	120	-	≥ 99 %	-	-
R2	H_3PO_4 (57%)	120	-	≥ 99 %	-	-
R3	H_2SO_4 (57%)	120	-	≥ 99 %	-	-
R4	$HClO_4$ (57%)	120	THF	≥ 99 %	-	-
R5	H_3PO_4 (57%)	120	THF	41.0 %	≥ 99 %	-
R6	H_2SO_4 (57%)	120	THF	94.6 %	-	-
R7	$HClO_4$ (57%)	60	THF	62.8 %	79.3 %	99.6 %
R8	H_3PO_4 (57%)	60	THF	0.96 %	1.20 %	2.33 %
R9	H_2SO_4 (57%)	60	THF	66.8 %	92.9 %	98.0 %

[a] 1 mol L^{-1}, [b] determined *via* GC

Table S4. GC screening for the conversion of limonene in the presence of H_2SO_4 (57%) in THF (1 mol L^{-1}).

	Equiv. H_2SO_4 (57%)	T / °C	Conversion of limonene (10 min)[a]	Conversion of limonene (60 min)[a]	Conversion of limonene (120 min)[a]	Conversion of limonene (24 h)[a]
R10	0.80	60	66.8 %	92.9 %	98.0 %	-
R11	0.40	60	35.9 %	64.4 %	87.9 %	100 %
R12	0.10	60	5.76 %	18.9 %	75.2 %	99.4 %
R13	0.80	20	2.71 %	8.64 %	16.3 %	80.6 %
R14	0.40	20	0.40 %	4.33 %	8.27 %	63.7 %
R15	0.10	20	0.00 %	0.00 %	2.16 %	24.2 %

[a] determined *via* GC

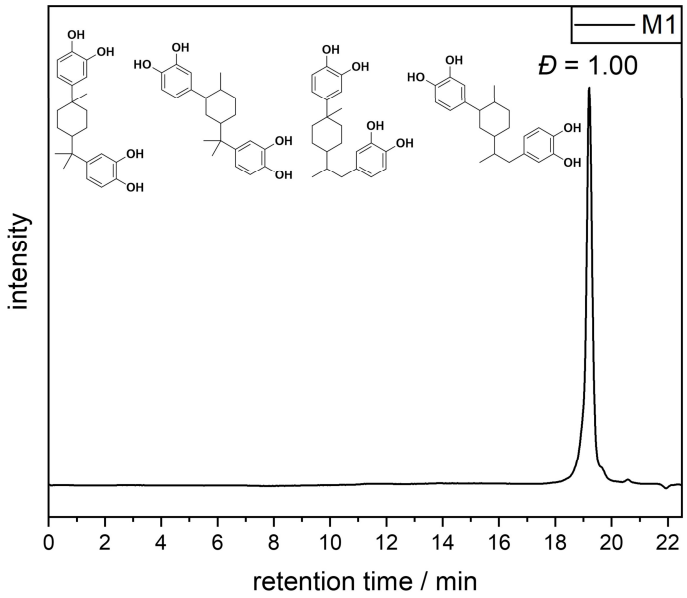

Figure S56. SEC traces of **M1** in THF + 250 ppm BHT.

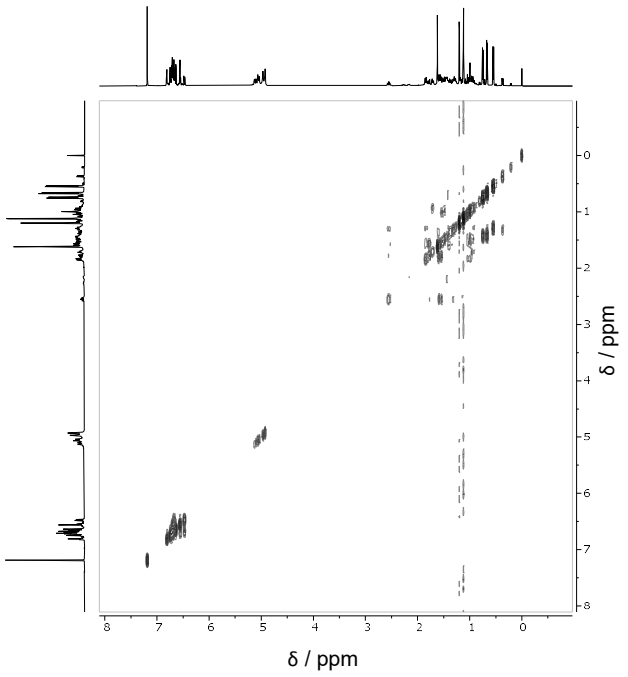

Figure S57. 2D ^{1}H ^{1}H COSY spectrum (400 MHz) of **M1** in $CDCl_3$ at ambient temperature.

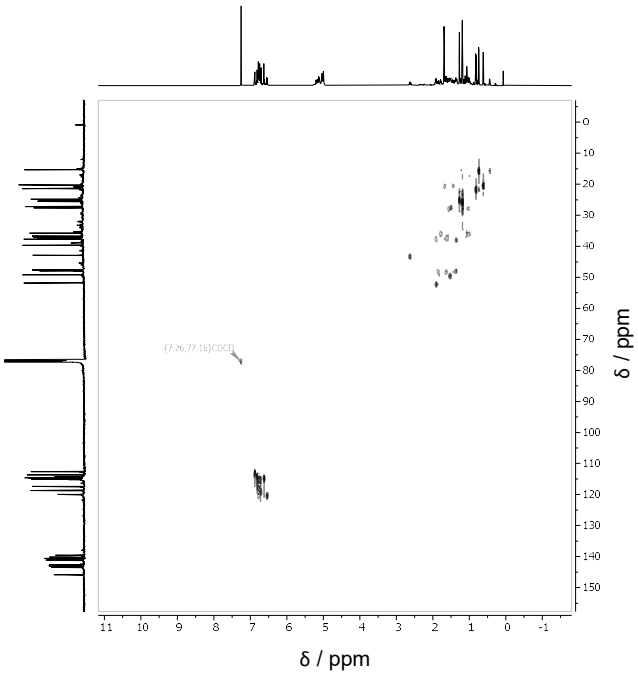

Figure S58. 2D ^{1}H ^{13}C HSQC spectrum of **M1** in $CDCl_3$ at ambient temperature.

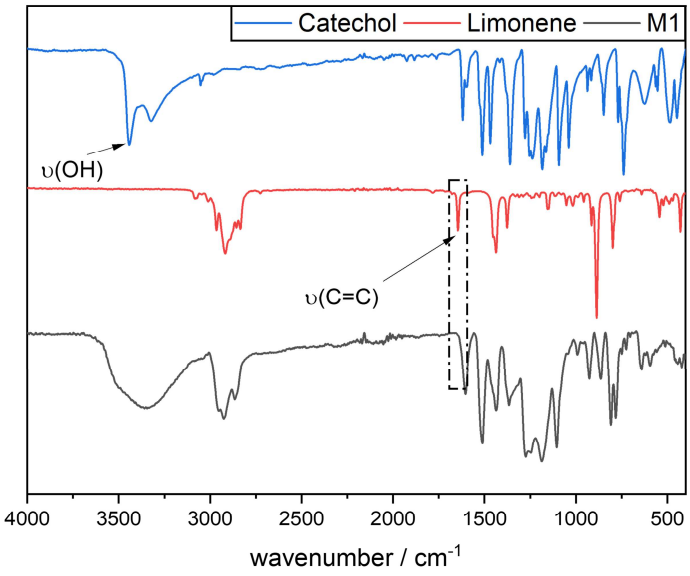

Figure S59. ATR-IR spectra of catechol (blue), limonene (red), and **M1** (black).

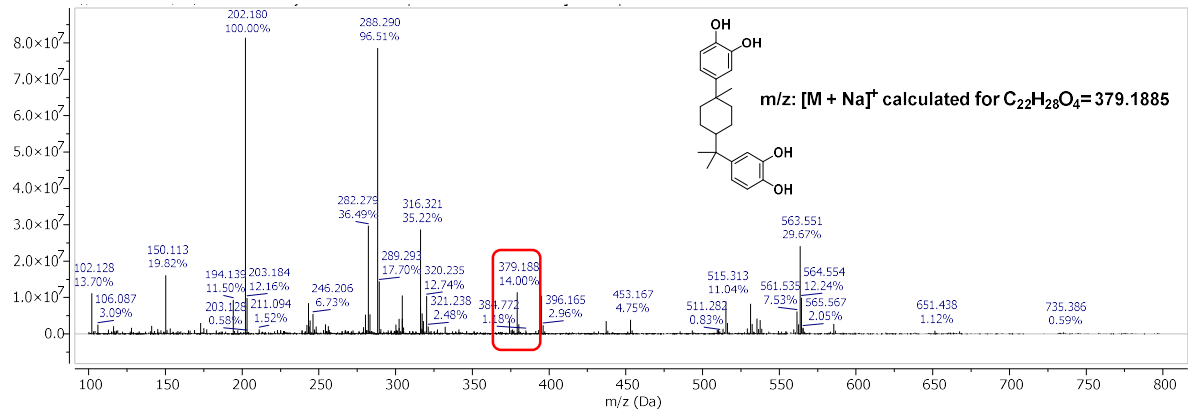

Figure S60. ESI-MS spectrum of **M1** in MeOH.

Table S5. GC screening for the conversion of methyl oleate in the presence of sulfuric acid (57%) and catechol in THF.[a]

	Equiv. H_2SO_4 (57%)	T / °C	Conversion methyl oleate (10 min)[b]	Conversion methyl oleate (60 min)[b]	Conversion methyl oleate (120 min)[b]	Conversion methyl oleate (24 h)[b]
R16	0.40	60	4.88 %	23.5 %	26.8 %	39.4 %
R17	0.20	60	2.50 %	5.98 %	10.5 %	21.9 %
R18	0.05	60	1.52 %	1.74 %	2.60 %	12.7 %
R19	0.40	20	0.00 %	1.90 %	6.74 %	22.7 %
R20	0.20	20	-	-	3.28 %	11.1 %
R21	0.05	20	-	-	0.11 %	2.59 %

[a] 1 mol L^{-1}, [b] determined via GC

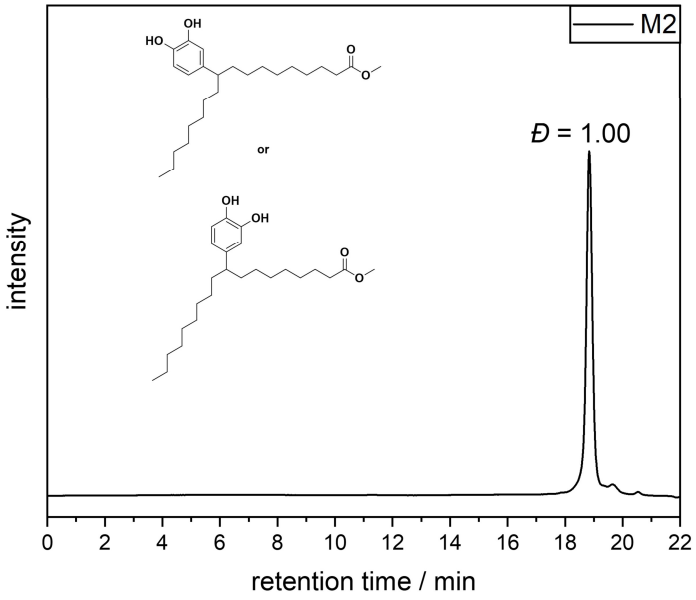

Figure S61. SEC traces of **M2** in THF + 250 ppm BHT.

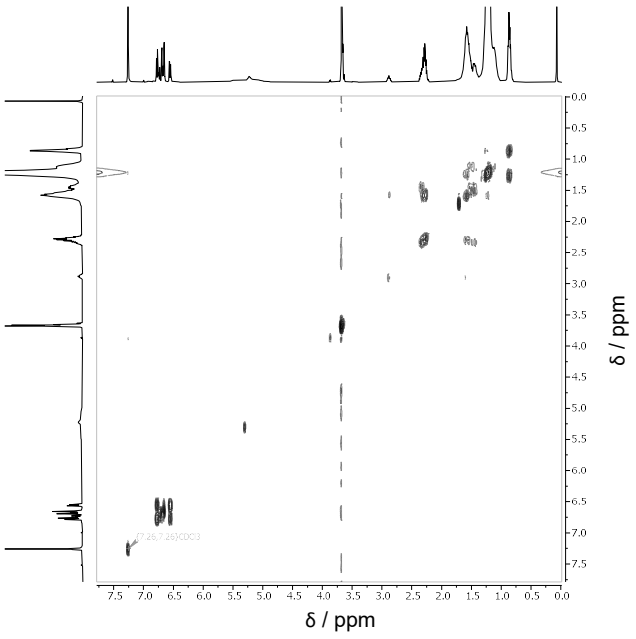

Figure S62. 2D ^{1}H ^{1}H COSY spectrum (400 MHz) of **M2** in $CDCl_3$ at ambient temperature.

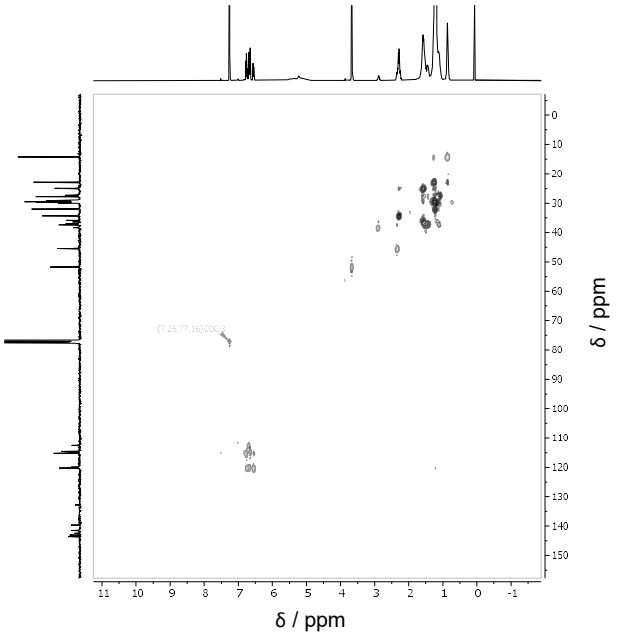

Figure S63. 2D ^{1}H ^{13}C HSQC spectrum of **M2** in $CDCl_3$ at ambient temperature.

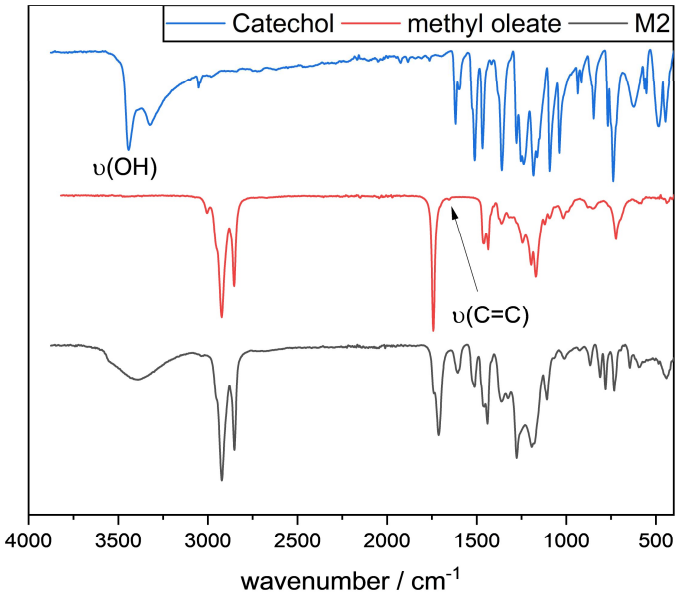

Figure S64. ATR-IR spectra of catechol (blue), methyl oleate (red), and **M2** (black).

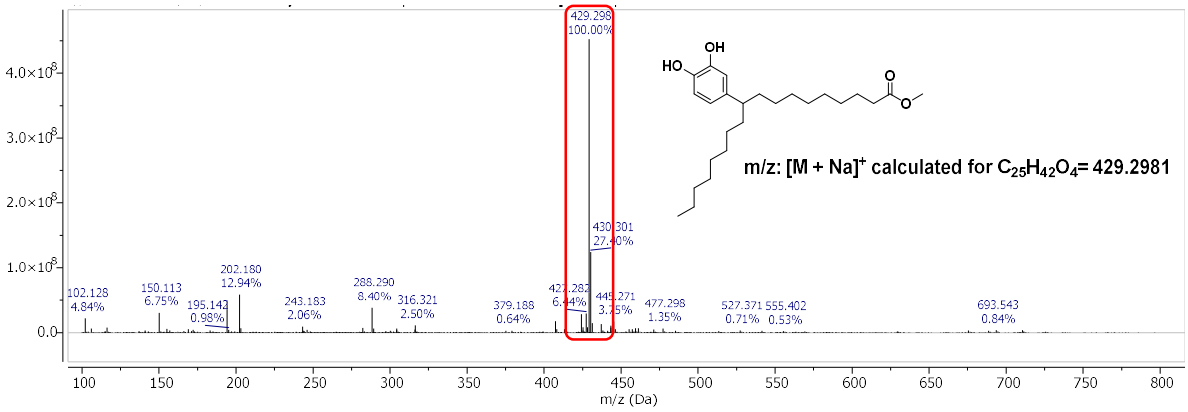

Figure S65. ESI-MS spectrum of **M2** in MeOH.

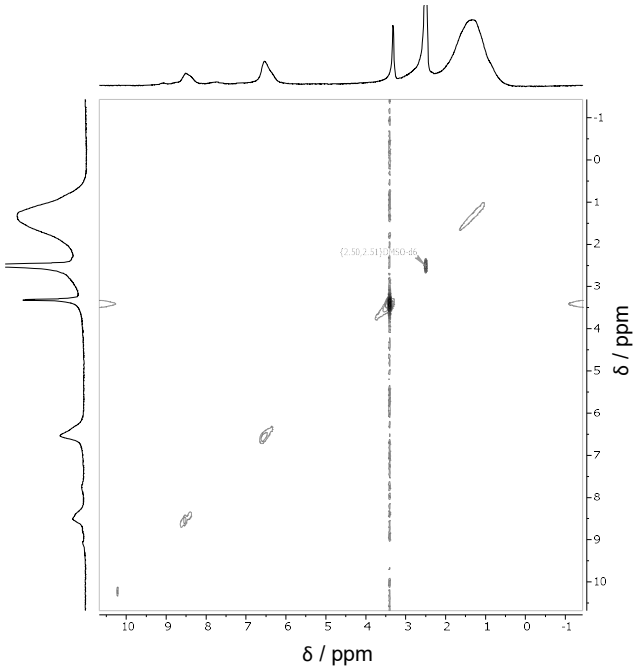

Figure S66. 2D ^{1}H ^{1}H COSY spectrum (400 MHz) of **P1** in DMSO-d_6 at ambient temperature.

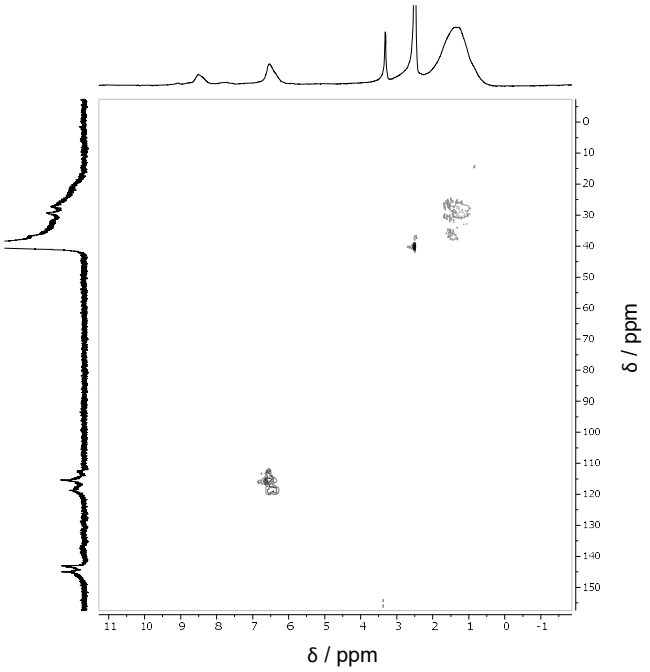

Figure S67. 2D ^{1}H ^{13}C HSQC spectra of **P1** in DMSO-d_6 at ambient temperature.

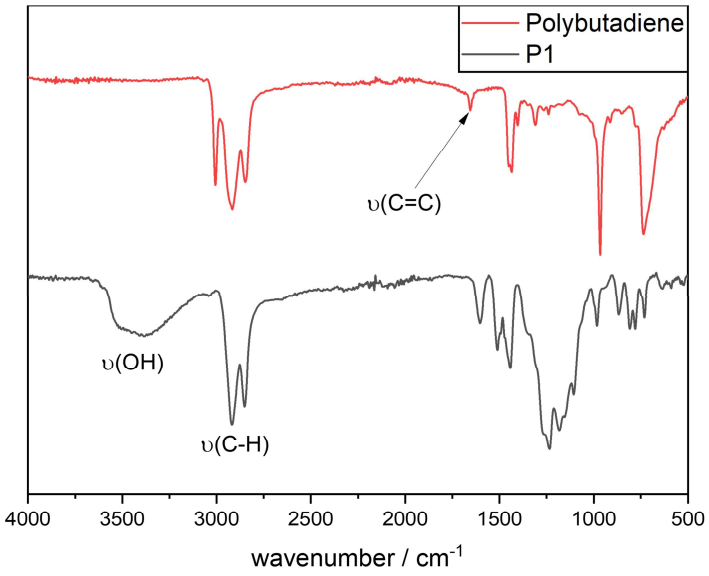

Figure S68. ATR-IR spectra of polybutadiene (red) and **P1** (black) after post polymerization modification.

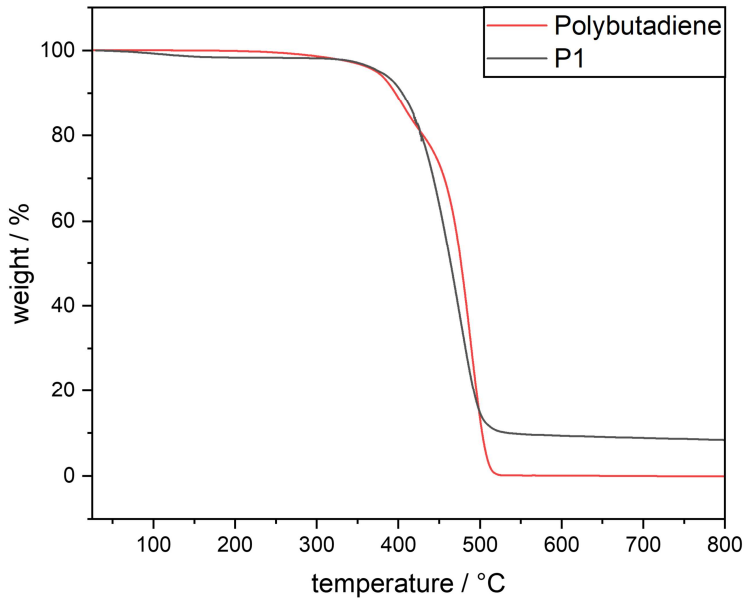

Figure S69. Thermogravimetric analysis (TGA) of polybutadiene (red) and **P1** (black) from 25 °C to 800 °C with a heating rate of 10 K min^{-1} under a nitrogen flow.

Table S6. Metal ion sorption studies.

Metal	C_i (mg L^{-1})	C_f (mg L^{-1})[a]
Pb	1.00	< 0.01
Al	1.00	0.02
Cu	1.00	0.09
Fe	1.00	0.03
Zn	1.00	0.14
Hg	1.00	0.02

[a] after stirring silica particles coated with **P1** in the respective aqueous metal ion solution for 24 h at ambient temperature.

6.6 Fully Renewable High Oleic Sunflower Oil (HOSO)-based Acetal Covalent Adaptable Networks (CANs) – Chapter 4.4

6.6.1 Synthesis of a Fully Renewable Polyol

Procedure for the Synthesis of HOSO-catechol

A 250 mL two neck round bottom flask equipped with a reflux condenser was charged with HOSO (5.00 g, 17.0 mmol of double bonds (based on the molecular weight of triolein (885.45 g mol^{-1})), 1.00 equiv.), catechol (14.9 g, 136 mmol, 8.00 equiv.) and a stirring bar. The reaction setup was heated to 120 °C and the suspension was stirred until catechol was completely molten (T_m = 105 °C) and a homogenous reaction mixture was obtained. Then, H_2SO_4 (≥95%, 365 µL, 665 mg, 6.80 mmol, 0.40 equiv.) was slowly added and the reaction solution was rapidly stirred for 30 minutes at 120 °C. Subsequently, the mixture was cooled down to room temperature, the residue was dissolved in THF and precipitated in 400 mL H_2O (2x). After precipitation, the highly viscous crude polyol was resolubilized in Et_2O and washed with saturated sodium bicarbonate solution (3x) in order to remove residual sulfuric acid. Afterwards, the organic phase was dried over anhydrous sodium sulfate, the solvent was removed under reduced pressure and the last traces of catechol were removed under high vacuum (1.8 x 10^{-3} mbar) at 150 °C. The product was obtained as dark red to black, highly viscous and sticky liquid (2.75 g, 39.9%).

^{1}H NMR: (400 MHz, $CDCl_3$) δ (ppm) = 7.10 – 6.35 (m, H_h, 9H), 5.77 – 5.30 (m, H_g, 6H), 5.31 – 5.00 (m, H_f, 1H), 4.49– 3.91 (m, H_e, 4H), 2.96 – 2.82 (m, H_d, 1.5H), 2.64 – 2.47 (m, H_d, 1.5H), 2.40 – 2.19 (m, H_c, 6H), 1.83 – 0.95 (m, H_b, 84H), 0.94 – 0.77 (m, H_a, 9H).

^{13}C NMR: (126 MHz, $CDCl_3$) δ (ppm) = 174 (C_g, 3C), 144 – 132 (C_f, 9C), 122 - 112 (C_e, 9C), 70.9 – 62.2 (C_e, 3C), 45.4 (C_d, 3C), 38.2 (C_c, 1C), 38.1 – 22.7 (C_b, 30C), 14.1 (C_a, 3C).

ATR-IR: v (cm^{-1}) = 2922 (vs), 2851 (s), 1720 (m), 1595 (w), 1508 (w), 1497 (w), 1464 (m), 1441 (w), 1364 (w), 1323 (w), 1277 (m), 1173 (s), 1159 (s), 1109 (m), 1043 (w), 868 (vw), 812 (w), 781 (w), 733 (m), 642 (vw), 623 (vw), 590 (vw), 453 (vw), 446 (vw), 432 (vw).

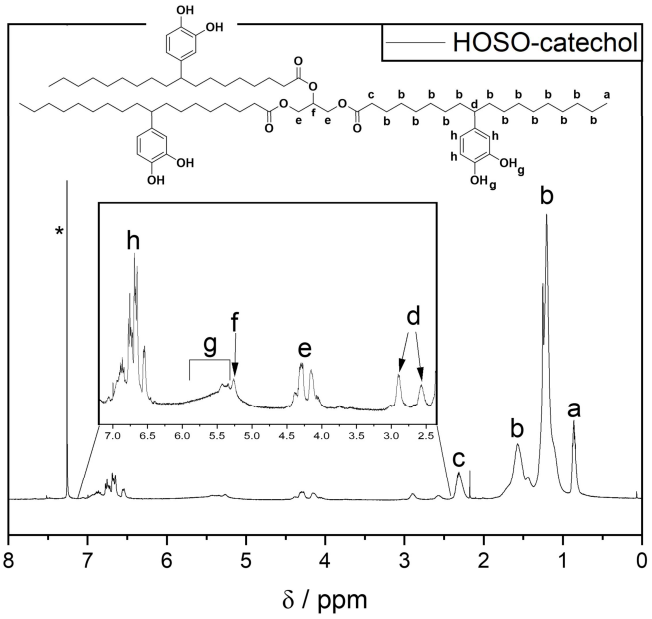

Figure S70. ^{1}H NMR (400 MHz) of **HOSO-catechol** in $CDCl_3$ (*) at ambient temperature.

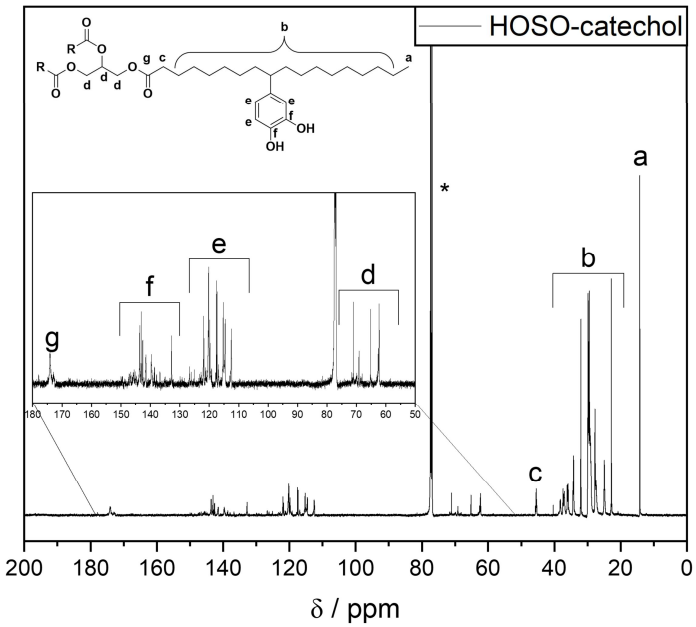

Figure S71. ^{13}C NMR (126 MHz) of **HOSO-catechol** in $CDCl_3$ (*) at ambient temperature.

6.6.2 Synthesis of Fully Renewable Acetal Covalent Adaptable Networks (CANs)

General Procedure for the Synthesis of Acetal CANs

HOSO-catechol (500 mg, 2.47 mmol OH groups (calculated based on the molecular weight of a quantitatively modified triolein structure $M_{HOSO\text{-}catechol}$ = 1215.78 g mol^{-1}), 1.00 equiv.) and 1,4-cyclohexanedimethanol divinyl ether (CVDE) were transferred in a certain ratio (**Table S7**) into a rectangular Teflon mold:

Table S7. General overview of the employed quantities of 1,4-Cyclohexanedimethanol divinyl ether (CVDE) for acetal CANs synthesis.

Material	Equivalents VE groups[a]	n_{CVDE} / mmol	m_{CVDE} / mg	V_{CVDE} / µL
P1-0.5	0.50	0.62	121	132
P2-0.7	0.70	0.87	169	184
P3-0.9	0.90	1.11	218	236

[a]related to OH groups

The mixture was subsequently carefully heated until both components could be manually mixed and a homogenous reaction mixture for the curing process could be prepared. The mold was then placed into an oven for 1h at 120 °C and 3h at 150 °C to obtain the final dark red to black materials.

P1-0.5

ATR-IR: ν (cm^{-1}) = 2920 (vs), 2851 (s), 1736 (m), 1722 (m), 1595 (w), 1504 (w), 1464 (m), 1443 (w), 1366 (w), 1323 (w), 1275 (m), 1159 (m), 1109 (m), 1040 (w), 868 (vw), 812 (w), 781 (w), 733 (w), 642 (vw), 623 (vw), 449 (vw).

P2-0.7

ATR-IR: ν (cm^{-1}) = 2920 (vs), 2851 (s), 1740 (m), 1593 (w), 1504 (w), 1466 (m), 1450 (m), 1379 (w), 1342 (w), 1265 (m), 1217 (w), 1130 (s), 1095 (s), 1034 (m), 1003 (w), 960 (w), 937 (vw), 906 (w), 885 (w), 820 (w), 781 (vw), 737 (w), 723 (w), 646 (vw), 455 (w), 447 (w).

P3-0.9

ATR-IR: ν (cm^{-1}) = 2920 (vs), 2851 (s), 1742 (m), 1605 (vw), 1593 (w), 1504 (w), 1466 (m), 1452 (m), 1379 (w), 1344 (w), 1263 (m), 1217 (w), 1200 (w), 1132 (s), 1099 (s), 1030 (m), 1003 (w), 960 (w), 939 (w), 906 (w), 885 (w), 818 (w), 781 (vw), 739 (w), 723 (w), 636 (w), 613 (w), 461 (vw), 449 (vw).

6.6.3 General Procedure for Swelling and Gel Content Tests

Swelling Ratio

Each crosslinked material, i.e. P1-0.5, P2-0.7, and P3-0.9, (~ 60 mg) was immersed in tetrahydrofuran (1.5 mL) for 24h at room temperature enabling the solubilization of unreacted starting materials and oligomeric chains. Subsequently, the materials were removed from the solvent and weighed. The swelling ratio is the amount of solvent that is soaked into the material and can therefore be calculated according to **Eqn. S9**:

$$Swelling\ ratio\ (\%) = \frac{m_{THF}}{m_o} \quad \text{(S9)}$$

m_{THF}: sample mass after storing the respective material in THF

m_0: initial sample mass before the gel content tests.

Gel Content

Each crosslinked material, i.e. P1-0.5, P2-0.7, and P3-0.9, (~ 60 mg) was immersed in tetrahydrofuran (1.5 mL) for 24h at room temperature enabling the solubilization of unreacted starting materials and oligomeric chains. Subsequently, the materials were removed from the solvent, dried under reduced pressure at 70 °C, and weighed. The gel content describes the percentage of mass that is insoluble in tetrahydrofuran and can therefore be calculated according to **Eqn. S10**:

$$Gel\ content\ (\%) = \frac{m_1}{m_o}\ x\ 100 \quad \text{(S10)}$$

m_1: dried sample mass after storing the respective material in THF

m_0: initial sample mass before the gel content tests.

6.6.4 Supporting Figures

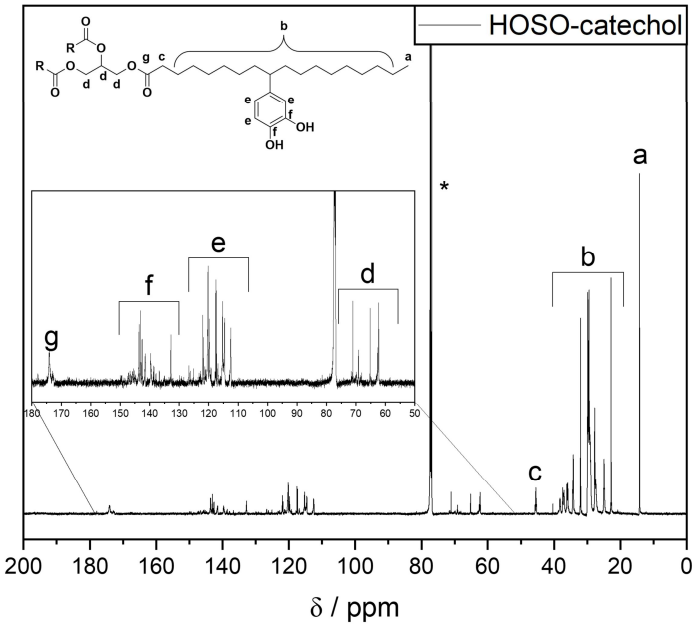

Figure S72. ^{13}C NMR (126 MHz) of **HOSO-catechol** in $CDCl_3$ (*) at ambient temperature.

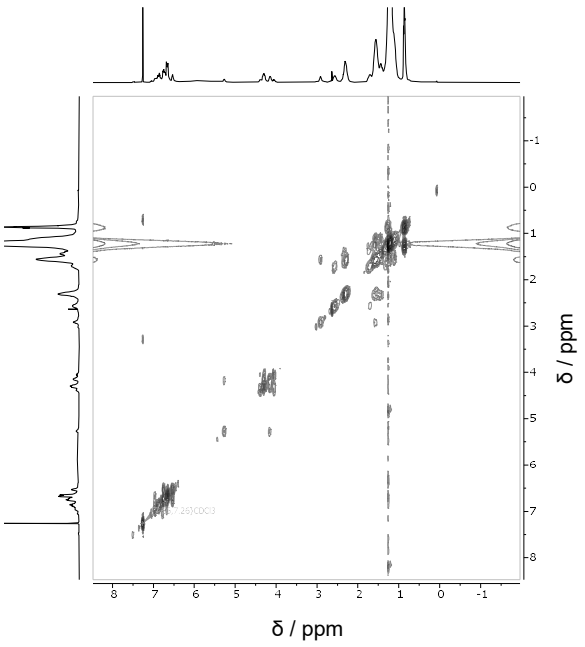

Figure S73. 2D ^{1}H ^{1}H COSY spectrum (400 MHz) of **HOSO-catechol** in $CDCl_3$ at ambient temperature.

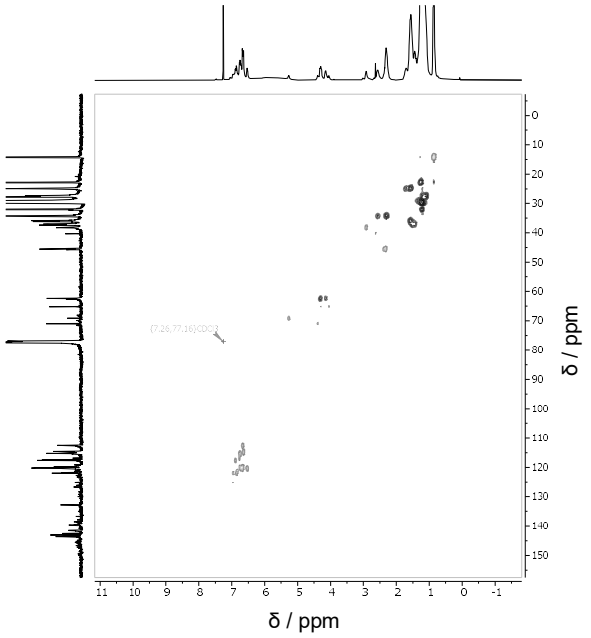

Figure S 74. 2D ^{1}H ^{13}C HSQC spectrum of **HOSO-catechol** in $CDCl_3$ at ambient temperature.

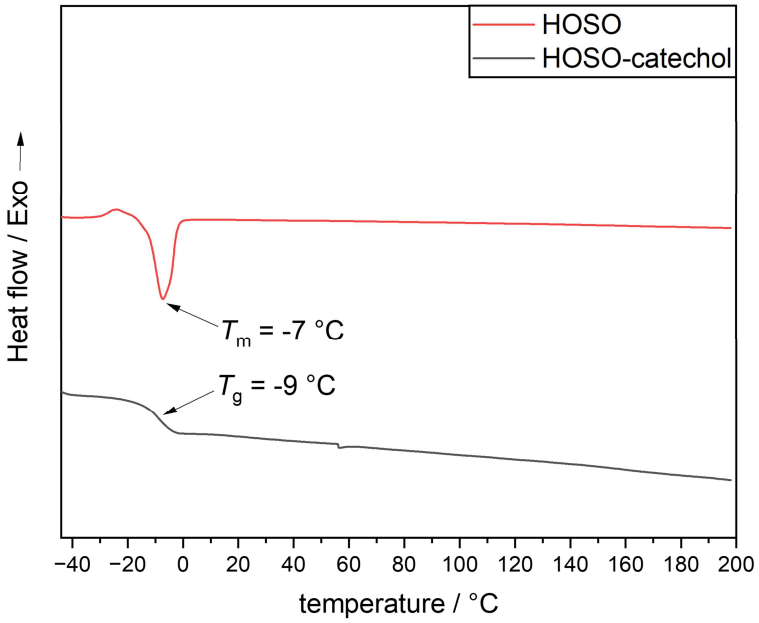

Figure S75. DSC studies (second heating run) of HOSO (red line) and **HOSO-catechol** (black line) −50 to 200 °C with a heating rate of 100 °C min^{-1}under a nitrogen flow.

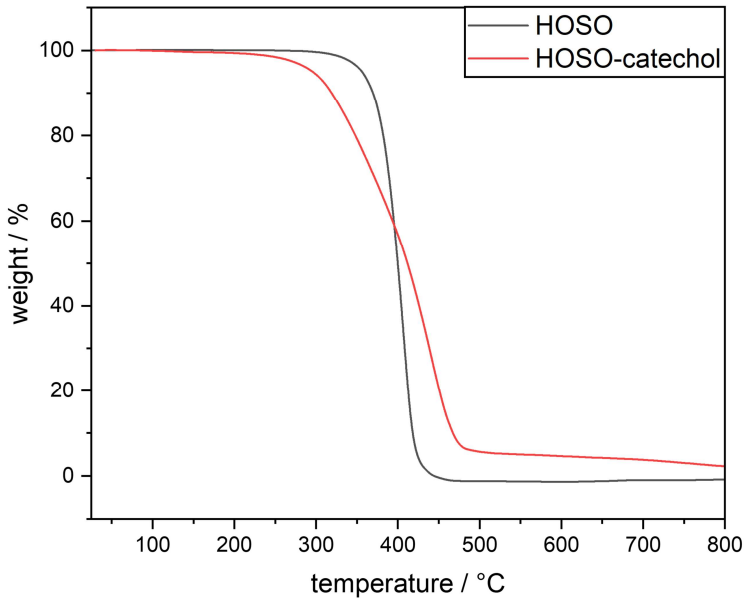

Figure S76. Thermogravimetric analysis (TGA) of HOSO (red) and **HOSO-catechol** (black) from 25 °C to 800 °C with a heating rate of 10 K min^{-1} under a nitrogen flow.

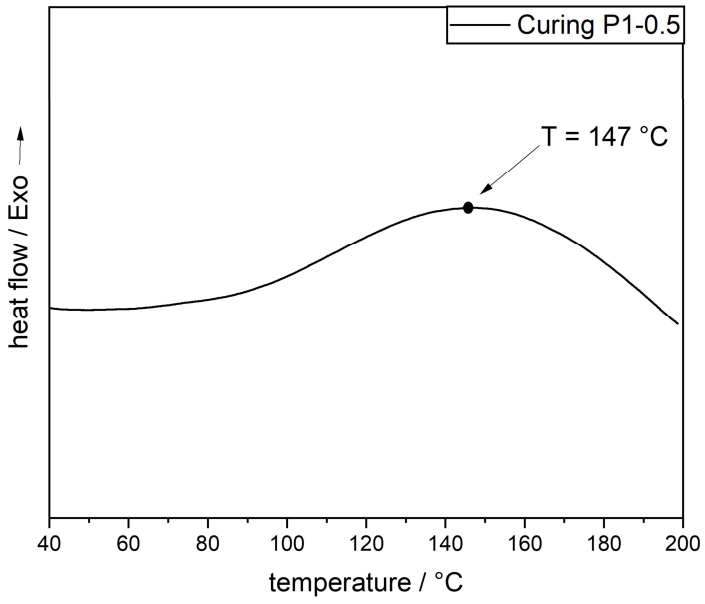

Figure S77. Non-isothermal DSC study (first heating run) of the curing process of **P1-0.5.**

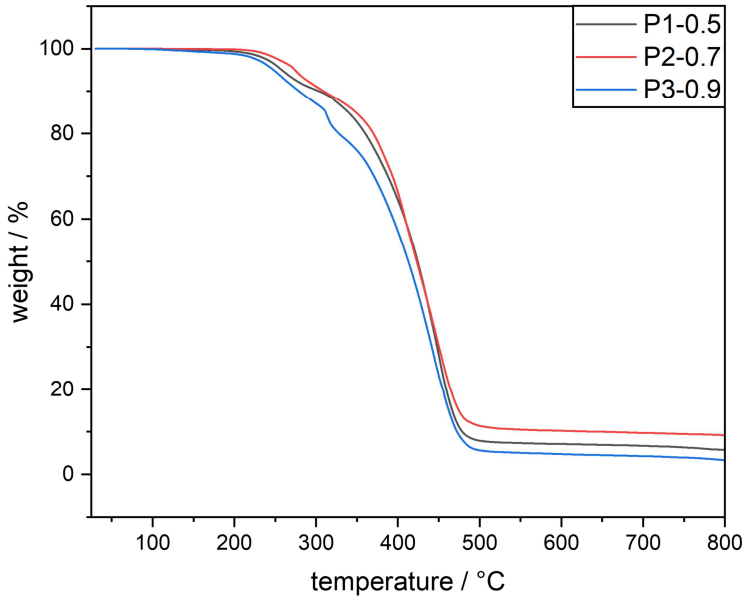

Figure S78. Thermogravimetric analysis (TGA) of **P1-0.5** (black), **P2-0.7** (red), and **P3-0.9** (blue) from 25 °C to 800 °C with a heating rate of 10 K min^{-1} under a nitrogen flow.

7 Appendix

7.1 List of Abbreviations

AAE	actual atom economy
AE	atom economy
AGU	anhydroglucose unit
AIBN	azobisisobutyronitrile
AMIMCl	1-allyl-3-methylimidazolium chloride
ATR-IR	attenuated total reflection infrared
BBr_3	boron tribromide
BMIMCl	1-butyl-3-methylimidazolium chloride
BPAGMA	bisphenol A glycerolate dimethacrylate
BSE	backscattered electron
CA	cellulose acetate
CAB	cellulose acetate butyrate
CAH	cellulose acetate hexanoate
CANs	covalent adaptable networks
CAO	cellulose acetate octanoate
CAP	cellulose acetate propionate
CAV	cellulose acetate valerate
CB	cellulose butyrate
cEF	complete *E* factor
CEs	cellulose esters
C_f	final mercury concentration
CH	cellulose hexanoate
C_i	initial mercury concentration
CMC	Carboxymethyl cellulose
CO	cellulose octanoate
CO_2	carbon dioxide
COSY	gradient selected correlation spectroscopy
CP	cellulose propionate
CS_2	carbon disulfide
CTA	cellulose triacetate
CV	cellulose valerate
CVDE	1,4-cyclohexanedimethanol divinyl ether
DABCO	1,4-diazabicyclo[2.2.2]octane
DBN	1,5-Diazabicyclo[4.3.0]non-5-ene
DBU	1,8-diazabicyclo-[5.4.0]-undec-7-ene
DDT	dichlorodiphenyltrichloroethane
DMA	dopamine methacrylamide
DMAc	*N,N*-dimethylacetamide
DMSO	dimethyl sulfoxide
DOPA	3,4-dihydroxyphenyl-l-alanine

DOSY	diffusion ordered spectroscopy
DP	degree of polymerization
DS_{1H}	degree of substitution
DSC	differential scanning calorimetry
DVB	1,2-divinyl benzene
E factor	environmental factor
EDX	energy-dispersive X-ray
EGDMA	ethylene glycol dimethacrylate
EMIMOAc	1-ethyl-3-methylimidazolium acetate
EPA	U.S. Environmental Protection Agency
ESI-MS	electrospray ionization mass spectrometry
FACEs	fatty acid cellulose esters
FCA	Friedel-Crafts alkylation
FDCA	furandicarboxylic acid
g	mass
GBDA	glyoxal bis(diallylacetal)
GC	gas chromatography
GSK	Glaxo Smith Kline
H_2SO_4	sulfuric acid
H_3PO_4	phosphoric acid
HBr	hydrogen bromide
$HClO_4$	perchloric acid
HCPM	2-hydroxy-3-cardanylpropyl methacrylate
HDDA	1,6-hexanediol dimethacrylate
HFIP	hexafluoro isopropanol
HOSO	high oleic sunflower oil
HSQC	heteronuclear single quantum coherence spectroscopy
ILs	ionic liquids
IR	infrared
K_d	distribution coefficient
LCA	Life Cycle Assessment
LCB	lignocellulosic biomass
LiCl	lithium chloride
MCC	microcrystalline cellulose
MEA	2-methoxyethyl acrylate
MI	mass intensity
MTBD	7-methyl-1,5,7-triazobicyclo[4.4.0]dec-5-ene
Na_2S	sodium sulfide
NaCl	sodium chloride
NADOPAMe	*N*-Ac-3,4-dihydroxyphenylalanine methyl ester
NaOH	sodium hydroxide
n-BuLi	*n*-butyl lithium
NCA	*N*-carboxyanhydride
NIPS	nonsolvent induced phase separation

NMMO	*N*-methylmorpholine-*N*-oxide
NMP	nitroxide mediated polymerization
NMR	nuclear magnetic resonance
PEF	poly(ethylene furanoate)
PET	poly(ethylene terephthalate)
PMI	process mass intensity
PPM	post polymerization modification
q_e	equilibrium extraction capacities
RAFT	reversible addition fragmentation transfer
RME	reaction mass efficiency
ROP	Ring opening polymerization
S_8	Elemental sulfur
SDGs	Sustainable Development Goals
SEC	Size exclusion chromatography
sEF	simple *E* factor
SEM	scanning electron microscopy
SO_2	sulfur dioxide
TAAs	trialkyl amines
TBAF	Tetra-butyl-ammonium fluoride
TBD	1,5,7-triazabicyclo-[4.4.0]-dec-5-en
TBDMS	*tert*-butyldimethylsilyl
TES	triethylsilyl
T_g	glass transition temperature
TGA	thermogravimetric analysis
THF	tetrahydrofuran
TMG	1,1,3,3-tetramethylguanidine
UN	United Nations
V	volume
VA	vinyl acetate
VE	vinyl ether
WCA	water contact angle
WHO	World Health Organization
$Zn(DTC)_2$	zinc diethyldithiocarbamate
τ^*	relaxation time

7.2 Scientific Contributions

List of publications in chronological order:

[5] F. Rhein, **T. Sehn**, M. A. R. Meier, Efficient and accurate determination of the degree of substitution of cellulose acetate using ATR-FTIR spectroscopy and machine learning, *Sci. Rep.* **2025**, *14*, 2904.

[4] **T. Sehn**, N. Kolb, A. Azzawi, M. A. R. Meier, Efficient One-Step Synthesis of Catechol Containing Polymers *via* Friedel−Crafts Alkylation and Their Use for Water Decontamination, *Macromolecules* **2024**, *57*, 10802−10811.

[3] **T. Sehn**, J. Fanelli, L. Wahl, M. A. R. Meier, High sulfur content composite materials from renewable fatty acid cellulose esters (FACEs) *via* inverse vulcanization, *RSC Sustainability* **2025**, *3*, 291–299.

[2] **T. Sehn**, M. A. R. Meier, Structure−Property Relationships of Short Chain (Mixed) Cellulose Esters Synthesized in a DMSO/TMG/CO_2 Switchable Solvent System, *Biomacromolecules* **2023**, *24*, 5255−5264.

[1] **T. Sehn**, B. Huber, J. Fanelli, H. Mutlu, Straightforward synthesis of aliphatic polydithiocarbonates from commercially available starting materials, *Polym. Chem.*, **2022**, *13*, 5965–5973.

List of conference contributions in chronological order:

[2] Presentation: Structure−Property Relationships of Short Chain (Mixed) Cellulose Esters Synthesized in a DMSO/TMG/CO_2 Switchable Solvent System at the *50th IUPAC World Polymer Congress* held at the University of Warwick, Coventry, England, **July 2024**.

[1] Presentation: Structure-property relationships of short chain (mixed) cellulose esters synthesized in a TMG/CO2 switchable solvent system at the ACS Fall Meeting held in San Francisco, United States, **August 2023.**

8 References

[1] E. B. Barbier, J. C. Burgess, *Economics* **2017**, *11*.

[2] L. Carlsen, R. Bruggemann, *International Journal of Sustainable Development & World Ecology* **2022**, *29*, 219-229.

[3] E.-S. Dalampira, S. A. Nastis, *Sustainable Development* **2020**, *28*, 46-55.

[4] P. Anastas, J. Warner, *Green Chemistry: Theory and Practice*, Oxford University Press: New York, **1998**.

[5] T. Keijer, V. Bakker, J. C. Slootweg, *Nature Chemistry* **2019**, *11*, 190-195.

[6] M. J. Mulvihill, E. S. Beach, J. B. Zimmerman, P. T. Anastas, *Annual Review of Environment and Resources* **2011**, *36*, 271-293.

[7] X. Li, H. Y. Yang, *Glob Chall* **2021**, *5*, 2000125.

[8] S. Sharma, A. Bhattacharya, *Applied Water Science* **2017**, *7*, 1043-1067.

[9] I. Mukherjee, U. K. Singh, R. P. Singh, in *Water Pollution and Management Practices* (Eds.: A. Singh, M. Agrawal, S. B. Agrawal), Springer Singapore, Singapore, **2021**, pp. 255-277.

[10] R. CARSON, *Silent Spring, Vol. 13*, **1963**.

[11] L. K. Caldwell, *The National Environmental Policy Act: an agenda for the future*, Indiana University Press, **1998**.

[12] G. W. Suter, II, *Integrated Environmental Assessment and Management* **2008**, *4*, 285-289.

[13] K. R. Walker, M. D. Ricciardone, J. Jensen, *International Journal of Hygiene and Environmental Health* **2003**, *206*, 423-435.

[14] R. A. Sheldon, *Green Chem.* **2016**, *18*, 3180-3183.

[15] M. L. Burnett, *Environmental Management* **1998**, *22*, 213-224.

[16] E. S. Beach, Z. Cui, P. T. Anastas, *Energy & Environmental Science* **2009**, *2*, 1038-1049.

[17] P. T. Anastas, M. M. Kirchhoff, *Acc. Chem. Res.* **2002**, *35*, 686-694.

[18] P. Anastas, N. Eghbali, *Chem. Soc. Rev.* **2010**, *39*, 301-312.

[19] S. Y. Tang, R. A. Bourne, R. L. Smith, M. Poliakoff, *Green Chem.* **2008**, *10*, 268-269.

[20] B. M. Trost, *Science* **1991**, *254*, 1471-1477.

[21] A. Albini, S. Protti, in *Paradigms in Green Chemistry and Technology* (Eds.: A. Albini, S. Protti), Springer International Publishing, Cham, **2016**, pp. 11-24.

[22] B. M. Trost, *Angewandte Chemie International Edition in English* **1995**, *34*, 259-281.

[23] R. A. Sheldon, *Green Chem.* **2007**, *9*, 1273-1283.

[24] R. A. Sheldon, *Green Chem.* **2023**, *25*, 1704-1728.

[25] R. A. Sheldon, *Chem. Ind. (London)* **1992**, 903-906.

[26] R. A. Sheldon, *Green Chem.* **2017**, *19*, 18-43.

[27] R. A. Sheldon, *Chem. Commun.* **2008**, 3352-3365.

[28] F. Roschangar, R. A. Sheldon, C. H. Senanayake, *Green Chem.* **2015**, *17*, 752-768.

[29] R. A. Sheldon, *J. Mol. Catal. A: Chem.* **1996**, *107*, 75-83.

[30] F. G. Calvo-Flores, *ChemSusChem* **2009**, *2*, 905-919.

[31] D. J. C. Constable, A. D. Curzons, V. L. Cunningham, *Green Chem.* **2002**, *4*, 521-527.

[32] C. Jimenez-Gonzalez, C. S. Ponder, Q. B. Broxterman, J. B. Manley, *Organic Process Research & Development* **2011**, *15*, 912-917.

[33] G. Finnveden, M. Z. Hauschild, T. Ekvall, J. Guinée, R. Heijungs, S. Hellweg, A. Koehler, D. Pennington, S. Suh, *Journal of Environmental Management* **2009**, *91*, 1-21.

[34] M. A. Curran, *Current Opinion in Chemical Engineering* **2013**, *2*, 273-277.

[35] D. Kralisch, D. Ott, D. Gericke, *Green Chem.* **2015**, *17*, 123-145.

[36] R. G. Hunt, W. E. Franklin, R. G. Hunt, *The International Journal of Life Cycle Assessment* **1996**, *1*, 4-7.

[37] L. M. Tufvesson, P. Tufvesson, J. M. Woodley, P. Börjesson, *The International Journal of Life Cycle Assessment* **2013**, *18*, 431-444.

[38] C. Okkerse, H. van Bekkum, *Green Chem.* **1999**, *1*, 107-114.

[39] H. Röper, *Starch - Stärke* **2002**, *54*, 89-99.

[40] D. Peters, *Biotechnology Journal* **2006**, *1*, 806-814.

[41] L. T. Mika, E. Cséfalvay, Á. Németh, *Chem. Rev.* **2018**, *118*, 505-613.

[42] T. Werpy, J. Holladay, J. White, **2004**.

[43] J. J. Bozell, G. R. Petersen, *Green Chem.* **2010**, *12*, 539-554.

[44] A. F. Sousa, R. Patrício, Z. Terzopoulou, D. N. Bikiaris, T. Stern, J. Wenger, K. Loos, N. Lotti, V. Siracusa, A. Szymczyk, S. Paszkiewicz, K. S. Triantafyllidis, A. Zamboulis, M. S. Nikolic, P. Spasojevic, S. Thiyagarajan, D. S. van Es, N. Guigo, *Green Chem.* **2021**, *23*, 8795-8820.

[45] S. K. Burgess, J. E. Leisen, B. E. Kraftschik, C. R. Mubarak, R. M. Kriegel, W. J. Koros, *Macromolecules* **2014**, *47*, 1383-1391.

[46] M. A. R. Meier, J. O. Metzger, U. S. Schubert, *Chem. Soc. Rev.* **2007**, *36*, 1788-1802.

[47] U. Biermann, U. T. Bornscheuer, I. Feussner, M. A. R. Meier, J. O. Metzger, *Angew. Chem. Int. Ed.* **2021**, *60*, 20144-20165.

[48] J. Salimon, N. Salih, E. Yousif, *Arabian Journal of Chemistry* **2012**, *5*, 135-145.

[49] I. Singh, S. K. Samal, S. Mohanty, S. K. Nayak, *Eur. J. Lipid Sci. Technol.* **2020**, *122*, 1900225.

[50] S. K. Sahoo, V. Khandelwal, G. Manik, *Polym. Adv. Technol.* **2018**, *29*, 2080-2090.

[51] S. Kumar, S. K. Samal, S. Mohanty, S. K. Nayak, *Ind. Eng. Chem. Res.* **2017**, *56*, 687-698.

[52] S. K. Sahoo, V. Khandelwal, G. Manik, *Ind. Eng. Chem. Res.* **2018**, *57*, 11323-11334.

[53] F. Campana, G. Brufani, F. Mauriello, R. Luque, L. Vaccaro, *Green Synthesis and Catalysis* **2024**.

[54] G. Lligadas, J. C. Ronda, M. Galià, V. Cádiz, *Biomacromolecules* **2010**, *11*, 2825-2835.

[55] M. Lawoko, L. Berglund, M. Johansson, *ACS Sustainable Chem. Eng.* **2021**, *9*, 5481-5485.

[56] O. Y. Abdelaziz, M. B. Vives, S. V. Mankar, N. Warlin, T. T. Nguyen, B. Zhang, C. P. Hulteberg, A. Khataee, *iScience* **2024**, *27*, 109418.

[57] F. Della Monica, A. W. Kleij, *Polym. Chem.* **2020**, *11*, 5109-5127.

[58] D. Klemm, B. Heublein, H.-P. Fink, A. Bohn, *Angew. Chem. Int. Ed.* **2005**, *44*, 3358-3393.

[59] X. Dang, N. Li, Z. Yu, X. Ji, M. Yang, X. Wang, *Carbohydr. Polym.* **2024**, *342*, 122385.

[60] A. Brogniart, A. Pelonze, R. Dumas, *Comptes Rendus* **1839**, *8*, 51-53.

[61] A. Payen, *Sci., a* **1838**, *7*, 1052.

[62] D. N. S. Hon, *Cellulose* **1994**, *1*, 1-25.

[63] W. Yan, J. Liu, X. Zheng, J. Zhang, K. Tang, *e-Polymers* **2023**, *23*.

[64] H. Staudinger, in *A Source Book in Chemistry, 1900-1950* (Ed.: M. L. Henry), Harvard University Press, Cambridge, MA and London, England, **1968**, pp. 259-264.

[65] H. Shaghaleh, X. Xu, S. Wang, *RSC Adv.* **2018**, *8*, 825-842.

[66] T. Heinze, in *Cellulose Chemistry and Properties: Fibers, Nanocelluloses and Advanced Materials* (Ed.: O. J. Rojas), Springer International Publishing, Cham, **2016**, pp. 1-52.

[67] A. Etale, A. J. Onyianta, S. R. Turner, S. J. Eichhorn, *Chem. Rev.* **2023**, *123*, 2016-2048.

[68] G. Fittolani, D. Vargová, P. H. Seeberger, Y. Ogawa, M. Delbianco, *J Am Chem Soc* **2022**, *144*, 12469-12475.

[69] M. P. Motloung, V. Ojijo, J. Bandyopadhyay, S. S. Ray, *Polymers* **2019**, *11*, 1270.

[70] T. Heinze, A. Koschella, T. Liebert, V. Harabagiu, S. Coseri, in *The European Polysaccharide Network of Excellence (EPNOE): Research Initiatives and Results* (Ed.: P. Navard), Springer Vienna, Vienna, **2012**, pp. 283-327.

[71] M. Wohlert, T. Benselfelt, L. Wågberg, I. Furó, L. A. Berglund, J. Wohlert, *Cellulose* **2022**, *29*, 1-23.

[72] B. B. Hallac, A. J. Ragauskas, *Biofuels, Bioproducts and Biorefining* **2011**, *5*, 215-225.

[73] R. Rinaldi, F. Schüth, *ChemSusChem* **2009**, *2*, 1096-1107.

[74] W. Faith, *Industrial & Engineering Chemistry* **1945**, *37*, 9-11.

[75] F. Bergius, *Industrial & Engineering Chemistry* **1937**, *29*, 247-253.

[76] L. P. Walker, D. B. Wilson, *Bioresour. Technol.* **1991**, *36*, 3-14.

[77] S. Kobayashi, J. Sakamoto, S. Kimura, *Prog. Polym. Sci.* **2001**, *26*, 1525-1560.

[78] D. P. Delmer, Y. Amor, *The Plant Cell* **1995**, *7*, 987-1000.

[79] A. F. Lehrhofer, T. Goto, T. Kawada, T. Rosenau, H. Hettegger, *Carbohydr. Polym.* **2022**, *285*, 119222.

[80] J. A. Figueiredo, M. I. Ismael, C. M. S. Anjo, A. P. Duarte, in *Carbohydrates in Sustainable Development I* (Eds.: A. P. Rauter, P. Vogel, Y. Queneau), Springer Berlin Heidelberg, Berlin, Heidelberg, **2010**, pp. 117-128.

[81] K. Jedvert, T. Heinze, *J. Polym. Eng.* **2017**, *37*, 845-860.

[82] Y.-L. Hsieh, *Cotton: Science and technology* **2007**, 3-34.

[83] D. Mboowa, *Biomass Conversion and Biorefinery* **2024**, *14*, 1-12.

[84] R. M. Brown, *Pure Appl. Chem.* **1999**, *71*, 767-775.

[85] R. M. Brown, Jr., J. H. Willison, C. L. Richardson, *Proc Natl Acad Sci U S A* **1976**, *73*, 4565-4569.

[86] R. M. Brown Jr, I. M. Saxena, *Plant Physiol. Biochem.* **2000**, *38*, 57-67.

[87] D. R. Nobles, D. K. Romanovicz, R. M. Brown Jr, *Plant physiology* **2001**, *127*, 529-542.

[88] S. Kobayashi, K. Kashiwa, T. Kawasaki, S. Shoda, *J. Am. Chem. Soc.* **1991**, *113*, 3079-3084.

[89] S. Kobayashi, H. Uyama, M. Ohmae, *Bull. Chem. Soc. Jpn.* **2002**, *74*, 613-635.

[90] F. Nakatsubo, H. Kamitakahara, M. Hori, *J. Am. Chem. Soc.* **1996**, *118*, 1677-1681.

[91] F. H. Isikgor, C. R. Becer, *Polym. Chem.* **2015**, *6*, 4497-4559.

[92] Preethi, G. M, G. Kumar, O. P. Karthikeyan, S. Varjani, R. B. J, *Environmental Technology & Innovation* **2021**, *24*, 102080.

[93] E. A. Cazier, T.-N. Pham, L. Cossus, M. Abla, T. Ilc, P. Lawrence, *Waste Manage. (Oxford)* **2024**, *188*, 11-38.

[94] Q. Wang, M. S. Jahan, S. Liu, Q. Miao, Y. Ni, *Bioresour. Technol.* **2014**, *164*, 380-385.

[95] H. L. Hintz, in *Encyclopedia of Materials: Science and Technology* (Eds.: K. H. J. Buschow, R. W. Cahn, M. C. Flemings, B. Ilschner, E. J. Kramer, S. Mahajan, P. Veyssière), Elsevier, Oxford, **2001**, pp. 6707-6711.

[96] P. Bajpai, in *Biotechnology for Pulp and Paper Processing* (Ed.: P. Bajpai), Springer US, Boston, MA, **2012**, pp. 67-92.

[97] De Gruyter, Berlin, New York, **2009**.

[98] G. K. Gupta, R. K. Kapoor, P. Shukla, in *Microbial Enzymes and Biotechniques: Interdisciplinary Perspectives* (Ed.: P. Shukla), Springer Singapore, Singapore, **2020**, pp. 43-56.

[99] P. Azadi, O. R. Inderwildi, R. Farnood, D. A. King, *Renewable and Sustainable Energy Reviews* **2013**, *21*, 506-523.

[100] M. Takada, R. Chandra, J. Wu, J. N. Saddler, *Bioresour. Technol.* **2020**, *302*, 122895.

[101] H. Tran, E. K. Vakkilainnen, *Tappi Kraft Pulping Short Course* **2008**, 1-8.

[102] C. J. Biermann, *Handbook of pulping and papermaking*, Elsevier, **1996**.

[103] O. Fearon, S. Kuitunen, K. s. Ruuttunen, V. Alopaeus, T. Vuorinen, *Ind. Eng. Chem. Res.* **2020**, *59*, 12977-12985.

[104] J. Gierer, L.-Å. Smedman, G. Cederberg, R. Jensen, C. T. Pederson, E. Larsen, *Acta Chem. Scand.* **1965**, *19*, 1103-1112.

[105] G. E. Miksche, *Acta Chem. Scand* **1972**, *26*.

[106] S. Ljungagren, *Sven. Papperstidn.;(Sweden)* **1980**, *83*.

[107] D. D. S. Argyropoulos, C. Crestini, C. Dahlstrand, E. Furusjö, C. Gioia, K. Jedvert, G. Henriksson, C. Hulteberg, M. Lawoko, C. Pierrou, J. S. M. Samec, E. Subbotina, H. Wallmo, M. Wimby, *ChemSusChem* **2023**, *16*, e202300492.

[108] M. Ragnar, G. Henriksson, M. E. Lindström, M. Wimby, J. Blechschmidt, S. Heinemann, in *Ullmann's Encyclopedia of Industrial Chemistry*, pp. 1-92.

[109] N. Sharma, B. J. Allardyce, R. Rajkhowa, R. Agrawal, *J. Polym. Environ.* **2024**, *32*, 1500-1512.

[110] S. Lou, Y. Huang, M. Wu, *Carbohydr. Polym.* **2023**, *302*, 120421.

[111] T. Liebert, in *Cellulose Solvents: For Analysis, Shaping and Chemical Modification, Vol. 1033*, American Chemical Society, **2010**, pp. 3-54.

[112] S. Acharya, S. Liyanage, P. Parajuli, S. S. Rumi, J. L. Shamshina, N. Abidi, *Polymers* **2021**, *13*, 4344.

[113] H. Nawaz, A. He, Z. Wu, X. Wang, Y. Jiang, A. Ullah, F. Xu, F. Xie, *Int. J. Biol. Macromol.* **2024**, *273*, 133012.

[114] B. Lindman, G. Karlström, L. Stigsson, *J. Mol. Liq.* **2010**, *156*, 76-81.

[115] L. Alves, B. Medronho, F. E. Antunes, D. Topgaard, B. Lindman, *Cellulose* **2016**, *23*, 247-258.

[116] E. Schweizer, *Journal für Praktische Chemie* **1857**, *72*, 109-111.

[117] K. Saalwächter, W. Burchard, P. Klüfers, G. Kettenbach, P. Mayer, D. Klemm, S. Dugarmaa, *Macromolecules* **2000**, *33*, 4094-4107.

[118] C. Woodings, in *Regenerated Cellulose Fibres* (Ed.: C. Woodings), Woodhead Publishing, **2001**, pp. 1-21.

[119] J. Chen, in *Textiles and Fashion* (Ed.: R. Sinclair), Woodhead Publishing, **2015**, pp. 79-95.

[120] C. F. B. Cross, E. J.; Beadle, C. , British, **1892**.

[121] D. Majumdar, A. Bhanarkar, C. Rao, D. Gouda, *Atmospheric Environment: X* **2022**, *13*, 100157.

[122] H. Tu, X. Li, Y. Liu, L. Luo, B. Duan, R. Zhang, *Carbohydr. Polym.* **2022**, *296*, 119942.

[123] J. Hu, *Laboratories* **2024**, *1*, 135-147.

[124] K. T. Ekman, O. T.; Huttunen, J. I., Finnish, **1982**.

[125] S. Paunonen, T. Kamppuri, L. Katajainen, C. Hohenthal, P. Heikkilä, A. Harlin, *Journal of Cleaner Production* **2019**, *222*, 871-881.

[126] R. A. Jacobson, *J. Am. Chem. Soc.* **1938**, *60*, 1742-1744.

[127] C. L. McCormick, D. K. Lichatowich, *Journal of Polymer Science: Polymer Letters Edition* **1979**, *17*, 479-484.

[128] B. Morgenstern, H. W. Kammer, W. Berger, P. Skrabal, *Acta Polym.* **1992**, *43*, 356-357.

[129] T. Heinze, R. Dicke, A. Koschella, A. H. Kull, E.-A. Klohr, W. Koch, *Macromol. Chem. Phys.* **2000**, *201*, 627-631.

[130] A. J. Sayyed, N. A. Deshmukh, D. V. Pinjari, *Cellulose* **2019**, *26*, 2913-2940.

[131] A. Pinkert, K. N. Marsh, S. Pang, *Ind. Eng. Chem. Res.* **2010**, *49*, 11121-11130.

[132] M. Shabbir, F. Mohammad, in *Sustainable Fibres and Textiles* (Ed.: S. S. Muthu), Woodhead Publishing, **2017**, pp. 171-189.

[133] C. Graenacher, United States, **1934**.

[134] R. P. Swatloski, S. K. Spear, J. D. Holbrey, R. D. Rogers, *J. Am. Chem. Soc.* **2002**, *124*, 4974-4975.

[135] R. P. Swatloski, J. D. Holbrey, S. K. Spear, R. D. Rogers, *ECS Proceedings Volumes* **2002**, *2002-19*, 155.

[136] S. Zhu, Y. Wu, Q. Chen, Z. Yu, C. Wang, S. Jin, Y. Ding, G. Wu, *Green Chem.* **2006**, *8*, 325-327.

[137] J. Zhang, J. Wu, J. Yu, X. Zhang, J. He, J. Zhang, *Materials Chemistry Frontiers* **2017**, *1*, 1273-1290.

[138] L. Berga, I. Bruce, T. W. J. Nicol, A. J. Holding, N. Isobe, S. Shimizu, A. J. Walker, J. E. S. J. Reid, *Cellulose* **2020**, *27*, 9593-9603.

[139] S. K. Singh, A. W. Savoy, *J. Mol. Liq.* **2020**, *297*, 112038.

[140] S. Tang, G. A. Baker, S. Ravula, J. E. Jones, H. Zhao, *Green Chem.* **2012**, *14*, 2922-2932.

[141] J. Pernak, R. Kordala, B. Markiewicz, F. Walkiewicz, M. Popławski, A. Fabiańska, S. Jankowski, M. Łożyński, *RSC Adv.* **2012**, *2*, 8429-8438.

[142] T. Heinze, K. Schwikal, S. Barthel, *Macromolecular Bioscience* **2005**, *5*, 520-525.

[143] E. S. Sashina, D. A. Kashirskii, M. Zaborski, S. Jankowski, *Russ. J. Gen. Chem.* **2012**, *82*, 1994-1998.

[144] Y. Fukaya, A. Sugimoto, H. Ohno, *Biomacromolecules* **2006**, *7*, 3295-3297.

[145] Y. Fukaya, K. Hayashi, M. Wada, H. Ohno, *Green Chem.* **2008**, *10*, 44-46.

[146] S. S. de Jesus, R. Maciel Filho, *Renewable and Sustainable Energy Reviews* **2022**, *157*, 112039.

[147] K. Kuroda, *New J. Chem.* **2022**, *46*, 20047-20052.

[148] A. J. S. McIntosh, J. Griffith, J. Gräsvik, in *Application, Purification, and Recovery of Ionic Liquids* (Eds.: O. Kuzmina, J. P. Hallett), Elsevier, Amsterdam, **2016**, pp. 59-99.

[149] P. G. Jessop, D. J. Heldebrant, X. Li, C. A. Eckert, C. L. Liotta, *Nature* **2005**, *436*, 1102-1102.

[150] H. Xie, X. Yu, Y. Yang, Z. K. Zhao, *Green Chem.* **2014**, *16*, 2422-2427.

[151] Q. Zhang, N. S. Oztekin, J. Barrault, K. De Oliveira Vigier, F. Jérôme, *ChemSusChem* **2013**, *6*, 593-596.

[152] K. N. Onwukamike, T. Tassaing, S. Grelier, E. Grau, H. Cramail, M. A. R. Meier, *ACS Sustainable Chem. Eng.* **2018**, *6*, 1496-1503.

[153] M. Gunnarsson, D. Bernin, M. Hasani, M. Lund, E. Bialik, *ACS Sustainable Chem. Eng.* **2021**, *9*, 14006-14011.

[154] E. Esen, P. Hädinger, M. A. R. Meier, *Biomacromolecules* **2021**, *22*, 586-593.

[155] Y. Zheng, Z. Li, M. Chen, J. Zuo, T. Yang, W. Miao, Y. Zhao, F. Liu, J. Wang, J. Zhu, *Chem. Eng. J.* **2024**, *501*, 157304.

[156] D. Prat, A. Wells, J. Hayler, H. Sneddon, C. R. McElroy, S. Abou-Shehada, P. J. Dunn, *Green Chem.* **2016**, *18*, 288-296.

[157] J. Wolfs, M. A. R. Meier, *Green Chem.* **2021**, *23*, 4410-4420.

[158] J. Verma, M. Petru, S. Goel, *Industrial Crops and Products* **2024**, *210*, 118078.

[159] S. Kamel, N. Ali, K. Jahangir, S. Shah, A. El-Gendy, *Express Polym Lett* **2008**, *2*, 758-778.

[160] F. Schoenbein, *Pogg. Ann.* **1846**, *70*, 220.

[161] J. W. Hyatt*, Vol. 50359A*, United States, **1865**.

[162] E. A. Carter, B. Swarbrick, T. M. Harrison, L. Ronai, *Heritage Science* **2020**, *8*, 51.

[163] J. F. Kennedy, C. J. Knill, in *Medical Textiles and Biomaterials for Healthcare* (Eds.: S. C. Anand, J. F. Kennedy, M. Miraftab, S. Rajendran), Woodhead Publishing, **2006**, pp. 3-22.

[164] H. Seddiqi, E. Oliaei, H. Honarkar, J. Jin, L. C. Geonzon, R. G. Bacabac, J. Klein-Nulend, *Cellulose* **2021**, *28*, 1893-1931.

[165] H. O. M. A. Moura, E. C. d. Souza, B. R. d. Silva, E. S. Pereira, T. d. C. Bicudo, E. Rodríguez-Castellón, L. S. d. Carvalho, *Industrial Crops and Products* **2024**, *220*, 119413.

[166] K. J. Edgar, C. M. Buchanan, J. S. Debenham, P. A. Rundquist, B. D. Seiler, M. C. Shelton, D. Tindall, *Prog. Polym. Sci.* **2001**, *26*, 1605-1688.

[167] T. Kawano, Y. Andou, *RSC Adv.* **2023**, *13*, 24286-24290.

[168] J. Ganster, H.-P. Fink, in *Bio-Based Plastics*, **2013**, pp. 35-62.

[169] K. J. Edgar, in *Encyclopedia of Polymer Science and Technology*, **2004**.

[170] I. R. Ahmad, D. Cane, J. H. Townsend, C. Triana, L. Mazzei, K. Curran, *Polym. Degrad. Stab.* **2020**, *172*, 109050.

[171] P. McNeice, B. L. Feringa, *Green Chem.* **2024**, *26*, 11747-11772.

[172] K. N. Onwukamike, S. Grelier, E. Grau, H. Cramail, M. A. R. Meier, *ACS Sustainable Chem. Eng.* **2019**, *7*, 1826-1840.

[173] K. N. Onwukamike, S. Grelier, E. Grau, H. Cramail, M. A. R. Meier, *ACS Sustainable Chem. Eng.* **2018**, *6*, 8826-8835.

[174] T. Kulomaa, J. Matikainen, P. Karhunen, M. Heikkilä, J. Fiskari, I. Kilpeläinen, *RSC Adv.* **2015**, *5*, 80702-80708.

[175] P. Willberg-Keyriläinen, J. Ropponen, *Heliyon* **2019**, *5*, e02898.

[176] V. Vatanpour, M. E. Pasaoglu, H. Barzegar, O. O. Teber, R. Kaya, M. Bastug, A. Khataee, I. Koyuncu, *Chemosphere* **2022**, *295*, 133914.

[177] C. Reid, E. Breton, *J. Appl. Polym. Sci.* **1959**, *1*, 133-143.

[178] A. Boretti, L. Rosa, *npj Clean Water* **2019**, *2*, 15.

[179] M. D. Islam, F. J. Uddin, T. U. Rashid, M. Shahruzzaman, *Mater. Adv.* **2023**, *4*, 4054-4102.

[180] R. Al-Wafi, M. K. Ahmed, S. F. Mansour, *Journal of Water Process Engineering* **2020**, *38*, 101543.

[181] H. E. Emam, M. El-Shahat, R. M. Abdelhameed, *J. Hazard. Mater.* **2021**, *414*, 125509.

[182] J. A. Ober, *USGS Report* **2018**, 2.

[183] T. Lee, P. T. Dirlam, J. T. Njardarson, R. S. Glass, J. Pyun, *J. Am. Chem. Soc.* **2022**, *144*, 5-22.

[184] M. Akiba, A. S. Hashim, *Prog. Polym. Sci.* **1997**, *22*, 475-521.

[185] M. King, M. Moats, W. G. Davenport, *Sulfuric acid manufacture: analysis, control and optimization*, Newnes, **2013**.

[186] P. Devendar, G.-F. Yang, *Top. Curr. Chem.* **2017**, *375*, 82.

[187] P. Conen, M. A. R. Meier, *Tetrahedron Chem* **2024**, *11*, 100086.

[188] A. Y. Coran, in *Science and Technology of Rubber (Second Edition)* (Eds.: J. E. Mark, B. Erman, F. R. Eirich), Academic Press, San Diego, **1994**, pp. 339-385.

[189] W. J. Chung, A. G. Simmonds, J. J. Griebel, E. T. Kim, H. S. Suh, I.-B. Shim, R. S. Glass, D. A. Loy, P. Theato, Y.-E. Sung, K. Char, J. Pyun, *Angew. Chem. Int. Ed.* **2011**, *50*, 11409-11412.

[190] W. J. Chung, J. J. Griebel, E. T. Kim, H. Yoon, A. G. Simmonds, H. J. Ji, P. T. Dirlam, R. S. Glass, J. J. Wie, N. A. Nguyen, B. W. Guralnick, J. Park, Á. Somogyi, P. Theato, M. E. Mackay, Y.-E. Sung, K. Char, J. Pyun, *Nature Chemistry* **2013**, *5*, 518-524.

[191] X. Wu, J. A. Smith, S. Petcher, B. Zhang, D. J. Parker, J. M. Griffin, T. Hasell, *Nature Communications* **2019**, *10*, 647.

[192] J. Jia, J. Liu, Z.-Q. Wang, T. Liu, P. Yan, X.-Q. Gong, C. Zhao, L. Chen, C. Miao, W. Zhao, S. Cai, X.-C. Wang, A. I. Cooper, X. Wu, T. Hasell, Z.-J. Quan, *Nature Chemistry* **2022**, *14*, 1249-1257.

[193] Z. Yang, P. Yan, X. Li, C. Miao, S. Cai, W. Ji, M. Song, L. J. Dodd, X. Wu, T. Hasell, P. Song, *Polym. Chem.* **2023**, *14*, 3686-3694.

[194] B. Zheng, L. Zhong, X. Wang, P. Lin, Z. Yang, T. Bai, H. Shen, H. Zhang, *Nature Communications* **2024**, *15*, 5507.

[195] L. J. Dodd, Ö. Omar, X. Wu, T. Hasell, *ACS Catalysis* **2021**, *11*, 4441-4455.

[196] J. H. Hwang, J. M. Lee, J. H. Seo, G. Y. Noh, W. Byun, S. Kim, W. Lee, S. Park, D.-G. Kim, Y. S. Kim, *Green Chem.* **2023**, *25*, 4641-4646.

[197] M. J. H. Worthington, R. L. Kucera, J. M. Chalker, *Green Chem.* **2017**, *19*, 2748-2761.

[198] C. Herrera, K. J. Ysinga, C. L. Jenkins, *ACS Applied Materials & Interfaces* **2019**, *11*, 35312-35318.

[199] A. Abbasi, M. M. Nasef, W. Z. N. Yahya, *Sustainable Chemistry and Pharmacy* **2019**, *13*, 100158.

[200] M. S. Karunarathna, M. K. Lauer, T. Thiounn, R. C. Smith, A. G. Tennyson, *Journal of Materials Chemistry A* **2019**, *7*, 15683-15690.

[201] M. K. Lauer, T. A. Estrada-Mendoza, C. D. McMillen, G. Chumanov, A. G. Tennyson, R. C. Smith, *Adv. Sustainable Syst.* **2019**, *3*, 1900062.

[202] M. K. Lauer, A. G. Tennyson, R. C. Smith, *ACS Appl. Polym. Mater.* **2020**, *2*, 3761-3765.

[203] A. Nayeem, M. F. Ali, J. H. Shariffuddin, *Materials Today: Proceedings* **2022**, *57*, 1095-1100.

[204] M. J. H. Worthington, R. L. Kucera, I. S. Albuquerque, C. T. Gibson, A. Sibley, A. D. Slattery, J. A. Campbell, S. F. K. Alboaiji, K. A. Muller, J. Young, N. Adamson, J. R. Gascooke, D. Jampaiah, Y. M. Sabri, S. K. Bhargava, S. J. Ippolito, D. A. Lewis, J. S. Quinton, A. V. Ellis, A. Johs, G. J. L. Bernardes, J. M. Chalker, *Chemistry – A European Journal* **2017**, *23*, 16219-16230.

[205] N. A. Lundquist, M. J. H. Worthington, N. Adamson, C. T. Gibson, M. R. Johnston, A. V. Ellis, J. M. Chalker, *RSC Adv.* **2018**, *8*, 1232-1236.

[206] A. D. Tikoalu, N. A. Lundquist, J. M. Chalker, *Adv. Sustainable Syst.* **2020**, *4*, 1900111.

[207] Z. Ren, X. Jiang, L. Liu, C. Yin, S. Wang, X. Yang, *J. Mol. Liq.* **2021**, *328*, 115437.

[208] A. G. Simmonds, J. J. Griebel, J. Park, K. R. Kim, W. J. Chung, V. P. Oleshko, J. Kim, E. T. Kim, R. S. Glass, C. L. Soles, Y.-E. Sung, K. Char, J. Pyun, *ACS Macro Letters* **2014**, *3*, 229-232.

[209] I. Gomez, O. Leonet, J. A. Blazquez, D. Mecerreyes, *ChemSusChem* **2016**, *9*, 3419-3425.

[210] F. Zhao, Y. Li, W. Feng, *Small Methods* **2018**, *2*, 1800156.

[211] P. Liu, J. M. Gardner, L. Kloo, *Chem. Commun.* **2015**, *51*, 14660-14662.

[212] A. Hoefling, Y. J. Lee, P. Theato, *Macromol. Chem. Phys.* **2017**, *218*, 1600303.

[213] S. F. Valle, A. S. Giroto, R. Klaic, G. G. F. Guimarães, C. Ribeiro, *Polym. Degrad. Stab.* **2019**, *162*, 102-105.

[214] A. Adharis, K. Loos, in *Methods Enzymol., Vol. 627* (Eds.: N. Bruns, K. Loos), Academic Press, **2019**, pp. 215-247.

[215] T. Kaur, R. P. Singh, in *Bioactive Natural products in Drug Discovery* (Eds.: J. Singh, V. Meshram, M. Gupta), Springer Singapore, Singapore, **2020**, pp. 517-545.

[216] M. K. Lauer, A. G. Tennyson, R. C. Smith, *Mater. Adv.* **2021**, *2*, 2391-2397.

[217] M. K. Lauer, A. G. Tennyson, R. C. Smith, *Mater. Adv.* **2022**, *3*, 4186-4193.

[218] P. Mischnick, D. Momcilovic, in *Adv. Carbohydr. Chem. Biochem., Vol. 64* (Ed.: D. Horton), Academic Press, **2010**, pp. 117-210.

[219] F. N. Omar, H. S. Hafid, J. Zhu, E. K. Bahrin, F. Z. M. Nadzri, M. Wakisaka, *Materials Today Communications* **2022**, *33*, 104392.

[220] D. J. Parker, S. T. Chong, T. Hasell, *RSC Adv.* **2018**, *8*, 27892-27899.

[221] D. J. Parker, H. A. Jones, S. Petcher, L. Cervini, J. M. Griffin, R. Akhtar, T. Hasell, *Journal of Materials Chemistry A* **2017**, *5*, 11682-11692.

[222] J. Kuwabara, K. Oi, M. M. Watanabe, T. Fukuda, T. Kanbara, *ACS Appl. Polym. Mater.* **2020**, *2*, 5173-5178.

[223] J. J. Dale, V. Hanna, T. Hasell, *ACS Appl. Polym. Mater.* **2023**, *5*, 6761-6765.

[224] M. R. Thomsett, J. C. Moore, A. Buchard, R. A. Stockman, S. M. Howdle, *Green Chem.* **2019**, *21*, 149-156.

[225] C. M. Byrne, S. D. Allen, E. B. Lobkovsky, G. W. Coates, *J. Am. Chem. Soc.* **2004**, *126*, 11404-11405.

[226] L. Kvittingen, B. J. Sjursnes, R. Schmid, *J. Chem. Educ.* **2021**, *98*, 3600-3607.

[227] M. P. Crockett, A. M. Evans, M. J. H. Worthington, I. S. Albuquerque, A. D. Slattery, C. T. Gibson, J. A. Campbell, D. A. Lewis, G. J. L. Bernardes, J. M. Chalker, *Angew. Chem. Int. Ed.* **2016**, *55*, 1714-1718.

[228] F. Wu, S. Chen, V. Srot, Y. Huang, S. K. Sinha, P. A. van Aken, J. Maier, Y. Yu, *Adv. Mater.* **2018**, *30*, 1706643.

[229] L. Hu, H. Pan, Y. Zhou, M. Zhang, *BioResources* **2011**, *6*.

[230] R. C. Kuhad, A. Singh, *Crit. Rev. Biotechnol.* **1993**, *13*, 151-172.

[231] S. c. d. Eswaran, S. Subramaniam, U. Sanyal, R. Rallo, X. Zhang, *Scientific Data* **2022**, *9*, 647.

[232] Y. C. Lin, Y. N. Hsu, Y. C. Chung, *RSC Adv.* **2014**, *4*, 22931-22937.

[233] K. J. Kramer, M. R. Kanost, T. L. Hopkins, H. Jiang, Y. C. Zhu, R. Xu, J. L. Kerwin, F. Turecek, *Tetrahedron* **2001**, *57*, 385-392.

[234] S. A. Mian, L.-M. Yang, L. C. Saha, E. Ahmed, M. Ajmal, E. Ganz, *Langmuir* **2014**, *30*, 6906-6914.

[235] H. Wang, L. Wang, S. Zhang, W. Zhang, J. Li, Y. Han, *Polym. Int.* **2021**, *70*, 1209-1224.

[236] N. Patil, C. Jérôme, C. Detrembleur, *Prog. Polym. Sci.* **2018**, *82*, 34-91.

[237] P. Kord Forooshani, B. P. Lee, *J. Polym. Sci., Part A: Polym. Chem.* **2017**, *55*, 9-33.

[238] J. Saiz-Poseu, J. Mancebo-Aracil, F. Nador, F. Busqué, D. Ruiz-Molina, *Angew. Chem. Int. Ed.* **2019**, *58*, 696-714.

[239] F. Coumes, A. Malfait, M. Bria, J. Lyskawa, P. Woisel, D. Fournier, *Polym. Chem.* **2016**, *7*, 4682-4692.

[240] Y. Suzuki, D. Kusuyama, T. Sugaya, S. Iwatsuki, M. Inamo, H. D. Takagi, K. Ishihara, *J. Org. Chem.* **2020**, *85*, 5255-5264.

[241] H. Gulley-Stahl, P. A. Hogan, II, W. L. Schmidt, S. J. Wall, A. Buhrlage, H. A. Bullen, *Environ. Sci. Technol.* **2010**, *44*, 4116-4121.

[242] S. Sakib, F. Bakhshandeh, S. Saha, L. Soleymani, I. Zhitomirsky, *Sol. RRL* **2021**, *5*, 2100512.

[243] G. Yan, G. Chen, Z. Peng, Z. Shen, X. Tang, Y. Sun, X. Zeng, L. Lin, *Adv. Mater. Interfaces* **2021**, *8*, 2100239.

[244] Z. Xu, *Sci. Rep.* **2013**, *3*, 2914.

[245] A. Petran, C. Lar, D. Bogdan, A. Caspari, N. D. Hadade, A. Vulcu, A. Popa, F. Simon, Z. Cordelia, J. Liebscher, *Polymer* **2024**, *312*, 127630.

[246] A. Lancelot, A. A. Putnam-Neeb, S. L. Huntington, J. M. Garcia-Rodriguez, N. Naren, C. L. Atencio-Martinez, J. J. Wilker, *Macromolecules* **2023**, *56*, 1141-1153.

[247] K. Hennig, W. Meyer, *Molecules* **2022**, *27*, 4027.

[248] T. Ratvijitvech, *J. Polym. Environ.* **2020**, *28*, 2211-2218.

[249] H. Lee, S. M. Dellatore, W. M. Miller, P. B. Messersmith, *science* **2007**, *318*, 426-430.

[250] Y. Liu, K. Ai, L. Lu, *Chem. Rev.* **2014**, *114*, 5057-5115.

[251] D. R. Dreyer, D. J. Miller, B. D. Freeman, D. R. Paul, C. W. Bielawski, *Chemical Science* **2013**, *4*, 3796-3802.

[252] D. Yang, X. Wang, Q. Ai, J. Shi, Z. Jiang, *RSC Adv.* **2015**, *5*, 42461-42467.

[253] H. Hu, J. C. Dyke, B. A. Bowman, C.-C. Ko, W. You, *Langmuir* **2016**, *32*, 9873-9882.

[254] Q. Lyu, J. Zhang, K. G. Neoh, C. Li Lin Chai, *Nanoscale* **2017**, *9*, 12409-12415.

[255] H. Wang, J. Wu, C. Cai, J. Guo, H. Fan, C. Zhu, H. Dong, N. Zhao, J. Xu, *ACS Applied Materials & Interfaces* **2014**, *6*, 5602-5608.

[256] H. Yamamoto, K. Ohkawa, *Amino Acids* **1993**, *5*, 71-75.

[257] M. J. Sever, J. J. Wilker, *Tetrahedron* **2001**, *57*, 6139-6146.

[258] T. J. Deming, *Nature* **1997**, *390*, 386-389.

[259] M. Yu, J. Hwang, T. J. Deming, *J. Am. Chem. Soc.* **1999**, *121*, 5825-5826.

[260] M. Yin, Y. Yuan, C. Liu, J. Wang, *Biomaterials* **2009**, *30*, 2764-2773.

[261] M. Yu, T. J. Deming, *Macromolecules* **1998**, *31*, 4739-4745.

[262] A. B. Samui, T. Kanai, *Int. J. Biol. Macromol.* **2019**, *140*, 522-537.

[263] M. Kharasch, F. KAWAHARA, W. NUDENBERG, *J. Org. Chem.* **1954**, *19*, 1977-1990.

[264] G. Moad, D. H. Solomon, *The chemistry of free radical polymerization, Vol. 3*, Pergamon Oxford, **1995**.

[265] C. Zhang, K. Li, J. Simonsen, *J. Appl. Polym. Sci.* **2003**, *89*, 1078-1084.

[266] A. GhavamiNejad, C. H. Park, C. S. Kim, *Biomacromolecules* **2016**, *17*, 1213-1223.

[267] J. Nishida, M. Kobayashi, A. Takahara, *J. Polym. Sci., Part A: Polym. Chem.* **2013**, *51*, 1058-1065.

[268] H. Xu, J. Nishida, W. Ma, H. Wu, M. Kobayashi, H. Otsuka, A. Takahara, *ACS Macro Letters* **2012**, *1*, 457-460.

[269] S.-B. Lee, C. González-Cabezas, K.-M. Kim, K.-N. Kim, K. Kuroda, *Biomacromolecules* **2015**, *16*, 2265-2275.

[270] Y. Mu, X. Wu, D. Pei, Z. Wu, C. Zhang, D. Zhou, X. Wan, *ACS Biomaterials Science & Engineering* **2017**, *3*, 3133-3140.

[271] J. D. White, J. J. Wilker, *Macromolecules* **2011**, *44*, 5085-5088.

[272] A. Isakova, P. D. Topham, A. J. Sutherland, *Macromolecules* **2014**, *47*, 2561-2568.

[273] S. Hou, P. X. Ma, *Chem. Mater.* **2015**, *27*, 7627-7635.

[274] H. O. Ham, Z. Liu, K. A. Lau, H. Lee, P. B. Messersmith, *Angew. Chem. Int. Ed.* **2011**, *50*, 732-736.

[275] H. N. Nguyen, E. T. Nadres, B. G. Alamani, D. F. Rodrigues, *Journal of Materials Chemistry B* **2017**, *5*, 6616-6628.

[276] Z. Gao, L. Duan, Y. Yang, W. Hu, G. Gao, *Appl. Surf. Sci.* **2018**, *427*, 74-82.

[277] J. Ko, Y.-J. Kim, Y. S. Kim, *ACS applied materials & interfaces* **2016**, *8*, 23854-23861.

[278] Y.-S. Choi, H. Kang, D.-G. Kim, S.-H. Cha, J.-C. Lee, *ACS applied materials & interfaces* **2014**, *6*, 21297-21307.

[279] H. J. Meredith, J. J. Wilker, *Adv. Funct. Mater.* **2015**, *25*, 5057-5065.

[280] X. Xue, G. Pasparakis, N. Halliday, K. Winzer, S. M. Howdle, C. J. Cramphorn, N. R. Cameron, P. M. Gardner, B. G. Davis, F. Fernández-Trillo, *Angew. Chem. Int. Ed.* **2011**, *50*, 9852-9856.

[281] A. Charlot, V. Sciannaméa, S. Lenoir, E. Faure, R. Jérôme, C. Jérôme, C. Van De Weerdt, J. Martial, C. Archambeau, N. Willet, *J. Mater. Chem.* **2009**, *19*, 4117-4125.

[282] J. Yang, J. Keijsers, M. Van Heek, A. Stuiver, M. A. C. Stuart, M. Kamperman, *Polym. Chem.* **2015**, *6*, 3121-3130.

[283] N. Rubio, H. Au, H. S. Leese, S. Hu, A. J. Clancy, M. S. P. Shaffer, *Macromolecules* **2017**, *50*, 7070-7079.

[284] S. Kim, J. M. Moon, J. S. Choi, W. K. Cho, S. M. Kang, *Adv. Funct. Mater.* **2016**, *26*, 4099-4105.

[285] C. Fan, J. Fu, W. Zhu, D.-A. Wang, *Acta biomaterialia* **2016**, *33*, 51-63.

[286] J. Lee, K. C. Yoo, J. Ko, B. Yoo, J. Shin, S.-J. Lee, D. Sohn, *Carbohydr. Polym.* **2017**, *164*, 309-316.

[287] M. Shin, S.-G. Park, B.-C. Oh, K. Kim, S. Jo, M. S. Lee, S. S. Oh, S.-H. Hong, E.-C. Shin, K.-S. Kim, *Nature materials* **2017**, *16*, 147-152.

[288] C. Nie, C. Cheng, L. Ma, J. Deng, C. Zhao, *Langmuir* **2016**, *32*, 5955-5965.

[289] S. Ryu, Y. Lee, J. W. Hwang, S. Hong, C. Kim, T. G. Park, H. Lee, S. H. Hong, *Adv. Mater.* **2011**, *23*, 1971-1975.

[290] L. Q. Xu, H. Jiang, K.-G. Neoh, E.-T. Kang, G. D. Fu, *Polym. Chem.* **2012**, *3*, 920-927.

[291] R. Wang, J. Li, W. Chen, T. Xu, S. Yun, Z. Xu, Z. Xu, T. Sato, B. Chi, H. Xu, *Adv. Funct. Mater.* **2017**, *27*, 1604894.

[292] L. J. Duan, Y. Liu, J. Kim, D. J. Chung, *J. Appl. Polym. Sci.* **2013**, *130*, 131-137.

[293] E. Grignon, S. Y. An, A. M. Battaglia, D. S. Seferos, *Macromolecules* **2022**, *55*, 10167-10175.

[294] J. Heo, T. Kang, S. G. Jang, D. S. Hwang, J. M. Spruell, K. L. Killops, J. H. Waite, C. J. Hawker, *J. Am. Chem. Soc.* **2012**, *134*, 20139-20145.

[295] Y. Mu, Z. Wu, Y. Ma, J. Zheng, W. Zhang, Z. Sun, X. Wang, D. Pei, L. Li, W. Jiang, *Journal of Materials Chemistry B* **2017**, *5*, 1742-1752.

[296] Y. Shi, P. Zhou, V. Jérôme, R. Freitag, S. Agarwal, *ACS Biomaterials Science & Engineering* **2015**, *1*, 971-977.

[297] P. Chapala, M. Bermeshev, S. Korchagina, R. Ashirov, E. Bermesheva, *Russ. Chem. Bull.* **2016**, *65*, 1061-1066.

[298] D. A. Jose, P. Kar, D. Koley, B. Ganguly, W. Thiel, H. N. Ghosh, A. Das, *Inorg. Chem.* **2007**, *46*, 5576-5584.

[299] E. Faure, C. Falentin-Daudré, C. Jérôme, J. Lyskawa, D. Fournier, P. Woisel, C. Detrembleur, *Prog. Polym. Sci.* **2013**, *38*, 236-270.

[300] J. Sedó, J. Saiz-Poseu, F. Busqué, D. Ruiz-Molina, *Adv. Mater.* **2013**, *25*, 653-701.

[301] M. Krogsgaard, V. Nue, H. Birkedal, *Chemistry–A European Journal* **2016**, *22*, 844-857.

[302] J. Niu, D. J. Lunn, A. Pusuluri, J. I. Yoo, M. A. O'Malley, S. Mitragotri, H. T. Soh, C. J. Hawker, *Nature Chemistry* **2017**, *9*, 537-545.

[303] Y. Song, G. Ye, Y. Lu, J. Chen, J. Wang, K. Matyjaszewski, *ACS Macro Letters* **2016**, *5*, 382-386.

[304] D. J. Phillips, G.-L. Davies, M. I. Gibson, *Journal of Materials Chemistry B* **2015**, *3*, 270-275.

[305] P.-X. Wang, Y.-S. Dong, X.-W. Lu, J. Du, Z.-Q. Wu, *Polym. Chem.* **2016**, *7*, 5563-5570.

[306] M. Arslan, T. N. Gevrek, J. Lyskawa, S. Szunerits, R. Boukherroub, R. Sanyal, P. Woisel, A. Sanyal, *Macromolecules* **2014**, *47*, 5124-5134.

[307] Q. Zhang, G. Nurumbetov, A. Simula, C. Zhu, M. Li, P. Wilson, K. Kempe, B. Yang, L. Tao, D. M. Haddleton, *Polym. Chem.* **2016**, *7*, 7002-7010.

[308] T. Sehn, M. A. R. Meier, *Biomacromolecules* **2023**, *24*, 5255-5264.

[309] S. Mi, Z. Yao, F. Liu, Y. Li, J. Wang, H. Na, J. Zhu, *Green Chem.* **2022**, *24*, 8677-8684.

[310] Z. Söyler, K. N. Onwukamike, S. Grelier, E. Grau, H. Cramail, M. A. R. Meier, *Green Chem.* **2018**, *20*, 214-224.

[311] J. Wolfs, R. Nickisch, L. Wanner, M. A. R. Meier, *J. Am. Chem. Soc.* **2021**, *143*, 18693-18702.

[312] Z. Yao, S. Mi, B. Chen, F. Liu, H. Na, J. Zhu, *ACS Sustainable Chem. Eng.* **2022**, *10*, 17327-17335.

[313] C.-G. Wang, N. Li, G. Wu, T. T. Lin, A. M. X. Lee, S.-W. Yang, Z. Li, D. H.-K. Luo, *Carbohydrate Polymer Technologies and Applications* **2022**, *3*, 100186.

[314] S. Tanaka, T. Iwata, M. Iji, *ACS Sustainable Chem. Eng.* **2017**, *5*, 1485-1493.

[315] T. Morooka, M. Norimoto, T. Yamada, N. Shiraishi, *J. Appl. Polym. Sci.* **1984**, *29*, 3981-3990.

[316] T. Danjo, T. Iwata, *Polymer* **2018**, *137*, 358-363.

[317] P. Willberg-Keyriläinen, J. Vartiainen, A. Harlin, J. Ropponen, *Cellulose* **2017**, *24*, 505-517.

[318] J. T. Jung, J. F. Kim, H. H. Wang, E. di Nicolo, E. Drioli, Y. M. Lee, *J. Membr. Sci.* **2016**, *514*, 250-263.

[319] T. Sehn, J. Fanelli, L. Wahl, M. A. R. Meier, *RSC Sustainability* **2025**, *3*, 291-299.

[320] A. W. T. King, J. Jalomäki, M. Granström, D. S. Argyropoulos, S. Heikkinen, I. Kilpeläinen, *Analytical Methods* **2010**, *2*, 1499-1505.

[321] M. Ioelovich, *Polymers* **2021**, *13*, 1241.

[322] M. J. H. Worthington, M. Mann, I. Y. Muhti, A. D. Tikoalu, C. T. Gibson, Z. Jia, A. D. Miller, J. M. Chalker, *Physical Chemistry Chemical Physics* **2022**, *24*, 12363-12373.

[323] J. M. Chalker, M. Mann, M. J. H. Worthington, L. J. Esdaile, *Organic Materials* **2021**, *03*, 362-373.

[324] T. Sehn, N. Kolb, A. Azzawi, M. A. R. Meier, *Macromolecules* **2024**, *57*, 10802-10811.

[325] T. N. Kocherova, N. O. Druzhkov, K. A. Martyanov, A. S. Shavyrin, M. V. Arsenyev, T. I. Kulikova, E. V. Baranov, V. A. Kuropatov, V. K. Cherkasov, *Russ. Chem. Bull.* **2020**, *69*, 2383-2389.

[326] H. Q. N. Gunaratne, T. J. Lotz, K. R. Seddon, *New J. Chem.* **2010**, *34*, 1821-1824.

[327] C. B. Campbell, A. Onopchenko, D. C. Young, *Ind. Eng. Chem. Res.* **1990**, *29*, 642-647.

[328] M. B. Smith, in *Organic Synthesis (Fourth Edition)* (Ed.: M. B. Smith), Academic Press, Boston, **2017**, pp. 605-657.

[329] A. P. Grimm, J. M. Scheiger, P. W. Roesky, P. Théato, *Polym. Chem.* **2022**, *13*, 5852-5860.

[330] Y. Shin, G. E. Fryxell, W. Um, K. Parker, S. V. Mattigod, R. Skaggs, *Adv. Funct. Mater.* **2007**, *17*, 2897-2901.

[331] Y.-L. Hou, Y. Diao, Q. Jia, L. Chen, *ACS Omega* **2020**, *5*, 7392-7398.

[332] in *Guidelines for drinking-water quality: Fourth edition incorporating the first and second addenda*, World Health Organization, Geneva, **2022**.

[333] C. J. Kloxin, T. F. Scott, B. J. Adzima, C. N. Bowman, *Macromolecules* **2010**, *43*, 2643-2653.

[334] S. Kamarulzaman, Z. M. Png, E. Q. Lim, I. Z. S. Lim, Z. Li, S. S. Goh, *Chem* **2023**, *9*, 2771-2816.

[335] L. Sougrati, A. Duval, L. Avérous, *Materials Science and Engineering: R: Reports* **2024**, *161*, 100882.

[336] W. Denissen, J. M. Winne, F. E. Du Prez, *Chemical Science* **2016**, *7*, 30-38.

[337] D. Yang, K. Zhao, R. Yang, S.-W. Zhou, M. Chen, H. Tian, D.-H. Qu, *Adv. Mater.* **2024**, *36*, 2403880.

[338] F. I. Altuna, V. Pettarin, R. J. Williams, *Green Chem.* **2013**, *15*, 3360-3366.

[339] J. Lyu, S. Lee, H. E. Bae, H. Jung, Y. I. Park, Y.-J. Jin, J.-E. Jeong, J. C. Kim, *Angew. Chem. Int. Ed.* **2024**, *63*, e202411397.

[340] Y. Ding, R. Miao, J. Liu, Z. Xin, C. Bao, *ACS Appl. Polym. Mater.* **2024**, *6*, 9008-9016.

[341] Q. Li, S. Ma, S. Wang, Y. Liu, M. A. Taher, B. Wang, K. Huang, X. Xu, Y. Han, J. Zhu, *Macromolecules* **2020**, *53*, 1474-1485.

[342] Q. Li, S. Ma, P. Li, B. Wang, Z. Yu, H. Feng, Y. Liu, J. Zhu, *Macromolecules* **2021**, *54*, 8423-8434.

[343] K. H. Kim, K. Jeong, J. Zhuang, H. J. Jeong, C. S. Kim, B. Koo, C. G. Yoo, *Industrial Crops and Products* **2021**, *159*, 113095.

[344] P.-C. Bian, W.-J. Xu, H.-Z. Gang, J.-F. Liu, B.-Z. Mu, S.-Z. Yang, *Int. J. Mass spectrom.* **2017**, *415*, 85-91.

[345] C. Berti, E. Binassi, M. Colonna, M. Fiorini, G. Kannan, S. Karanam, M. Mazzacurati, I. Odeh, M. Vannini, **2010**.

[346] N. Kasmi, M. Majdoub, G. Z. Papageorgiou, D. N. Bikiaris, *Polym. Degrad. Stab.* **2018**, *152*, 177-190.

[347] A. Moreno, M. Morsali, M. H. Sipponen, *ACS Applied Materials & Interfaces* **2021**, *13*, 57952-57961.

[348] L. Santos Correa, S. Leidenheimer, M. A. R. Meier, *Polym. Chem.* **2025**, *16*, 821-832.